



Institut für Geowissenschaften (IFG)

EBERHARD KARLS
UNIVERSITÄT
TÜBINGEN



Institut für Geowissenschaften (IFG)

TÜBINGER GEOWISSENSCHAFTLICHE ARBEITEN (TGA)

Reihe A: Geologie, Paläontologie, Stratigraphie

Schriftleitung: W. Frisch & J. Kuhlemann

Volker Schuller

**Evolution and geodynamic
significance of the Upper
Cretaceous Gosau basin in the
Apuseni Mountains (Romania)**

TGA, A70, 2004

Tübinger Geowissenschaftliche Arbeiten	A	70	112 S.	88 Abb. 15 Tab.	Tübingen, Juli 2004
---	---	----	--------	--------------------	---------------------------

Band 70

Evolution and geodynamic significance of the Upper Cretaceous Gosau basin in the Apuseni Mountains (Romania)

Volker Schuller

Tübingen

2004

Anschrift des Verfassers: Volker Schuller
Inst. für Geowissenschaften, Univ. Tübingen, Sigwartstr. 10, 72076 Tübingen

Key words: Apuseni Mts., Gosau basin, basin modelling, vitrinite reflectance, fission track thermochronology

Copyright © Volker Schuller 2004. All rights reserved. Alle Rechte vorbehalten.

Copyright © Universität Tübingen 2004 (TGA Series A, ISSN 0953-4921).

Citations of this volume should take the form:

Schuller, V. (2004): Evolution and geodynamic significance of the Upper Cretaceous Gosau basin in the Apuseni Mountains (Romania). *Tübinger Geowiss. Arb., Reihe A* **70**, 1-112

Please note that according to German transcription rules, 'Tübinger' transcribes to 'Tuebinger' in case of lack of the character 'ü'.

Library of Congress Cataloging-in-Publication Data

Evolution and geodynamic significance of the Upper Cretaceous Gosau basin in the Apuseni Mountains (Romania). / Schuller, Volker

p. cm. — (Publication / Geological and Palaeontological Institute, University of Tuebingen, Germany; no. 70)

Includes bibliographical references.

ISSN 0953-4921

1. Geology, Geophysics

I. Title. II. Series.

551.8—dc21

This work is subject to copyright. All rights are reserved, whether the whole or part of the material is concerned, specifically the right of translation, reprinting, re-use of illustrations, recitation, broadcasting, reproduction on microfilms or in other ways, and storage in data banks including publication via the internet or other computer network.

The storage of the abstract of the volume in its entirety together with the name(s) of the author(s) and the title of the volume is allowed for citation purposes provided that the copyright notice appears.

www.uni-tuebingen.de

Printed in Germany

Bisher erschienen in dieser Reihe:

- Nr. 1 RING, U. (1989): Tectogenesis of the Penninic/Austroalpine boundary zone: the Arosa Zone (Grisons-Rätikon area, Swiss-Austrian Alps).
- Nr. 2 BETZLER, C. (1989): The Upper Paleocene to Middle Eocene between the Rio Segre and the Rio Llobregat (eastern South Pyrenees): facies, stratigraphy and structural evolution.

- Nr. 3 HEINZ, W. (1989): Vulkanoklastische Komponenten und deren geodynamische Bedeutung für die Entwicklung der Southern Uplands von Schottland.
- Nr. 4 SICK, M. (1989): Paleomagnetism of ophiolite complexes from the southern Middle American Landbridge (Costa Rica and western Panama).
- Nr. 5 BRÜCKMANN, W. (1989): Typische Kompaktionsabläufe mariner Sedimente und ihre Modifikation in einem rezenten Akkretionskeil (Barbados Ridge).
- Nr. 6 VAVRA, G. (1989): Die Entwicklung des penninischen Grundgebirges im östlichen und zentralen Tauernfenster der Ostalpen – Geochemie, Zirkonmorphologie, U/Pb-Radiometrie.
- Nr. 7 SCHWENTKE, W. (1990): Upper Cretaceous tectono-sedimentary and facies evolution of the Basque Pyrenees (Spain).
- Nr. 8 RICHTER, C. (1990): The anisotropy of magnetic susceptibility – Numeric models, deformation experiments, and practical application in structural geology.
- Nr. 9 HEINZLER-JONCZYK, G. (1992): PTt-Paths in the southeast Tauern Window (Eastern Alps).
- Nr. 10 HAIB, N. (1992): Untersuchungen zur Genese von Plagioklasgneisen im Basiskristallin der Ostalpen (Gleinalm- Ötztal- und Silvrettakristallin).
- Nr. 11 KRAUS, S. (1992): Stratigraphy and facies of the "Garumnian" – Late Cretaceous to Early Paleogene – in the Treppe region, central southern Pyrenees.
- Nr. 12 SFEIKOS, A. (1992): Geology, analysis of deformation and kinematics of the Pelagonian nappe system, Kamvounia mountains (North Thessaly, Greece).
- Nr. 13 LIU, G. (1992): Permian to Eocene sediments and Indian passive margin evolution in the Tibet Himalayas.
- Nr. 14 BECKER, B. (1993): The Structural Evolution of the Radstadt Thrust System, Eastern Alps, Austria – Kinematics, Thrust Geometries, Strain Analysis.
- * Nr. 15 DÜRR, S.B. (1993): The Mid- to Early-Late Cretaceous Xigaze forearc basin (south Tibet); Sedimentary evolution and provenance of clastic sediments. [13 EUR]
- * Nr. 16 MICHEL, G. (1993): Neokinematics along the North Anatolian Fault. [15 EUR]
- * Nr. 17 HERRMANN, U.R. (1993): The origin of a „Terrane“: U/Pb zircon systematics, geochemistry and tectonics of the Xolapa complex (southern Mexico). [12 EUR]
- Nr. 18 GRÄFE, K.-U. (1994): Sequence Stratigraphy in the Cretaceous and Paleogene (Aptian to Eocene) of the Basco-Cantabrian Basin (N. Spain).
- Nr. 19 PROKOPH, A. (1994): Zyklische Sedimentation im Oberalb des Norddeutschen Beckens.
- * Nr. 20 REICHERTER, K. (1994): The Mesozoic tectono-sedimentary evolution of the Central Betic seaway (external Betic Cordillera, Southern Spain). [15 EUR]
- * Nr. 21 RATSCHBACHER, L., SPERNER, B., MESCHÉDE, M. & FRISCH, W. (1994): Computer techniques and applications: A program library for stress and strain analysis. [10 EUR]
- * Nr. 22 MESCHÉDE, M. (1994): Tectonic evolution of the northwestern margin of the Caribbean Plate in the light of the "terrane concept": Structural and geochemical studies in southern Mexico and Costa Rica. [13 EUR]

- * Nr. 23 KÖLBL-EBERT, M. (1995): Paläozoische Ganggesteine (Rhyodazite/Dazite und Lamprophyre) des Südschwarzwaldes. [14 EUR]
- Nr. 24 JIN, J. (1995): Dynamic stratigraphic analysis and modeling in the south-eastern German molasse basin.
- Nr. 25 PATZELT, A. (1996): Palaeo- and rockmagnetism of Cretaceous to Tertiary sediments from the Tethyan Himalaya: evidence for crustal shortening and deformation of the northern Indian margin due to the collision with Eurasia.
- * Nr. 26 LÄUFER, A.L. (1996): Variscan and Alpine tectonometamorphic evolution of the Carnic Alps (Southern Alps) – Structural analysis, illite crystallinity, K-Ar and Ar-Ar geochronology. [13 EUR]
- * Nr. 27 SPERNER, B. (1996): Computer programs for the kinematic analysis of brittle deformation structures and the Tertiary tectonic evolution of the Western Carpathians (Slovakia). [13 EUR]
- Nr. 28 MAYER, H. (1996): Magnetostratigraphic and Cyclostratigraphic Investigations of the Early Cretaceous Biancone Formation at Cison and Pra da Stua (Southern Alps, Italy) with Palaeoclimatical, Geochronological and Geomathematical Implications.
- * Nr. 29 PFÄNDER, Jörg (1996): TWIST – Ein Computerprogramm zur Strainberechnung aus Calcit-Zwillingsdaten und seine Anwendung in der Deformationsanalyse des alpinen Vorlandes. [10 EUR]
- * Nr. 30 WINKLER, M. (1996): Genese und geodynamische Stellung der Zentralgneise im Tauernfenster. [13 EUR]
- Nr. 31 SCHUSTER, F. (1996): Paleocology of Paleocene and Eocene Corals from the Kharga and Farafra Oases (Western Desert, Egypt) and the Depositional History of the Abu Tartur Carbonate Platform, Kharga Oasis.
- Nr. 32 GÜLDENPFENNIG, M. (1997): Geologische Neuaufnahme der Zone von Badenweiler-Lenzkirch (Südschwarzwald) unter besonderer Berücksichtigung unterkarbonischer Vulkanite und Grauwacken.
- * Nr. 33 ZWEIGEL, P. (1997): The Tertiary tectonic evolution of the Eastern Carpathians (Romania): Orogenic arc formation in response to microplate movements. [13 EUR]
- * Nr. 34 NOUFAL, A.W. (1997): Geology and tectonic evolution of the Gulf of Suez, West-Central Sinai, Egypt. [15 EUR]
- * Nr. 35 GÎRBACEA, R.A. (1997): The Pliocene to Recent Tectonic Evolution of the Eastern Carpathians (Romania) [13 EUR]
- Nr. 36 SCHAUER, M. (1998): Dynamische Stratigraphie, Diagenese, und Rohstoffpotential des Oberjura (Kimmeridge 1-5) der mittleren Schwäbischen Alb.
- Nr. 37 LEHMANN, J. (1998): Systematic palaeontology of the ammonites of the Cenomanian-Lower Turonian (Upper Cretaceous) of northern Westphalia, North Germany.
- Nr. 38 RÖSLER, W. (1998): Magnetostratigraphy of Neogene fluvial sediments: results from a high resolution study and several new sections in the Nepalese Siwaliks.
- * Nr. 39 GRÄFE, K. (1998): Exhumation and thermal evolution of the Cordillera de Talamanca (Costa Rica): constraints from fission track analysis, ^{40}Ar - ^{39}Ar , and ^{87}Rb - ^{87}Sr chronology. [13 EUR]
- * Nr. 40 BRÜGEL, A. (1998): Provenances of alluvial conglomerates from the Eastalpine foreland: Oligo-/Miocene denudation history and drainage evolution of the Eastern Alps. [15 EUR]
- Nr. 41 HU, S. (1998): A magnetic study on lacustrine sediments from Zoigê Basin, Eastern Tibetan Plateau, China.

- * Nr. 42 ELIAS, J. (1998): The thermal history of the Ötztal-Stubai-complex (Tirol; Austria/Italy) in the light of the lateral extrusion model. [15 EUR]
- Nr. 43 ASPRION, U. (1998): Ground-penetrating Radar (GPR) analysis in aquifer-sedimentology: Case studies, with an emphasis on glacial systems of SW Germany.
- * Nr. 44 FETSCHER, M. (1998): Strukturelle und petrologische Entwicklung des Terraba-Forearcs im zentralen Bereich des flach subduzierten Cocos-Rückens, Süd-Costa Rica.
MORITZ, E. (1998): Interpretation von LWD-Daten mit Hilfe von künstlichen neuronalen Netzen und genetischen Algorithmen (unter Anwendung auf Daten des ODP Leg 170, Costa Rica Convergent Margin). [15 EUR]
- * Nr. 45 WALDHÖR, M. (1999): The Small-circle reconstruction in paleomagnetism and its application to paleomagnetic data from the Pamirs. [13 EUR]
- * Nr. 46 ABD EL-NABY, H.H. (1999): Geology, petrochemistry and tectogenesis of the Wadi Um Ghalaga area, eastern desert, Egypt. [14 EUR]
- Nr. 47 RÖHL, H.-J. (1999): Hochauflösende palökologische und sedimentologische Untersuchungen im Posidonien-schiefer (Lias ϵ) von SW-Deutschland.
- Nr. 48 SCHMID-RÖHL, A. (1999): Hochauflösende geochemische Untersuchungen im Posidonienschiefer (Lias ϵ) von SW-Deutschland.
- * Nr. 49 CHINCHILLA CHAVES, A.L. (1999): Geologie und Struktur des Ophiolith-Komplexes der Nicoya-Halbinsel (Costa Rica). [13 EUR]
- * Nr. 50 HUSSEIN MOHAMMED, B. (1999): The geology, structure and geochemistry of the crystalline rocks of the Moyale area, Southern Ethiopia: Implications for the tectogenesis of the Precambrian basement. [13 EUR]
- Nr. 51 PÖPPELREITER, M. (1999): Controls on epeiric successions exemplified with the mixed siliciclastic-carbonate Lower Keuper (Ladinian, German Basin).
- * Nr. 52 SZÉKELY, B., FRISCH, W., KUHLEMANN, J., & DUNKL, I. (1999): 4th Workshop on Alpine Geological Studies. 21-24 September 1999, Tübingen (Germany). [20 EUR]
- * Nr. 53 LÓPEZ, A. (1999): Neo- and paleostress partitioning in the SW corner of the Caribbean plate and its fault reactivation potential. [20 EUR]
- Nr. 54 LÖFFLER, S.-B. (1999): Systematische Neubearbeitung und paläoökologische Aspekte der unteroligozänen Molluskenfauna aus den Zementmergeln von Bad Häring (Unterinntal, Tirol).
- * Nr. 55 REINECKER, J. (2000): Stress and deformation: Miocene to present-day tectonics in the Eastern Alps. [13 EUR]
- Nr. 56 HORNING, J. (1999): Dynamische Stratigraphie, Reservoir- und Aquifer-Sedimentologie einer alluvialen Ebene: Der Stubensandstein in Baden-Württemberg (Obere Trias, mittlerer Keuper).
- * Nr. 57 SCHNEIDERMEIER, T. (2000): Paläolithische Fundschichten in quartären Lockersedimenten (Südwestdeutschland): Prospektionsmethoden, Stratigraphie und Paläoökologie. [15 EUR]
- * Nr. 58 HUBICH, D. (2000): Geodynamische Entwicklung der Karnischen Alpen. [13 EUR]

- * Nr. 59 TRAUTWEIN, B. (2000): Detritus provenance and thermal history of the Rhenodanubian flysch zone: mosaicstones for the reconstruction of the Eastern Alps. [13 EUR]
- * Nr. 60 SZÉKELY, B. (2001): On the surface of the Eastern Alps – a DEM study. [13 EUR]
- * Nr. 61 PAWELLEK, T. (2001): Fazies,- Sequenz-und Gamma-Ray-Analyse im höheren Malm der Schwäbischen Alb (SW-Deutschland) mit Bemerkungen zur Rohstoffgeologie (hochreine Kalke). [30 EUR]
- * Nr. 62 CAMPOS BEJARANO, L. (2001): Geology and basins history of Middle Costa Rica: an intraoceanic island arc in the convergence between the Caribbean and the Central Pacific plates. [13 EUR]
- * Nr. 63 MOSER, F. (2001): Tertiäre Deformation in den Rumänischen Südkarpaten: Strukturelle Analyse eines Blattverschiebungskorridors am Westrand der Moesischen Plattform. [13 EUR]
- * Nr. 64 Dakrory, A.M. (2002): Biostratigraphy, paleoenvironment and tectonic evolution of the Late Cretaceous-Early Paleogene succession on the North African plate (Sinai, Egypt) and a comparison with some European and Asian sections. [20 EUR]
- * Nr. 65 Dünkel, I. (2002): The genesis of East Elba iron ore deposits and their interrelation with Messinian tectonics. [15 EUR]
- Nr. 66 Most, T. (2003): Geodynamic evolution of the Eastern Pelagonian Zone in north-western Greece and the Republic of Macedonia. Implications from U/Pb, Rb/Sr, K/Ar, ⁴⁰Ar/³⁹Ar geochronology and fission track thermochronology. TOBIAS LIB online
- Nr. 67 Most, P. (2003): Late Alpine cooling histories of tectonic blocks along the central part of the TRANSALP-traverse (Inntal-Gardertal): Constraints from geochronology. *Tübinger Geowiss. Arb., Reihe A* 67, 1-97.
- * Nr. 68 Helbing, H. (2003): No suture in the Sardinian Variscides: A structural, petrological, and geochronological analysis. [15 EUR]
- Nr. 69 Junghans, W.-D. (2003): Fazies, Zyklizität, Petrophysik und Paläomagnetik im Buntsandstein der Bohrung Kraichgau 1002 (SW-Deutschland).
- * Nr. 70 Schuller, V. (2004): Evolution and geodynamic significance of the Upper Cretaceous Gosau basin in the Apuseni Mountains (Romania). [15 EUR]

Herausgeber: Institut für Geowissenschaften, Universität Tübingen

Sigwartstraße 10, D-72076 Tübingen

ISSN 0953-4921

* zu beziehen über: Dr. Joachim KUHLEMANN, Institut und Museum für Geologie und Paläontologie der Universität Tübingen, Sigwartstraße 10, D-72076 Tübingen, Fax: ++49 7071 5059, e-mail: kuhlemann@uni-tuebingen.de

Aktueller Stand erschienener Bände über: http://www.uni-tuebingen.de/geo/gpi/tga/reihe_a.html

Preise sind ohne Gewähr. Prices are subject to change.

Contents

Abstract	1
Zusammenfassung	2
1. Introduction	3
1.2 The Gosau sediments of the Eastern Alps	5
2. The Apuseni Mountains – geology and structural division	8
3. Methods and results	14
3.1 Sedimentological records of the Upper Cretaceous	
Gosau successions	14
3.1.1 Drocea occurrence	14
3.1.2 Vidra occurrence	18
3.1.3 Sălciua-Ocoliş occurrence	21
3.1.4 Gilău-Haşdate occurrence	24
3.1.5 Vlădeasa occurrence	26
3.1.6 Borod occurrence	28
3.1.7 Roşia occurrence	29
3.1.8 Stratigraphic range	31
3.2 Heavy mineral analysis	35
3.3 Vitrinite reflection and basin modeling	44
3.3.1 Data overview	44
3.3.2 Basin modeling	48
3.3.2.1 Basin model of the Gosau succession	48
3.3.2.2 Basin model of the outer flysch succession (Geoagiu formation, Bozeş flysch)	51
3.4 Kinematic analysis	54
3.5 Fission-track analysis	58
3.5.1 Zircon fission-track data	58
3.5.2 Apatite fission-track data	64
4. Interpretation and discussion	68
4.1 Gosau basin evolution of the Apuseni Mts.	68
4.2 Geodynamic model	68
4.3 Discussion	73
5. Conclusions and paleogeographic implications	76

References	79
Appendix	
A.1 Nannofossil determination	83
A.2 Heavy mineral analysis	86
A.3 Paleocurrent data	91
A.4 Vitrinite reflection	92
A.5 Kinematic analysis	99
A.6 Fission-track analysis	103
References	111
Acknowledgements	112

Abstract

The present-day shape of the Alpine chain is a consequence of Mesozoic to Tertiary plate movements within the Tethys region. As part of this orogen, the Apuseni Mts. were formed during the Upper Cretaceous convergence between the Tisia and Dacia microplates. The subduction of the Transylvanian ocean between the Tisia and Dacia microcontinents can be traced into the East-Alpine region, where the South Penninic ocean was subducted at the same time. In both orogens (the Apuseni Mts. and the Eastern Alps) an Upper Cretaceous basin evolved, which commonly is known as Gosau basin. This work focuses on the sedimentologic and geodynamic evolution of the Gosau basins of the Apuseni Mts.. It combines various methods, which enable a reconstruction of the geological evolution in the sedimentation area and allow direct comparison to the well studied Austroalpine Gosau sediments in the Eastern Alps.

Sedimentologic records yield facies differences within the Apuseni Mts: the southern and eastern parts of the Apuseni Mts. record both, deep marine and shallow marine sediments, which, according to the Austroalpine definition, are grouped into the Lower Gosau Subgroup (shallow marine facies) and Upper Gosau Subgroup (deep marine facies). In the northern Apuseni Mts. only shallow marine sediments were deposited. Paleontological data constrain the stratigraphic range: sedimentation started in Upper Turonian time and ended in the uppermost Cretaceous. The sedimentation onset of the Lower Gosau Subgroup occurred diachronously with a lateral shift from southwest to northeast. The sedimentation onset of the Upper Gosau Subgroup does not show a diachronous pattern. Heavy mineral assemblages prove the erosion of areas lying on both sides of the elongated basin. Basin modeling based on vitrinite reflectance confirms maximum sediment thickness of approximately 3000 m, similar to what is known from the Eastern Alps. Fission-track age populations of detrital zircons from the Gosau sediments reflect three Mesozoic tectonothermal events in the hinterland: at 90 – 110 Ma, 130 – 150 Ma and 170 - 200 Ma. Two additional age populations record Paleozoic ages (250 – 300 Ma and ~ 400 Ma). The convergence of the Tisia and Dacia microplates resulted in a “soft” collision, which is indicated by non-resetting of detrital apatite fission-track ages from the Gosau sediments. However, there was increased exhumation in the crystalline hinterland, which is shown by thermal modeling of apatite fission-track lengths.

The achieved data lead to a reinterpretation of the plate tectonic evolution of the studied area and the proposal of a geodynamic model for the generation of such type of basins. Initial basin subsidence is a consequence of high-strain forced subduction with high frictional shear at the contact between the overriding and subducting plate, accompanied by flexure of the overriding plate and low basin subsidence rates during the deposition of the Lower Gosau Subgroup. Change to retreating subduction due to dehydrating and thus increasing slab density, accompanied by downward pull from the downbending plate, is responsible for the rapid basin subsidence and sedimentation of the Upper Gosau Subgroup. The installation of a cornerflow after the beginning of retreating subduction is inferred to be responsible for the Late Cretaceous banatite magmatism. Retreating subduction resulted in a “soft” continental collision, which occurred around the Cretaceous/Tertiary boundary.

The similarities to the Gosau occurrences of the Eastern Alps lead to direct correlation with the Alpine paleogeographic evolution and the assumption that a continuous ocean basin (South Penninic and Transylvanian ocean basin) has been consumed during Upper Cretaceous times.

Depositioning of Upper Cretaceous flysch sediments (e.g. Bozeş flysch, South Apuseni Mts.) occurred into a second basin, which is interpreted as a deep sea subduction-trench basin. The difference to the Gosau basin is supported by basin modeling based on vitrinite reflectance.

Zusammenfassung

Die mesozoischen bis tertiären plattentektonischen Bewegungen im Tethysraum verursachten die gegenwärtige Form der alpinen Gebirgskette. Das Apusenigebirge ist Teil dieses Orogens. Es entstand als Folge der Konvergenz der beiden Mikroplatten Tisia und Dacia. Die hierfür verantwortliche Subduktion des Transilvanischen Ozeans kann bis in den ostalpinen Raum verfolgt werden. Hier wurde zur gleichen Zeit der Südpenninische Ozean subduziert. In beiden Orogenen (Apusenigebirge und Ostalpen) bildet sich während der Oberkreide ein Becken, das als Gosaubecken bezeichnet wird. Die vorliegende Arbeit richtet ihr Augenmerk auf die Gosauablagerungen des Apusenigebirges. Zur Untersuchung der Gosauabfolgen wurden unterschiedliche Methoden angewandt, mit deren Hilfe die geologische Entwicklung im Sedimentationsraum rekonstruiert werden kann und ein direkter Vergleich zu den alpinen Gosausedimenten ermöglicht wird.

Anhand von detaillierten sedimentologischen Untersuchungen wurden sedimentfazielle Unterschiede festgestellt: im südlichen und östlichen Apusenigebirge lagerten sich flachmarine und tiefmarine Sedimente ab, die, vergleichbar zu den Ostalpen, in Untere Gosau (flachmarine Fazies) und Obere Gosau (tiefmarine Fazies) eingeteilt werden. Im Nordapusenien wurden nur Flachwassersedimente abgelagert. Der stratigraphische Umfang der Gosauablagerungen ist durch paläontologische Untersuchungen für die Zeit vom obersten Turon bis ins oberste Maastricht eingegrenzt worden. Die Sedimentation der Unteren Gosau setzte diachron ein, wobei ein Wandern des Sedimentationsbeginns von Südwesten nach Nordosten festgestellt wurde. Der Wechsel zur Oberen Gosau findet ohne diachrones Wandern statt. Schwermineralanalysen zeigen Erosion und Sedimenttransport von beiden Seiten des länglich geformten Beckens. Die maximale Sedimentmächtigkeit der Gosausedimente wurde anhand von Beckenmodellierungen mit Hilfe von Vitritreflexion auf ca. 3000 m berechnet und weist ähnliche Werte wie die der ostalpinen Gosauabfolgen auf. Aus den Spaltspurenaltern detritischer Zirkone wurden fünf Alterspopulationen separiert: drei mesozoische (90 – 110 Ma, 130 – 150 Ma und 170 – 200 Ma) und zwei paläozoische (250 – 300 Ma und ~ 400 Ma), die thermische Überprägungen im Hinterland anzeigen. Die Konvergenz zwischen den Mikroplatten Tisia und Dacia führt zu einer „weichen“ Kollision, da die Spaltspurenalter detritischer Apatite aus den Gosauabfolgen keine postsedimentäre thermische Überprägung aufweisen. Thermische Modellierungen anhand von Apatit-Spaltspurenlängen des kristallinen Autochthons zeigen, daß die Kollision der beiden Krustenblöcke mit einer Hebung des Hinterlandes verbunden ist.

Aufgrund dieser Daten wird die plattentektonische Entwicklung des Untersuchungsgebietes neu interpretiert und ein geodynamisches Modell für die Entstehung des Gosaubeckens erstellt. Als Folge der erzwungenen Subduktion und der damit verbundenen hohen Spannung an der Kontaktfläche zwischen der Oberplatte und der subduzierten Kruste wurde in der Oberplatte eine Flexur erzeugt. In dem hierdurch gebildeten flachmarinen Becken wurden die Sedimente der Unteren Gosau abgelagert. Aufgrund der Dehydrierung und Dichtezunahme der subduzierten ozeanischen Kruste wurde ein Wechsel im Ablauf der Subduktionsprozesse eingeleitet. Die nun folgende rückschreitende Subduktion war Ursache für die rasche Beckensubsidenz im Sedimentationsraum. Eine im Mantelkeil einsetzende Konvektion mit Winkelfluß war für den kalk-alkalinen Banatit-Magmatismus verantwortlich. Als Folge der rückschreitenden Subduktion kam es zu einer „weichen“ Kollision an der Kreide/Tertiär Grenze.

Die Ähnlichkeiten zu den Gosau Abfolgen der Ostalpen ermöglichen eine Korrelation der beiden Sedimentationsräume und führen zur Annahme, daß ein von den Ostalpen bis zum Apusenien Gebirge durchgehender Ozean (Südpenninischer und Transilvanischer Ozean) während der Oberkreide subduziert wurde.

Zeitgleich zur Gosausedimentation wurden im Südapusenien bis in die oberste Kreide Turbidite (Bozeş Flysch) in eine Tiefseerinne abgelagert. Beckenmodellierungen mit Hilfe von Vitritreflexion zeigen deutliche Unterschiede dieser beiden Sedimentationsräume und legen somit den Schluß nahe, daß während der Oberkreide zwei unterschiedliche Becken im Apuseniengebirge existierten.

1. Introduction

During Mesozoic to Tertiary plate movements several mountain belts formed within the Alpine–Carpathian orogen. The Apuseni Mts. are part of this mountain belt, although situated in an isolated position between the Pannonian and the Transylvanian Basin (Figure 1-1). The region has attracted many geologists mainly because of several ore deposits. The mountain range is separated by basins from the surrounding Southern, Eastern and the Western Carpathians, and also from other Alpine mountains to the west. The region covers 5200 km², which is rather small compared to the surface covered by the Eastern and Southern Carpathians. The highest peak is the Vlădeasa summit (1849 m) in the northern part of the Apuseni Mts.. Their average altitude is about 700 m.

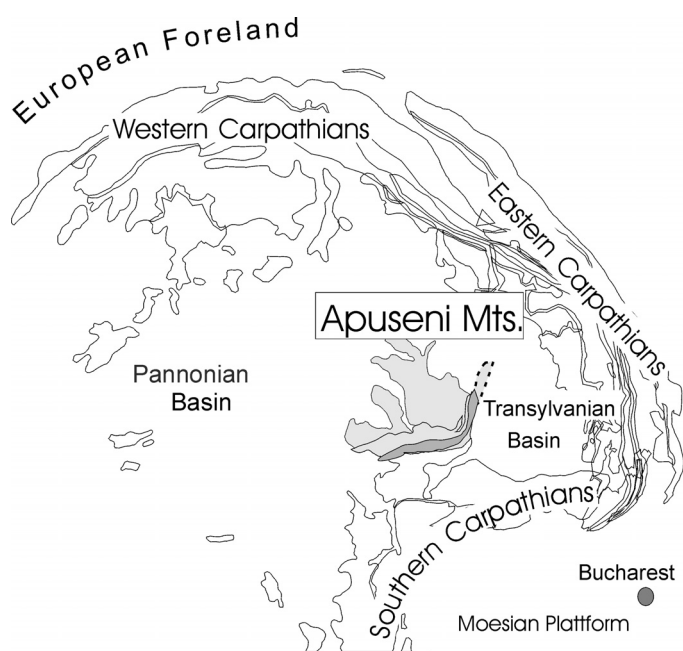


Fig. 1-1: Geological setting of the Apuseni Mts. (grey). The Moesian platform and the European foreland are forming the pre-Alpine continental basement. Dark grey (within the Apuseni Mts.) shows the suture between the two microplates Tisia and Dacia (see Fig. 2). The dashed line is the prolongation of the suture in the Transylvanian basin, covered by Neogene sediments.

The Apuseni Mts. have been formed during Cretaceous times as a result of the convergence and collision of the two microplates Tisia and Dacia (Fig. 1-2). The suture within the newly created Tisia-Dacia block crops out in the south and southeast of the Apuseni Mts.. Its prolongation towards NE is covered by Neogene sediments of the Transylvanian basin. However, its existence is known from geophysical data.

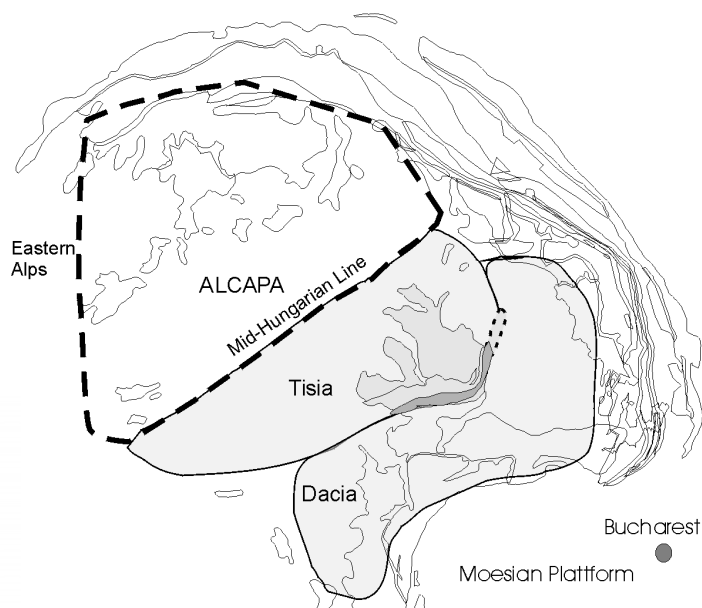


Fig. 1-2: Position of the two microplates Tisia and Dacia. The ALCAPA (Alpine-Carpathian-Pannonian) block is situated west of the Tisia block. The dark grey area illustrates the exposed suture between the two microplates (dashed-line: covered suture).

Many works have been carried out to reconstruct the microplate constellations and drift patterns within the Alpine-Carpathian-Dinaridic region (Săndulescu, 1984; Csontos et al., 1992; Csontos, 1995; Tari, 1995; Zweigel, 1997; Linzer et al., 1998; Moser, 2001). The present geologic setting within the Carpathian orogen is a consequence of the Mesozoic and Tertiary plate movement of the Tisia-Dacia block and the ALCAPA (Alpine-Carpathian-Pannonian) block. The Mid-Hungarian Line represents the boundary between the two microplates (Csontos et al., 1992). The Tisia-Dacia block underwent Late Tertiary N-S shortening (Csontos, 1995)

accompanied by a 70°-90° clockwise rotation in Early to Middle Miocene time (Pătarșcu et al., 1994; Panaiotu et al., 1997; Zweigel, 1997). Based on kinematic data, Zweigel (1997) proposes a Late Cretaceous northward drift of a non-fragmented continental block which comprises the Eastern Alps, Western-, Eastern-, Southern-Carpathians and the Balkanides (Fig. 1-3). Due to collision in the southern part of Moesia, the block has been divided by dextral faults. The ongoing subduction resulted in a northward advance of the fragmented blocks during the Paleogene. The counterclockwise rotation of the ALCAPA block (Mauritsch et al., 1995) was followed by the continental collision in the Western Carpathians. The clockwise rotation of the Tisia-Dacia block was accompanied and succeeded by retreating subduction (Royden, 1993) of the Ceahlău ocean (Zweigel, 1997), an eastward prolongation of the Penninic ocean. Neogene collision of the Tisia-Dacia block with the European margin formed the Eastern Carpathians.

One target of this study is to shed light on the geodynamic evolution at the end of the Mesozoic and the beginning of Tertiary times. The Upper Cretaceous sediments of the Apuseni Mts. seem to be a key for understanding the formation of the orogen and the geodynamic evolution within this area. Therefore this study focuses on these syn-orogenic sediments. A second aim of the study is to compare the Upper Cretaceous deposits of the Apuseni Mts. with similar sedimentary successions of the Eastern Alps (Gosau Group). The common characters of the Upper Cretaceous successions of the Apuseni Mts. with those of the Eastern Alps have been described by several geologists, generally on the basis of classical sedimentologic and paleontologic data (e.g. Lupu, 1970; Lupu & Lupu, 1983; Pitulea & Lupu, 1987; Lupu & Zacher, 1996). Most of the Upper Cretaceous sediments of the Apuseni Mts. have been described as sediments belonging to Gosau facies. Gosau type successions of the Eastern Alps and the Apuseni Mts. display the following similarities:

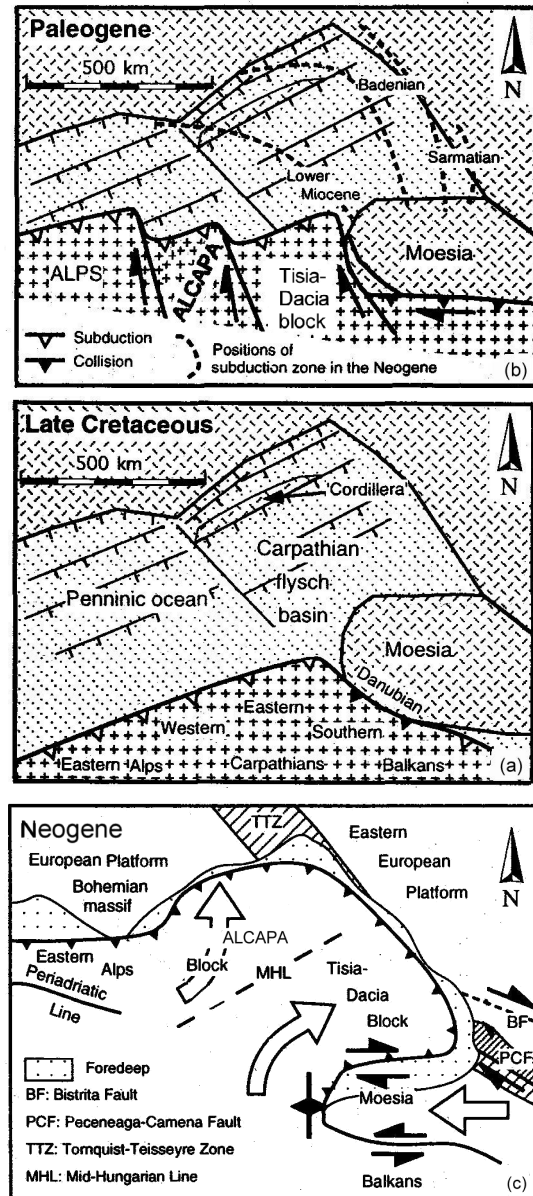


Fig. 1-3: Late Cretaceous to Neogene palinspastic reconstruction of the Carpathian-Pannonian region. Late Cretaceous collision (a) on the western edge of Moesia led to segmentation of the continental block (b). The Tisia-Dacia block rotated clockwise and drifted into the Carpathian bay (c), followed by Neogene continent-continent collision (modified after Zweigel, 1997).

- same stratigraphic range
- same sedimentological facies succession
- sedimentation in a similar geodynamic and tectonic frame

With respect to these similarities I will use the name Gosau sediments, succession or

group for the Upper Cretaceous sediments of the Apuseni Mts. as it has been done by most of the geologist who worked in the Apuseni Mts. in the past.

1.2 The Gosau sediments of the Eastern Alps

The remnants of the Upper Cretaceous Gosau sediments of the Eastern Alps have been in the focus of many geologists since their description in 1782 by J. Bohdasch. The term Gosau as a facies and sedimentary succession has been named after the village of Gosau in the Salzkammergut, southeast of Salzburg. Several publications are dealing with each Upper Cretaceous Gosau occurrence within the Eastern Alps (Tollmann, 1976 and references therein). Brinkmann (1934, 1935), Kühn (1947), Oberhauser (1965) described the successions and discussed the litho-stratigraphic range of the Gosau

occurrences of the entire Eastern Alps. Recent work (Leiss, 1990; Ortner 1994, 2001; Wagreich, 1994, 1995, 2001) focused mostly on basin evolution and geodynamic implications.

The Gosau sediments of the Eastern Alps are mainly located in the Northern Calcareous Alps (NCA), a subunit of the Austroalpine nappe complex (Fig. 1-4). Some occurrences are also exposed in the Central-Alpine region, which belongs to the Austroalpine Unit south of the NCA and north of the Periadriatic Line. The Gosau sediments have been deposited unconformably upon the nappe complexes of the Austroalpine which have been formed during the Eoalpine tectogenesis. In several places the Gosau succession seals the nappe contacts of the Austroalpine nappe complexes. Together with the Gosau sediments, the Northern Calcareous Alps have been affected by later Tertiary shortening. Thus, most of the

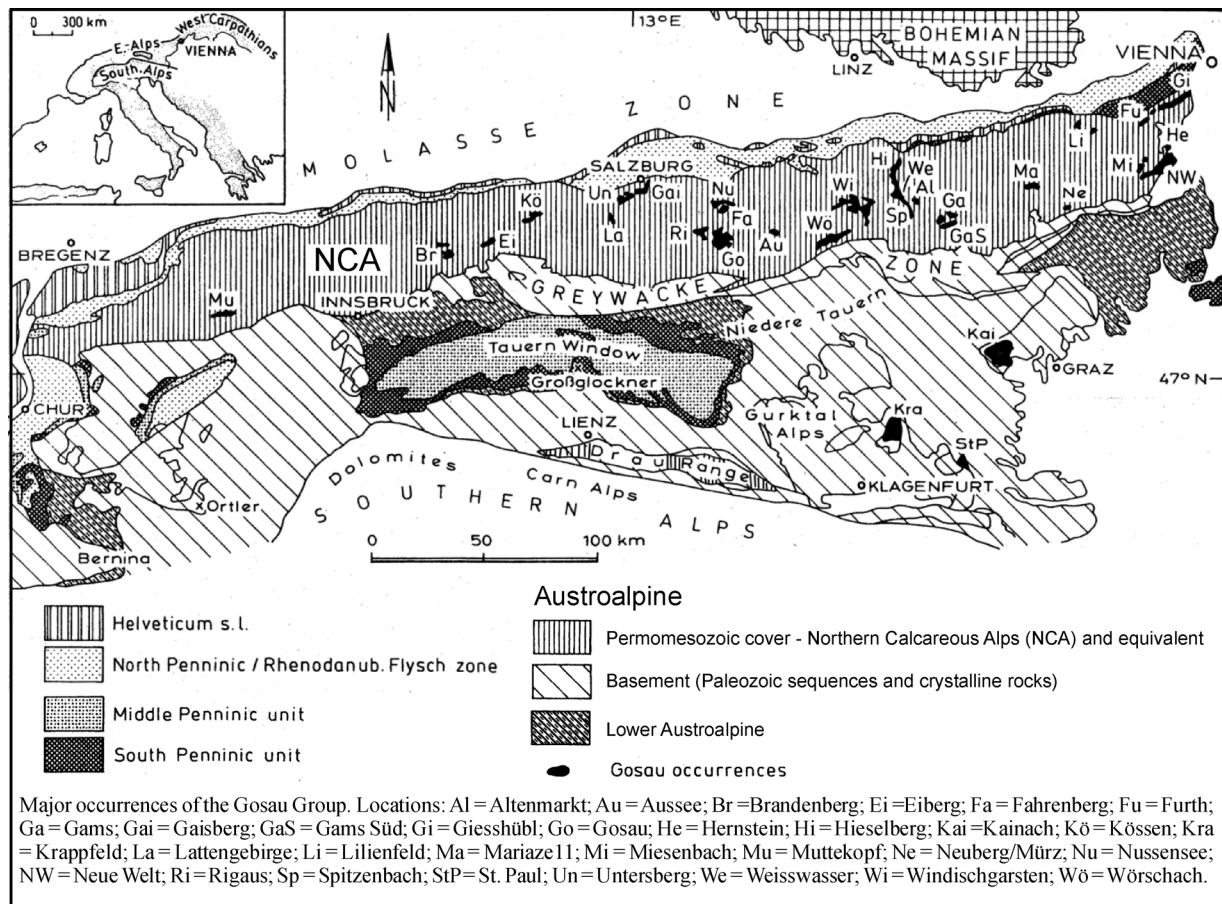


Fig. 1-4: Overview of the main Gosau occurrences of the Eastern Alps (Tollmann, 1976; Wagreich, 1994).

sediments are characterized by post-sedimentary faults, folds and overthrusting.

The successions of the Gosau deposits record identical facies associations within the Eastern Alps. Most authors agree on the first order division into a Lower Gosau Subgroup, comprising alluvial and shallow marine deposits, and the Upper Gosau Subgroup, represented by deep marine turbidites. The sedimentation started with clast supported basal conglomerates with

Santonian/Campanian in the east. The same pattern has also been proven for the second subsidence phase. The change from the shallow marine to deep marine sedimentation - respectively Lower to Upper Gosau Subgroup - first happened in the northwest (Turonian/Coniacian) and successively moved towards southeast, where the first deep water sediments record Maastrichtian ages (Wagreich, 1995; Fig. 1-5). In some occurrences the continuous basin subsidence led to

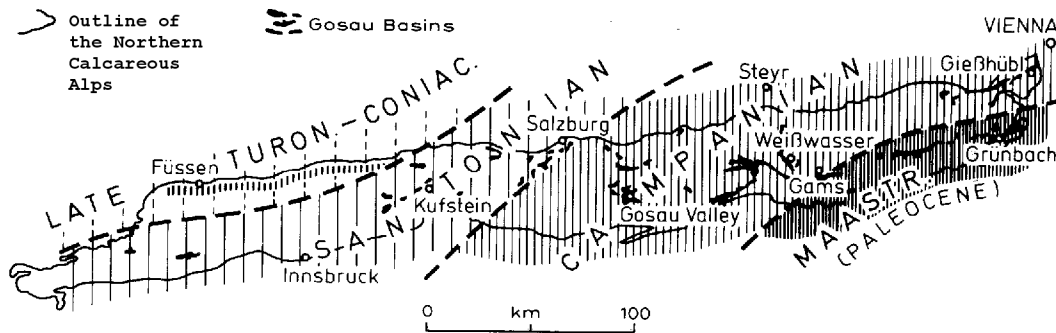


Fig. 1-5: Diachronous start of the deep water sedimentation (Upper Gosau Subgroup) within the Northern Calcareous Alps. The isolines illustrate the time shift from northwest to southeast (after Wagreich, 1995).

a reddish matrix and a base-breccia. Upsection, the succession turns into a marine fan delta facies with conglomerates, sandstones and siltstones sometimes rich in marine fossils. Upsection shallow marine sediments follow. The alternation of sandstones, sandy limestones, rudist-bearing limestones, marls and tempestites reflects a shallow marine inner and outer, storm-influenced shelf facies. The evidence of a hemipelagic character upsection is proven by a fining upward trend and also in the appearance and dominance of planktonic foraminifera (Wagreich et al., 1994). The succession turns into a turbiditic deep water facies (Upper Gosau Subgroup). Gravity flows with coarse grained to fine grained siliciclastic sequences represent deposits of a the upper, middle and lower fan of deep marine turbiditic aprons. Partly carbonate-free sedimentation proves deposition below the CCD.

The initial sedimentation of the Lower Gosau Subgroup records a diachronous onset from Late Turonian in the west, to

sedimentation of deep water deposits up to the Eocene (Wagreich, 2001).

The change from shallow water to deep water sedimentation is of crucial importance, since the geotectonic mechanism which led to this rapid basin subsidence is still a subject of debate. Leiss (1990) proposes that basin

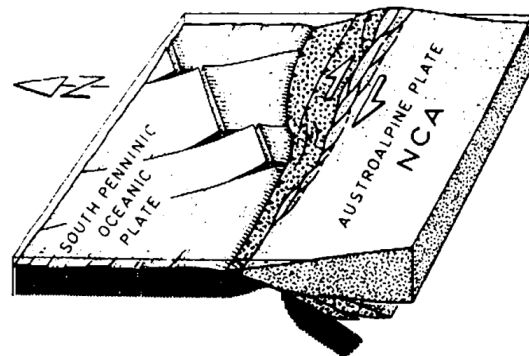


Fig. 1-6: Model sketches the subduction tectonic erosion. Oblique subduction of the oceanic crust led to diachronous collision and subduction of the oceanic ridge. This resulted in a laterally onset of the basin subsidence within the Austroalpine plate (Wagreich, 1995).

subsidence was due to orogenic compression which led to formation of intraplate troughs. Waggreich et al. (1994) suggested a model based on subduction erosion and an extensional tectonic regime. Their model is also able to explain the diachronous onset of the subsidence phases. According to these authors, the South Penninic ocean has been subducted towards the south. The collision and subduction of an "intraplate-high" (e.g. oceanic ridge) led to subduction erosion of material from the accretionary wedge as well as from parts of the continental crust (Fig. 1-6). Thinning of the overriding plate was accompanied by rapid basin subsidence. Because of the oblique movement of the two plates (South Penninic Ocean and Austroalpine Unit), the subduction of the an "intraplate-high" occurred with a lateral shift from west to east.

2. The Apuseni Mountains – geology and structural division

The Apuseni Mts. are built up of several tectonic units which were formed during Mesozoic to Early Tertiary tectonic events (Fig. 2-1, 2-2). The division into Northern and Southern Apuseni Mts. has been made because the Northern Apuseni Mts. mainly consist of a pre-Alpine basement with Permo-Mesozoic cover, whereas the Southern Apuseni Mts. are mostly built up by Jurassic to Cretaceous sedimentary

rocks and igneous rocks. The Arieş river and its prolongation towards the west divides the Northern and Southern Apuseni Mts.. In the following sections, the geology of the Apuseni Mts. is summarized, mainly by concerning the division of the main tectonic units (Ianovici et al., 1976, Săndulescu, 1984, Balintoni, 1997). This division has been made based on the age of the tectonic phases and their corresponding nappe emplacements. The main units are the Transylvanides and Apusenides. The Apusenides comprise

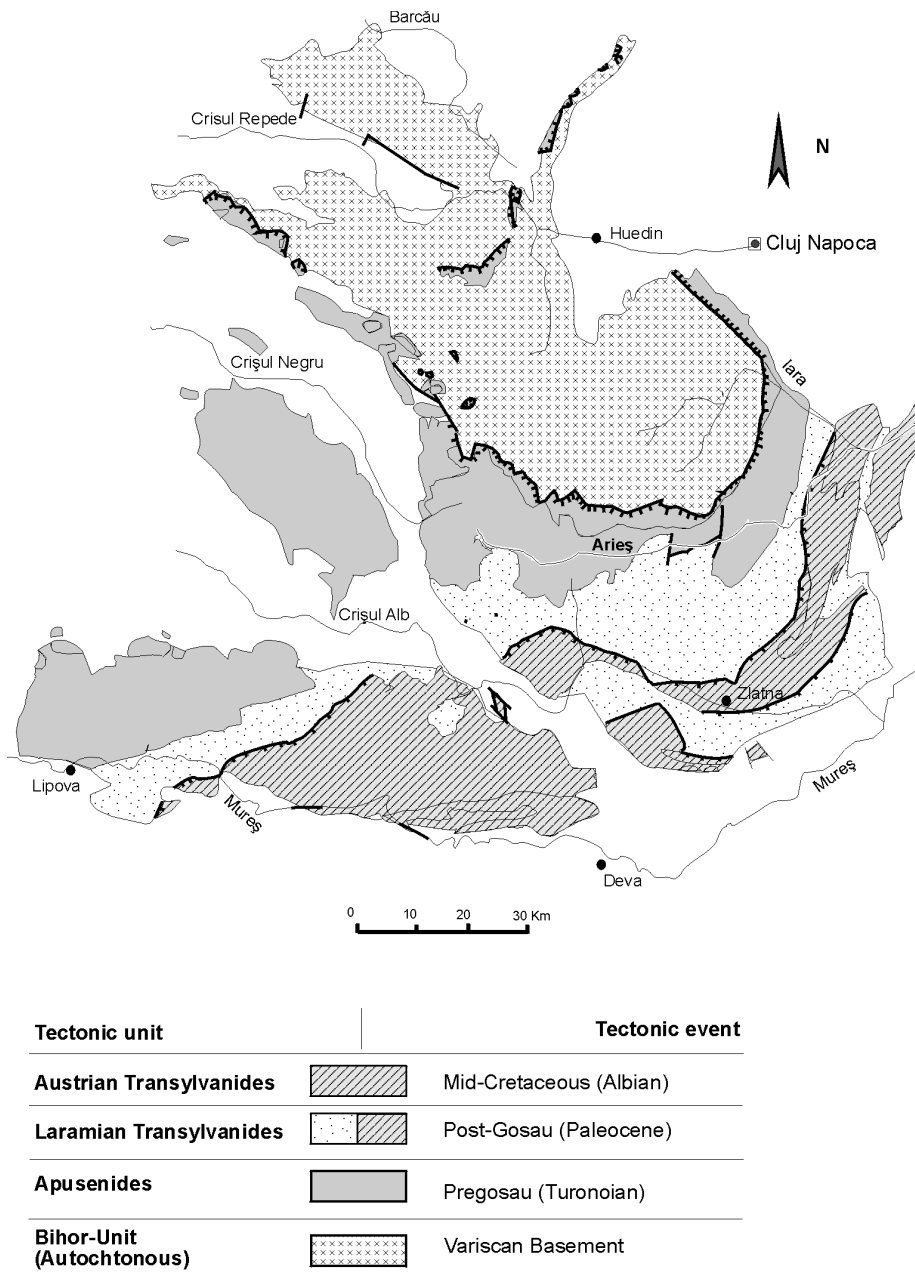


Fig. 2-1: Division of the main tectonic units of the Apuseni Mts. after Balintoni (1997). The Laramian Transylvanides incorporate also the mid-Cretaceous Austrian Transylvanides.

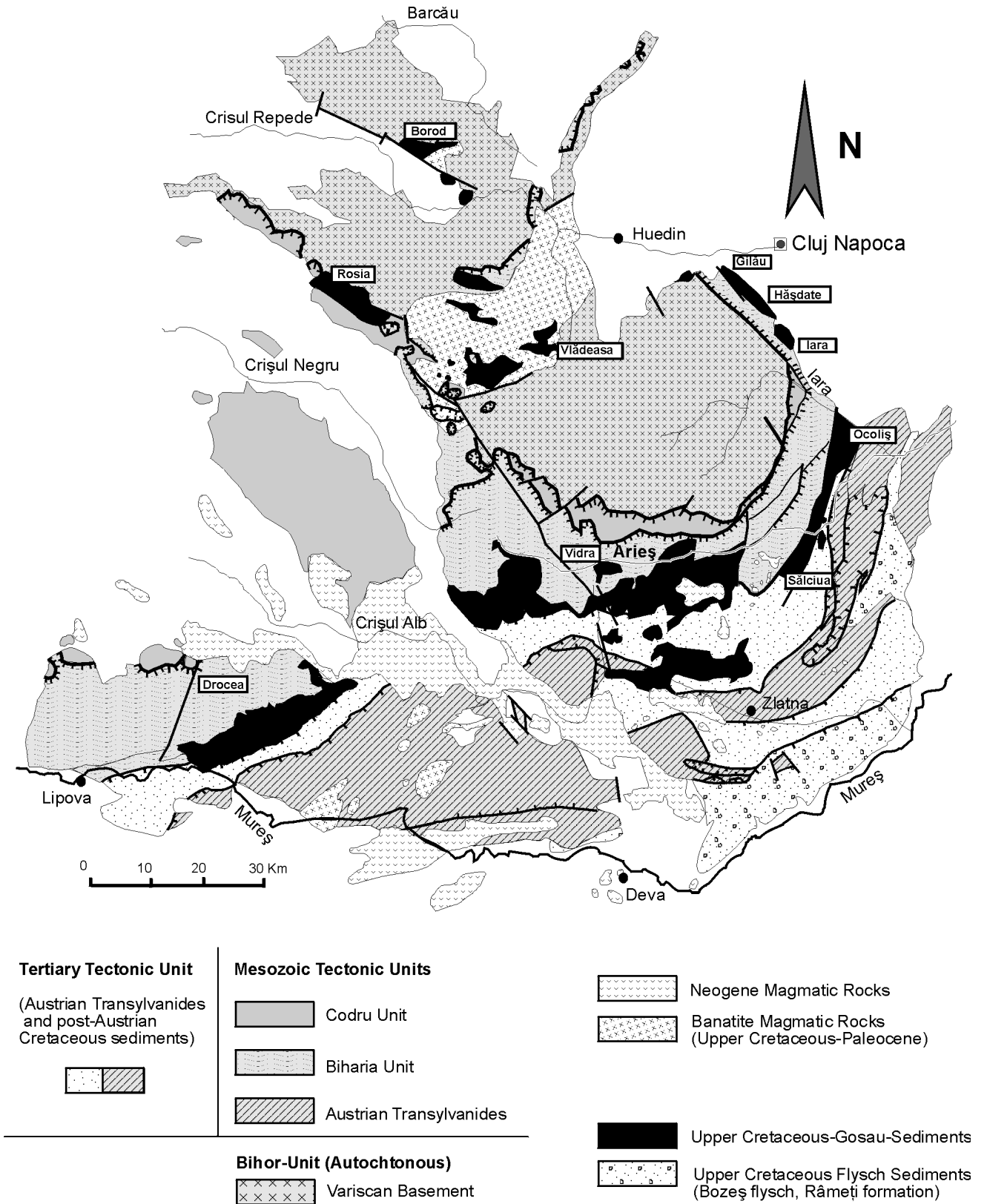


Fig. 2-2: Structural map of the Apuseni Mts. (after Ianovici et al., 1976; Balintoni, 1997). The denominations of the main Upper Cretaceous Gosau sediment occurrences are shown in the white squares. The Gosau sediments of the South Apuseni Mts. appertain to the Tertiary Tectonic unit.

the nappes of the Codru and the Biharia Units. The nappe emplacement happened during Turonian time (Săndulescu, 1984), prior to Gosau sedimentation. In Romanian literature this tectonic event is named Pre-Gosau tectogenesis.

Since Balintoni (1997) proposed the division of the Transylvanides into the Austrian and Laramian Transylvanides, some explanation could help to understand this subdivision. The Austrian Transylvanides are considered to comprise rocks which are part of the tectonic units that have been formed during the mid-Cretaceous tectogenesis, particularly during the Albian (Austrian tectogenesis in Romanian literature). The Early Tertiary tectogenesis again incorporates the Austrian Transylvanides, and "Post-Austrian" (mid-Cretaceous and Upper Cretaceous) sediments and forms the Laramian Transylvanides. Since Laramian is the name for an orogen in the North American plate, which is not associated with the Alpine orogenesis, I will avoid this denomination. For further descriptions and discussions I will divide all the tectonic units into the Mesozoic Tectonic Units and a Tertiary Tectonic Unit (Fig. 2-2). Thus, the Austrian Transylvanides and the Apusenides (comprising the Codru and Biharia nappe complexes) are forming the Mesozoic Tectonic Unit (or Pre-Gosau Unit) which has been formed before the sedimentation of the Upper Cretaceous Gosau sediments. The second unit will be the Tertiary Tectonic Unit which has been formed after the last sedimentary record of the Gosau deposits (uppermost Maastrichtian) and before the deposition of the first sediments of the Transylvanian Basin in the lowermost Eocene (Ypresian). Thus the Tertiary Tectonic Unit comprises the Laramian Transylvanides and therefore replaces this name.

The nappes of the Mesozoic tectonic unit are west vergent and the contact between the nappes is characterized by steep thrust planes. The lowermost and stratigraphically youngest unit is the Codru nappe complex which lies upon the Bihor autochthonous unit (Fig. 2-3). The

uppermost unit are the Austrian Transylvanides. They are the tectonically highest and stratigraphically oldest nappe complex. The Tertiary tectogenesis affects the southern part of the Apuseni Mts. and is characterized by faults, folds and out-of-sequence thrusts.

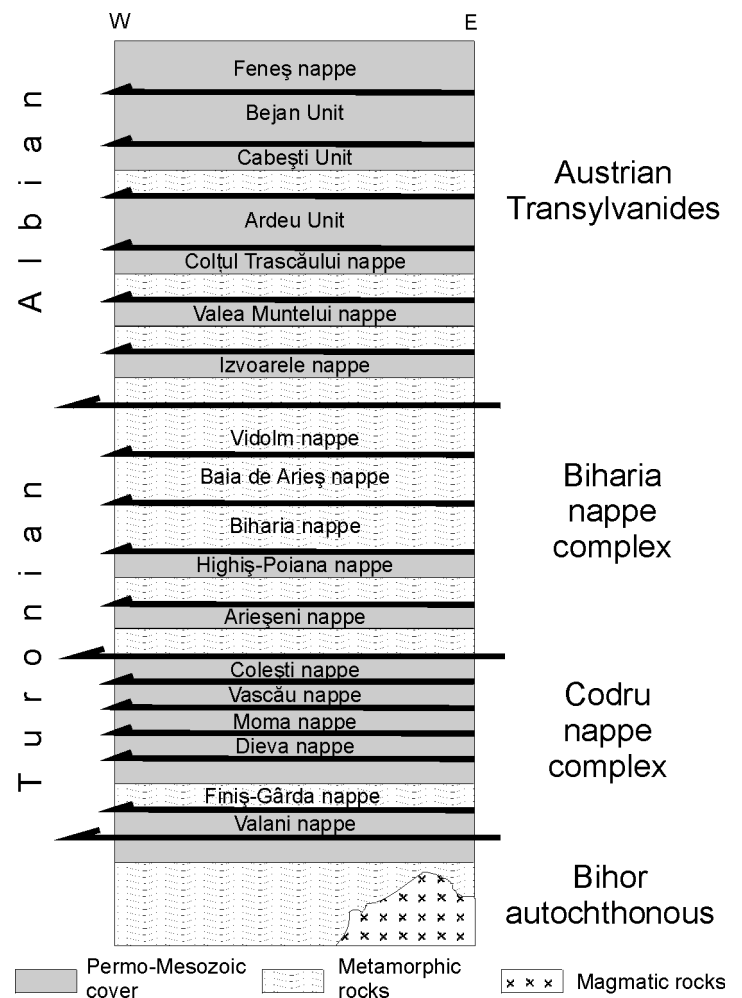


Fig. 2-3: Tectonostratigraphic positions of nappe complexes of the Mesozoic Tectonic Units (after Săndulescu, 1984 and Balintoni, 1997). The Austrian Transylvanides are the oldest (Albian), whereas the Codru and Biharia nappe complexes are the youngest (Turonian).

The Bihor Autochthonous Unit

The Bihor autochthonous unit is situated in the northern part of the Apuseni Mts.. It is composed of several metamorphic rocks (which form the Someş unit), a Variscan granite (Granit de Muntele Mare) and Permo-Mesozoic sediments (Ianovici et al., 1976). The Someş unit comprises

micaschists, amphibolites and gneisses, which record medium-grade metamorphism. Its age has been dated by the Ar/Ar method on hornblende and it shows a uniform range of about 300 Ma (Dallmeyer et al., 1994, Dallmeyer et al., 1999). The Muntele Mare granite intrudes into the metamorphic unit. It is the largest magmatic intrusion in the Apuseni Mts. composed of porphyric granites which record Ar/Ar muscovite ages between 122 and 190 Ma (Dallmeyer et al., 1994, Dallmeyer et al., 1999).

The Permo-Mesozoic cover comprises the following stratigraphic-sedimentary succession (Fig. 2-4, after Ianovici et al., 1976):

- Permian: fluvial conglomerates, breccias and sandstones, and volcanic tuffs, followed by a hiatus.
- Lower Triassic (Werfenian, Skythian): conglomerates, quartz-sandstones, claystones and in some areas dolomites. These rocks are similar in facies to the Werfen beds in the Northern Calcareous Alps (Mantea, 1985).
- Middle to Upper Triassic: the sedimentary facies of these deposits is also similar to that of the Alpine Triassic. The sediments comprise thick limestones and dolomites in the Middle Triassic and red limestones interbedded with claystones and thick limestones in the Upper Triassic. The Triassic sequence closes with a hiatus at the uppermost Triassic.
- Jurassic: the succession starts with conglomerates and fine-grained clastic sediments, limestones and marls in the Lower Jurassic. Thick platform carbonates were deposited during the Middle and Upper Jurassic. Two short discontinuities – within the Bajocian and the Callovian - are known within this succession.
- Cretaceous: a hiatus at the lowermost Cretaceous is responsible for the workable bauxite deposits of the Apuseni Mts. The sedimentation starts with limestones and marly limestones (Barremian). Siliciclastic deposits predominate in the upper part of the Lower Cretaceous. The latest

sedimentation (sandstones and conglomerates) is recorded from the lowermost Turonian.

Remnants of the Upper Cretaceous Gosau sediments have been deposited in the areas of the Bihor autochthonous unit as well as in all other tectonic units. But because they are considered as post-tectonic cover (at least in terms of Mesozoic tectogenesis), they will be described separately (chapter 3.1).

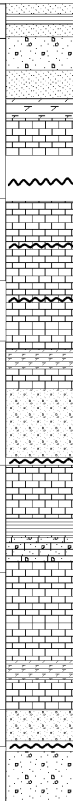
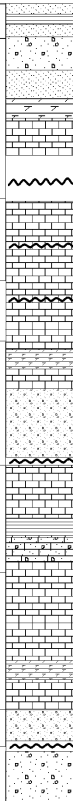
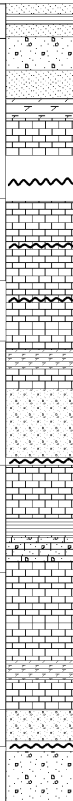
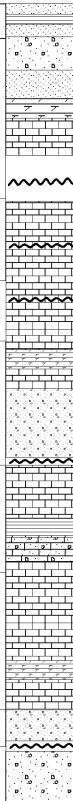
Cretaceous	Upper		sandstones, siltstones, claystones conglomerates, sandstones, marls
	Lower		limestones, marls, sandstones Barremian limestones Bauxites
Jurassic	Upper		limestones
	Middle		limestones and marls
	Lower		conglomerates and sandstones (Gersten facies)
Triassic	Upper		limestones red claystones limestone conglomerates
	Middle		limestones (Wetterstein facies) limestones and dolomites
	Lower		Sandstones, conglomerates (Werfen facies)
Permian			fluvial sediments (breccias and conglomerates) hiatus

Fig. 2-4: Sedimentary cover of the Bihor autochthonous unit after Ianovici et al. (1976).

The Mesozoic Tectonic Units

The Apusenides

The **Codru Unit** represents the lowermost nappe complex of the Apusenides comprising several nappes (Fig. 2-3). The crystalline rocks consists of medium- to low-grade metamorphic rocks. The assemblage of micaschist, gneiss and amphibolite is cut by Variscan granodioritic intrusions. Ar/Ar data of the metamorphic

rocks record ages around 400 Ma (Dallmeyer et al., 1994, 1999).

The Permo-Mesozoic cover of the Codru Unit consists of the same sediments as those of the Bihor autochthonous unit described above.

The nappes of the **Biharia Unit** are built up of predominantly crystalline rocks. They record very low- to medium-grade P/T conditions. Metaconglomerates and some micaschists of the Biharia nappe give Ar/Ar ages about 300 Ma. Some amphibolites of the Baia de Arieș nappe show Ar/Ar ages of 155 Ma (Dallmeyer et al, 1994, 1999). Mylonites within the entire Biharia nappe complex report Ar/Ar ages which scatter between 120 and 110 Ma. These data reflect that the Biharia nappe complex is the only unit that has been partly affected by the Mesozoic tectogenesis.

Remnants of the Permo-Mesozoic sedimentary cover (as described for the Bihor autochthonous unit) are also known from several small outcrops within the Biharia nappe complex.

The Austrian Transylvanides

Within the Mesozoic Tectonic Unit the Austrian Transylvanides are the uppermost nappe complex. Because of the ophiolitic rocks within this nappe complex, Săndulescu (1984) proposed the term “obduction nappes”. The nappes of the Transylvanides are composed of a metamorphic basement (greenschists, phyllites, marbles) with unmetamorphosed basic intrusive dikes, Jurassic ophiolites with deep marine sediments (radiolarites), Upper Jurassic to Lower Cretaceous platform carbonates (Stramberg facies) and Lower Cretaceous siliciclastic sediments (marls, sandstones and flysch sediments).

The Tertiary Tectonic Unit

Balintoni (1997) proposed to divide the Transylvanides into two tectonic units (Austrian and Laramian Transylvanides) in order to differentiate the tectonic events: a Cretaceous and an Early Tertiary one. The Tertiary Tectonic Unit comprises the

nappes of the Austrian Transylvanides, Lower Cretaceous to Upper Cretaceous flysch deposits and the Upper Cretaceous Gosau sediments. Some Upper Cretaceous deposits (e.g. Geoagiu flysch, Bolbâlna sequence, Râmeți sequence) do not belong to the Gosau succession, mainly because of their external position. This issue is still subject of controversial discussion and it also will be a focus within this study.

The Early Tertiary tectonics affects the Apuseni Mts. only in their southern part. Although obvious tectonic compression is recorded this tectogenesis does not build up nappes in its proper sense. The Early Tertiary tectonics causes faults, folds and out of sequence thrusts but no large scale faulting with low angle thrust planes.

The Upper Cretaceous magmatic rocks (banatites)

Bernhard von Cotta (1864) was the first geologist who described the calc-alkaline magmatic rocks of the Apuseni Mts. and proposed the term banatites (after Banat, an area situated in the southwestern part of the Apuseni Mts.). Especially from economical point of view they have been in the focus of interest, since metasomatic mineralisations and the hydrothermal stage of the magmatic intrusions generated Cu, Au, Mo, Zn, Pb and Fe deposits. However, most ore deposits are Skarn ores, formed during Upper Cretaceous magmatic intrusions, mainly into Jurassic limestones.

The banatite magmatism generated primarily acidic to intermediate plutonic and volcanic rocks. The center of the eruptions is located in the Vlădeasa massif, in the central part of the northern Apuseni Mts.. This volcano-plutonic complex is characterized by large subvolcanic dacites and rhyolites and a volcano-sedimentary succession (Ștefan, 1980; Mantea, 1985). Within the entire Apuseni Mts. intrusions (granites, granodiorites and diorites), sills, dikes and tuffs can be found.

Similar intrusive and extrusive rocks are also known from the South Carpathians (Poiana Rusca Mts.), northern Serbia

(Timok) and northern Bulgaria (Srednogorie). Together with the Apuseni Mts., they build up a chain of similar Upper Cretaceous to Paleocene magmatic rocks which extends from the Balkans to the west and along the southern part of the South Carpathians towards the north into the Apuseni Mts. (Berza et. al., 1998; Neubauer, 2002). Several ages of the banatite rocks in Romania have been determined but few within the Apuseni Mts.. Bleahu et al. (1984) presents K/Ar ages which range from 76 Ma to 61 Ma. K/Ar ages on Andesites from the Apuseni Mts. show ages between 45 and 40 Ma (Har, 2001). Banatites in the southern part of Romania gave ages that scatter between 79 and 66 Ma (Neubauer, 2002 and references therein).

The Neogene magmatism

The mainly calc-alkaline Neogene magmatism was active only in the southern part of the Apuseni Mts.. Subvolcanic, volcanic and volcano-sedimentary rocks range from rhyolites to dacites and mainly andesites, reflecting the acidic to intermediate character of this magmatism. Furthermore, some basic subvolcanic intrusions are also associated with this magmatism. The Neogene magmatism is responsible for the Au-rich ore deposits of the Apuseni Mts. (Roşia Montana) which have been mined for more than 2000 years. Several radiometric age datings (Har, 2001 and references therein) show that the magmatic activity starts at about 16 Ma and ends at beginning of the Quaternary time.

3. Methods and results

Several methods have been applied to analyze the Upper Cretaceous Gosau sediments. Some of these methods are the same as those used for the investigations on the Gosau sediments of the Eastern Alps. Thus, the results can directly be compared. Some additional methods have been used, particularly fission-track analyses. For detailed explanations concerning the methodology of rock sample preparing and analyzing, see the Appendix.

3.1 Sedimentological records of the Upper Cretaceous Gosau successions

The main occurrences of Gosau sediments are shown in Fig. 3-1. In this chapter some of these occurrences will be presented. The division into Northern and Southern Apuseni Mts. is applicable for the Gosau sediments, although the original division of the Apuseni Mts. is based on other particularities. The Gosau sediments of the Southern Apuseni Mts. (Drocea, Vidra, Câmpeni-Abrud, Sălcium, Ocoliș, Hașdate and Gilău) record similar sedimentary facies successions: shallow marine deposits (Lower Gosau Subgroup) followed by deep marine turbidites (Upper Gosau Subgroup). The sedimentary succession in the Northern Apuseni Mts. (Vlădeasa and Borod) is characterized by only shallow marine deposits. However, the occurrence of Roșia plays a transitional role with a short turbiditic sedimentation phase, although it is part of the Northern Apuseni Mts..

3.1.1 Drocea occurrence

The Gosau sediments of the Drocea area are the westernmost occurrence of the Apuseni Mts. (Fig. 3-1, Fig. 3-2). They are named after the Highiș-Drocea Mts., a low mountain range at the southwestern edge of the Apuseni Mts.. The sediments are situated between the crystalline rocks of the Biharia nappe complex (in the north) and the Middle Jurassic to Lower Cretaceous limestones, deep marine

clays, jaspers, and tholeiitic basalts (in the south). The originally transgressive contact between the crystalline basement and the Gosau deposits was tectonically overprinted by the Tertiary orogeny. The bedding dips generally to the south-southeast by angles between 15 to 70°. The angle of dip increases towards the south-southeast.

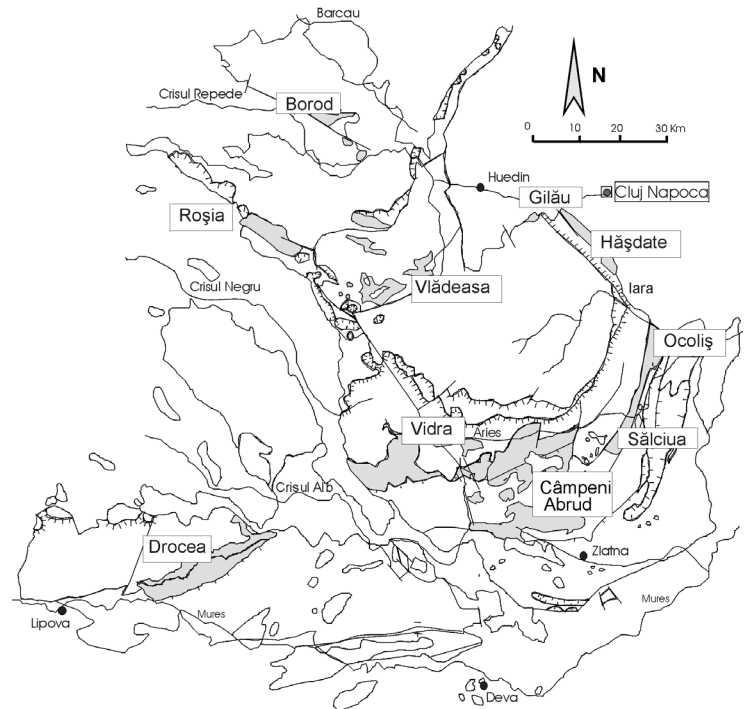


Fig. 3-1: Main occurrences of Upper Cretaceous Gosau sediments of the Apuseni Mts..

The succession starts with conglomeratic breccias, conglomerates and sandstones intercalated by fine-grained claystone layers with organic matter. The pebbles derive from a metamorphic source. The thickness of the basal conglomerates varies between 0 and 15 m. Their absence and/or variety indicates filling of a paleorelief or later tectonic activity with thrusting. The overlying shallow marine sequences are characterized by alternation of claystones, siltstones, sandstones and conglomerates intercalated by organic or fossil-rich layers. Figure 3-3 shows a profile from the lower part of the shallow marine sequence. Upsection, the succession is characterized by increasingly fine-grained, marly

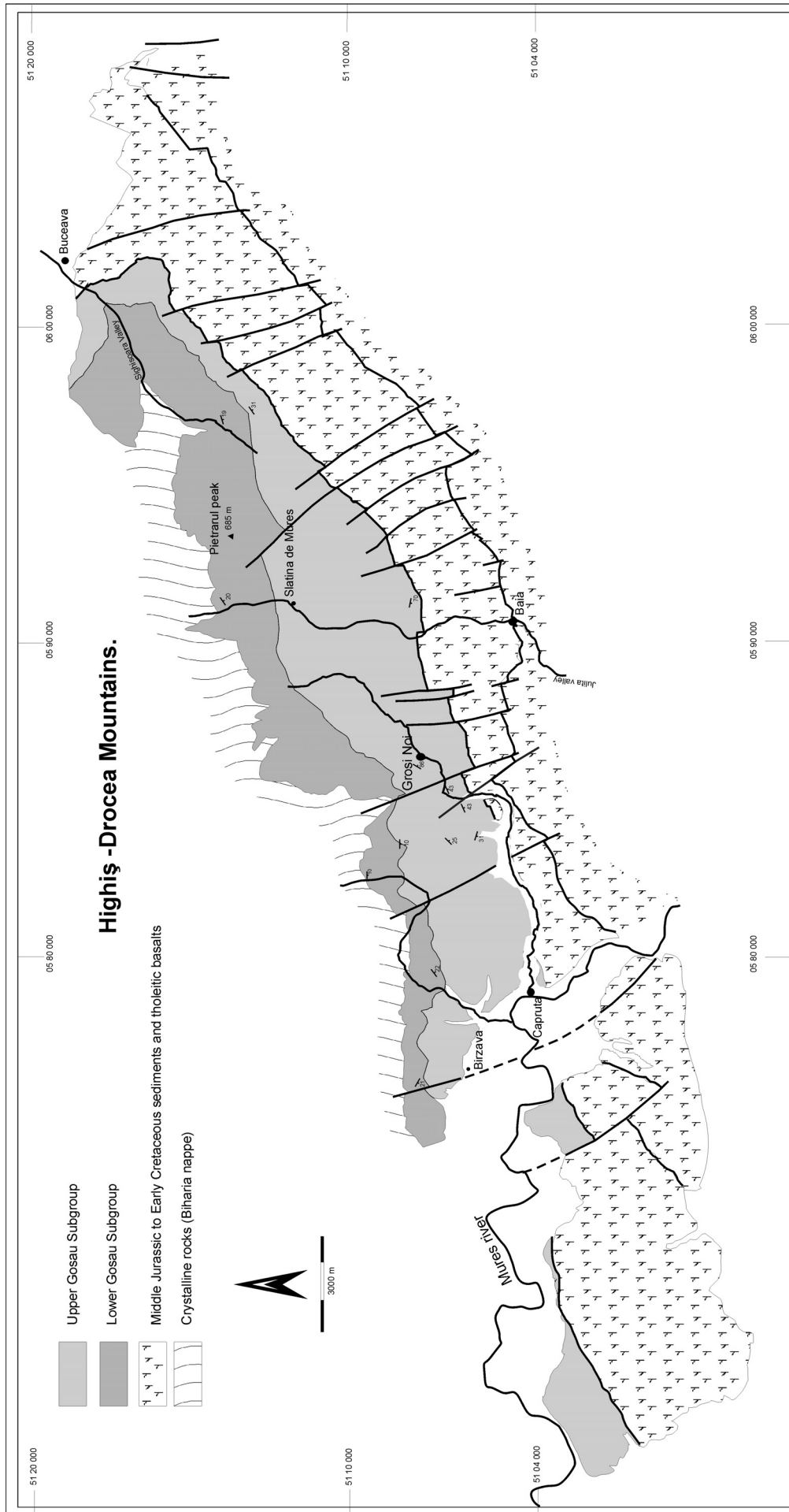


Fig. 3-2: Upper Cretaceous deposits of the Drocea occurrence (modified after Lupu et al., 1993).

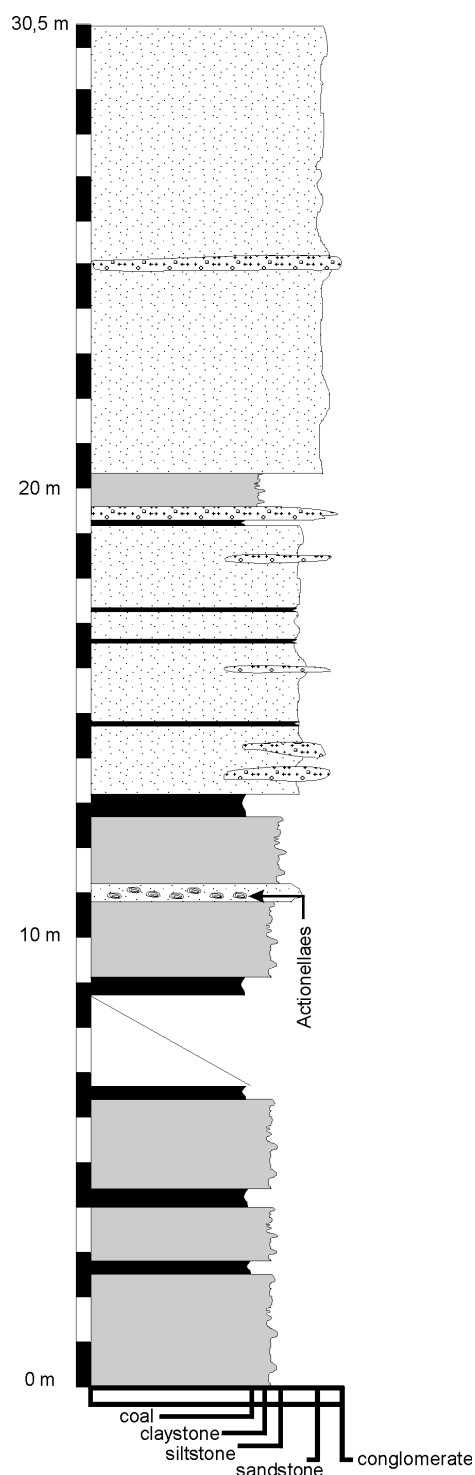
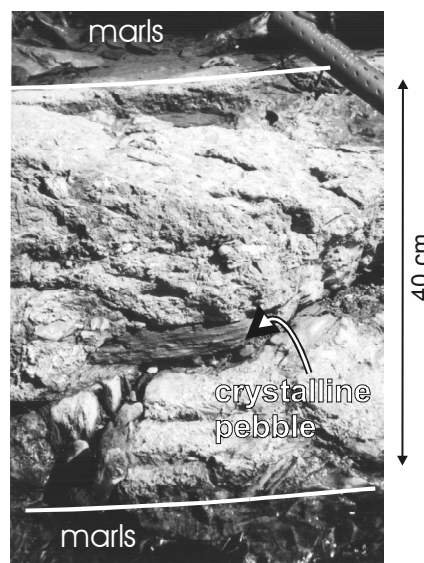


Fig. 3-3: Profile of a succession of the Lower Gosau Subgroup of the Drocea occurrence (Pos.: 05 79 401/51 07 443)

deposits, with sporadically inter-calated coarse-grained, conglomeratic layers which represent tempestites (Fig. 3-4). Several small fan deltas with partly coarse

Fig. 3-4: Tempestite layer within the Lower Gosau Subgroup. The 40 cm thick layer consists of extraclasts (mainly crystalline pebbles) with diameters up to 15 cm, intraclasts (marls, siltstones) and microscopic to macroscopic fragments of shales and rudists. The poorly sorted layer closes with a 5 cm thick fine grained sandstone (Pos. 06 43 990/51 37 110)



grained deposits formed due to syn-sedimentary tectonics (cf. Fig. 3-19). Storm events reworked these sediments and deposited them together with biocalstic fragments as tempestite layers. The thickness of the shallow marine sequence varies between 300 and 600 m. The flysch deposits of the Upper Gosau Subgroup start with typical turbiditic sequences: rhythmic changes of sandstones and claystones or marly limestones. The sandstone beds do not exceed 30 cm in thickness. Upsection, a coarsening-upward trend is observed (Fig. 3-5). The sandstone beds reach thicknesses of up to 2.5 m. In the upper part of the Upper Gosau Subgroup the facies changes to wildflysch with debris flows and olistoliths. The debris flow horizon forms a 20-100 m thick, mainly matrix supported and chaotic conglomeratic succession which can be laterally traced over several kilometers (Lupu et. al., 1993). The Upper Jurassic to Lower Cretaceous limestone-olistoliths have diameters of up to 15 m. In the upper part of the deep water succession the turbidites record a fining-upward trend with sandstone beds which do not exceed 20 cm in thickness (Fig. 3-5). Some outcrops with discordant sedimentary contacts reflect active tectonics during sedimentation (Fig. 3-6). A composite profile shows a thickness of about 1500 to 2000 m of the Upper Gosau Subgroup.

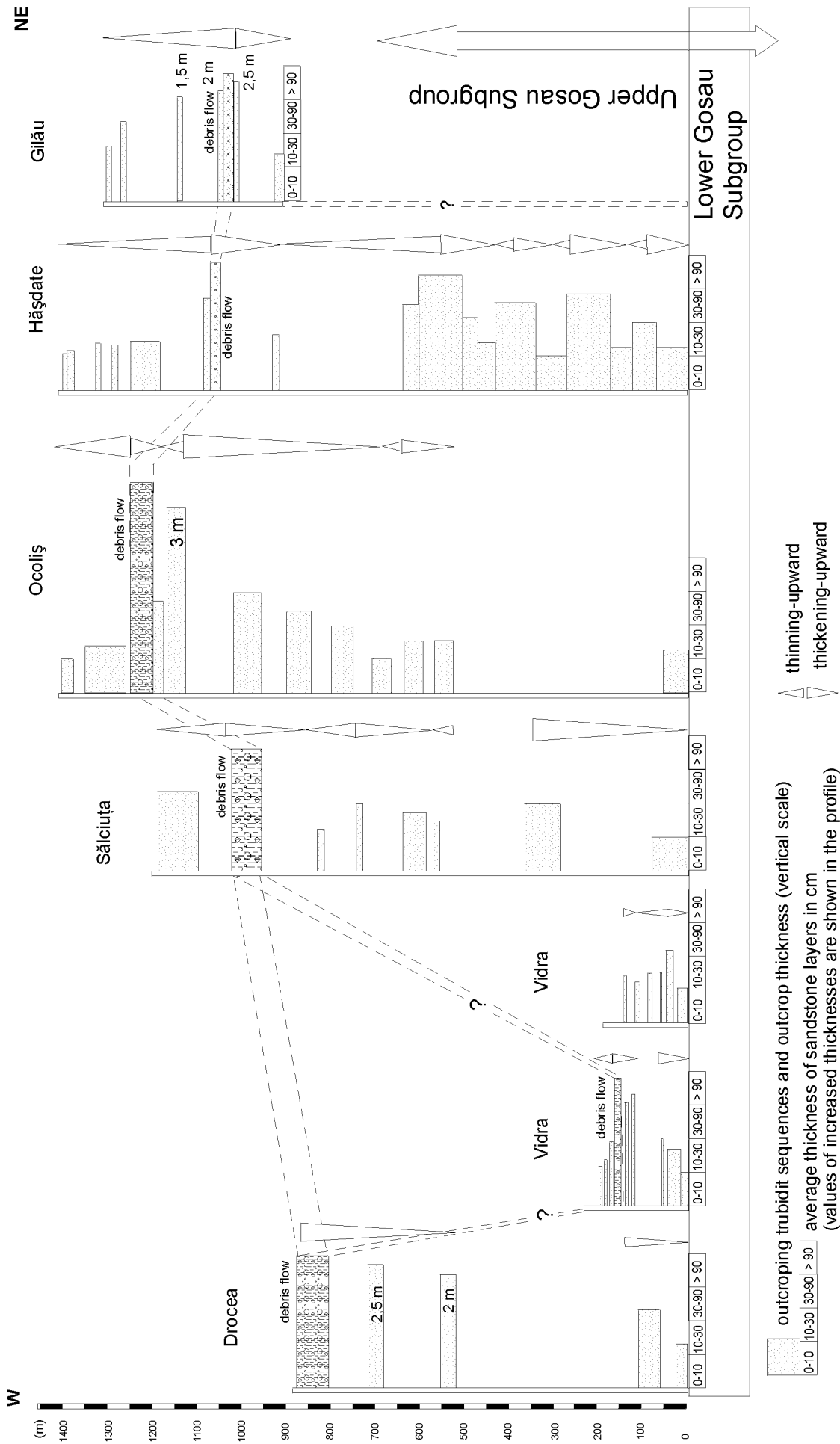


Fig. 3-5.: Correlation of the turbidite succession of the Upper Gosau Subgroup. Each column within a profile illustrates an outcrop with its thickness (vertical scale) and the average thickness of the sandstone layers (horizontal scale). A thickening-upward trend until the debris flow horizon can be seen, as well as a thinning-upward trend after the debris flow horizon.



Fig. 3-6: Proximal turbidit deposits with discordant bedding within the Upper Gosau Subgroup of the Drocea occurrence (Pos. 05 78 050/ 51 07 306).

3.1.2 Vidra occurrence

The Vidra occurrence (Fig 3-7) is situated at the border to the Northern Apuseni Mts., in the area of the Arieșul Mic river, which is a headwater of the Arieș river. The Upper Cretaceous Gosau sediments unconformably overlie the crystalline basement of the Biharia nappe complex. They seal the nappe contact between the Arieșeni and the Muncel-Lupșa nappe (Dimitrescu et al., 1977). The stratification of the Lower Gosau Subgroup is nearly horizontal, whereas the Upper Gosau Subgroup records dipping values up to 84°. The sedimentation starts with basal conglomerate whose thickness strongly varies (20 – 300 m). A 20 m thick profile in

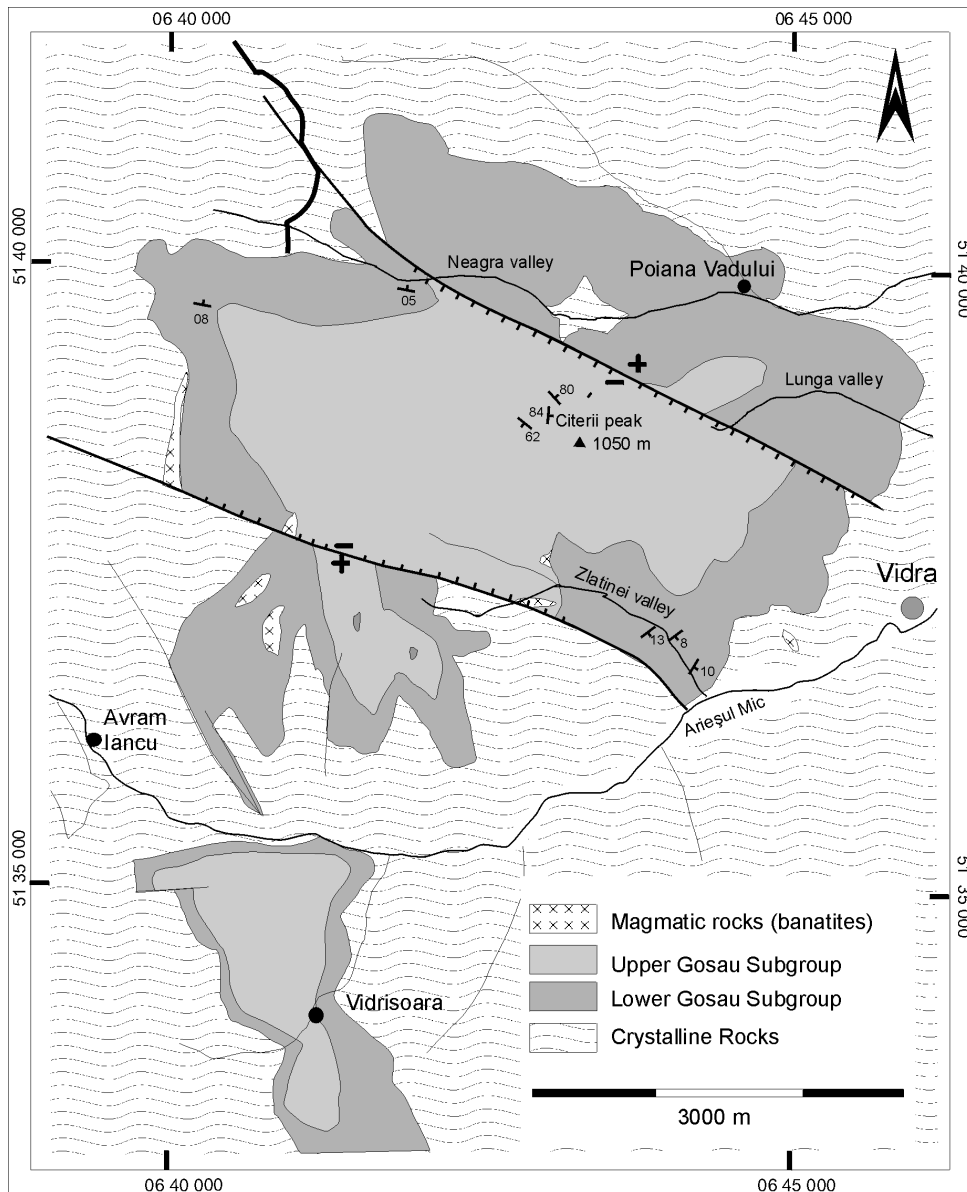


Fig. 3-7: Geological map of the Gosau sediments of the Vidra occurrence (modified after Dimitrescu et al., 1977).

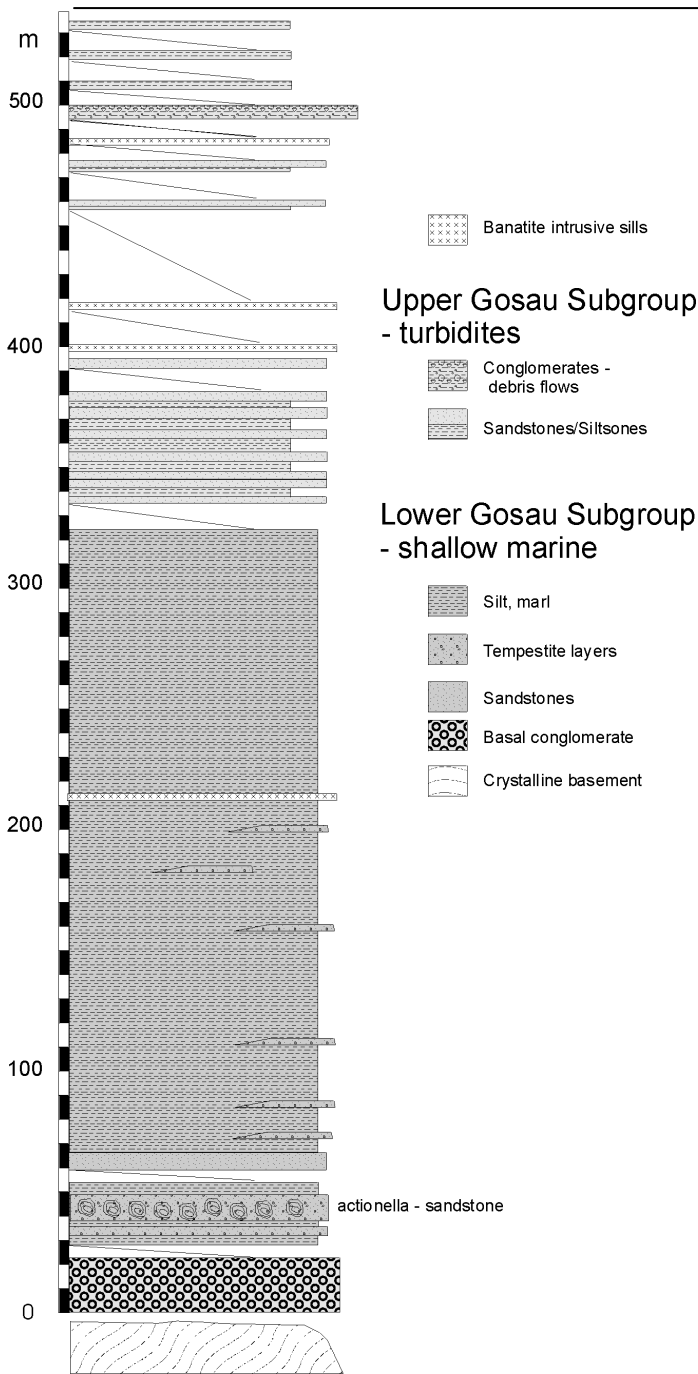


Fig. 3-8: Profile of the Gosau sediments of the Zlatinei valley.

the Lunga valley gives a representative succession through the basal conglomerates of all the Gosau occurrences of the Apuseni Mts.. The profile comprises an alternation of clast supported conglomerates with imbricated clasts, matrix supported conglomerates, cross-bedded microconglomerates, and cross-bedded to planar sandstones. The lenticular, up to 2 m thick coarse-grained

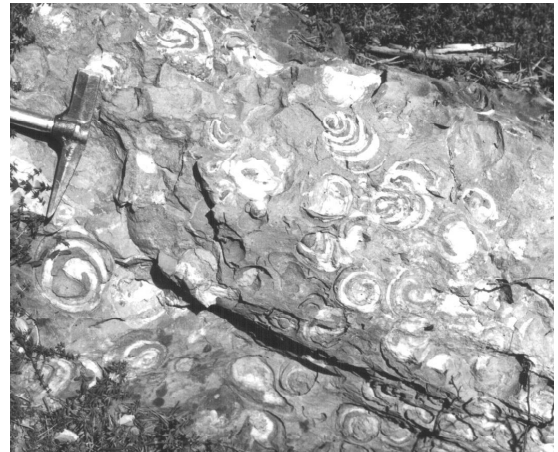


Fig. 3-9: Coastal sandstone with *Actionella* (Pos. 06 44 571/ 71 36 746).

layers represent channel fills. They erosively cut into fine-grained, cross bedded or planar sandstones which have been deposited on terraces beneath the active channels. A general fining-upward trend in this profile is observed, as well as an increase in the matrix proportion. The red to yellowish color change of the matrix suggests that the alluvial fan is prograding into a lake or the sea causing a change in the redox state of the deposited material. The overlying sequences are deposits of coastal, shallow marine and shelf facies (Fig. 3-8). Several meters thick, partly fossil-rich sandstones (Fig. 3-9) representing beach and shoreface deposits are followed by fine grained sandstones with intercalation of coarse-grained to conglomeratic layers. These up to 1.5 m thick, poorly sorted, non-graded conglomerate layers are tempestites, which often contain fossil fragments. They can be found even in the higher parts of the profile showing that the sedimentation of the Lower Gosau Subgroup was mainly in a shallow marine environment which did not exceed 20-30 m water depth, at least until the last tempestite layer. A fining-upward trend can be observed (Fig. 3-10), as well as a change to calcareous sandstones and marls in the upper part of the Lower Gosau Subgroup.

The Upper Gosau Subgroup starts with thin bedded alternations of fine grained sandstones and limy silts. The thickness of the sandstone layers successively

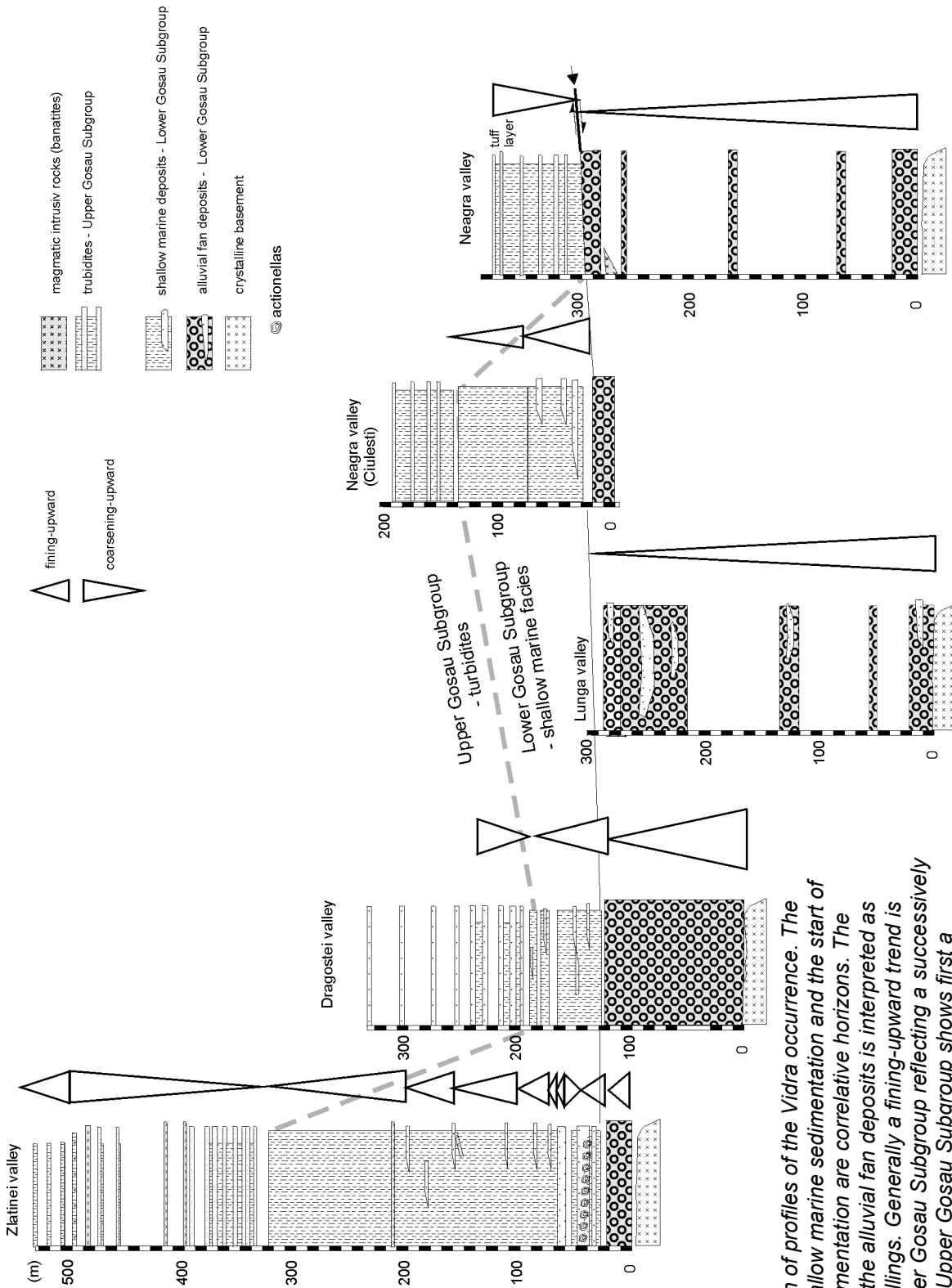


Fig 3-10: Correlation of profiles of the Vidra occurrence. The beginning of the shallow marine sedimentation and the start of the deep water sedimentation are correlative horizons. The thickness variety of the alluvial fan deposits is interpreted as distinct paleorelief fillings. Generally a fining-upward trend is recorded in the Lower Gosau Subgroup reflecting a successively basin opening. The Upper Gosau Subgroup shows first a coarsening-upward with increasing sandstone layer thicknesses of the turbidite sequences. The profile closes with a fining upward cyclicity (silt-mudstone alternation).

increases, reflecting a coarsening-upward trend (Fig. 3-10). The sandstone-mudstone alternations often appear as complete Bouma sequences: coarse grained sandstones representing the erosive Ta layer, followed by the parallel laminated Tb layer, the convolute or ripple bedded Tc layer, fine-grained parallel laminated Td and the pelagic mudstones of the Te layer (Fig. 3-11). After a 6 m thick sequence with debris flow deposits,

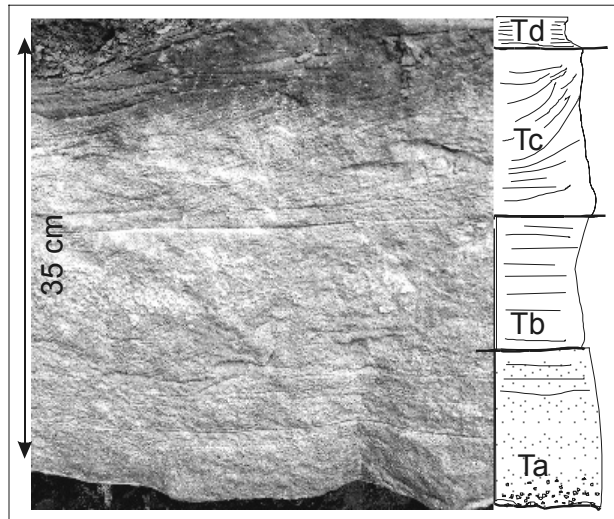


Fig. 3-11: Bouma sequence of a turbidite layer of the Upper Gosau Subgroup. This 35 cm thick layer comprises a graded sandstone (Ta), laminated sandstone (Tb), convolute- and cross-bedded sandstone (Tc) and a fine-grained parallel laminated sandstone (Td).

the succession records a fining-upward trend (Fig. 3-10). Thin bedded sandstones and Bouma sequences with only Tb to Te layers are deposits of a more distal turbiditic fan.

Banatite magmatic rocks are represented as fine grained porphyritic rhyolites intruding as subvolcanic dikes and sills (up to 2 m thick) but also as tuff layers. The post-sedimentary extensional tectonics led to the formation of a horst-and-graben structure (Dimitrescu et al., 1977).

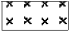





3.1.3 Sălciua-Ocoliș occurrence

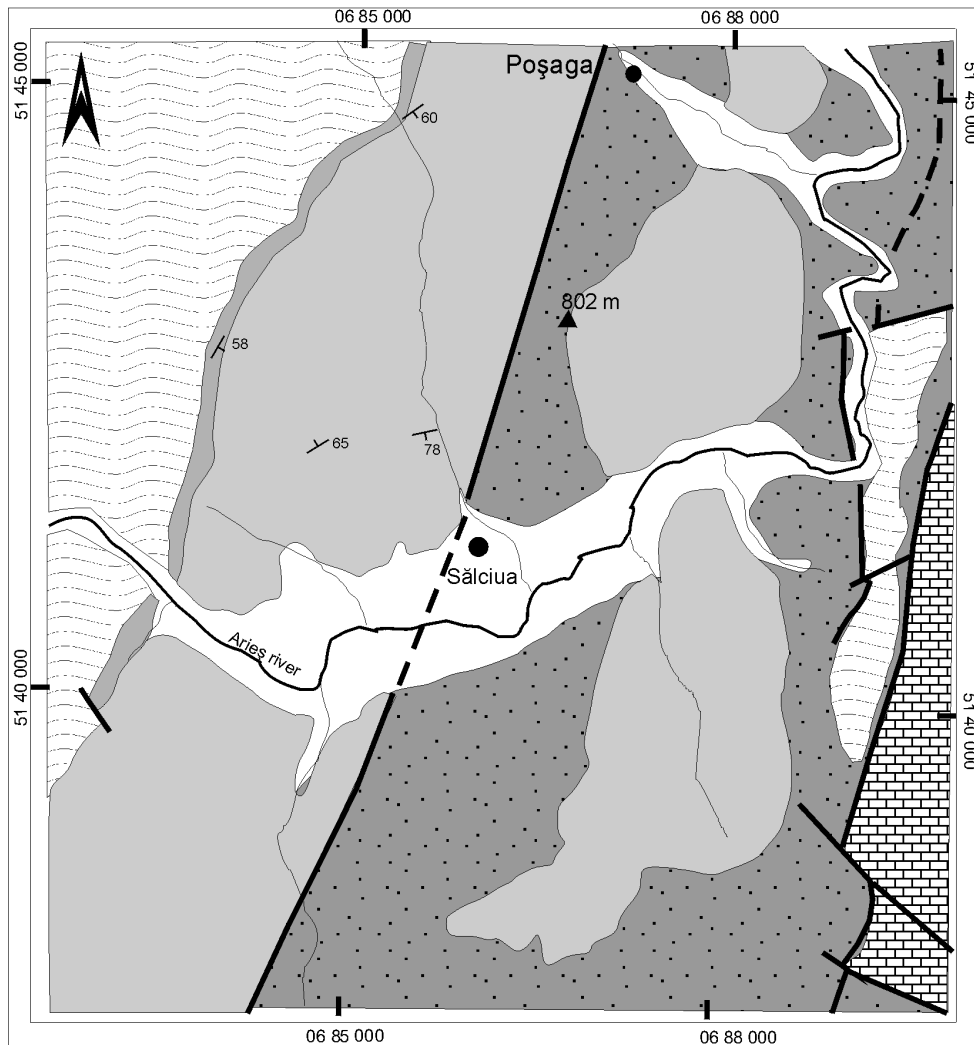
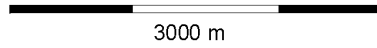
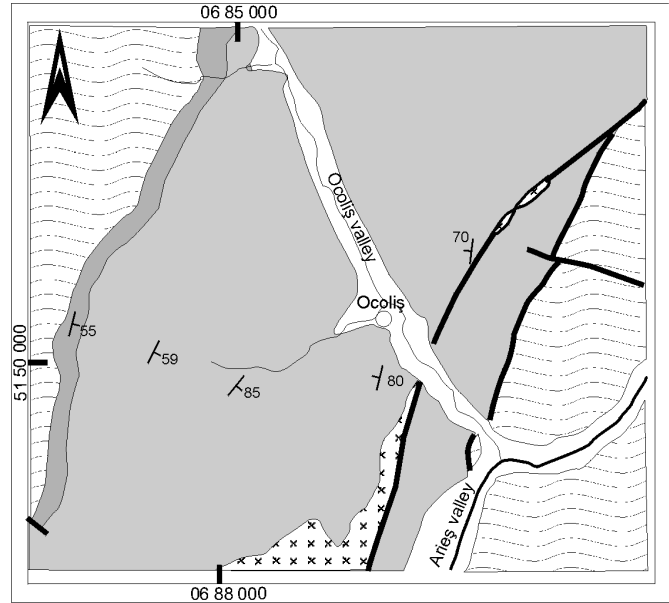
The Upper Cretaceous Gosau sediments of the Sălciua-Ocoliș occurrence are cropping out in the eastern part of the

Apuseni Mts.. Surrounded by the crystalline rocks of the Biharia nappe complex (particularly the Baia de Arieș nappe) in the northwest and the Transylvanides in the southeast, they cover the nappe contact between these both nappe complexes (Balintoni et al., 1987). The Gosau sediments unconformably overlie crystalline rocks in the northeast and Lower Cretaceous turbidites in the southeast (Fig. 3-12). The sedimentary succession has strongly been affected by the Tertiary compressive tectonics. The sediments are thrust over the crystalline basement, folded and tilted. As a result of this compression, the shallow marine sequence is not thicker than 350 m, since the entire Gosau succession was first tilted and then thrust over the shallow marine succession. The discordant contact between the crystalline basement and the breccias of the first Gosau deposits is shown in Figure 3-13. The breccias are succeeded by coarse-grained fluvial sediments. Normal faulting, visualized in Figure 3-13, is a result of the Neogene extensive tectonics (see chapter 3.4).

The basal conglomerate and shallow marine deposits record the same succession as described for the Vidra and Drocea occurrences. The thickness of the Sălciua-Ocoliș occurrence is smaller. The deep water turbidites also show the same succession as described for the other occurrences, including the debris flow deposit in the upper part of the succession. In both, the Sălciua and the Ocoliș valley, this part of the succession is better exposed as in the Vidra occurrence. Especially in the Ocoliș valley the debris flow builds up a 35 m thick profile (Pos. 06 88 966/51 50 422). It comprises clast supported conglomerates in a muddy matrix with chaotic layering, fine layered mudstones with internal folding and sporadically embedded pebbles with diameters up to 50 cm (Fig. 3-14), but also matrix supported microconglomerates without gradation reflecting the high sedimentation energy due to syn-sedimentary active tectonics. Pebbles of radiolarites indicate that the material

Fig. 3-12: Upper Cretaceous sediments of the Sălciua-Ocoliş occurrence (modified after Balintoni et al., 1987).

-  Magmatic rocks (banatites)
-  Upper Gosau subgroup
-  Lower Gosau subgroup
-  Lower Cretaceous sediments
-  Upper Jurassic limestones
-  Crystalline rocks



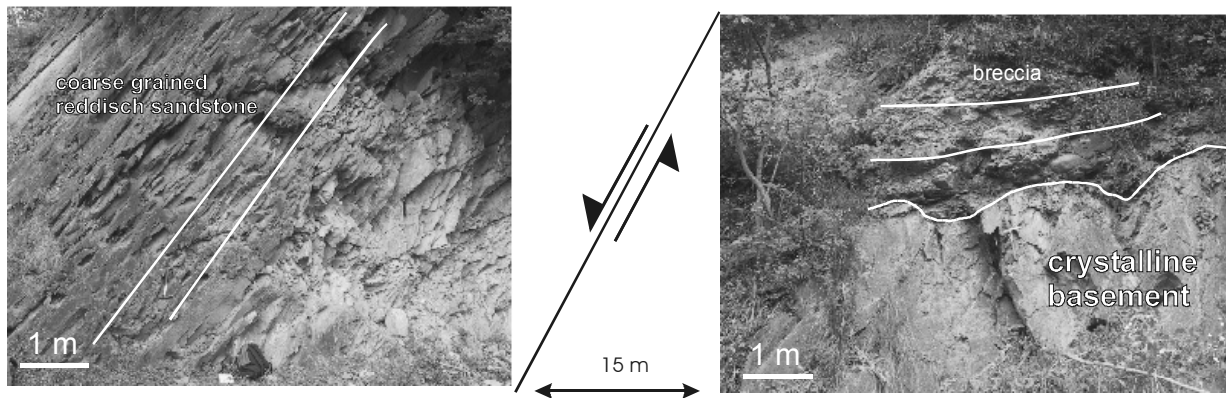


Fig. 3-13: Both pictures show the alluvial succession of the first Gosau sediments. In the right picture, the discordant contact between the crystalline basement and the first breccias is shown. The breccias lie almost horizontally. The left picture is 15 m aside showing reddish coarse grained sandstones of the alluvial fan deposits with a dipping of 55°. The normal faulting is a result of the Neogene extensive tectonics (Pos. 06 87 133/51 50 289).

derived from the Transylvanides in the southeast (in present coordinates). The turbiditic succession records a thickening-upward trend until the debris flow horizon, followed by a thinning-upward trend at the top of the succession (Fig. 3-5). Because of the post-sedimentary Tertiary tectonics, a reconstruction of the profile is difficult. Paleontological data (nannoplankton), kinematic data (fault planes with lineations) and vitrinite reflection data helped to reconstruct a profile along the Gosau succession along the Sălcuia valley, which is shown in Figure 3-15.



Fig. 3-14: Debris flow with crystalline pebble within a folded muddy matrix (Pos. 06 88 966/51 50 422).

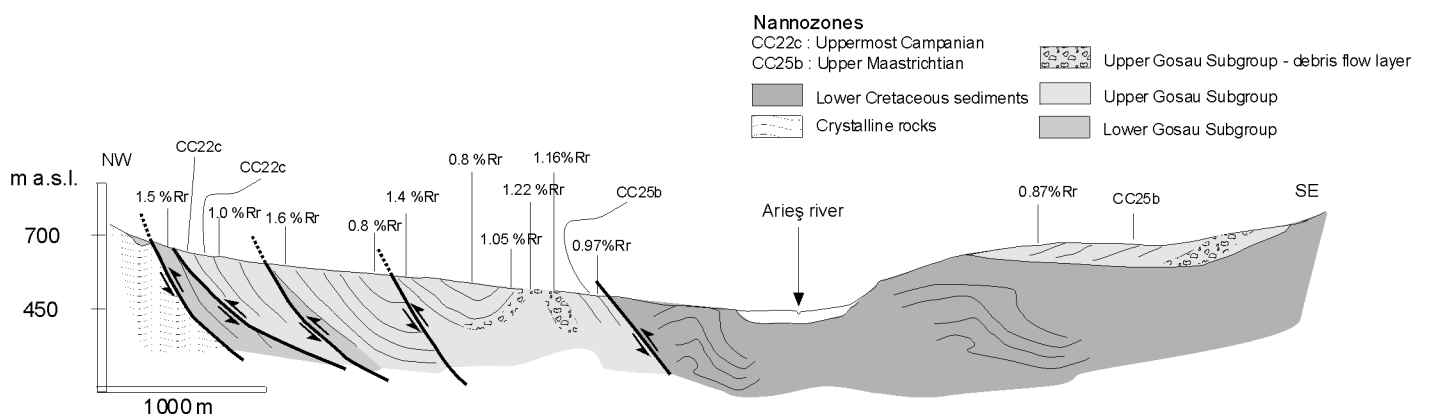


Fig. 3-15: Exaggerated profile through the Arieș valley at Sălcuia village. The numbers show the vitrinite reflection values measured on organic matter from samples at the indicated points. Generally a decrease of the reflectance values from NW to SE can be seen within each unit, indicating that the higher parts of the succession experienced lower thermal overprint.

3.1.4 Gilău-Hășdate occurrence

The Gilău-Hășdate occurrence is situated on the northeastern edge of the Apuseni Mts.. The characteristic of this occurrence are the thick carbonate rocks of the Lower Gosau Subgroup. Although carbonates with rudists of the Lower Gosau Subgroup can be found also in other areas, the largest outcrops are those in the

lăra-Gilău-Hășdate region (Fig. 3-1, 3-16). The Gosau sediments unconformably overlie the crystalline nappes of the Biharia nappe complex. In the east they are discordantly covered by terrestrial sediments of Thanetian-Ypresian age (Baciu, 2003). These sediments already belong to the deposits of the Transylvanian basin.

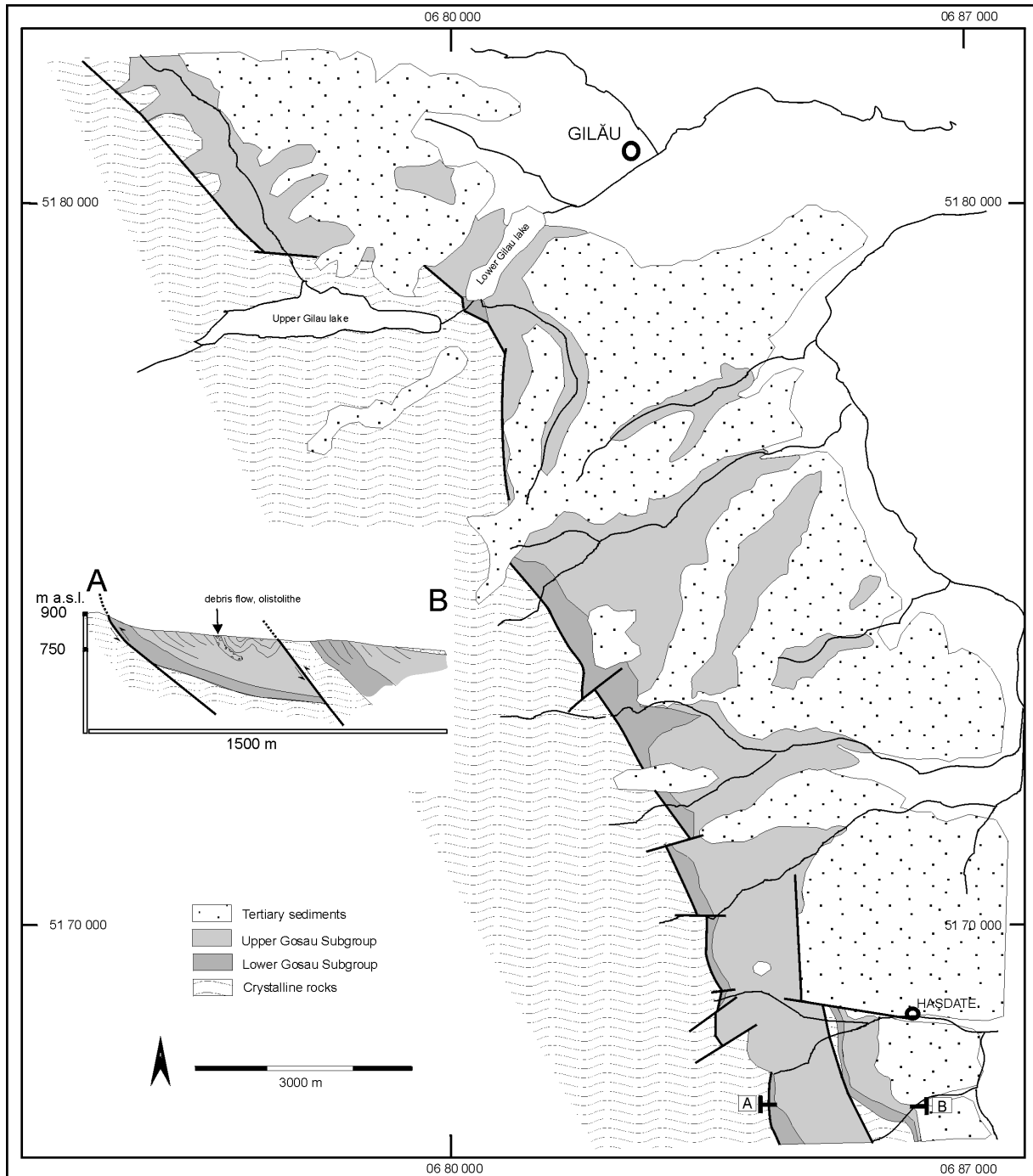


Fig. 3-16: Upper Cretaceous sediments of the Gilău-Hășdate occurrence (modified after Dimitrescu, 1996; Hârtoapanu, 1982).

The succession of the Gosau deposits is strongly deformed due to the post-sedimentary tectonics. The sediments have been wedged in between the nappes of the Biharia complex in the west and the Transylvanides in the east. East of Gilău-Hășdate the Transylvanides are covered by the Tertiary sediments of the Transylvanian basin.

The sedimentary succession starts with the basal conglomerate, which sometimes is missing due to overthrusting. Fine grained marine sandstones, limy siltstones and mudstones interlock with limestones. The limestones are built up mainly by rudists and corals which form isolated patch reefs. Figure 3-17 shows a profile record of the carbonatic succession at

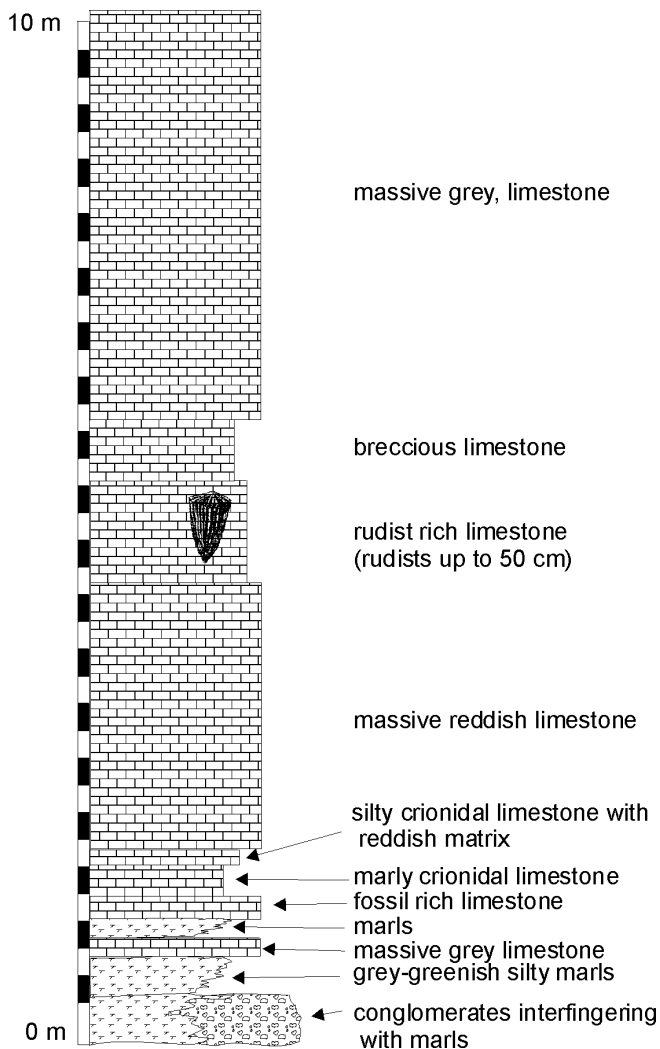


Fig. 3-17: Profile through the carbonatic sequence at Hășdate (Pos. 06 83 497/51 69 346).

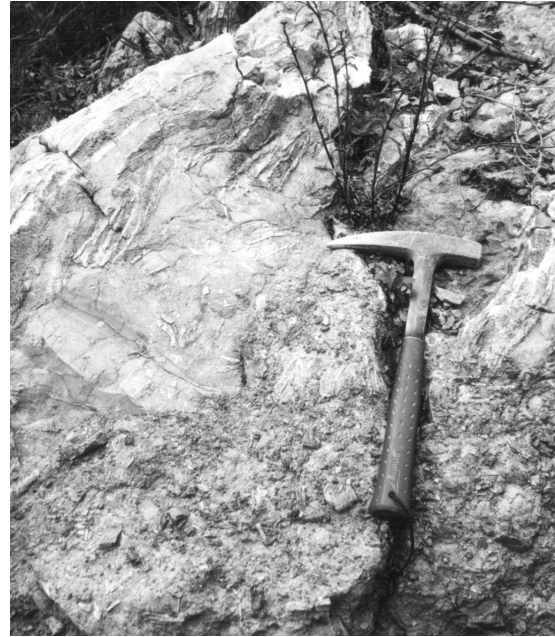


Fig. 3-18: Limestone with rudist fragments and a conglomeratic layer in the lower part of the picture (Pos. 06 83 630/51 69 844).

Hășdate. The 70 m thick limestone succession which overlies the profile in Figure 3-10 records the same variety in facies. The alternation of massive sandstones (partly reddish), silty layers with reddish matrix and conglomerates interfingering with calcareous sequences reflect the dynamic sedimentation environment. Patch reefs installed near high energy sedimentation areas (Fig. 3-18). Small alluvial fans prograded into the marine environment, but laterally rudist colonies could grow. Active tectonics caused increased input of clastic material which resulted in periodical coverage of the carbonate reefs. Tilting and uplift of the carbonatic rocks above sea-level caused small scale karstification or is responsible for the partly reddish color of the limestones. Figure 3-19 sketches the possible environment during the deposition of the shallow marine Lower Gosau Subgroup.

The upper part of the Gosau succession is analogous to the before described occurrences. A debris-flow, olistolith horizon appears in the upper part of the turbidite sequence (Fig. 3-20). Recent studies proved that the limestone olistoliths derived from east (present day

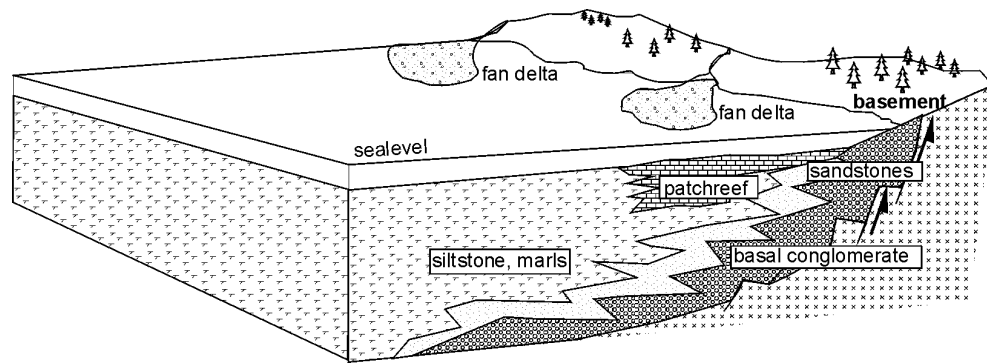


Fig. 3-19: Schematic reconstruction of the paleoenvironment during the deposition of the Lower Gosau Subgroup. Active tectonics caused cyclic sedimentation and pro-/retrogradation of the fan delta. This led to interfingering of carbonate and clastic material but also complete covering of carbonates by clastic strata.

coordinates), particularly from the Transylvanides (Bucur et al. 2004). The topmost part of the turbiditic deposits is characterized by silt/mudstone alternations, reflecting the fining-upward trend of the entire succession (Fig. 3-5). These Bouma Tc to Te sequences are deposits of the distal turbidite fan indicating the ongoing basin opening respectively basin subsidence. Particularly this part of the succession is strongly folded because the rocks were not lithified during the active tectonics. The Tertiary compression resulted in formation of faults and out of sequence thrusts (profile in Fig. 3-16).

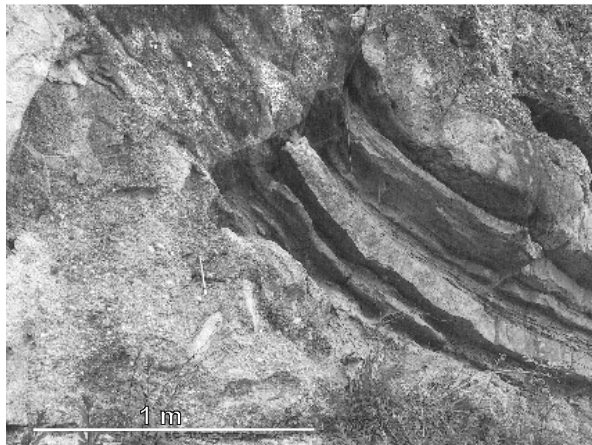


Fig. 3-20: Grain supported slide containing undeformed sandstone layer (Pos. 06 80 498/51 79 259).

3.1.5 Vlădeasa occurrence

The Vlădeasa occurrence (Fig. 3-21) is located in the central part and the highest region of the Apuseni Mts.. The altitude at which the Gosau sediments are exposed reaches up to 1600 m above sea level. The comparison to the altitude ranges of the Drocea occurrence (about 400 m a.s.l.) reflects the relative uplift of the crystalline Bihor autochthonous unit and the Vlădeasa massif.

Together with the Borod occurrence (see next chapter: 3.1.6) the Vlădeasa occurrence does not record deep water flysch deposits. The shallow marine sedimentation shows a similar succession as described for the other occurrences. Dragoş (1971) precisely describes the facies succession of the Vlădeasa region. The succession is divided into four formations. The first formation is the basal conglomerate (1) with breccias at the bottom and a fining-upward trend. It unconformably lies on crystalline or Permo-Mesozoic rocks and is followed by a fossil-rich calcareous facies (2), which includes layers of *Actionella*, bivalves, ammonites, and rudists. The overlying succession (3) is characterized by detrital deposits (silt-, sandstones) and is followed by a marly/silty sequence (4). Due to bad outcrop conditions and the post-sedimentary tectonics, a reconstruction of the thicknesses based on surface geology is not possible. Drillings, however, show a

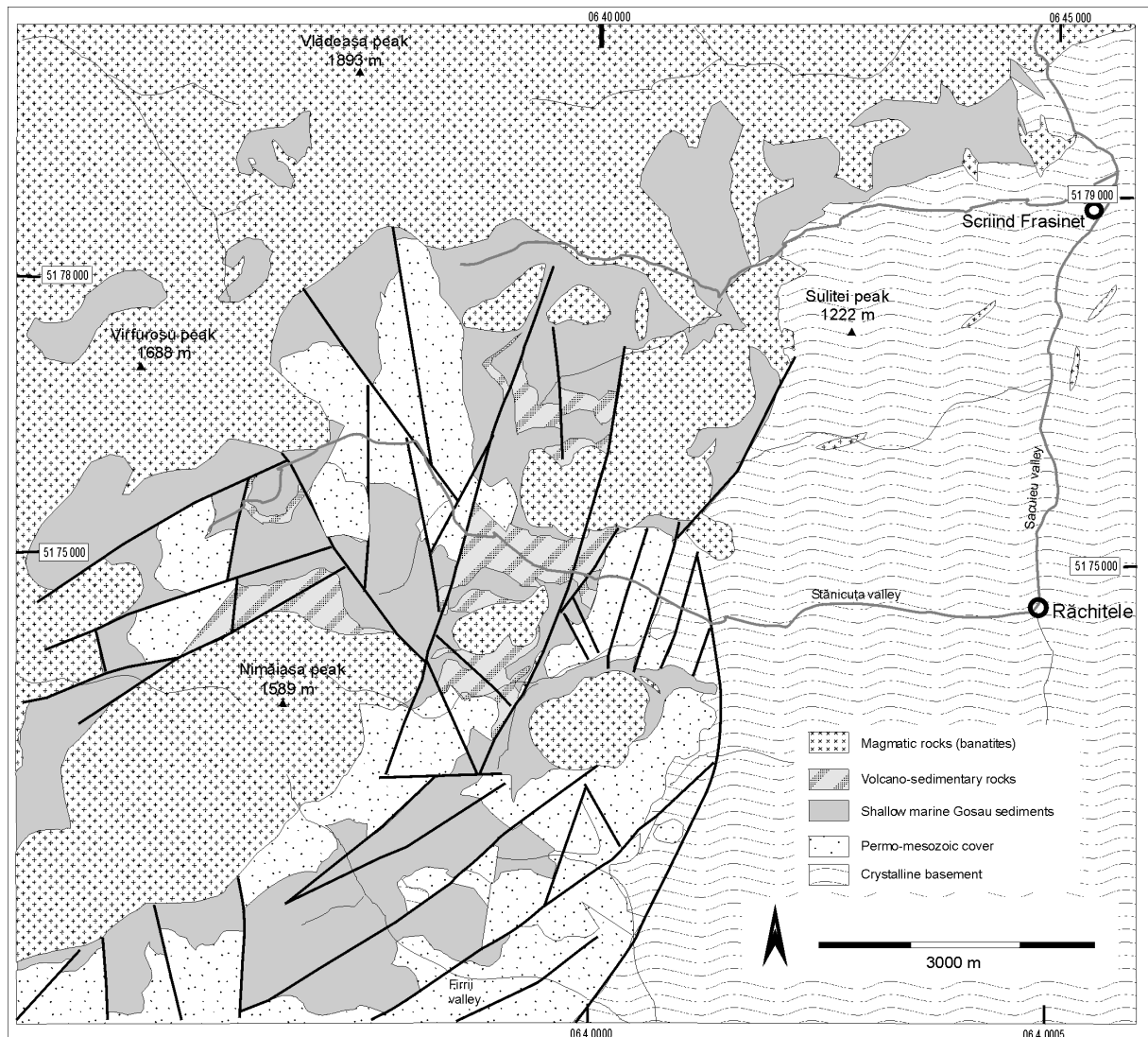


Fig. 3-21: Upper Cretaceous sediments of the Vlădeasa occurrence (modified after Mantea et al., 1987).

thickness of 180 m of the shallow marine deposits (Mantea, 1985). The shallow marine deposits (formations 1 to 4) are overlain by a volcano-sedimentary succession. It consists of an alternation of sandstones, volcanic tuffs, tuffites and conglomerates, with pebble diameters up to 50 cm, which derive from the surrounding geological units (limestones, sandstones, Permian conglomerates, granites and schists). The conglomerates are predominating within the volcano-sedimentary succession. The sandy matrix alternates with a tuffitic, greenish matrix. The volcano-sedimentary succession comprise the first extrusive rocks of the banatite magmatism (Mantea, 1985). The center of the eruption was situated near

Vlădeasa, building up probably several strato volcanoes. During eruption, the rising magma dislocated rocks of older geological units and deposited them in a fluvial or shallow marine environment. The volcano-sedimentary succession is exposed in a small creek at a length of 200 m. It is not possible to measure its thickness, because no stratification is visible. Although the before mentioned drilling records a thickness of 6 m, it is evident that the volcano-sedimentary succession is locally much thicker (Ștefan, 1980; own field observations).

West of the outcropping Gosau sediments the volcanic activity of the banatite magmatism builds up the largest eruptive

subvolcanic formations (rhyolites and dacites) of the Apuseni Mts..

3.1.6 Borod occurrence

The Borod occurrence is situated in the northwestern Apuseni Mts. (Fig. 3-1, 3-22). It is the northernmost outcrop of the Gosau succession. Different from other occurrences, it is built up only by the

shallow marine sequence of the Lower Gosau Subgroup. The succession starts with the basal conglomerate with varying thicknesses. It discordantly overlies the crystalline basement. An alternation of conglomerates, microconglomerates, bioclast-rich sandy limestones (grainstones and floatstones) and sandstones characterizes the beginning of the sedimentary succession (Fig. 3-23). The

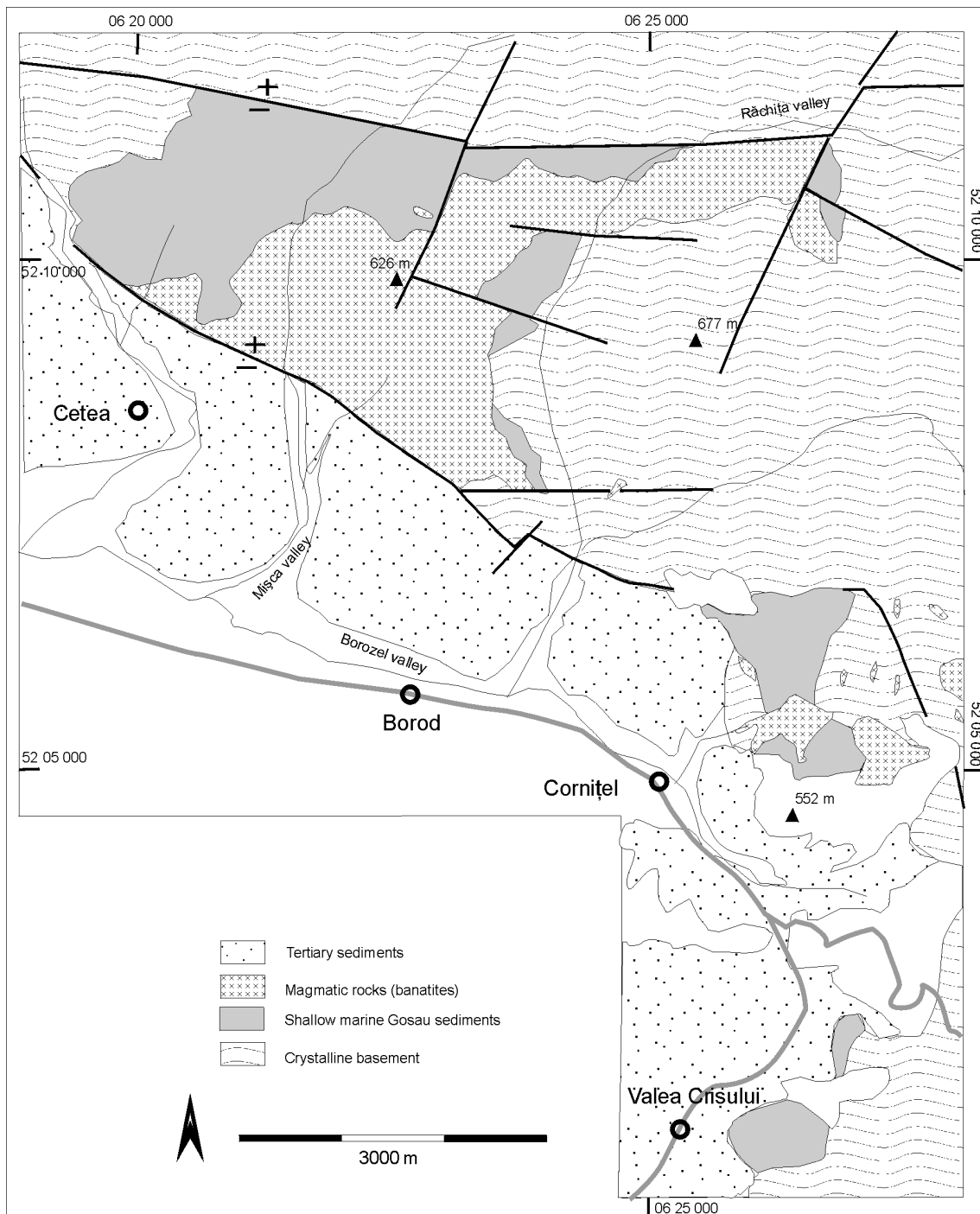


Fig 3-22: Gosau sediments of the Borod occurrence (modified after Patrușiu et al., 1973, Papaianopol et al., 1977).

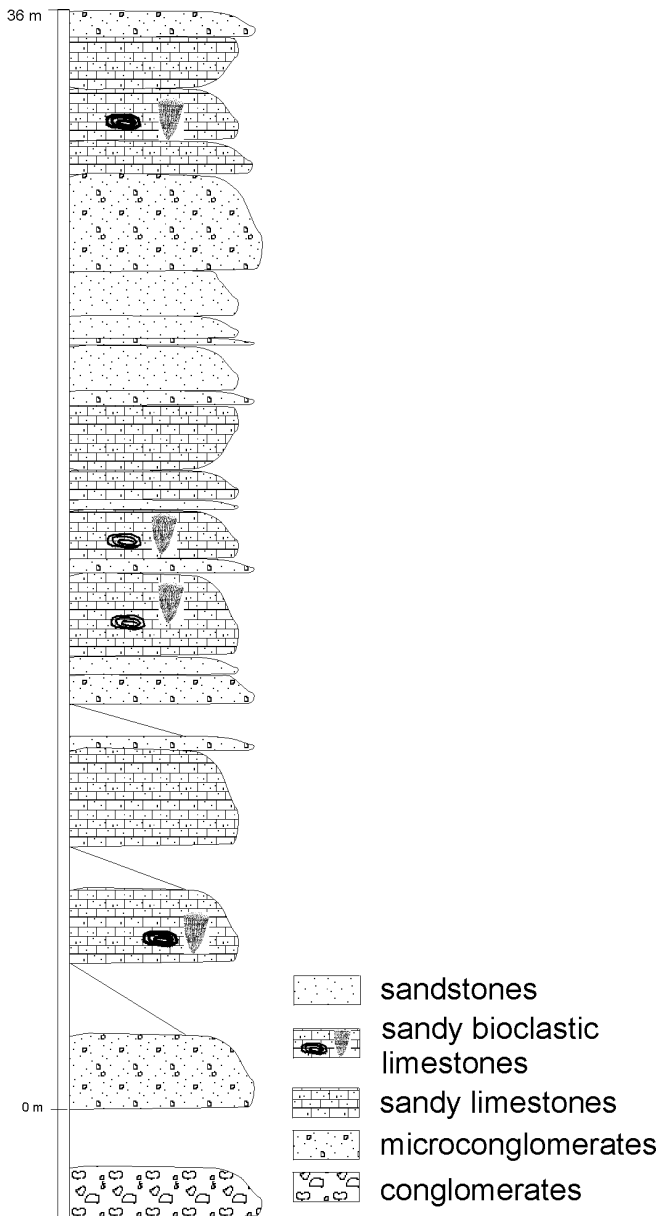


Fig. 3-23: Profile of the Gosau succession at the Borod occurrence (Crişului valley, Pos.: 06 26 103/52 01 651)

profile illustrates the dynamic sedimentation due the active tectonics. Within short periods limestones with rudist colonies were installed but have been periodically covered by siliciclastic input. The following succession shows a general fining-upward trend. It is marked by an alternation of siltstones, calcareous sandstones and mudstones, often rich in organic material. The succession ends with a shallow marine limestone, without showing records of pelagic sedimentation. Based on field records and literature data

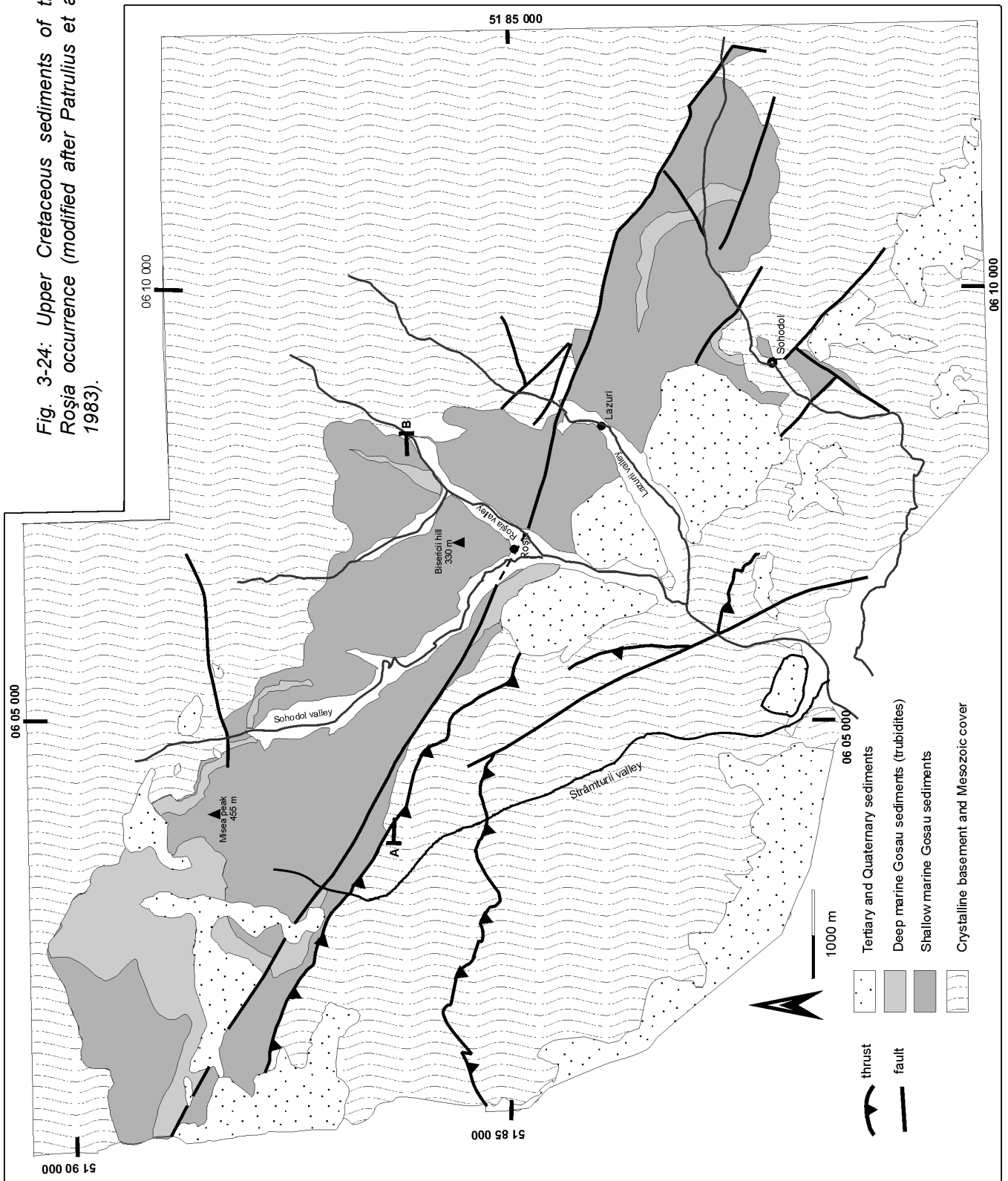
(Patrulius et al., 1973, Papaianopol et al., 1977) the entire succession is about 400 m thick.

The post-sedimentary banatite magmatism caused large subvolcanic intrusions, mainly into the Gosau sediments.

3.1.7 Roşia occurrence

The Roşia occurrence is located on the western part of the Northern Apuseni Mts.. (Fig. 3-1, 3-24). Because of its short turbiditic sedimentation it plays a transitional role between the occurrences of the Northern and those of the Southern Apuseni Mts.. The Gosau sediments unconformably overlie the Permo-Mesozoic and crystalline rocks of the Bihor autochthonous unit and the Codru nappe system (Patrulius et al., 1983). The Lower Gosau Subgroup is represented by the basal conglomerates, sandstones, marls, tuffs and limestones which are mainly exposed in the northern Roşia basin (Patrulius, 1974). The approximately 80 m thick succession of turbidites is overlying the shallow marine succession. The deep marine sequence has not been described or recognized before. Former studies concentrated on biostratigraphy of the shallow marine deposits, whereas the short succession of deep marine deposits was described as sandstone-siltstone alternation, without sedimentary facies interpretation (Lupu, 1974, 1976; Patrulius et al., 1983). The character of the turbiditic sequence can be seen in an outcrop in the Roşia valley (Pos. 06 07 715/ 51 85 875, Fig. 3-26). The alternation of coarse to fine grained (up to 50 cm thick) sandstone and mudstone layers mainly record entire Bouma sequences with typical sole marks at the base of the Ta layer. Within the entire succession a fining-upward trend can be recognized. Nannoplankton (see also following chapters) shows a stratigraphic age of Lower Maastrichtian (CC24). Based on these data, literature data and field observations (strata dipping, fault data records) a profile interpretation is performed in Figure 3-25.

Fig. 3-24: Upper Cretaceous sediments of the Roşia occurrence (modified after Patruilus et al., 1983).



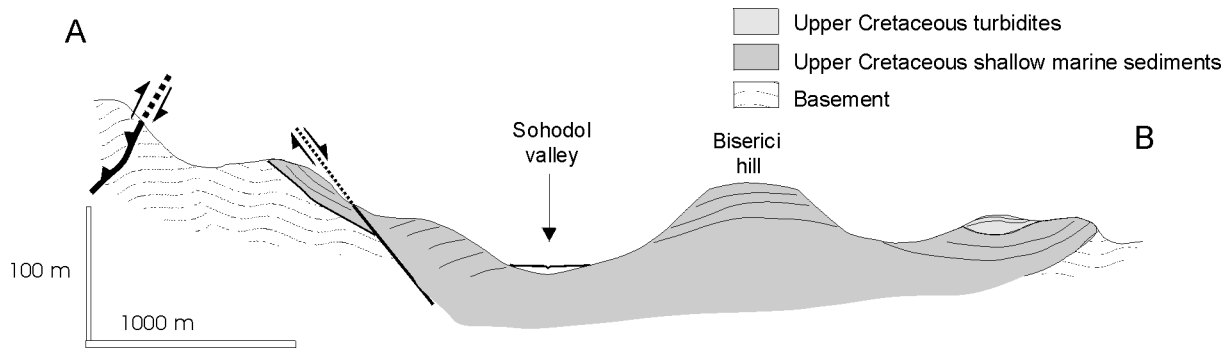


Fig. 3-25: Exaggerated profile through the Roşia basin. The extensive tectonic during the Neogene caused horst-and-graben structures. Nevertheless, syn-sedimentary compressional tectonics caused folding of the Upper Cretaceous sediments.



Fig. 3-26: Sandstone layers of the turbidite succession of the Roşia occurrence (Pos. 06 07 765/51 83 302).

3.1.8 Stratigraphic range

Several works have been carried out to determine the limits of the Gosau succession of the Apuseni Mts. (e.g. Dragoş, 1971; Lupu, 1974; Lupu, 1976; Lupu et al., 1978; Pitulea et al., 1978). Most of the biostratigraphic investigations are restricted to the Lower Gosau Subgroup. For this work, the fossil-poor deep water sediments of the Upper Gosau Subgroup have been dated with nanofossil assemblages after the zonations of Sissingh (1977) and Perch-Nielsen (1985). Several samples for biostratigraphic dating based on foraminifera have been processed. However, it was not possible to extract

determinable fossils since they contain only fragments of foraminifera.

The following data are a compilation of own data (23 nanofossil samples) and literature data (most references have been made in chapters 3.1.1 to 3.1.7). Within the Gosau succession the oldest sediments have been found in the Drocea occurrence, recording an Upper Turonian age (CC12). The youngest Gosau deposits have been sampled at Sălcia-Ocoliş showing Upper Maastrichtian age (CC25c).

The onset of sedimentation (Lower Gosau Subgroup) did not happen simultaneously. In the southwestern part of the Apuseni Mts., the first marine Gosau sediments were deposited in the Upper Turonian. In the northeast (Ocoliş occurrence) the marine sedimentation started in the Upper Santonian/Lower Campanian (Balintoni et al., 1987). Own data of the same occurrence record nanoplankton assemblages of Upper Campanian age for the Lower Gosau Subgroup. After compiling this data, it is evident that onset of sedimentation successively moved from southwest to northeast (Fig. 3-27).

The change from shallow marine to deep marine sedimentation scatters within Campanian to Lower Maastrichtian time (Fig. 3-28). The oldest turbidites have been sampled at Gilău showing a Santonian/Campanian age (CC17). At Drocea the first deep water sediments record Campanian/Maastrichtian ages (CC232c). At this occurrence the Lower Maastrichtian age (CC24) of shallow marine deposits and the Campanian/Maastrichtian (CC22c) age for the first deep marine deposits reflects the concurrent deposition of deep water and

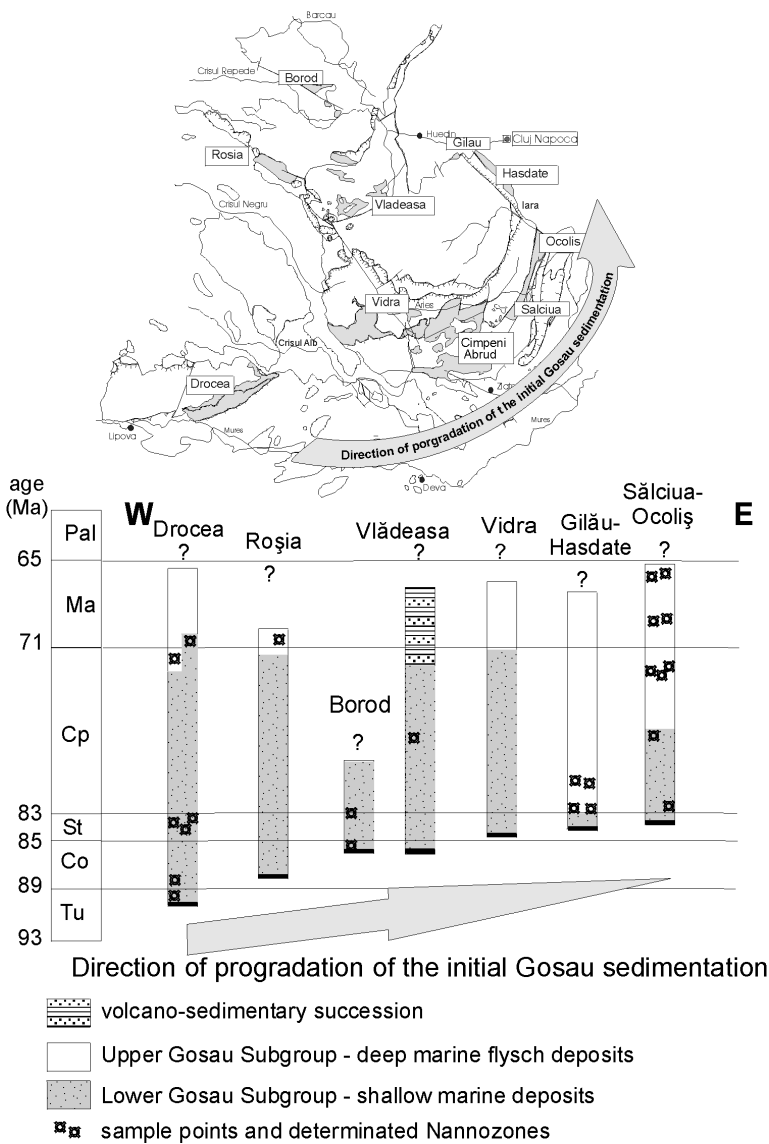
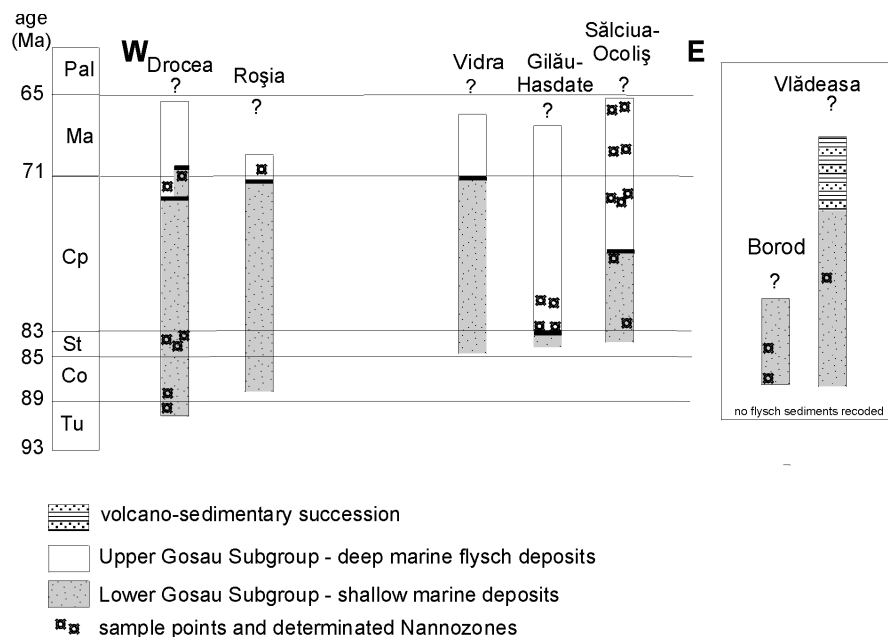


Fig. 3-27: Diachronous progradation of the initial Gosau sedimentation. First sediments have been deposited in the southwest (Drocea). The initial sedimentation successively moves to the northeast (Sălciua-Ocoliș). Question marks at the top of each column indicate that due to postsedimentary basin inversion erosion of the uppermost succession parts is presumed.

Fig. 3-28: Asynchronous onset of the Upper Gosau sedimentation. The change to the deep marine facies does not show a laterally movement, as it has been recorded for the initial sedimentation of the Gosau sediments. Question marks at the top of each column indicate that due to postsedimentary basin inversion erosion of the uppermost succession parts is presumed.



shallow marine sediments. The sudden subsidence and beginning of deep water sedimentation did not lead to an uniform drop of the basin floor. More likely a ramp-slope-deep basin constellation, separated through normal faults was responsible for the synchronous deposition of deep water and shallow marine sediments. A similar scenario was proposed by Wagneich (2001) for the Gosau sediments of the Eastern Alps. This basin segmentation is probably also valid for the other Gosau occurrences within the Apuseni Mts.. However, the attempt of high resolution biostratigraphic dating around the border of the facies change was not successful.

A time shift for the change from the shallow marine facies (Lower Gosau Subgroup) to the deep marine facies (Upper Gosau Subgroup), like for the start of the Gosau sedimentation, can not be recognized (Fig. 3-28). Although this event did not occur synchronously as well, there is no systematic shift in time and space.

Summary of depositional evolution

Reviewing the presented results, three major features which describe the sedimentary evolution of the Upper Cretaceous Gosau sediments of the Apuseni Mts. are evident:

1. The sedimentation started diachronously (Lower Gosau Subgroup) with a successive time shift from southwest to northeast, from the Upper Turonian to the Upper Santonian.
2. The change to deep water sedimentation (Upper Gosau Subgroup) happened asynchronously. No pattern of a lateral time shift at the change of the sedimentation facies has been detected.

3. A division of the Gosau occurrences based on their sedimentary facies record is possible (Fig. 3-29). In the northwest of the Apuseni Mts., only shallow marine sediments have been deposited. In the south and southeast, both, shallow marine and deep marine sedimentation took place. The Roşia occurrence occupies a transitional position with short deep water sedimentation in the Lower Maastrichtian (CC24).

Comparing the Gosau sediments of the Eastern Alps with the Gosau succession of the Apuseni Mts., lithostratigraphic and biostratigraphic similarities are evident. The sedimentary facies association allows a division into a Lower and an Upper Gosau Subgroup. The initial Gosau sedimentation records a diachronous

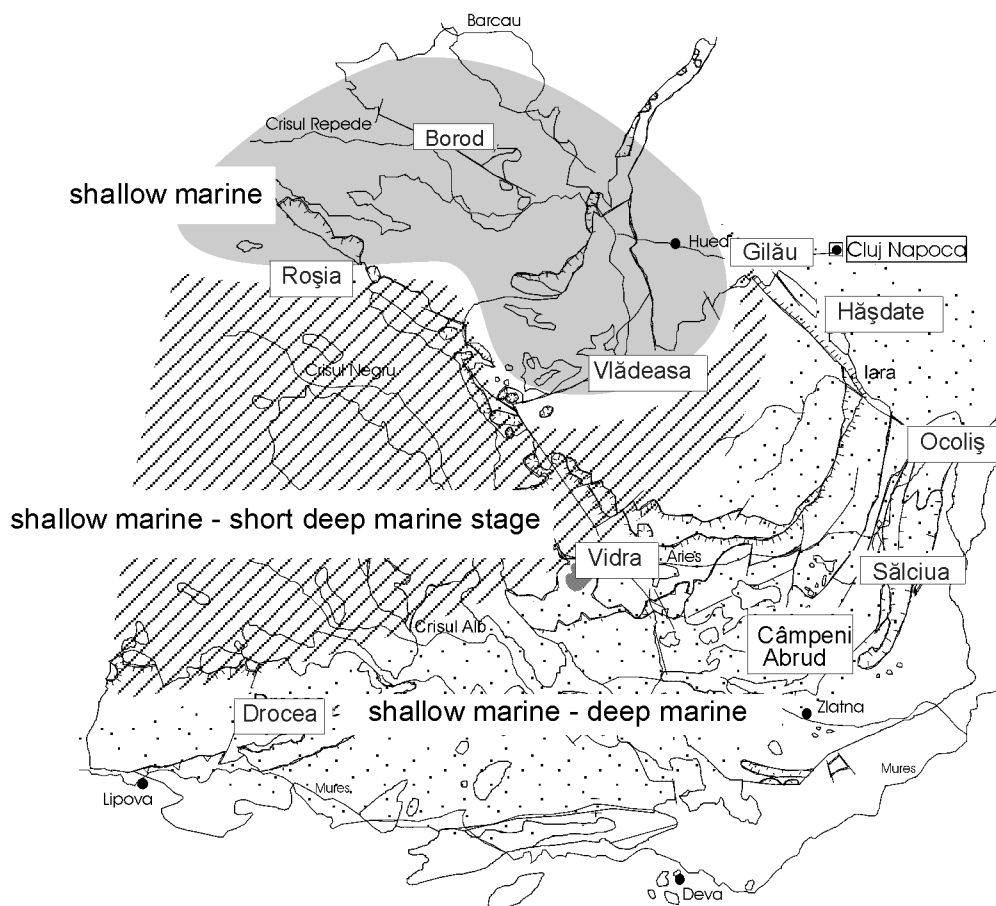


Fig. 3-29: Distribution of the sedimentary facies of the Gosau succession. In the South Apuseni Mts. shallow marine and deep marine sediments have been deposited, whereas in the north, only shallow marine deposition took place. The transition zone (Roşia occurrence) records a short deep marine deposition stage.

onset as it is known for the Alpine Gosau. However, an important difference is obvious. In the Eastern Alps the diachronous onset of the initial Gosau sedimentation shifted from west to east. In contrast, in the Apuseni Mts. the shift was from southeast to northwest, considering the Neogene 70-90° clockwise rotation of the Tisia-Dacia block.

Rapid basin subsidence led to a continuous sedimentation of deep marine sediments in the Eastern Alps as well as in the Apuseni Mts.. The onset of the second subsidence phase shows a diachronous shift from west to east for the Gosau sediments of the Eastern Alps. Although in the Apuseni Mts. the change from shallow to deep marine sedimentation was asynchronous, it does not show a systematic shift. The onset of the second subsidence phase scatters without showing a pattern, within a range of about 12-14 My (Campanian to lowermost Maastrichtian).

In the southern parts of the Eastern Alps (Central-Alpine Gosau, Wagreich, 1994) only few deep marine sediments have been deposited (until lowermost Maastrichtian) above the shallow marine

Lower Gosau Subgroup. Considering the Neogene rotation of the Tisia-Dacia block, a similar pattern is recognizable for the Apuseni Mts.: areas with few or absent Upper Gosau sediments (Roşia, Vădeasa, Borod) will then be situated in the southwest, whereas successions which comprise thick sequences of both facies subgroups have been deposited in the north, east and southeast (Fig. 3-30). The fluvial, volcano-sedimentary succession of the Vlădeasa region, heavy mineral assemblages and apatite fission-track data indicate an uplift of the Northern Apuseni Mts. and the end of the marine sedimentation during Maastrichtian time (see following chapters).

The stratigraphical range of the Gosau sediments of the Apuseni Mts. is restricted to the Upper Cretaceous. Paleocene sedimentation is not recorded within the Apuseni Mts.. Uppermost Paleocene /Lower Eocene alluvial deposits unconformably overlie the Gosau sediments. In contrast, the Gosau sediments of the Eastern Alps record continuous marine sedimentation until lowermost Eocene.

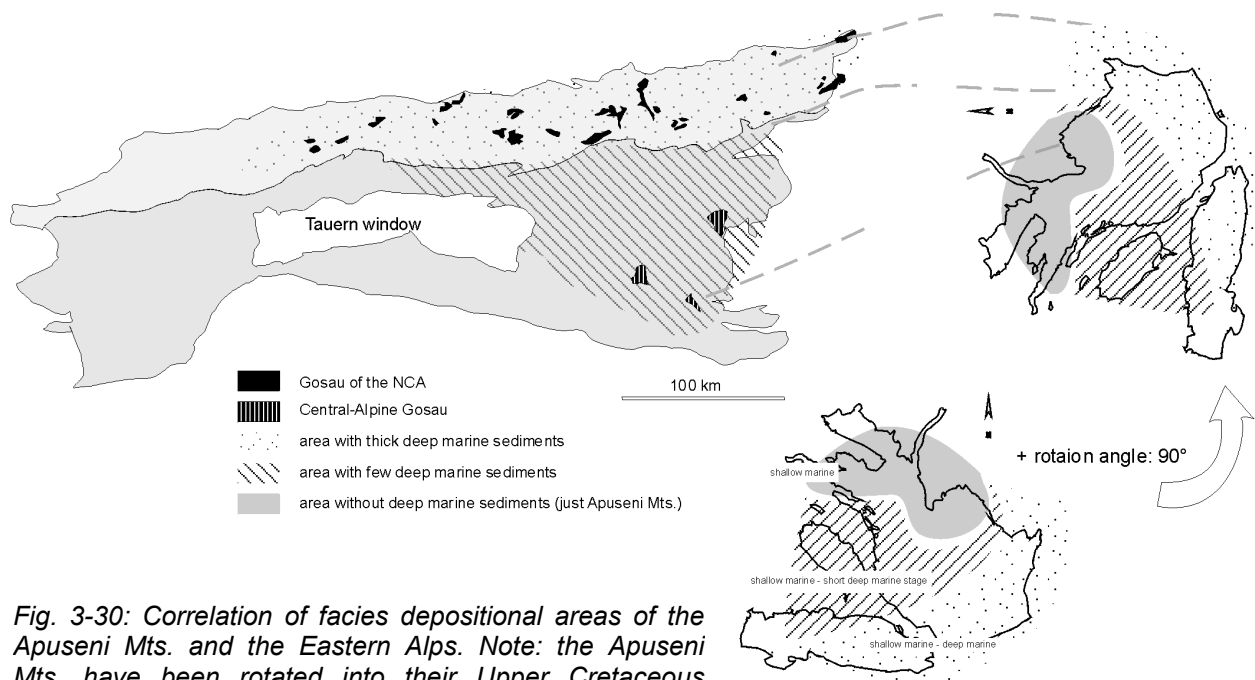


Fig. 3-30: Correlation of facies depositional areas of the Apuseni Mts. and the Eastern Alps. Note: the Apuseni Mts. have been rotated into their Upper Cretaceous position (for details compare Fig. 3-29, 1-4).

3.2. Heavy mineral analysis

To localize and characterize the source area of the Gosau sediments, 67 samples for heavy mineral analysis have been collected. Outcrops have been selected with respect to the litho-stratigraphic sequence along an entire succession of each Gosau occurrence.

The mineral spectra of the analyzed samples record a wide variety of different heavy minerals deriving from diverse rock types. The dominating minerals are garnet, staurolite, tourmaline, zircon, apatite and rutile (in this order). Minerals like spinel, chloritoid, glaucophane or orthite (allanite) are marginal but of high interest concerning the erosional source. The following chapter presents the heavy mineral spectra, a compilation for the Gosau sediments of the entire Apuseni Mts. and implications on their provenance. Figures 3-31 to 3-37 show the mineral distributions in a litho-stratigraphical order and the change within a profile succession. Figure 3-39 illustrates all samples in respect to their stratigraphical position. It has been tried to cover a

complete succession within a Gosau occurrence, in order to illustrate the change in the mineral assemblage of the entire sequence. For better exemplification and concerning the stability, but also the lithospecific formation and origin of each heavy mineral, some minerals have been grouped. Thus, staurolite, epidote and zoisite build a group of relative stable minerals deriving from low- to medium-grade metamorphic rocks. Zircon and tourmaline have been grouped because of their extreme weathering resistivity and transport stability. Although rutile belongs to the group of extreme stable minerals as well, it was separated from this group, because its origin is primarily related to high-pressure metamorphic rocks.

The mineral assemblage of the **Drocea** occurrence (Fig. 3-31) records mainly minerals deriving from metamorphic rock sources (garnet, staurolite, rutile). Within the zircon-tourmaline group, tourmaline dominates with 81%. The source of tourmaline is proposed to be either the medium-grade metamorphic complexes of the autochthonous unit and the Codru nappe complex, but more likely the Variscan granites and pegmatites

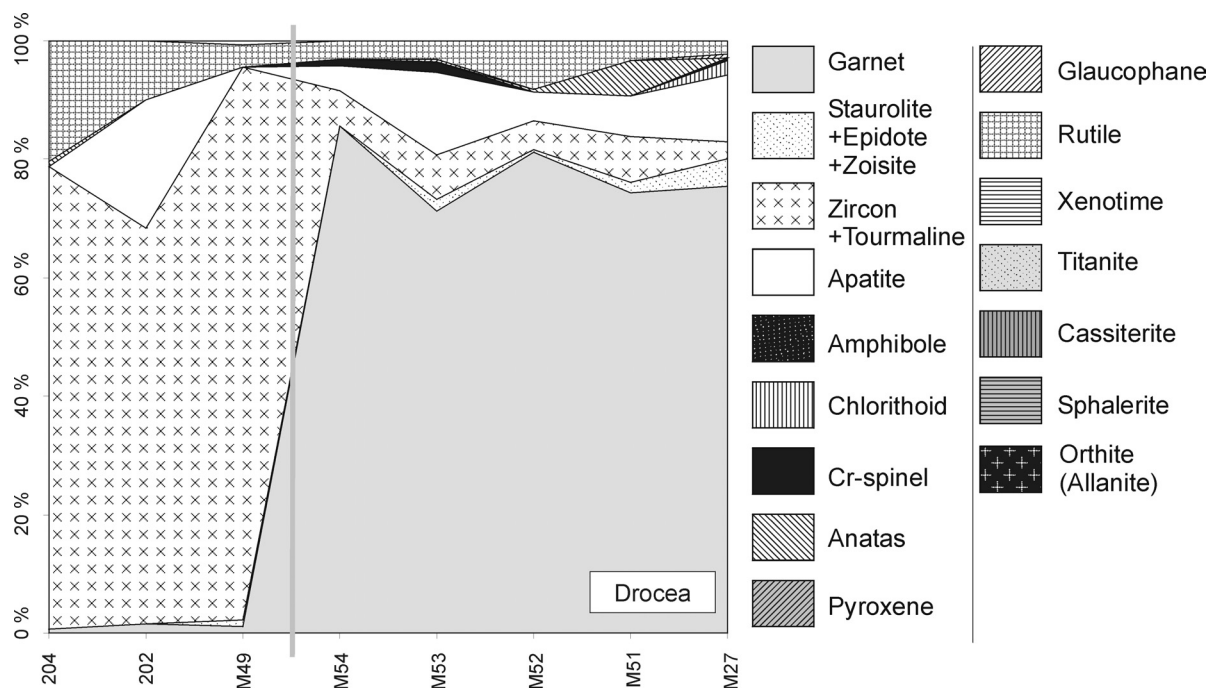


Fig. 3-31: Change of the mineral assemblage from the Drocea occurrence. X-axis shows the sample number. The grey line marks the boundary between Lower Gosau and Upper Gosau Subgroup. The samples are in stratigraphic order (oldest left), but age differences are not equivalent.

(Muntele Mare granite). Although present in low amounts only (3%), Cr-spinel proofs the erosion of the ophiolites situated in the south-southeast of the Drocea occurrence (resp. Austrian Transylvanides, Fig. 2-1). This shows that rocks in the south were uplifted above sea level during Maastrichtian time (Fig. 3-40). Although also present in low amounts only (1%), glaucophane as a high-pressure/low-temperature metamorphic mineral witnesses exposure of a subduction zone. The remnants of these high-pressure rocks have been completely eroded, since glaucophane bearing rocks are not known from the Apuseni Mts.. The dominance of metamorphic minerals increases in the upper part of the succession, respectively within the Upper Gosau Subgroup. The facies change of the Lower to the Upper Gosau Subgroup is situated between sample number 33 and 65 (grey line). Garnet becomes the predominant mineral within the Upper Gosau Subgroup.

Within the succession of the **Vidra** occurrence (Fig. 3-32) minerals which derive from metamorphic rocks predominate and, similar to the data from

Drocea, the predominance increases within the Upper Gosau Subgroup. Tourmaline is the main mineral (90%) within the zircon-tourmaline group. In the lower part of the sequence apatite probably derives from the Variscan magmatic intrusions (e.g. Muntele Mare granite) but also from the metamorphic rocks of the Codru and Biharia nappe systems. Within the Upper Gosau Subgroup the apatite probably derives mainly from the coeval banatite magmatism, which also can be proven by the appearance of minerals like cassiterite and sphalerite. Since the banatite magmatism started around the Upper Campanian-Lower Maastrichtian boundary (see following chapters), it is presumed that apatite, which was eroded before this time, mainly derived from the Variscan granite. After Lower Maastrichtian, the apatite was additionally supplied from the banatite magmatic rocks. Cr-spinel again indicates erosion of ophiolitic rocks and that sediment transport took place from south to north (in present coordinates). This is also proven by paleocurrent measurements (see following paragraphs).

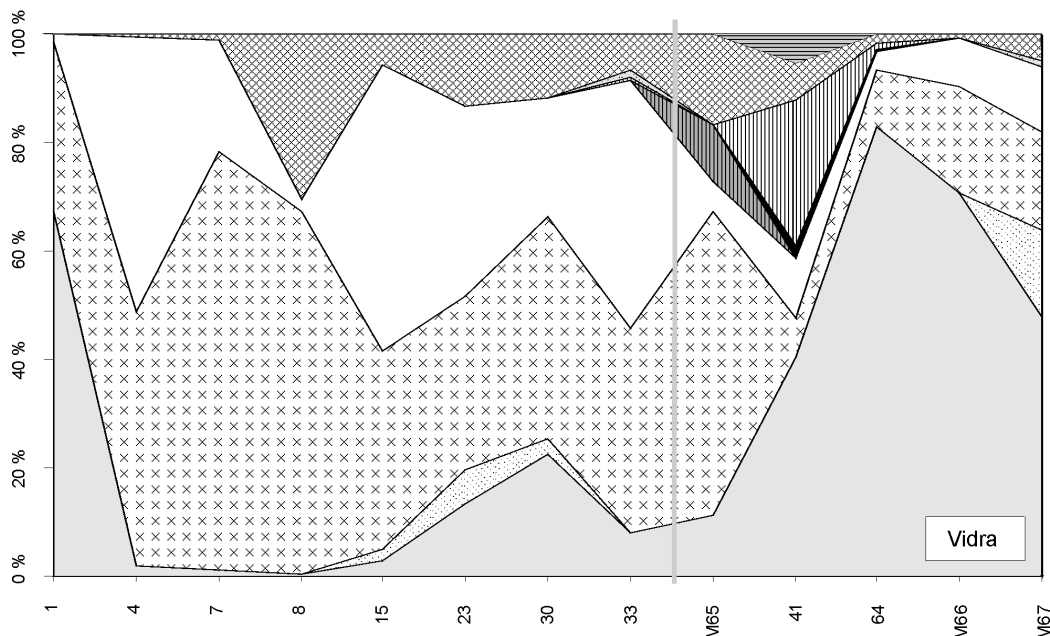


Fig. 3-32: Change of the mineral assemblage from the Vidra occurrence. X-axis shows the sample number. The grey line marks the boundary between Lower Gosau and Upper Gosau Subgroup. For symbols see Fig. 3-31.

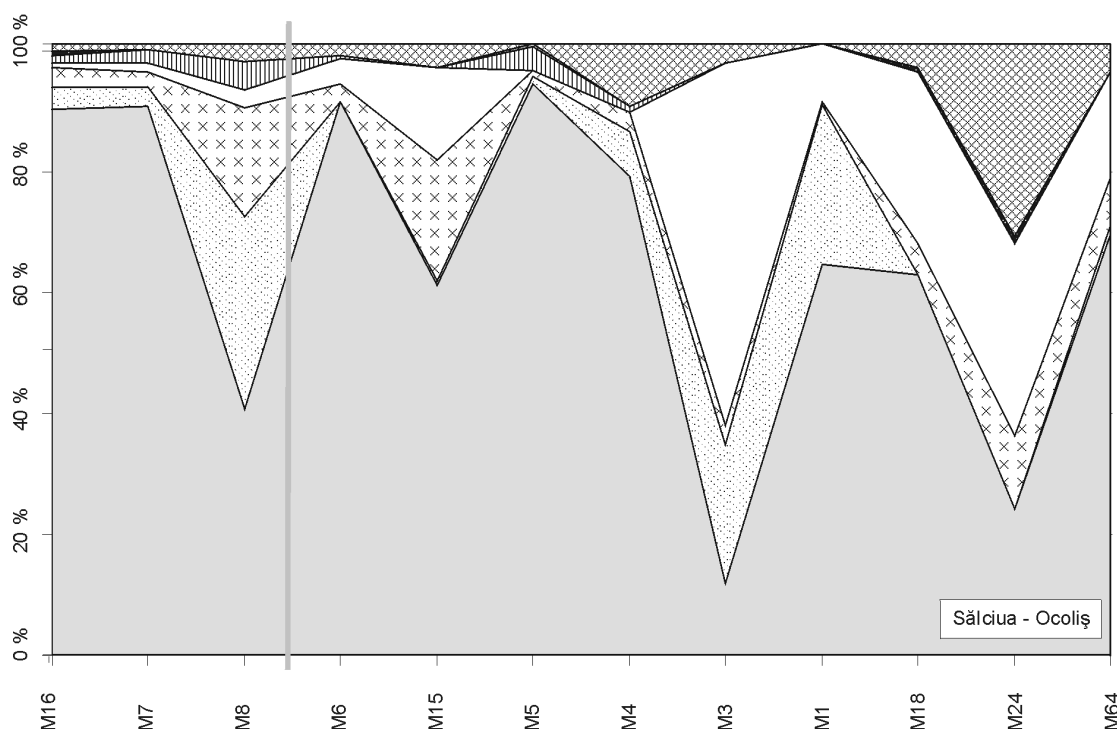


Fig. 3-33: Change of the mineral assemblage from the Sălciuma-Ocoliș occurrence. X-axis shows the sample number. The grey line marks the boundary between Lower Gosau and Upper Gosau Subgroup. Small amounts of pyroxene have been found in sample M5 (0.5%). Amphibole also appears in small amounts in sample M16 (0.6%), M18 (0.7%) and M24 (1.1%). For symbols see Fig. 3-31.

In the heavy mineral spectra of the **Sălciuma-Ocoliș** (Fig. 3-33) occurrence, minerals of metamorphic rock provenance (mainly garnet: 65%) predominate. The increasing amount of apatite in the Upper Gosau succession coincides with the beginning of the banatite magmatism and probably is related to this event. The increase of rutile in the upper part of the succession reflects the erosion of a high-pressure metamorphic rock complex. The only high-pressure rocks known from some small outcrops within the Austrian Transylvanides (Fig. 2-1) are eclogites (Szadetzki, 1930). This fact, together with the appearance of Cr-spinel – which also derived from the the Austrian Transylvanides and the obducted ocean floor of the Transylvanian ocean - proofs that transport of material occurred from south to north and southeast to northwest (in present coordinates).

The mineral assemblages of **Gilău** and **Hășdate** (Fig. 3-34) reflect the already

recognized pattern: predominance of metamorphic minerals and increase of this predominance within the Upper Gosau Subgroup. This is also evident by an increasing percentage of the metamorphic minerals of the staurolite-epidote-zoisite group. The high percentage of rutile (especially at the Gilău succession) can be explained by the erosion of high-grade metamorphic rocks of the Transylvanides. The Gilău succession comprises high amounts of apatite within the deep marine sediments (Upper Gosau Subgroup) of Lower Campanian age. Since the banatite magmatism started around the Upper Campanian-Lower Maastrichtian boundary, the apatite will rather be derived from the Bihor autochthonous unit, respectively from the Muntele Mare granite.

Metamorphic minerals predominate in the heavy mineral suite of the **Roșia** succession as well (Fig. 3-35). Within the zircon-tourmaline group, tourmaline is the dominating mineral (80%) reflecting the erosion of metamorphic units and/or

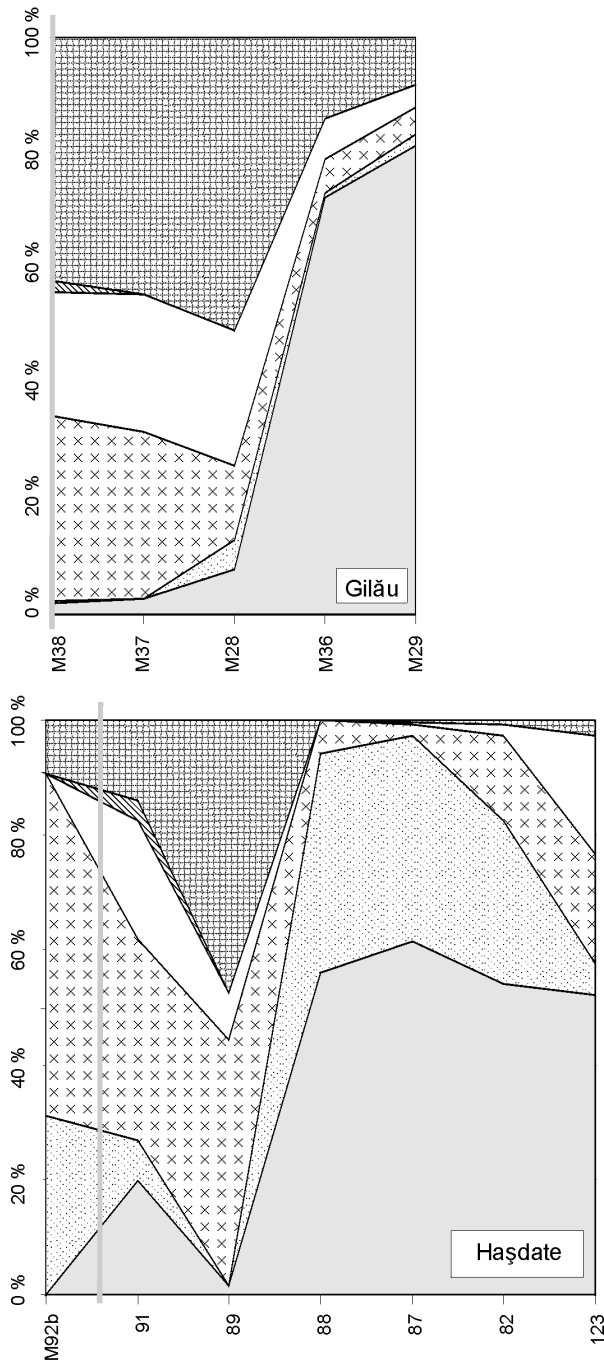


Fig. 3-34: Change of the mineral assemblage from Gilău and Hășdate occurrences. X-axis shows the sample number. The grey line marks the boundary between Lower Gosau and Upper Gosau Subgroup. For the Gilău occurrence only samples from the Upper Gosau Subgroup have been processed. For symbols see Fig. 3-31.

Variscan pegmatites. This is the case for the entire succession, except for sample M60, where zircon reaches 45% within the zircon-tourmaline group, which probably is

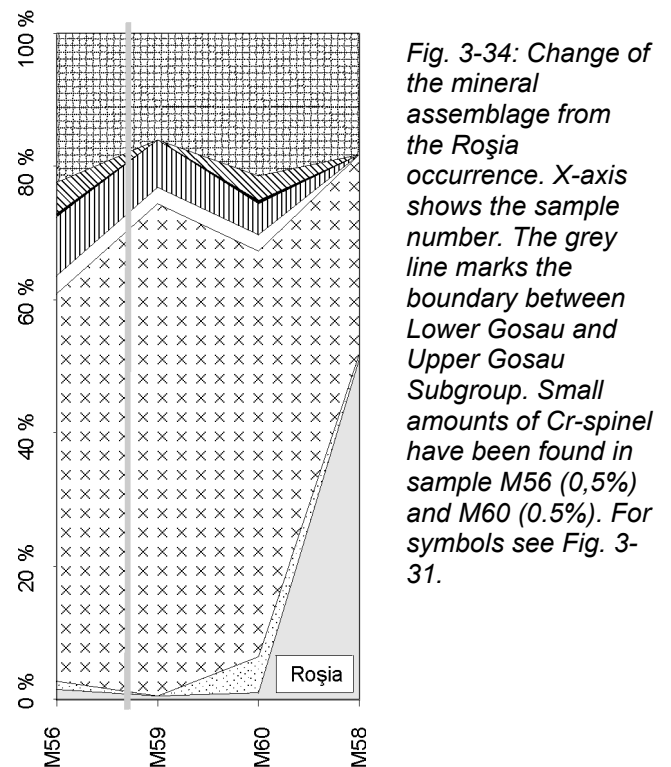


Fig. 3-34: Change of the mineral assemblage from the Roșia occurrence. X-axis shows the sample number. The grey line marks the boundary between Lower Gosau and Upper Gosau Subgroup. Small amounts of Cr-spinel have been found in sample M56 (0.5%) and M60 (0.5%). For symbols see Fig. 3-31.

related to the banatite magmatism. Although a minor amount of Cr-spinel (0.5% for each sample M56 and M60) has been identified, it proves that ultrabasic rocks of the ophiolites of the Transylvanides have been transported from south into the depositing area of the Roșia occurrence (in present coordinates). The high amount of rutile indicates the erosion of high-grade metamorphic units of the Transylvanides.

The **Vlădeasa** (Fig. 3-36) occurrence records a balanced proportion of metamorphic and magmatic minerals. The relative high amount of apatite in sample 162 (21%) is probably related to the erosion of the Muntele Mare granite. Since the age of this sample might be younger than Middle Campanian (Fig. 3-39), the banatite magmatism is also a possible source. At least the high orthite (allanite) content in sample 163 reflects the coeval banatite magmatism. This sample has been taken from the matrix of the volcano-sedimentary deposits of the Vlădeasa succession. It is also worth to mention the Cr-spinel in sample M26, as it indicates a transport and probable source from south (in present coordinates), from the ophiolitic rocks of the Transylvanides.

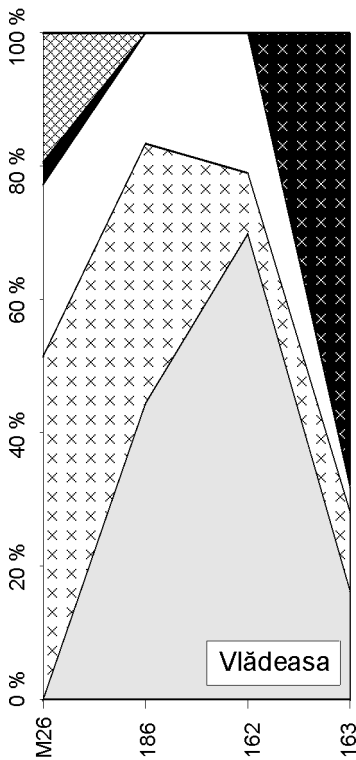


Fig. 3-36: Change of the mineral assemblage from the Vlădeasa occurrence. X-axis shows the sample number. For symbols see Fig. 3-31.

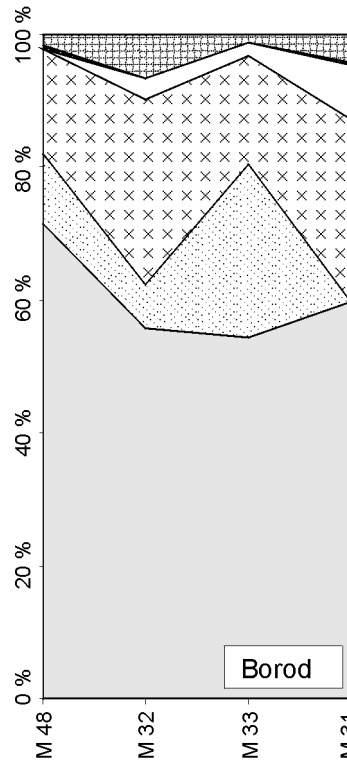


Fig. 3-37: Change of the mineral assemblage from the Borod occurrence. X-axis shows the sample number. For symbols see Fig. 3-31.

The heavy mineral assemblage of the **Borod** occurrence (Fig. 3-37) records a strong dominance of minerals deriving from metamorphic rocks. Within the zircon-tourmaline group of the entire succession tourmaline is predominating (87%). Moreover, the relative high percentage of the staurolite-epidote-zoisite mineral group supports the evidence of erosion of mainly metamorphic rocks.

presents a qualitative overview of the main and most important minerals (concerning the deductive provenance) and their inferred parent lithologies.

Figure 3-38 summarizes the above presented data, showing the heavy mineral suites identified in the Gosau sediments of the Apuseni Mts.. The table

For concluding statements concerning the heavy mineral assemblages and their variations for all Gosau occurrences of the Apuseni Mts., a compilation is helpful, which considers the stratigraphic ages of the samples within a profile as well as the facies change (Lower to Upper Gosau Subgroup). Since the sedimentation and facies change did not happen synchronously, this is a difficult issue.

Figure 3-39 illustrates the change of the

Characteristic minerals											Inferred principal parent lithologies	Presently exposed basement units (possible source terrains in the Apuseni Mts. and their surroundings)			
GARNET	STAUROLITE	EPIDOTE/ZOISITE	ZIRCON	TOURMALINE	RUTILE	APATITE	CHLORITOID	CR-SPINEL	GLAUCOPHANE	AMPHIBOLE			ORTHITE	SPHALERTITE	CASSITERITE
														GRANITE	Bihor Unit (autochthonous) "Granit de Muntele Mare"
														PERMIAN - LOWER CRETACEOUS SEDIMENTS	PERMIAN - LOWER CRETACEOUS SEDIMENTS
														OPHIOLITES	Mureş Ophiolite: Transylvanian Ocean
														COEVAL VOLCANICS	Banatitic Magmatism
														LOW-GRADE METAMORPHICS	Biharia Unit/Someş Unit (autochton, retrograde Series)
														MEDIUM-GRADE METAMORPHICS	Someş Unit (autochton), Codru Unit
														HIGH-PRESSURE METAMORPHICS	Transylvanides ?

Fig. 3-38: Qualitative overview of the identified heavy minerals and their assumed provenience. Light gray fields display secondary or uncertain provenances, dark fields indicate well isolated associations.

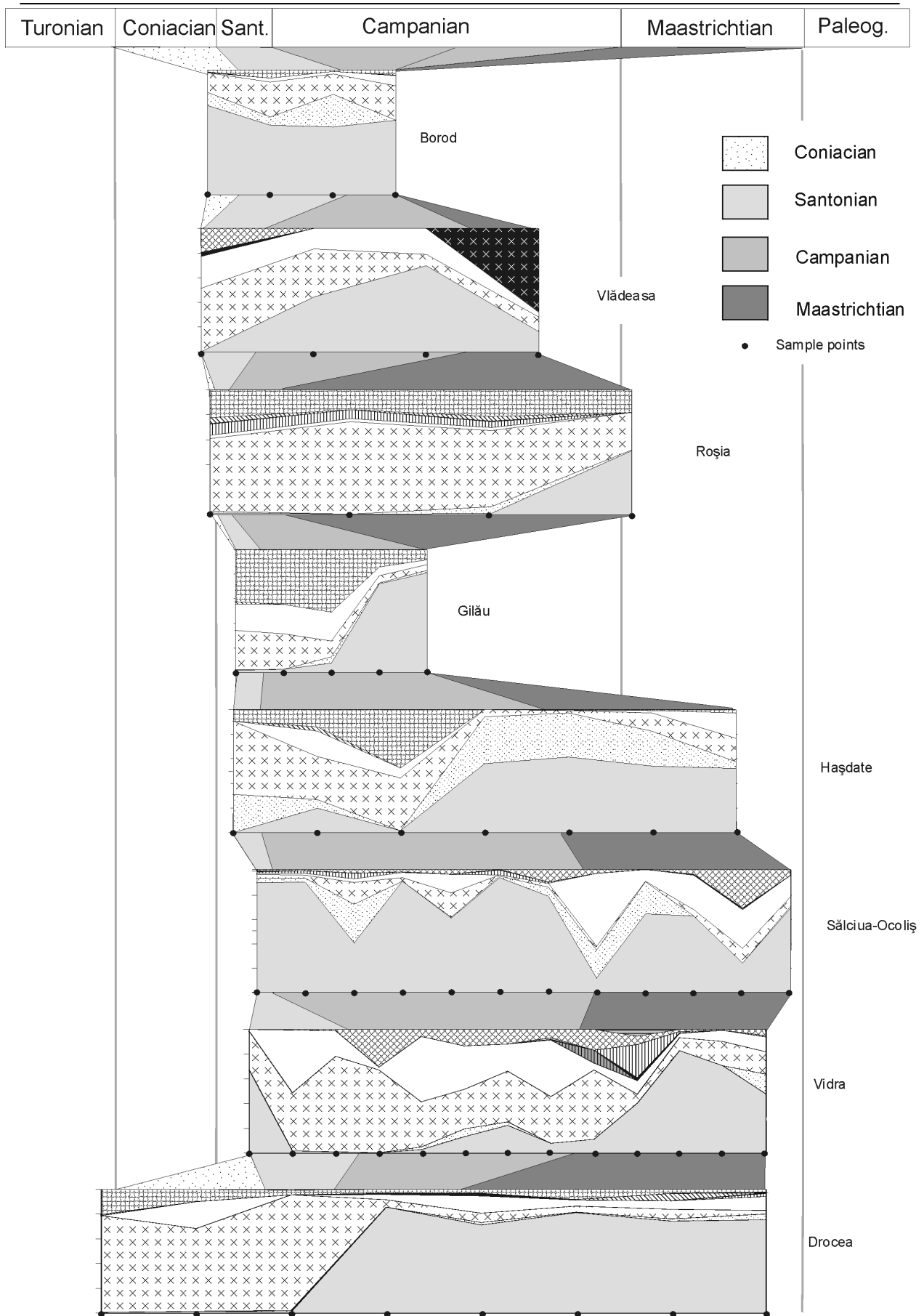


Fig. 3-39: Alternation of heavy mineral assemblages of the main Gosau occurrences of the Apuseni Mts. with stratigraphical relations of sample points. For further explanations see text. For comparison of each occurrence see Fig. 3-31 to 3-37.

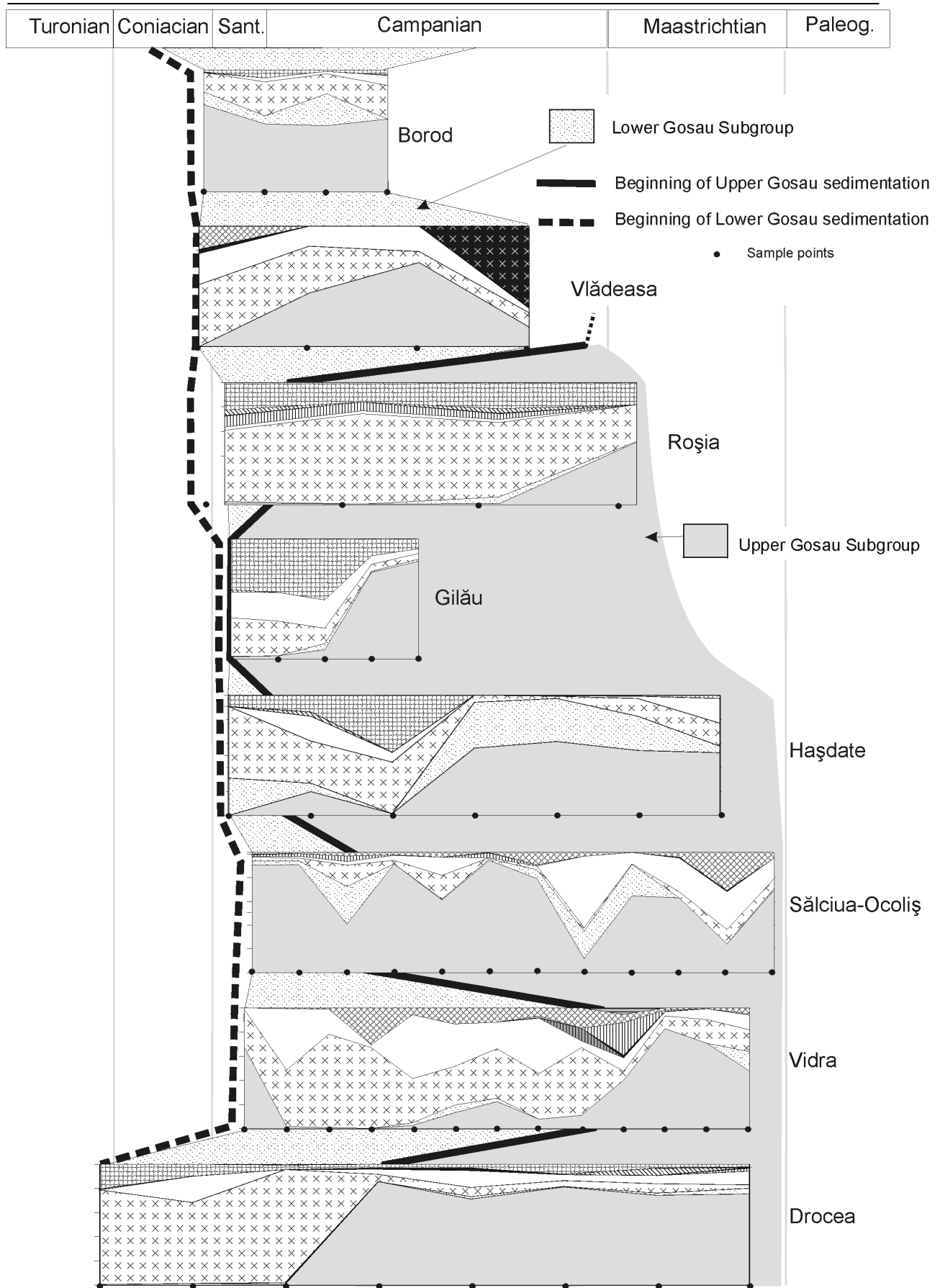


Fig. 3-40: Alternation of heavy mineral assemblages of the main Gosau occurrences of the Apuseni Mts.. The dark line marks the facies change from Lower to Upper Gosau Subgroup. For further explanations see text. For comparison of each occurrence see Fig. 3-31 to 3-37.

mineral assemblages of all occurrences. As an example, the first sample of the Drocea occurrence is situated in uppermost Turonian and the youngest in the uppermost Maastrichtian. The samples in between are not in their exact stratigraphical position, but isolines separate the chronostratigraphical stages within each profile. Although the increasing predominance of metamorphic minerals is already recognizable, figure 3-40 illustrates the change in the heavy mineral assemblages in coherence with the facies change from Lower Gosau to Upper Gosau Subgroup. In nearly every profile the change from Lower to Upper Gosau Subgroup is evident. The Borod and Vlădeasa occurrences do not record Upper Gosau sediments. However, they are surrounded by the metamorphic units of the Bihor autochthonous unit and thus the high percentage of metamorphic minerals is allegeable. The garnet dominance within the Lower Gosau Subgroup of the Sălciua-Ocoliș occurrence is probably due to mainly sedimentary supply from the metamorphic rocks of the Biharia nappe complex to the north. Although the Vidra occurrence records high percentages of apatite within the Lower Gosau Subgroup (deriving presumably from the Variscan granites) it is more probable that the obvious appearance of apatite after the Upper Campanian/Lower Maastrichtian is related to the beginning of the banatite magmatism. This assumption is also based on the fact that minerals like cassiterite, sphalerite and orthite (allanite) appear in Lower Maastrichtian parts of the successions.

The exhumation to erosional level of rock complexes situated south, southeast and east (in present coordinates) of the Gosau sedimentation area is evident since Cr-spinel, which can be supplied only from the ultrabasic rocks of the Transylvanides is present in some samples. The evidence therefore is also proven by the occurrence of radiolarite pebbles within the debris flow horizon and in olistoliths (Bucur et al., 2004), both deriving from rock units known only from the Transylvanides.

Furthermore, paleocurrent measurements support the assumption that sedimentary material has been supplied from both sides of the basin, from north and south (present day coordinates). The measurements have been taken from the Lower and Upper Gosau Subgroup. They are based on pebble imbrications, oblique lamination, and erosion marks on the base of Ta layers within the turbidites. Since some of the erosion marks do not indicate an unequivocal transport direction (e.g., most groove casts) and because of bad preservation, the presented data are grouped into bimodal and unimodal directions. Each measured data has been rotated into its original horizontal position by the amount of the layer dipping. Figure 3-41 shows a compilation of all measurements for each Gosau occurrence classified into unimodal and bimodal datasets and divided into Lower and Upper Gosau Subgroup. Bimodal datasets indicate that sediment transport may have occurred from both directions, e.g. north to south and south to north. Also the unimodal paleocurrent directions record transport from both directions for the Lower and the Upper Gosau Subgroup. From this direction deviating measurement (e.g. Roșia, Câmpeni) may be explained by horizontal block rotation during basin subsidence or post-sedimentary tectonics. The heavy mineral assemblages and the change within the lithostratigraphic successions of the Gosau sediments reflect a dynamic evolution. Basin subsidence, exhumation of the crystalline hinterland and uplift of the forearc region seem to be processes which occurred simultaneously.

The heavy mineral assemblages of the Gosau sediments of the Eastern Alps record a similar dynamic evolution as those of the Apuseni Mts.. Cr-spinel as the predominant mineral in the Lower Gosau Subgroup of the Eastern Alps (Woletz, 1967; Faupl & Wagneich, 1992) gives evidence of the erosion of ophiolites deriving from the accretionary wedge situated north of the basins, south of the Southpenninic ocean. Within the Upper Gosau Subgroup garnet as a metamorphic

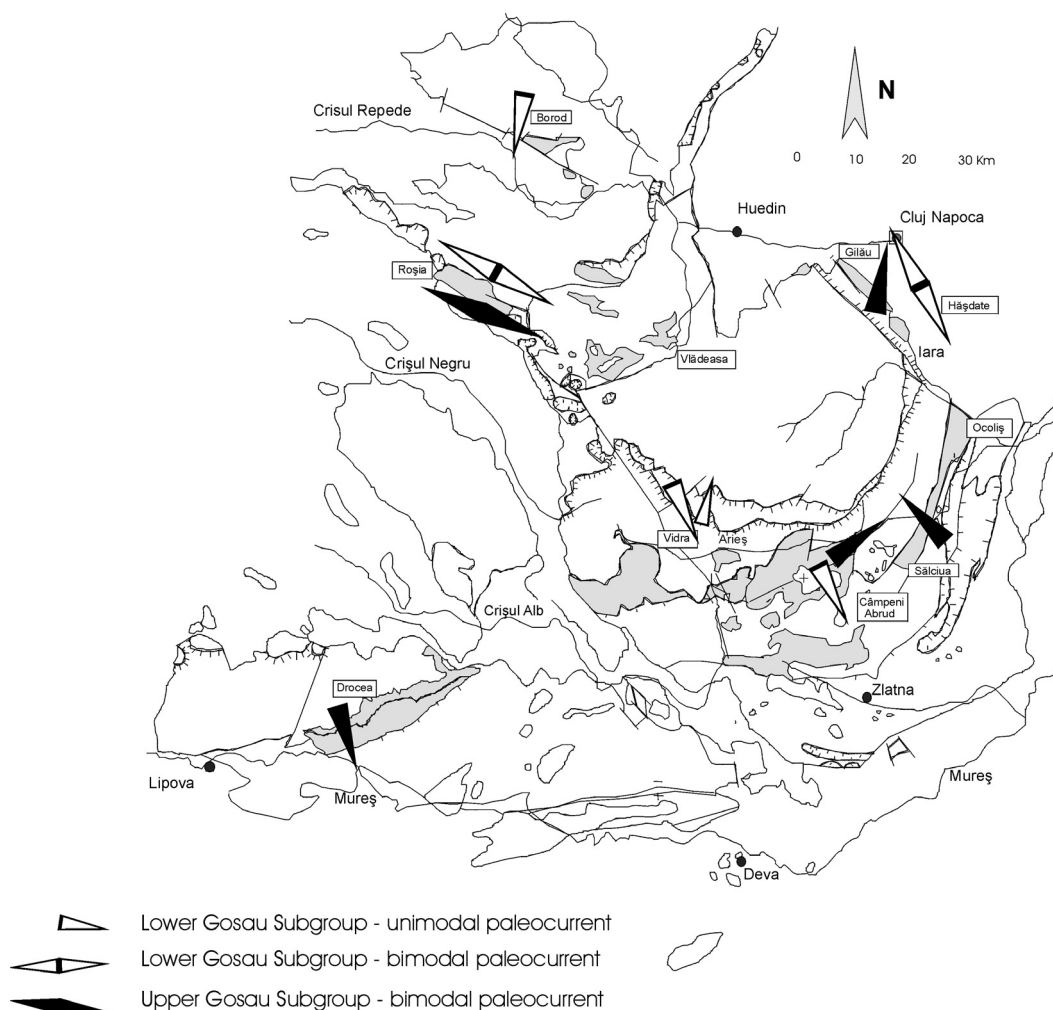


Fig. 3-41: Direction of paleocurrents of the Gosau sediments of the Apuseni Mts.. Bimodal measurements do not record finite transport directions. Each arrow illustrates an average of a dataset with several measurements.

mineral predominates indicating the uplift and exhumation of the Central Alpine crystalline complex in the south (Faupl & Wagneich, 1992; Wagneich & Faupl, 1994). Although the Cr-spinel is not dominating in the heavy mineral suites of the Apuseni Mts., it indicates the exhumation of the forearc region during the basin formation. The erosion of a fore arc region is also supported by the appearance of glaucophane as a characteristic mineral forming at high-pressure/low-temperature conditions which occur on convergent plate margins. Glaucophane-bearing rocks are not exposed in the Apuseni Mts., thus have completely been eroded. The obducted ophiolites are still largely exposed in the Apuseni Mts., whereas in the Eastern Alps remnants of the South

Penninic oceanic crust are known from comparable smaller outcrops only. Predominance of garnet and other metamorphic minerals in the Upper Gosau succession of the Apuseni Mts. is in line with the heavy mineral data known from the Eastern Alps. Like in the Eastern Alps, in the Apuseni Mts. this predominance is evidence for the Upper Campanian to Maastrichtian exhumation of a metamorphic hinterland, particularly of the Bihor autochthonous unit.

3.3. Vitrinite reflection and basin modeling

3.3.1. Data overview

In sedimentary basins, the coalification of macerals helps to reconstruct depositional, stratigraphic, and tectonic settings. For this study the coalification rank has been determined by the reflectivity of vitrinite (random vitrinite reflectance: %Rr), a member of the coal maceral group. Due to progressive burial of strata during deposition, the vitrinite reflectance gives a first clue of the stratigraphic succession due to sediment loading: the coalification increases with increasing depth. Thus, as a first deductive result stratigraphic relations can be recognized. Tectonic activity often leads to displacements within a sedimentary succession. Consequently, faults can be identified by sudden jumps in

a coalification rank profile. Since it is a useful tool in petrol and coal geology, the reconstruction of the thermal history based on the reflectivity of vitrinite has a long tradition. The “memory effect” of the vitrinite and its reflectance values allow the modeling of paleobasins and their burial history, even if these basins underwent later inversion and erosion.

Sedimentary rocks with organic content have been sampled with respect to their lithostratigraphic position from the main Gosau occurrences of the Apuseni Mts.. More than 150 samples have been processed. Due to lack of organic content or increased oxidation of organic matter only 74 samples were measured. The vitrinite reflection values are presented in Figure 3-42. They display a wide range beginning with coalification ranks from 0.37%Rr to 5.08%Rr. The latter value already enters into the rank of anthracite

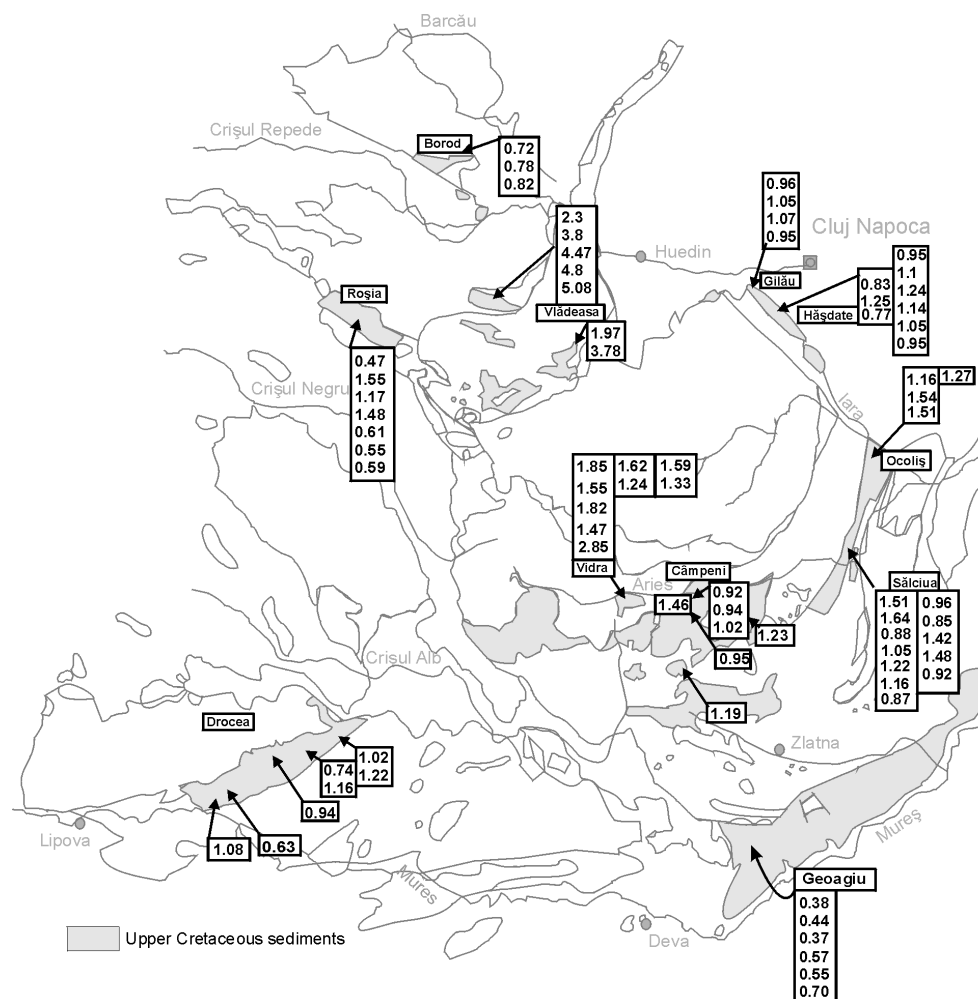


Fig. 3-42: Vitrinite reflectance values (%Rr) of the Upper Cretaceous deposits of the Apuseni Mts..

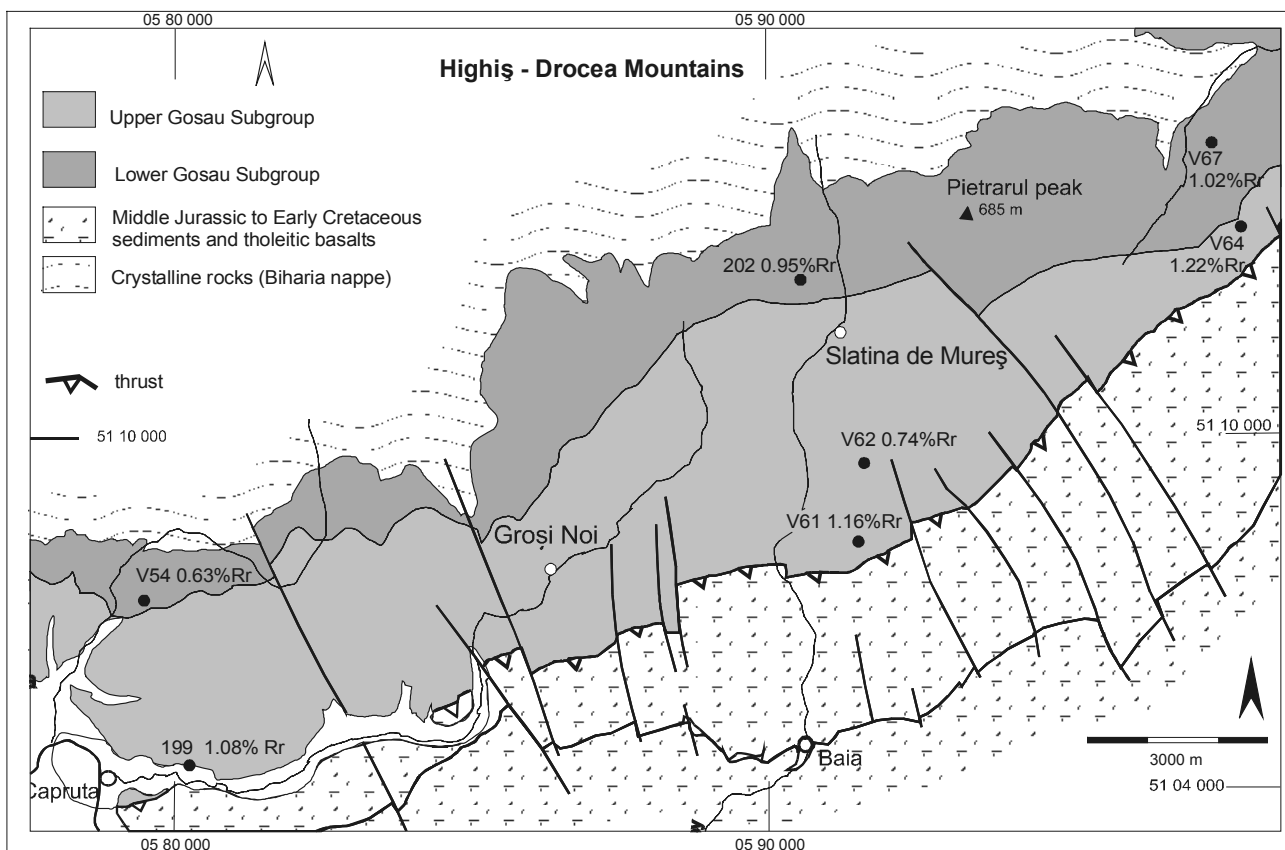


Fig. 3-43: Vitrinite reflectance values of the Drocea occurrence.

and meta-anthracite (Stach et al., 1982).

The coalification pattern in the eastern part of the **Drocea** area (Fig. 3-43) shows reflectance values between 0.95 and 1.02 %Rr within the Lower Gosau Subgroup. Only one sample meets the expectation of upsection decreasing reflectance (sample V62: 0.74%Rr). On the southern margin of the Gosau occurrence, close to the lowermost Tertiary thrust plane, vitrinite reflectance values increase up to 1.22%Rr. The generally lower reflectance values in the western part of the Drocea occurrence might be due to a lower profile thickness of the entire Gosau succession in this area.

The Gosau deposits of the **Vidra** occurrence (Fig. 3-44) show relatively high reflectance values, which can be explained by the increasing heat flow related to the banatite magmatism (see following paragraphs). The highest value (sample 25: 2.85%Rr) was taken near a

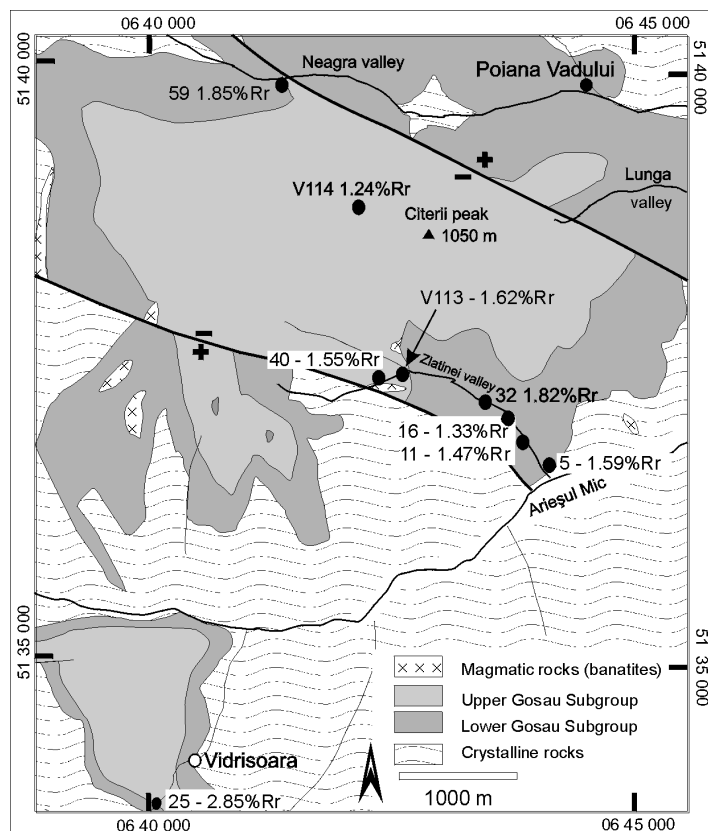


Fig. 3-44: Vitrinite reflectance values of the Vidra occurrence.

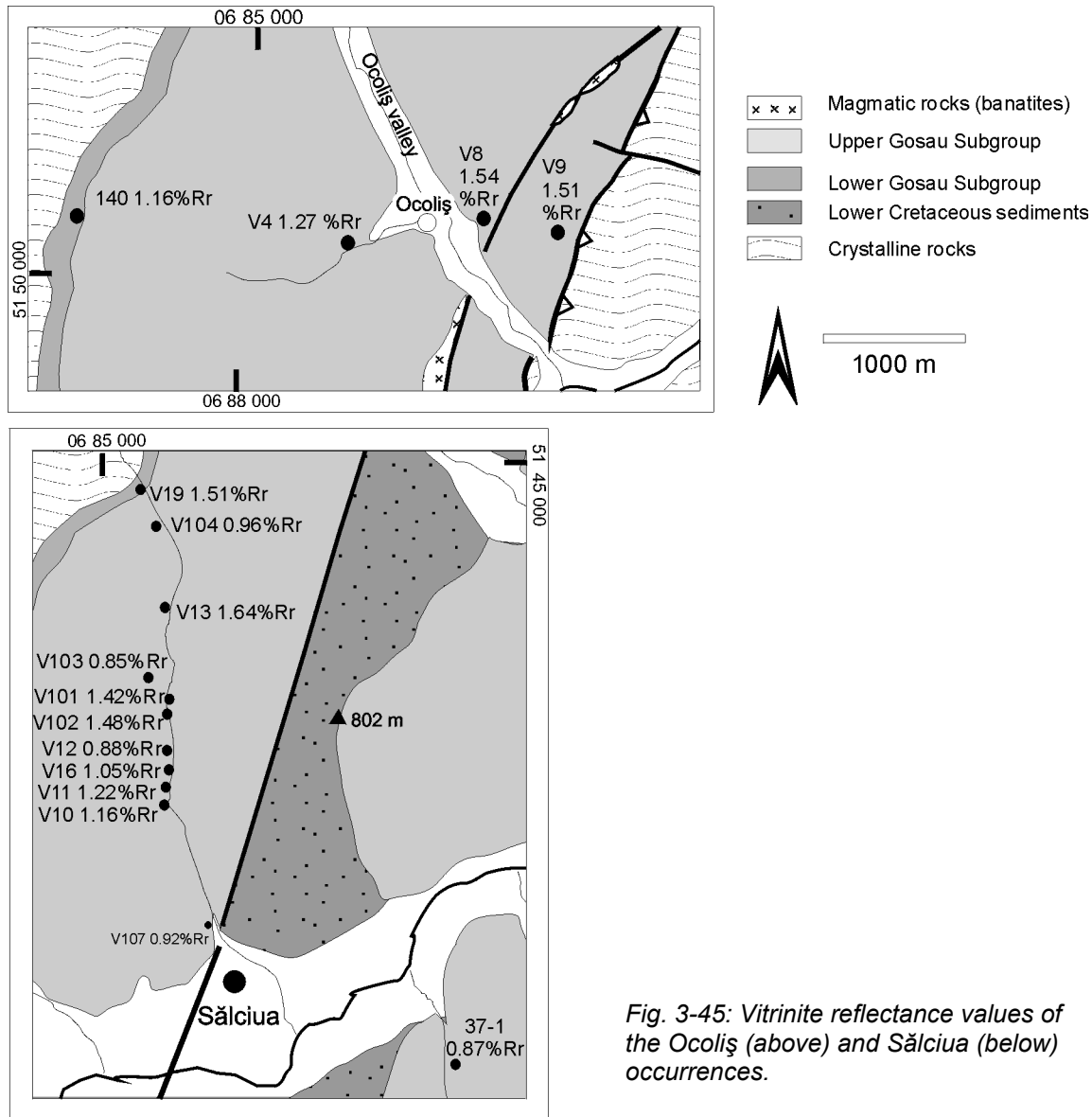


Fig. 3-45: Vitrinite reflectance values of the Ocoliş (above) and Sălciua (below) occurrences.

cataclastic fault zone. The other samples generally show scattering and increased reflectance values within both, the Lower and the Upper Gosau Subgroup. The lowest reflectance value (sample V114: 1.24%Rr) belongs to the uppermost levels of the succession.

The same range of reflectance values has been measured at the **Sălciua-Ocoliş** occurrence (Fig. 3-45). In contrast to the Vidra occurrence, higher parts of the Upper Gosau Subgroup are still preserved. Thus, a low reflectance value has been measured in the highest part of the succession (Upper Maastricht, sample 37-1: 0.87%Rr). Figure 3-15 shows a reconstructed profile through the Sălciua

basin, with increasing reflectance values due to compressional tectonics and decreasing values in the higher parts of the succession. This pattern is not visible in the Ocoliş area. Here, the Upper Gosau shows higher reflectance values than the sample of the Lower Gosau, which can be explained by vicinity of banatite intrusions and/or thrusting of the crystalline rocks of the Austrian Transylvanides over the eastern parts of the Gosau sediments of the Ocoliş area.

The coalification pattern of the **Hăşdate** occurrence is similar to the that of the Ocoliş area (Fig. 3-46). Increasing reflectance values towards the upper parts of the succession are probably also a

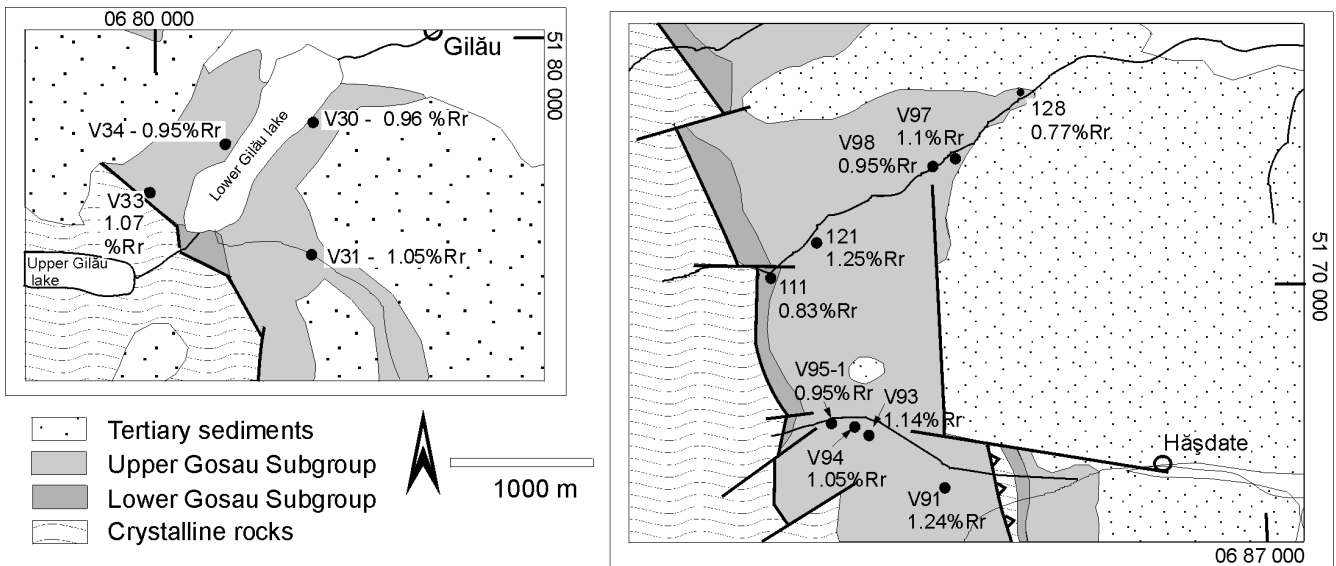


Fig. 3-46: Vitrinite reflectance values of the Gilău (left) and Hășdate (right) occurrences.

consequence of thrust loading (Profile in Figure 3-16). In the **Gilău** area the reflectance values scatter within a small range only. All samples belong to the Upper Gosau Subgroup and cover only a short stratigraphic interval (Fig. 3-17).

Generally, an upward decrease of the

reflectance values can also be seen within the succession of the **Roșia** occurrence (Fig. 3-47). The turbidites of the uppermost sequences of the succession record the lowest coalification ranks. Figure 3-48 shows a profile from the southern part of the Roșia occurrence. The plotted reflectance values give

Fig. 3-47: Vitrinite reflectance values of the Roșia occurrence.

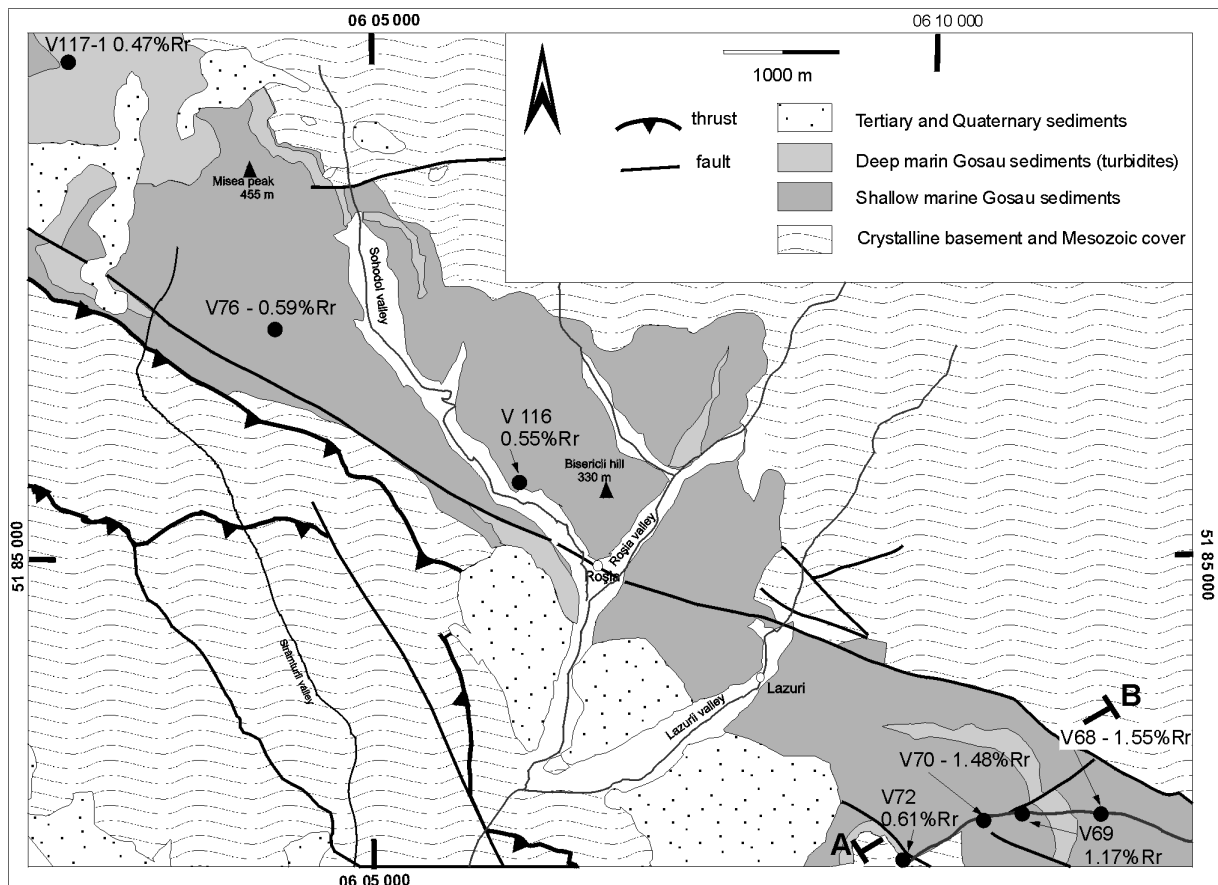
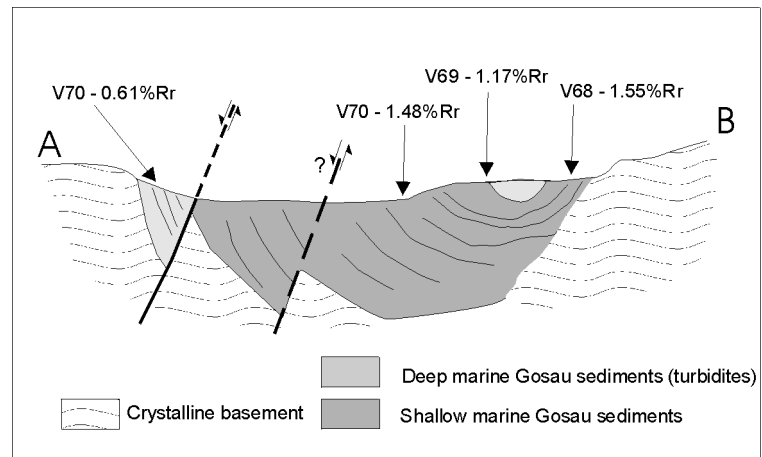


Fig. 3-48: Exaggerated profile through the Gosau sediments of the Roşia occurrence (for location of the profile line, see Fig. 3-3-6). The measured vitrinite reflectance values reflect the tectonic relations.



evidence for the Neogene extensional tectonics with normal faulting (see also chapter 3.4).

The high vitrinite reflectance values of the **Viădeasa** region (Fig. 3-42) cannot be used for sedimentologic or tectonic purposes. At least these measurements prove the increased heat flow during and after the banatite magmatism.

Basically, all measurements of the Apuseni Mts. give evidence for the following presumptions:

- The banatite magmatism is responsible for an increase of the heat flow within the Apuseni Mts.. The coalification ranks increase towards the center of the eruption (Viădeasa region), as well as in the areas where banatite intrusive bodies occur (Vidra, Câmpeni, Sălciua-Ocoliş, Gilău-Hăşdate). Thus, the Gosau sediments of the Drocea, Roşia and Borod occurrences and the deposits of the Geoagiu flysch (see following paragraphs) show the lowest coalification ranks.
- The increased coalification rank of the Vidra, Sălciua-Ocoliş and Gilău-Hăşdate occurrences are, beside the before mentioned banatite magmatism, also a consequence of the post-sedimentary tectonic activity.

3.3.2 Basin modeling

Basin modeling based on surface geology and vitrinite reflectance is a difficult issue, especially if post-sedimentary tectonics

aggravates a profile reconstruction, like it is the case for the Gosau sediments of the Apuseni Mts.. It has been attempted to find a continuous profile with no duplication of sequences due to faulting or folding. The most suitable profile was found near Câmpeni (Fig. 3-49). A second profile for vitrinite reflection measurements and basin modeling has been sampled within the Upper Cretaceous sediments (Geoagiu formation, Bozeş flysch) of the South Apuseni Mts. (Fig. 3-51, Fig. 2-2). The purpose of this modeling is to prove similarities and/or distinctions to the basin evolution of the Gosau sediments.

3.3.2.1 Basin model of the Gosau succession

The profile of the Gosau deposits of the **Câmpeni** area is based on outcrop (sedimentary facies and bedding dips) and literature data (Dimitrescu et al., 1974). The succession starts with a basal conglomerate followed by limestones and shallow marine marls (Fig. 3-50-a). This part of the succession represents the Lower Gosau Subgroup. The overlying turbidites of the Upper Gosau Subgroup have a thickness of 1300 m. Since no Paleogene sediments are known from the Apuseni Mts., erosion of the Cretaceous sediments has been assumed after the Maastrichtian/Paleogene boundary.

The burial history shows a rapid basin subsidence at the beginning of the sedimentation (Fig. 3-50-a). The shallow marine sedimentation phase of the Lower

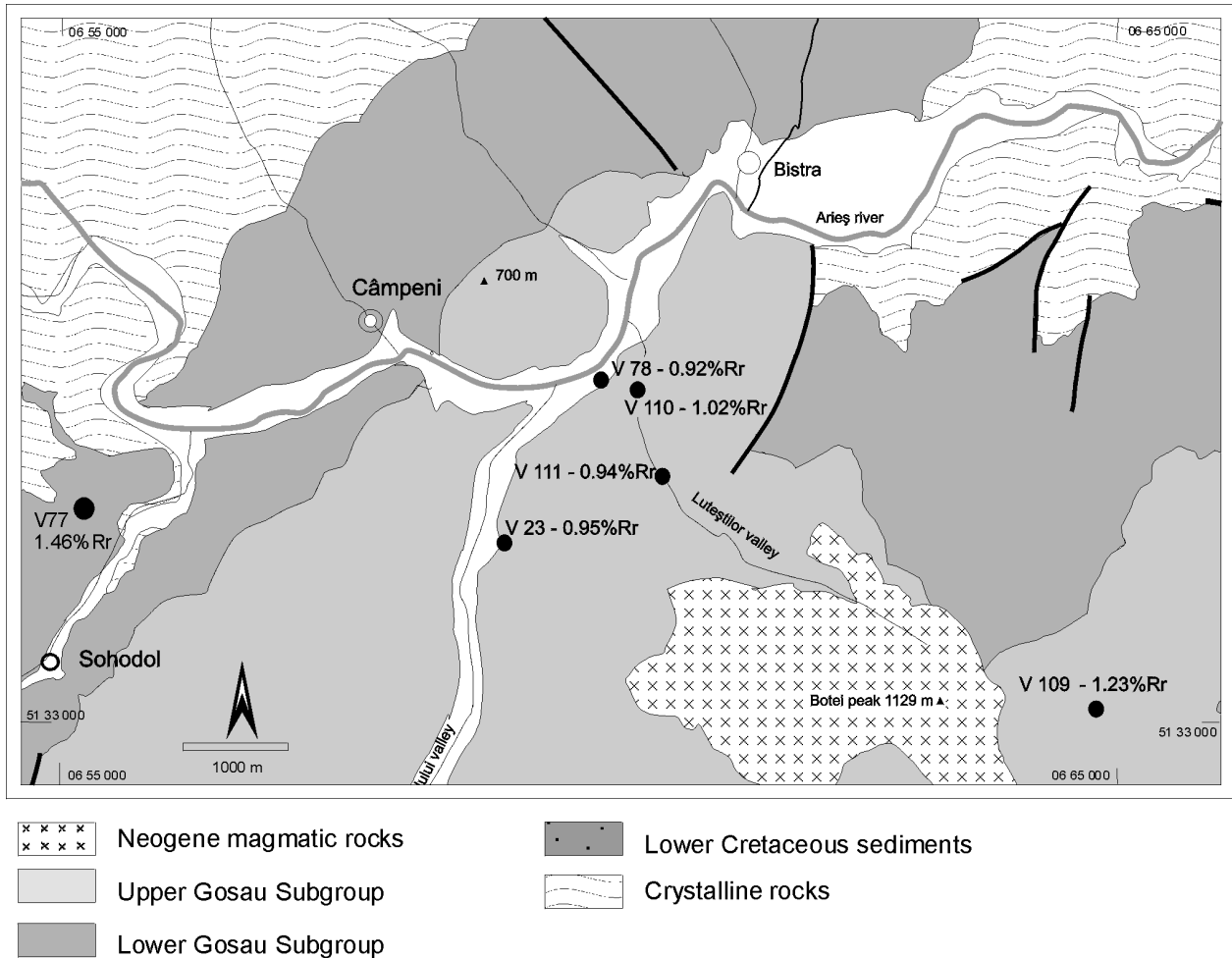


Fig. 3-49: Vitrinite reflectance values of Câmpeni area.

Gosau Subgroup records low subsidence rates (~ 0.33 mm/a), whereas the Upper Gosau Subgroup is characterized by increased subsidence rates (~ 2 mm/a). The post-sedimentary basin inversion as visualized in Figure 3-50-a is based on the modeling shown in Figures 3-50-b and 3-50-c. The samples and vitrinite reflection values have been plotted in the diagram in Figure 3-50-b. This diagram represents a pseudo-well based on the surface geology described above. The black line is the computed best-fit curve to the measured vitrinite reflectance values. This curve has been calculated with the assumptions of 1100 m eroded Gosau sediments, a high heat flow (< 108 mW/m²) during the Upper Cretaceous /Lower Paleogene and a slightly increased heat flow during Neogene (< 71 mW/m², black line in Fig. 3-50-c). The heat flow values are

explained with the banatite magmatism and the Neogene magmatism. The dashed and dotted gray lines (Fig. 3-50-b and 3-50-c) show calculations with either lower heat flow values in the Upper Cretaceous/Lower Paleogene or high heat flow during Neogene. It can be seen, that only a high heat flow during the Upper Cretaceous /Lower Paleogene can explain the measured coalification ranks. It is also evident, that the Neogene magmatism has no influence on the maturity of the organic matter of the Gosau sediments. The solid gray line is the computed curve with an assumed erosion of 1800 m and high heat flow values in the Upper Cretaceous /Lower Paleogene (black line in Fig. 3-50-c). Higher erosion thicknesses lead to increased coalification in the lower part of the succession. The same high erosion thicknesses, but lower heat flow values

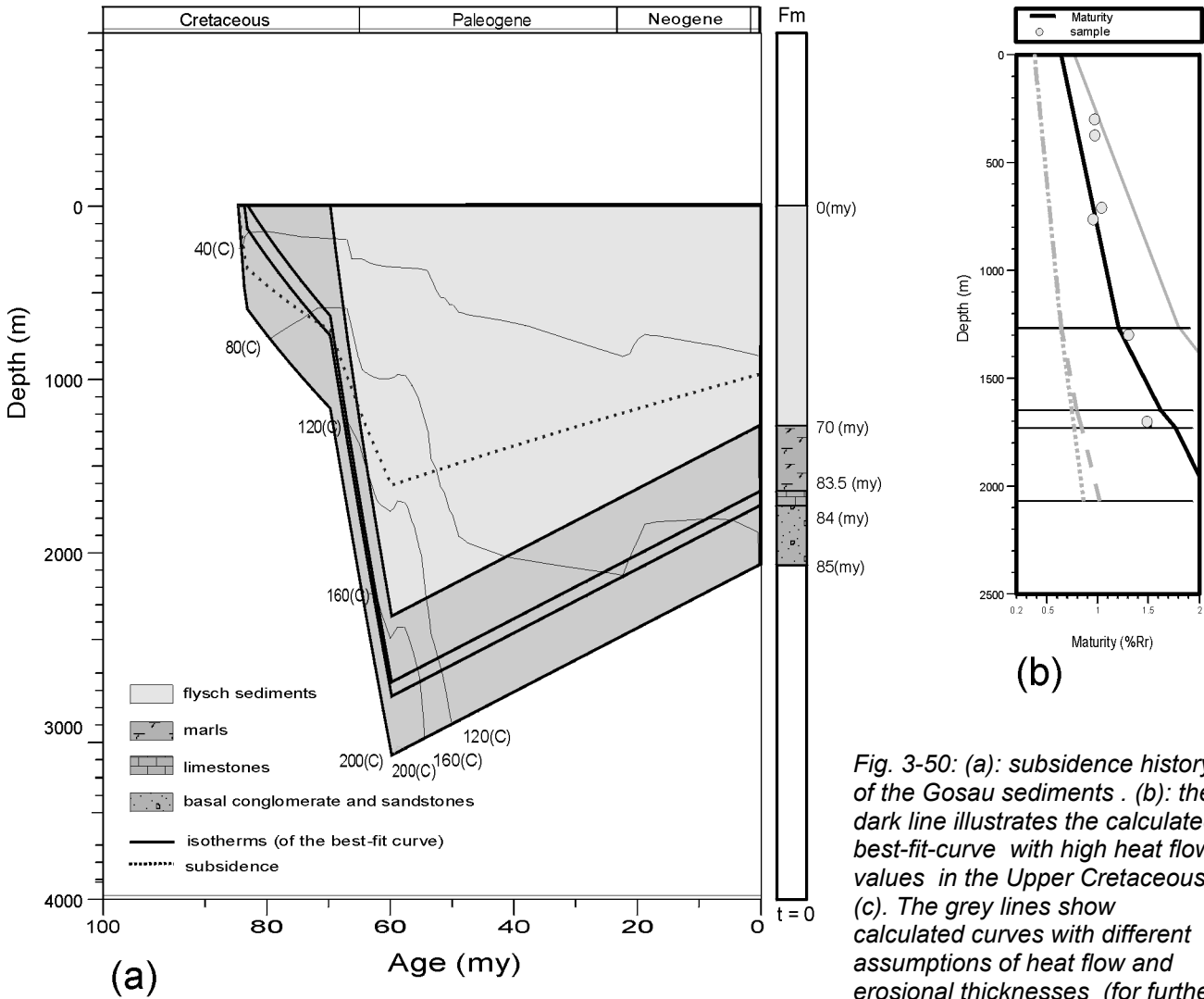
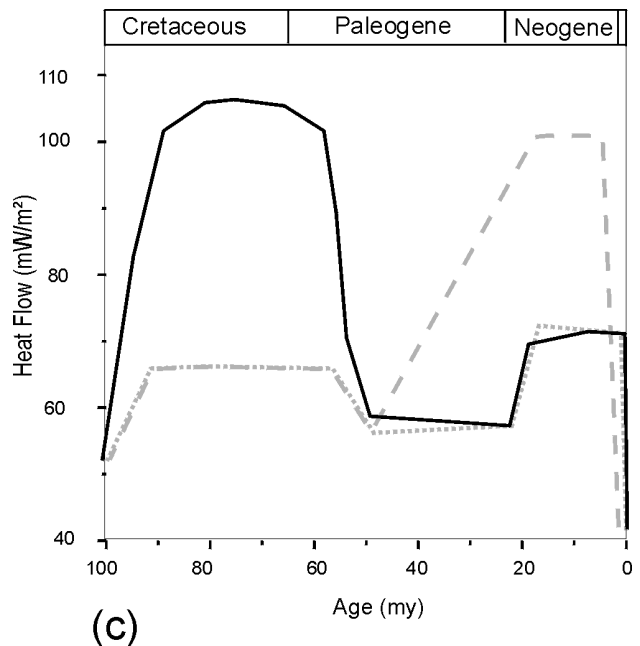


Fig. 3-50: (a): subsidence history of the Gosau sediments . (b): the dark line illustrates the calculated best-fit-curve with high heat flow values in the Upper Cretaceous (c). The grey lines show calculated curves with different assumptions of heat flow and erosional thicknesses (for further explanations, see text).

during the Upper Cretaceous/Lower Paleogene would cause too low coalification within the upper part of the succession, and still to high reflectance values within the lower part of the succession.

As concluding remarks, the following statements concerning burial history and basin evolution of the Gosau sediments based on vitrinite reflectance can be made:

- The entire Gosau succession reached total thicknesses of approximately 3200 m (2100 m preserved and 1100 m eroded sediments). Similar thicknesses are known for the Gosau successions of the Eastern Alps (Wagreich, 1993).
- The banatite magmatism is responsible for high heat flow values and relatively high coalification ranks. In



the Eastern Alps no magmatic activity occurred during the Upper Cretaceous, thus vitrinite reflectance values scatter between 0.4 and 0.65 %Rr (Sachsenhofer, 1987).

- The high heat flow within the sedimentary basins shows that they were situated near the volcanic arc, within the orogenic wedge.

3.3.2.2 Basin model of the outer flysch succession (Geoagiu formation, Bozeş flysch)

For the second basin modeling the organic matter of the Upper Cretaceous sediments of the **Geoagiu formation** and the **Bozeş**

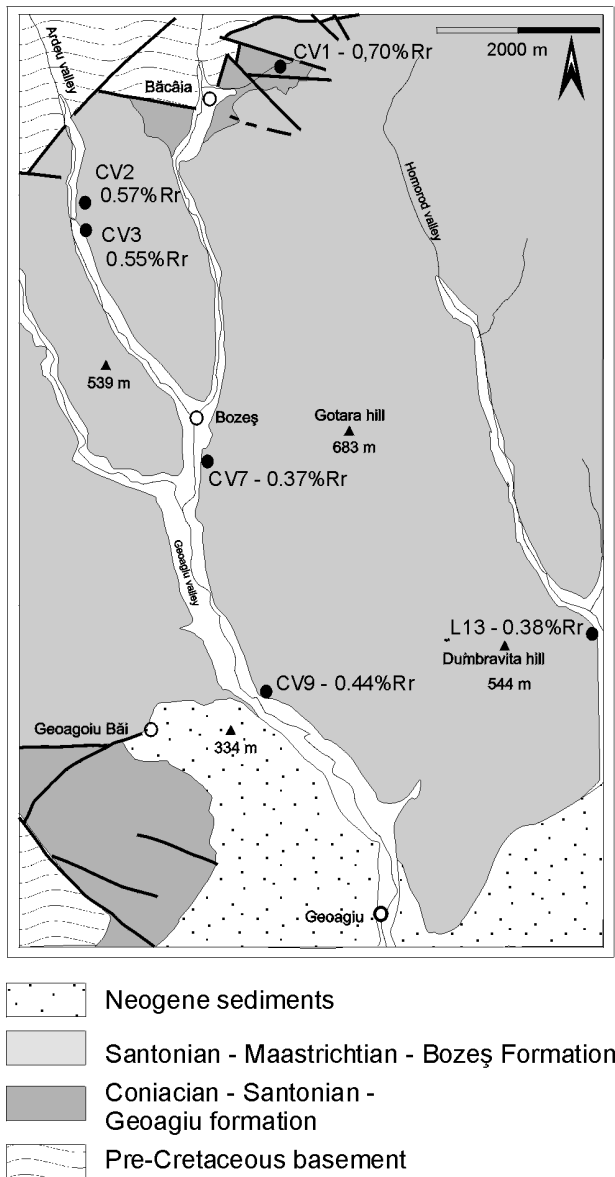


Fig. 3-51: Vitrinite reflectance values of the Geoagiu and Bozeş formation.

flysch have been analysed. The samples were collected along a profile within the Geoagiu and the Homorod valley (Fig. 3-51). The Geoagiu formation (Coniacian-Lower Campanian), is represented by conglomerates and shallow marine deposits. The overlying Bozeş flysch is characterized by rhythmic changes of coarse- to fine-grained sandstones, siltstones and claystone layers. The first turbidites within the succession record thick, partly amalgamated sandstone layers with Bouma Ta to Td horizons, which represent the proximal facies of a turbiditic fan (Fig. 3-52). The entire flysch



Fig. 3-52: Coarse-grained turbidite sequences of the Bozeş flysch.

succession shows a fining-upward trend. The uppermost sequences comprise thin-bedded silt layers with thick claystone intercalations (Fig. 3-53). The profile reconstruction is based on outcrop records (sedimentary facies and bedding dips) and literature data (Bordea et al., 1978; Borcoş et al., 1981). The Upper Cretaceous succession generally records bedding dips of 25° towards SE, which likely is a consequence of the Neogene extensional tectonics and the formation of the adjacent Transylvanian basin. In the south, Neogene sediments of the Transylvanian basin overlie the Upper Cretaceous sediments.



Fig. 3-53: Distal turbidite sequences of the Bozeş flysch.

Figures 3-54 a to c illustrate the basin history with calculated vitrinite reflection curves and estimated heat flow values. The subsidence curve shows a rapid subsidence with the beginning of the flysch sedimentation, followed by an erosive phase in the Paleogene. The best approach to the measured vitrinite reflectance data (black line in Fig. 3-54-b) has been calculated for the assumption of a very low heat flow during Upper Cretaceous, a high heat flow during the Neogene (black line in Fig. 3-54-c) and an erosion of 4000 m of Upper Cretaceous sediments during the Paleogene. The increased heat flow can be explained by the Neogene magmatic activity, which in the southern part of the South Apuseni Mts. had stronger effects than in the northern part. Lower heat flow values during the Neogene would cause low coalification in the lower part of the succession (dotted gray line in Fig. 3-54-b and c). Higher heat flow during the Upper Cretaceous on the other hand, would cause higher coalification in the Upper Cretaceous succession. An estimated erosion of only 2000 m (solid gray line in Fig. 3-54-b and black line in Fig. 3-54-c) would lead to lower coalification ranks in the upper part of the succession.

Furthermore, an increased heat flow during Upper Cretaceous (up to 60 mW/m²) and very low to no erosion would cause moderate coalification within the upper part of the profile and very high reflectance values in the lower part (dashed gray line in Fig. 3-54-b and c).

No significant erosion of Neogene sediments has been assumed. Since these deposits belong to the Transylvanian basin and the studied area is situated on the border of the Transylvanian basin, the thickness of the Neogene deposits was only negligibly higher than the present day thickness.

The basin modeling of the Upper Cretaceous Geoagiu and Bozeş formations give evidence for the following assumptions:

- The best approach to the measured vitrinite reflectance data indicates that the sediments have been deposited in a basin type with a very low heat flow. Such low heat flow values are only known from basins situated in trenches on convergent plate margins or fore-arc basins unrelated to arc magmatism. Since the arc magmatism (banatite magmatism) is documented, the basin type must be that of an ocean trench. Consequently, it has to be assumed that this basin was isolated to that of the Gosau deposition area and its evolution has to be interpreted differently.
- The calculated total thickness of approx. 6600 m would also indicate that these sediments have not been deposited within an orogenic wedge, like it is supposed for the Gosau sediments. Such high turbidite thicknesses would also support the suggested trench-basin evolution.

Compared to the Eastern Alps, these sediments would have their analogue in the Piemont flysch, which has been deposited on oceanic crust of the South Penninic Ocean (Oberhauser, 1995).

As final remarks concerning these results, it has to be pointed out that the calculated data are an approach. The difficulties of basin modeling based on surface geology

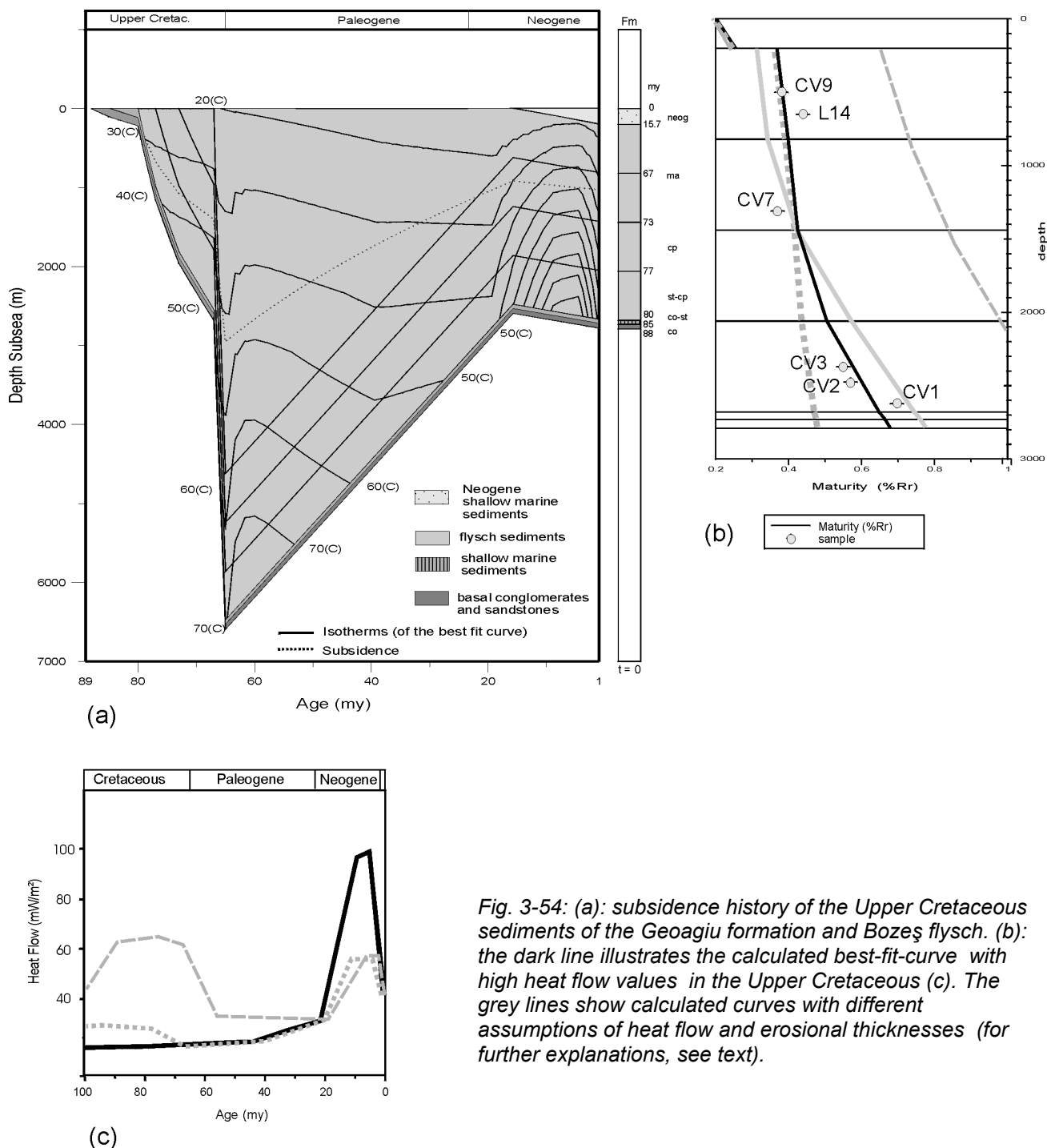


Fig. 3-54: (a): subsidence history of the Upper Cretaceous sediments of the Geoagiu formation and Bozeş flysch. (b): the dark line illustrates the calculated best-fit-curve with high heat flow values in the Upper Cretaceous (c). The grey lines show calculated curves with different assumptions of heat flow and erosional thicknesses (for further explanations, see text).

have been described before. However, the modeling shows an approximate range with definite limits. It has been shown that thick parts of the Gosau sediments have been eroded. For the calculated profile, the erosion value scatters around 1000 m, and definitely will not be higher than 1500 m. Thus, it can be assumed that total thickness of the Gosau successions did not exceed 3500 m. The basin modeling of

the Geoagiu formation and Bozeş flysch shows high erosion thickness, which surely is above 3000 m. The resulting total thickness together with the calculated heat flow indicates that - compared to the Gosau basins - a different basin evolution has to be presumed.

3.4 Kinematic analysis

For the calculation of compressional and extensional axes outcrop data of fault planes with distinct kinematic indicators (sense of slip), fold axes and axial fold planes have been measured within the Gosau sediments. The presented data are the result of processed measurements, showing calculated mean vectors with resulting principal paleostress directions. For further descriptions concerning processing methods, calculation and used software, see Appendix. The fault plane analysis resulted in separation of different fault plane populations which have been correlated with individual tectonic events.

The processed and assorted data set of the Gosau deposits of the **Hășdate** occurrence display two kinematic events (Fig. 3-55). The 1st, compressional event calculated from fault planes shows approx. E-W orientated directions. The compressive axis of the fault planes is corroborated by the orientation of the compressive axis deduced from fold axes and axial planes. The kinematic axis of the 2nd, extensional event shows ENE-WSW direction. Several fault planes record both, older compressional kinematic indicators, and cutting extensional ones. The relation of young, normal faults and older reverse faults is shown in Fig. 3-56.

The same kinematic pattern is recorded for the **Sălcium-Ocoliș** occurrence (including measurements in the Arieș valley). The 1st, E-W compressional event has been detected by fault planes, and is confirmed by compressional axes deriving from folds. The 2nd extensional event shows ESE-WNW paleostress directions.

Two fault plane populations have been separated from the data set of the **Viadeasa** region, which probably belong to the same tectonic event. The first population shows NE-SW extension with a vertical compressional mean vector. Although the mean compressional vector of the second population is horizontally orientated, the NE-SW orientation of the extensional axis indicates that this data set together with the first one belongs to a

tectonic event with NE-SW orientated extensional directions.

The coherent data set and fault plane analysis of the **Roșia** area shows NNE-SSE extensional direction, with a SSW-NNE direction. In one outcrop fold axes have been measured, showing a NE-SW orientated compressive direction.

The kinematic analysis of fault planes of the **Vidra** occurrence resulted in separation of two data sets (Fig. 3-57). The 1st population shows SW-NE orientated extension, which goes in line with the orientation of the normal faults and horst-and-graben structure shown in Figure 3-7. The 2nd population shows E-W compression with a horizontally extensional kinematic axis, resulting in mainly strike-slip faults.

Although the kinematic data from the **Drocea** occurrence show scattered vectors for the P-T-B-axes of each fault plane measurement, it was not possible to separate this data set in order to obtain more distinct values and/or subhorizontal (resp. subvertical) orientation for the main kinematic axes. However, the main compressional ENE-WSW orientated kinematic axis shows similar direction as the compression direction deduced from fold axes.

By compiling the presented kinematic axes, three principle paleostress directions can be assigned to regional tectonic events: (1) an E-W to NE-SW orientated compression, (2) an ENE-WSW to ESE-WNW orientated extension and (3) an NNE-SSW to NE-SW orientated extension (Fig. 3-57).

The mainly E-W orientated directions of the compressional event (1) have been measured in the Vidra, Sălcium-Ocoliș and Hășdate occurrences. This compressional event is related to the mid-Cretaceous to Lower Paleogene convergent movements of the Tisia and Dacia microplates. Although supported by only few data, the NE-SW compression of Roșia occurrences is assigned to the E-W compressional event. Block rotation during the later Neogene extensional tectonics is probably responsible for the rotation of the fold axis and the change in the paleostress

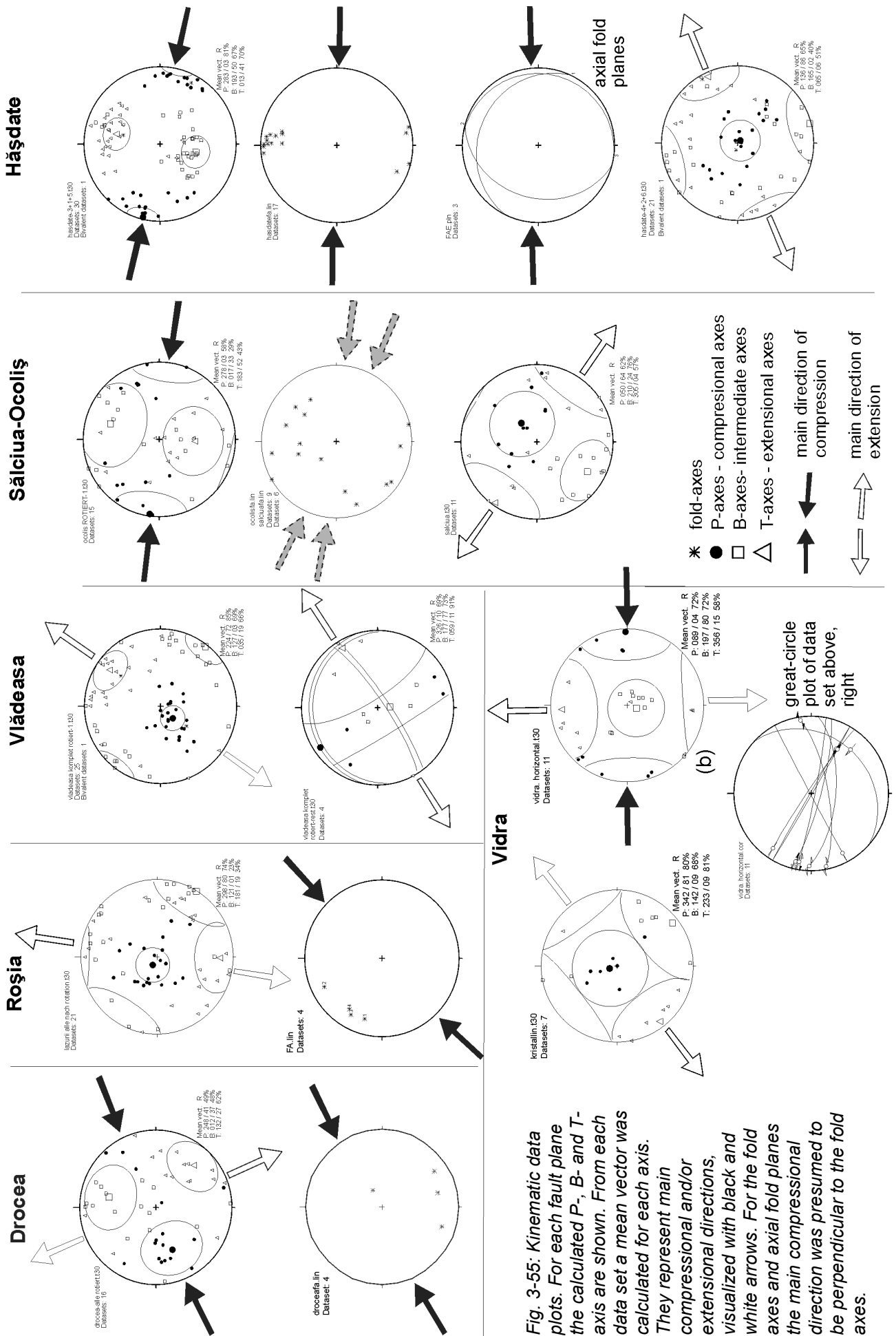


Fig. 3-55: Kinematic data plots. For each fault plane the calculated P-, B- and T- axes are shown. From each data set a mean vector was calculated for each axis. They represent the main compressional and/or extensional directions, visualized with black and white arrows. For the fold axes and axial fold planes the main compressional direction was presumed to be perpendicular to the fold axes.

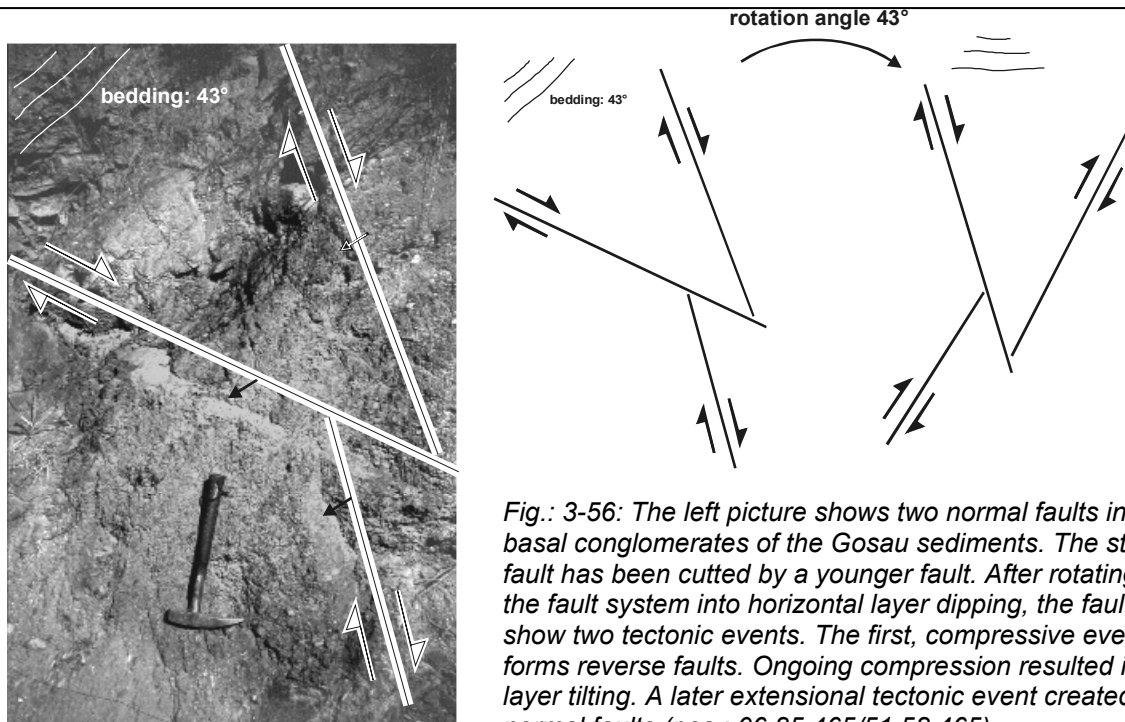


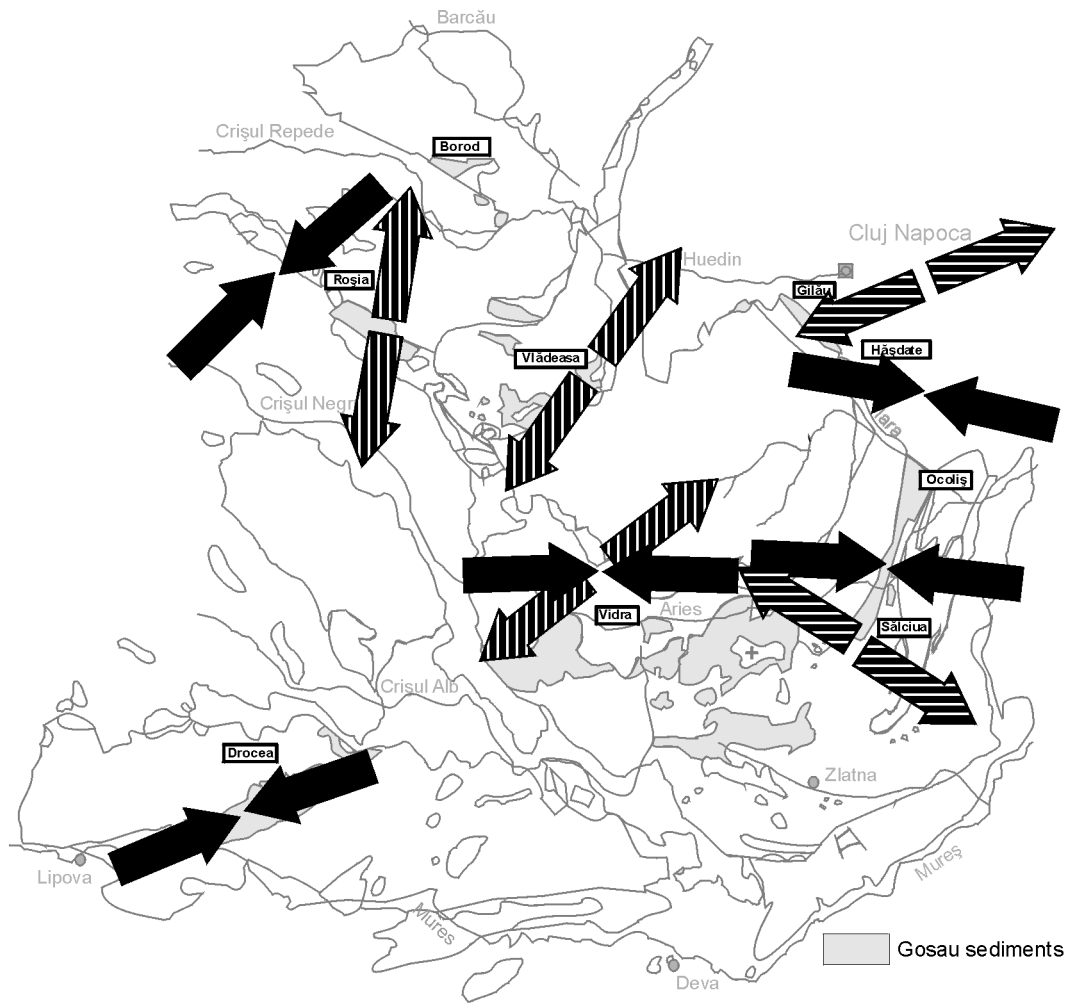
Fig.: 3-56: The left picture shows two normal faults in the basal conglomerates of the Gosau sediments. The steep fault has been cutted by a younger fault. After rotating the fault system into horizontal layer dipping, the faults show two tectonic events. The first, compressive event forms reverse faults. Ongoing compression resulted in layer tilting. A later extensional tectonic event created normal faults (pos.: 06 85 465/51 58 465).

direction. The ENE-WSW compression recorded for the Drocea occurrence is also assigned to the E-W compressional tectonic event. The deviation is probably a consequence of the Late Oligocene to Miocene strike-slip movements on the border between the Tisia-Dacia block and the Moesian platform (Fig. 1-3; Zweigel, 1997).

The approximately E-W extension (2) of the Sălciua-Ocoliş and the Hăşdate occurrence, and of the Arieş valley is inferred to correlate with the extensional processes and subsidence of the Transylvanian basin. Particularly at the Hăşdate occurrence (located on the border to the Transylvanian basin), the strong influence of the Neogene extension and subsidence of the Transylvanian basin causes kinematic features which record E-W extension. Although the outcrop situation suggests shortening (tilted and partly strongly folded sediments), the overprint of the later Neogene extension is obvious in this area.

The NNE-SSW to NE-SW extensional directions (3) measured in the Vlădeasa and Roşia occurrences are supposed to be related to the extensional tectonics in Miocene times. These faults were created during the formation of the Neogene

Borod, Beiuş and Zarand basins. The basins evolved in an extensional regime during the Miocene clockwise rotation of the Tisia-Dacia block (Zweigel, 1997; Har, 2001).



compression extension

NNE - SSW - extension
 NE - SW - extension:
Neogene extensional tectonics
 (related to the Beiuș, Borod, Zarand basins)



ENE - WSW - extension,
 ESE - WNW - extension:
Neogene extensional tectonics
 (related to the Transylvanian basin)



E - W-, NE - SW - compression:
mid-Cretaceous to Lower Paleogene compression
 (related to the convergent plate movement)



Fig. 3-57: Main tectonic features of the Apuseni Mts. with mean kinematic axes. Each compressional/extensional direction has been assigned to individual regional tectonic events (see text).

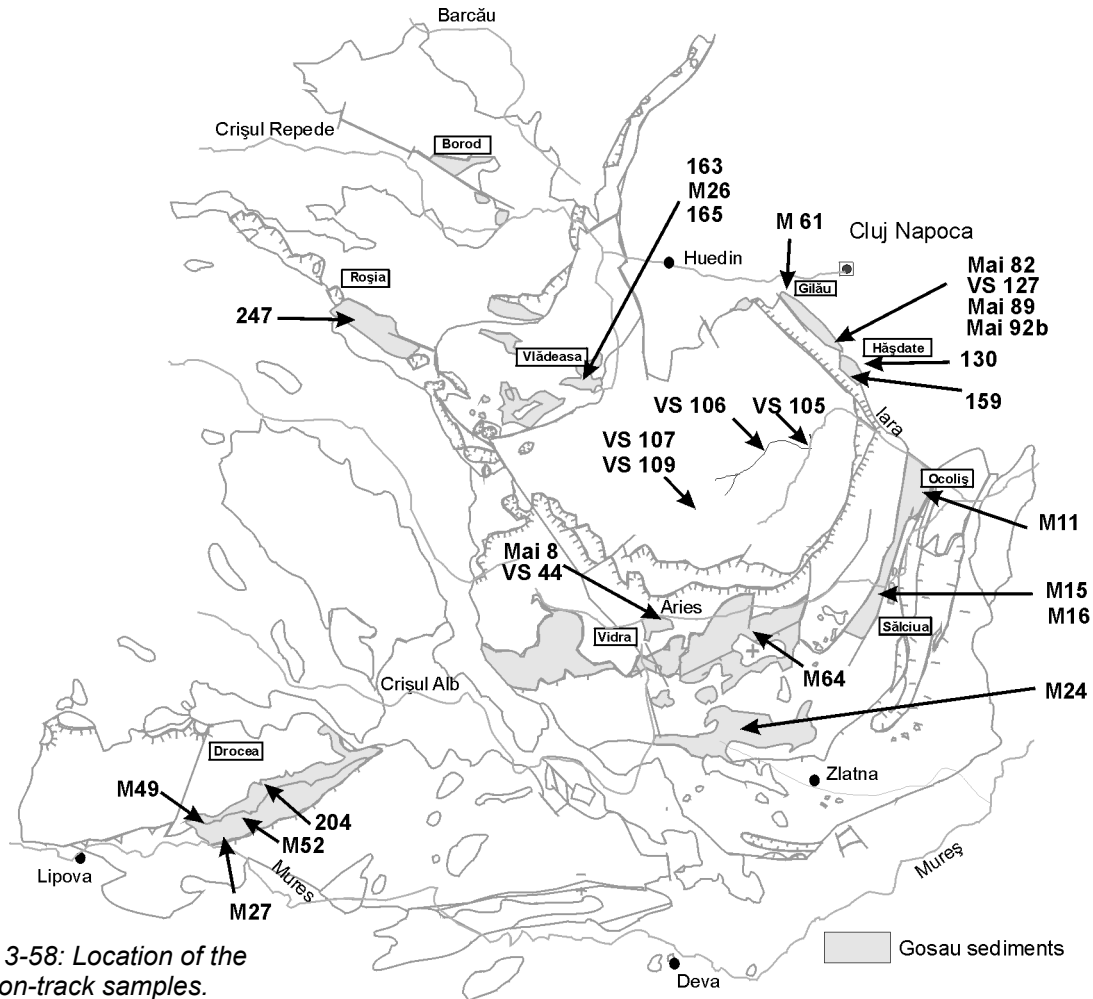


Fig. 3-58: Location of the fission-track samples.

3.5 Fission-track analysis

3.5.1 Zircon fission-track data

Samples for thermochronological investigations have been collected from the Gosau sediments and the surrounding geological units. The detrital zircon fission-track ages underwent statistical processing in order to differentiate age populations, which then can be correlated to distinct thermotectonic events. Figure 3-58 shows the location of the analyzed samples, a simplified profile with their lithologic and stratigraphic correlations is shown in Figure 3-59.

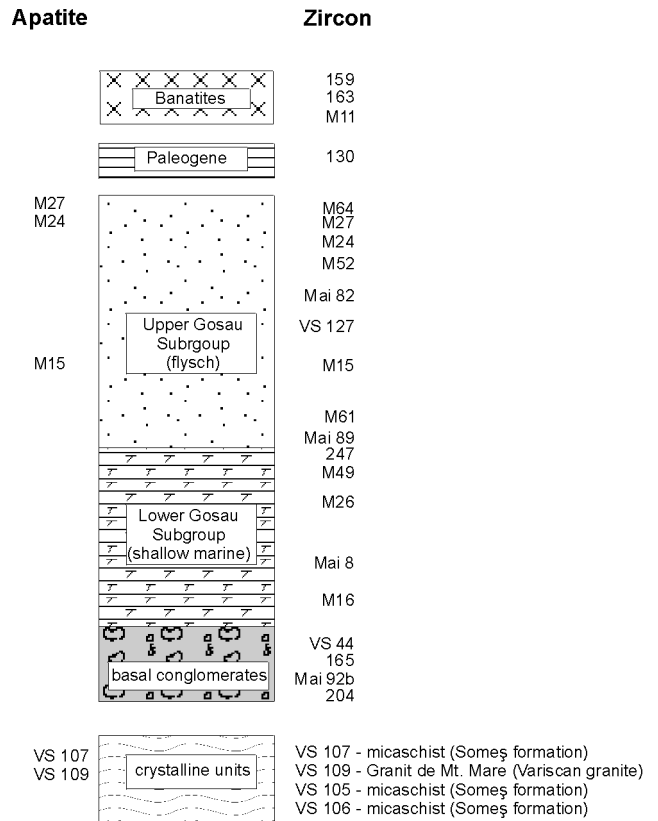


Fig. 3-59: Simplified profile with apatite and zircon fission-track sample points and lithologic/stratigraphic correlation. The samples of the Gosau succession are in stratigraphic order.

sample nr.	location	geological unit	age of sedimentation (Ma)	central age (Ma)	error (Ma)	Population error (Ma)				
						1	2	3	4	5
159	Băișoara			70.0	2.7					
163	Viădeasa	banatites		70.4	2.9					
M11	Ocoliș			64.4	2.7					
130	Linteni	Paleogene (fluvial sediments)	54	107.8	5.9	115.5	5.5	154	85.4	295.7 17.3
M64	Mușca	Upper Gosau	66	274.2	14					216.9 17.3 290.2 11.75 398.7 17.3
M24	Abrud-Zlatna	Upper Gosau	67	148.3	10.8	96.2	37.6			180.5 29.6 255.4 9.8
M27	Drocea	Upper Gosau	69	112.6	4.4	109.5	21.1	150.8	2.4	
M52	Drocea	Upper Gosau	70	149.5	8.0			139.4	13.9	171.6 34.3
M15	Sălciuma	Upper Gosau	72	110.9	7.1	79.4	9.9	134.7	52.2	
VS 127	Hășdate	Upper Gosau	78	107.7	5.3	108.2	28.4	140.8	49.5	
M26	Viădeasa	Lower Gosau	78	144.2	7.8	110.5	16.0	143.0	1.9	172.6 63.0
Mai 82	Hășdate	Upper Gosau	79	94.8	3.8	85.7	17.2	127.8	7.4	
247	Roșia	Lower Gosau	80	111.4	11.7	98.0	41.5			201.0 37.5
Mai 8	Vidra	Lower Gosau	82	99.1	4.1	93.0	17.9	133.0	19.8	
Mai89	Hășdate	Upper Gosau	83	104.6	5.1	102.1	24.0			178.0 13.0
M61	Gilau	Upper Gosau	83	128.9	7.3	85.9	5.7	122.4	9.7	170.0 69.8
VS 44	Vidra	Lower Gosau	83	102.5	5.0	97.9	22.7	152.8	11.5	
M 49	Drocea	Lower Gosau	84	166.9	10.4	89.2	0.95	128.3	3.35	216 32.9
Mai 92	Hășdate	Lower Gosau	85	106.9	5.0	85.0	10.7	129.0	14.4	
M16	Sălciuma	Lower Gosau	87	108.5	5.3	104.0	25.6			166.9 47.9
165	Viădeasa	Lower Gosau	87	91.4	3.7	91.4	3.7			
204	Drocea	Lower Gosau	89	121.4	7.0	95.7	28.2	145.6	15.8	205.8 21.1
VS 107	Muntele mare			94.9	4.7					
VS109	Băișoara Mt.			85.5	3.8					
VS105	lara valley	crystalline units		94.5	4.5					
VS106	lara valley			86.2	6.2					

Fig. 3-60: Results of zircon fission-track dating of all rock samples including the calculated age populations for the sediments (Gosau and Paleogene). Note: the euhedral crystals of the detrital zircon data sets have been deselected in the upper part of the succession (samples younger 80 Ma) to avoid rejuvenation of the populations due to banatite magmatism.

Zircon fission-track data of the banatites and the crystalline rocks

The analyzed banatite samples are hypabyssal, subvolcanic dacites and rhyolites showing a fine porphyritic texture with small phenocrysts, which proves that these rocks experienced relatively rapid cooling. Thus, it can be assumed that the difference of crystallization age and cooling age is negligible. The determined samples record ages which range from 64.4 ± 2.7 to 70.0 ± 2.7 Ma (Fig. 3-60). The results confirm published banatite ages (cf. chapter 2).

Published Ar/Ar data of the crystalline rocks of the Apuseni Mts. record hornblende and muscovite ages of ~ 300 Ma, and 120 to 190 Ma (cf. chapter 2; Dallmeyer et al., 1994, 1999). Since the closing temperature for zircon fission-track ages ($\sim 240^\circ\text{C}$) is below that of hornblende and muscovite ($490^\circ\text{--}550^\circ\text{C}$ and $\sim 350^\circ\text{C}$ resp.), the zircons show younger ages than minerals determined by the Ar/Ar method. The zircon fission-track ages of the crystalline rocks of the Bihar autochthonous unit record a narrow range of 85.5 ± 3.8 to 94.9 ± 4.7 Ma (Fig. 3-60). This shows that the analyzed rocks already cooled below approx. 240°C during Upper Cretaceous times and thus, where located in high crustal levels.

Fission-track ages of detrital zircons

The separated age populations of the detrital zircon ages are presented in Figure 3-60. The separation of each population has been made by using statistical methods. To avoid rejuvenation of the data sets due to banatite magmatism, euhedral crystals partly have been deselected before the calculation. Since the banatite magmatism is supposed to have occurred later than 80 Ma, every data set of samples with sedimentation ages younger than 80 Ma underwent this deselection process. Consequently, the resulting age populations are supposed to represent cooling ages of thermotectonic events. The effect of the deselection procedure is shown in Figures 3-61 and 3-62. Most revised data sets record higher ages for the first age population. Sample 130 for instance shows that the youngest population (79.5 Ma) completely disappears after deselection of euhedral crystals (Fig. 3-61 a and b). Thus, it has been assumed that this population is associated to the banatite magmatism. Figure 3-62-b illustrates the age populations after deselection. The regression lines slightly rise towards the samples with younger sedimentation ages.

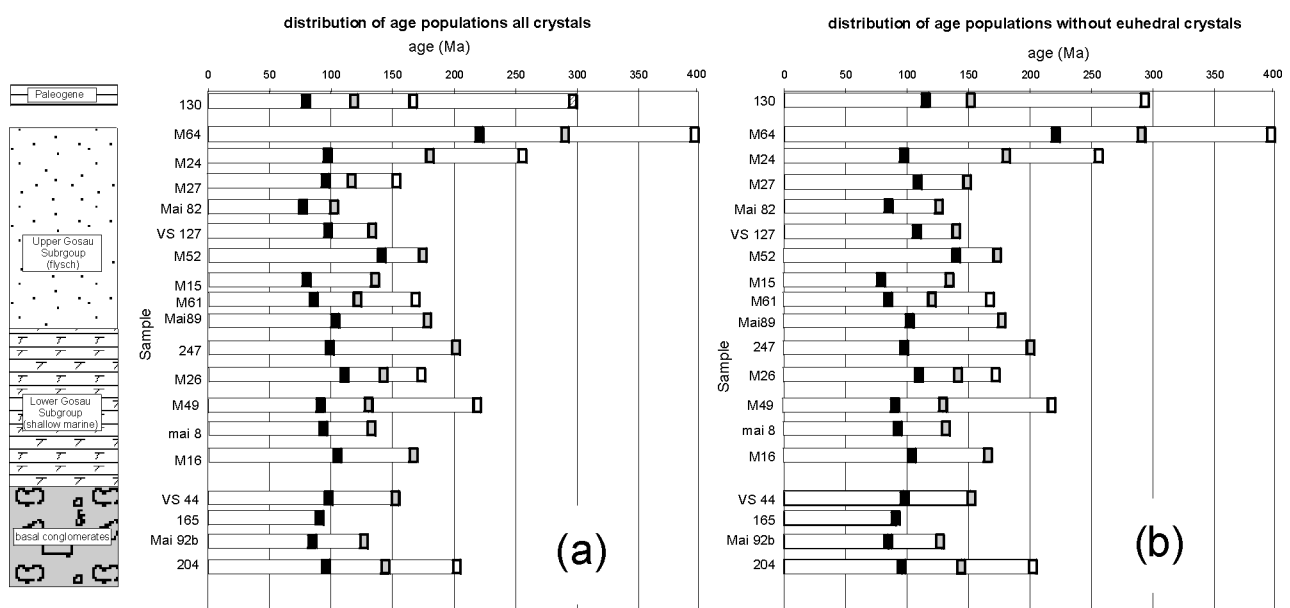


Fig. 3-61: Age populations of the detrital zircons (mean age). The first diagram (a) shows the age populations before deselection of euhedral crystals from samples with sedimentation ages younger 80 ma. The second diagram illustrates the age populations with deselected euhedral crystals.

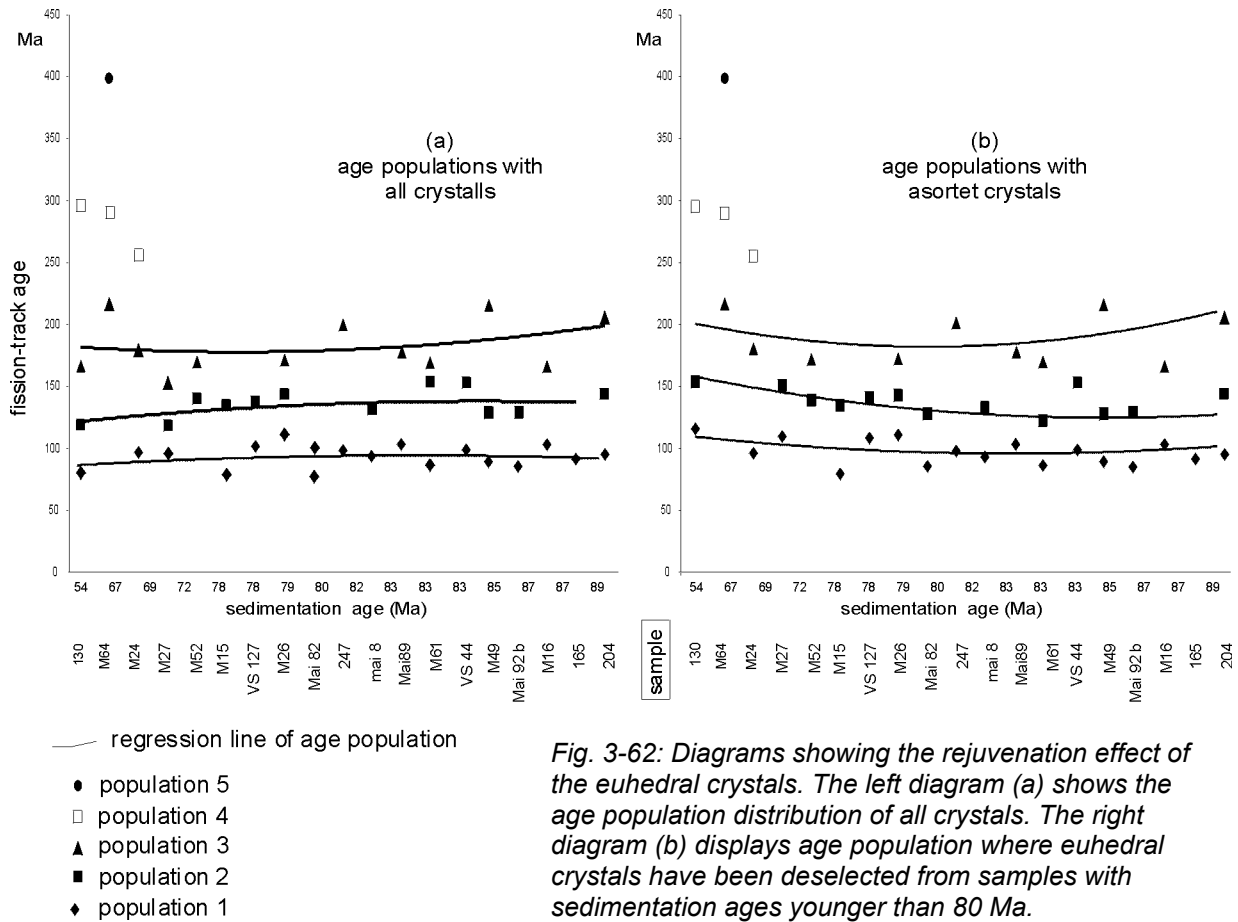


Fig. 3-62: Diagrams showing the rejuvenation effect of the euhedral crystals. The left diagram (a) shows the age population distribution of all crystals. The right diagram (b) displays age population where euhedral crystals have been deselected from samples with sedimentation ages younger than 80 Ma.

The statistically isolated age distributions of the Gosau sediments concentrate on 3 age populations: (1) 90-110 Ma, (2) 130-150 Ma and (3) 170-200 Ma (Figure 3-63). Two additional age populations, (4) and (5), isolated from the youngest samples of the Gosau deposits and from the Paleogene fluvial sandstone of the first deposits of the Transylvanian basin (Jibou formation), record ages of 250-300 Ma and approx. 400 Ma.

The first three populations show similar age ranges in all samples, irrespective of their stratigraphic position. This signifies that during the entire Gosau evolution the basin has been supplied with sediments deriving from geological units which underwent one of the first three isolated thermotectonic events. It also shows that during mid-Cretaceous time rocks with older thermotectonic overprints (population 2 and 3) have already been transported to higher crustal levels and did not undergo the thermal overprint of the first age population. Another interesting fact is the

appearance of the 4th and 5th age populations in the uppermost part of the Gosau succession and in the Paleogene sediments. Two conclusions can be made from this observation: (1) The rocks of the 4th and 5th populations did not suffer an overprint by one of the first three thermotectonic events, and thus have been situated at shallow crustal levels (above 240°C) since 250-300 Ma, and 400 Ma, respectively. (2) A tectonic event exhumed these rocks after uppermost Cretaceous time, and the ongoing uplift of the crystalline hinterland exposed them for erosion.

No age population shows systematic changes in age with respect to stratigraphic position of the sample. The flat regression lines (dashed lines in Fig. 3-63) indicate erosion of plane areas with rock units comprising uniform age characteristics.

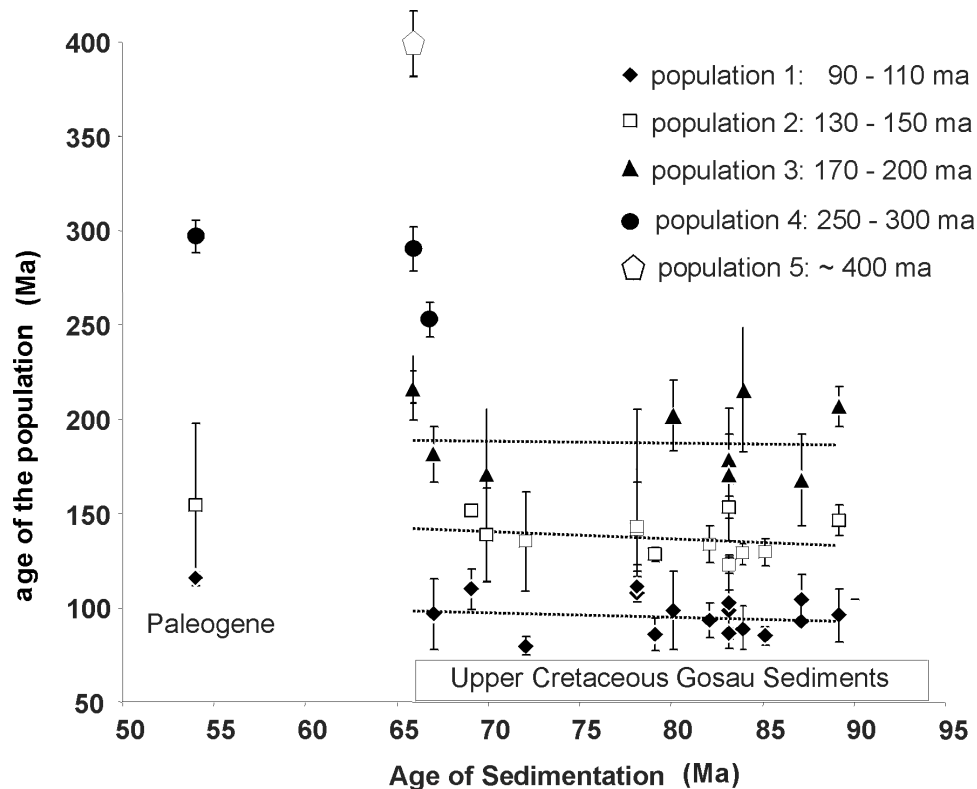


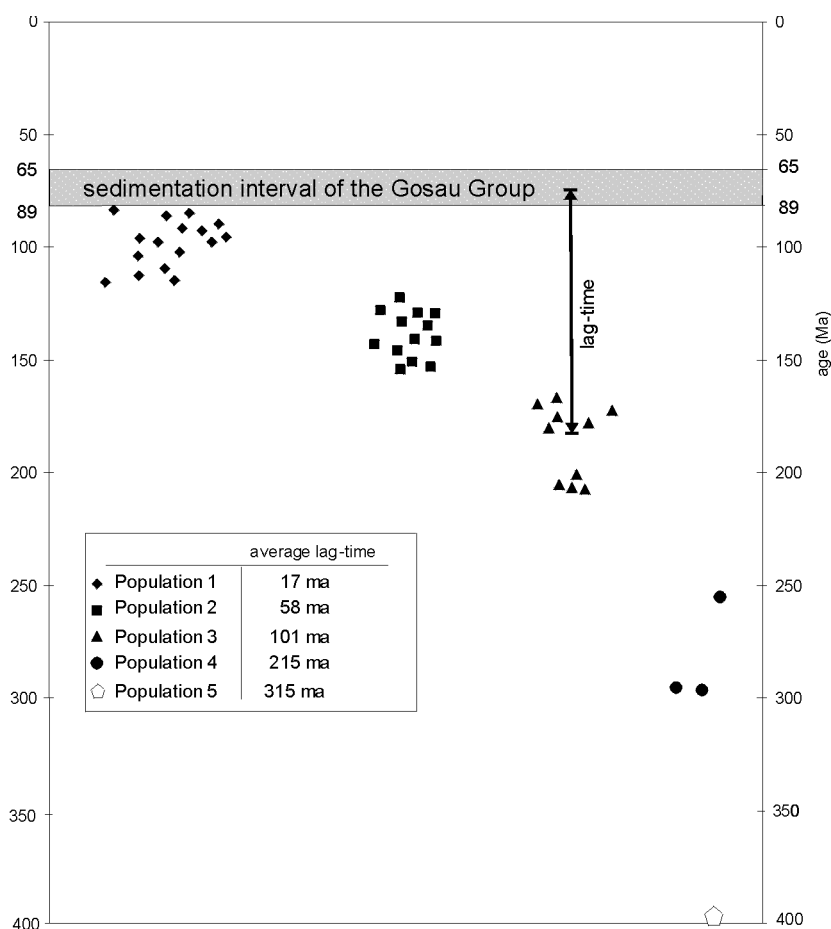
Fig. 3-63: Isolated age populations of the detrital zircon fission-track ages with correlation to thermotectonic events. Note: the Paleogene sample does not belong to the Gosau sediments.

A lag-time calculation can help to prove exhumation dynamics. The lag-time is the difference of sedimentation age and determined cooling age, and thus shows the time interval of exhumation and deposition. The lag-time was calculated for each age within each age population and for each sample. Within a profile, a successively increasing lag-time will display decreasing exhumation rates, because the time interval from zircon cooling to sedimentation increases. However, for the Gosau sediments the calculated lag-time of the first age population records a broad dispersion of 6 to 29 Ma, which does not allow a identification of successive decreasing or increasing lag-time values within the sedimentary succession (one sample has not been used for this calculation since for this sample the cooling age and sedimentation age were identical). An average of the lag-times has been calculated for each population (Fig. 3-64). A mean lag-time of 16 Ma was calculated for the first age population. This means that the rocks of this age population

needed 16 Ma for exhumation from passing the PAZ, erosion and deposition. If a geothermal gradient of 40°C/km (increased gradient due to banatite magmatism) is assumed, the rocks had passed the PAZ at 6000 m depth. This would result in an average exhumation rate of approx. 0.35 mm/a. By using the minimum and maximum lag-time values, exhumation rates scatter between 2 and 0.15 mm/a. The average exhumation rate for the other populations shows values of 0.1 mm/a (for population 2), 0.06 mm/a (for population 3), 0.03 mm/a (for population 4) and 0.02 mm/a (for population 5).

A correlation of the three isolated age populations with their inferred source rock units is difficult, due to the lack of zircon fission-track data from the Apuseni Mts.. At least the correlation of the first age population with the crystalline rocks of the Bihor autochthonous unit can be made by using the own measurements (Fig. 3-60). The correlation of zircon fission-track data with other geochronologic data can be

Fig. 3-64: Diagram illustrating age populations and lag-time. The lag-time is the difference between the cooling age and sedimentation age. It is the value for the exhumation-sedimentation time interval (x-axis arbitrary).



made as an approach only. As already mentioned above, Ar/Ar cooling ages of hornblende and muscovite should generally show higher ages, since these minerals have higher closing temperatures. Ar/Ar data (Dallmeyer et al., 1999), which scatter from 100 to 120 Ma, have mainly been measured on rocks of the Baia de Arieş Unit, a subunit of the Biharia Unit (Fig. 2-2, 2-3), and on mylonites of the Bihor autochthonous unit. These ages can be correlated with the 1st population (90 – 100 Ma) of the zircon fission-track ages. Ar/Ar ages that scatter from 120 to 216 Ma have been determined on rocks of the Biharia Unit and the Someş Unit (the latter is a metamorphic subunit of the Bihor autochthonous unit). These rocks can roughly be assigned to the 2nd and 3rd population. A distinct correlation can not be made, since both units record ages that scatter from 120 to 216 Ma. The Codru Unit – the lowermost nappe complex of the Apusenides (Fig. 2-3) - generally records Ar/Ar ages above

330 Ma. Also parts of the Bihor autochthonous unit record this time range. These ages can be correlated with the 4th and 5th age population of the detrital zircons. Consequently, this means that the Codru nappe complex and at least parts of the Bihor autochthonous unit have been exhumed above the PAZ in the Late Paleozoic, but firstly exposed for erosion in the uppermost Cretaceous, since no other older samples of the sedimentary succession contain zircons of the 4th (250 to 300 Ma) and 5th (~ 400 Ma) age populations.

Although a clear correlation of each age population with its supplying source rocks can not be made, they can be associated with thermotectonic events, which are known from other geochronological data:

- 1- The 1st age population (90 - 110 ma) is assigned to the mid-Cretaceous tectogenesis which led to the nappe emplacement of the Transylvanides and the Apusenides. Dallmeyer et al.

- (1999) came to the same conclusion based on Ar/Ar thermochronology.
- 2- The 2nd age-population (130 – 150 Ma) can be correlated with the Upper Jurassic compressive tectonic and obducting processes within the Vardar ocean, on the northern margin of the Apulian and the southeastern margin of the Tisia block (Săndulescu, 1984). The compressional structures of the Upper Jurassic tectonics are known from the middle and external Dacides of the Southern and Eastern Carpathians (Săndulescu, 1984). Based on Ar/Ar data, Dallmeyer et al. (1999) detected an Upper Jurassic thermotectonic event in the Apuseni Mts.. The authors interpret these data as an effect of regional diachronous tectonism and resetting. They correlate this thermotectonic event also with an Upper Jurassic blueschist metamorphism known from the Western Carpathians.
 - 3- The 3rd age population (170-200 Ma) is assigned to the extensional tectonics in the Lower to Middle Jurassic, which was accompanied by crustal thinning, rifting and formation of oceanic crust of the Transylvanian ocean. The increasing temperature and lifting of the PAZ to shallow crustal levels resulted in total annealing of the zircon fission tracks and resetting of the ages.
 - 4- The 4th and 5th age populations (250-300 Ma, ~400 Ma) can be correlated with the pre-Variscan tectogenesis and/or Late Variscan magmatism, the latter of which has its witness in the Muntele Mare granite of the Bihor autochthonous unit. This thermotectonic event is also recorded by Ar/Ar data from the Apuseni Mts. (Dallmeyer et al, 1999).

Lack of fission-track data from the Gosau sediments of the Eastern Alps hampers comparison with the Apuseni Mts. in this respect. Nevertheless, a comparison of the obtained results is possible, since thermotectonic events within the Eastern Alps are well defined. Three Mesozoic thermotectonic events of similar age are also known from the Eastern Alps. The

mid-Cretaceous tectonics of the Eastern Alps led to nappe emplacement in the external parts of the Northern Calcareous Alps (NCA). This would coincide with the first age population, respectively thermotectonic event. The second age population would correlate with the Upper Jurassic nappe emplacement in the internal parts of the NCA (e.g., Hallstatt unit) on the southern border of the Austroalpine mega-unit (Frisch & Gawlick, 2003). A thermal heating period during crustal thinning and rifting processes (due to the opening of the Penninic ocean) is proposed to have occurred in the Austroalpine realm during Upper Triassic to Lower Jurassic times (Dunkl, 1999). The third age population from the Gosau sediments of the Apuseni Mts. is proposed to derive from rocks which underwent a similar tectonothermal evolution in an equivalent geodynamic frame. The oldest age populations are related to Variscan orogenesis which is known in both, the Eastern Alps and the Apuseni Mts..

3.5.2 Apatite fission-track data

Apatite fission-track data of the Gosau succession

Three samples for detrital apatite fission-track analysis have been collected from three distant points in the Gosau sediments (Fig. 3-65). The main purpose was to prove whether possible thermal overprint after sedimentation could have caused shortening or annealing of the spontaneous tracks and thus resetting of the cooling ages. It was suspected that the Late Cretaceous to Early Paleogene compressive tectonics could have been responsible for age resetting. Since the compressive structures are only known from the southern and eastern parts of the Apuseni Mts., the samples were collected in this area. Figure 3-66 displays the results. The data of each sample passed the chi-square test ($P > 20\%$), indicating that the detrital apatites within each sample belong to one age population. The ages vary between 71.2 ± 4.0 and 81.0 ± 3.9 Ma. None of the measured samples records age resetting, since their

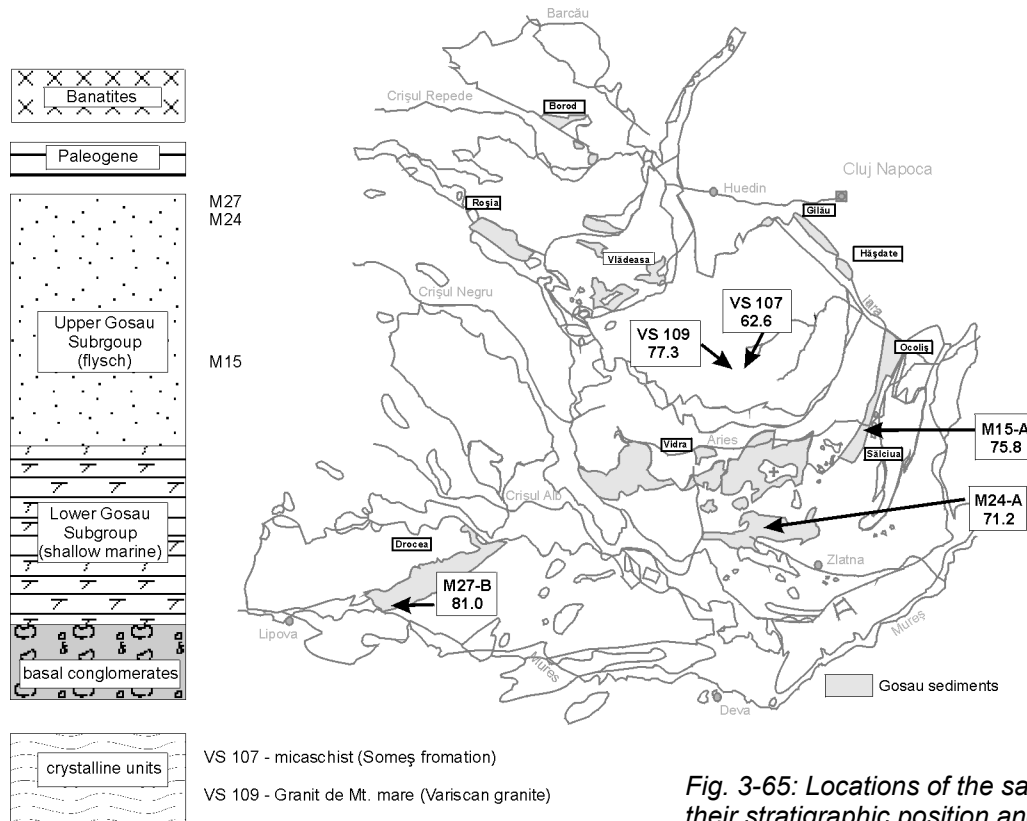


Fig. 3-65: Locations of the samples with their stratigraphic position and apatite fission-track ages in Ma.

sedimentation ages are younger than the measured cooling ages (Fig. 3-66). The relative short lag-time (average 6.6 Ma) indicate that the apatite crystals mainly derive from banatites. The result proves that the Late Cretaceous to Paleogene compressive tectonics (“Laramian tectogenesis” after Balintoni, 1997) did not have detectable thermal effects on the apatite ages. Although strong compressive structures can be found in all Gosau occurrences in the Southern and Eastern Apuseni Mts., this tectonics did not cause

large-scale-thrusting. Since the closing temperature of apatite lies around 100°C, even thin skinned thrusting would at least cause partial annealing of the fission tracks, and thus rejuvenation of the ages. Consequently it can be concluded that the Late Cretaceous to Early Paleogene tectonics in fact led to intensive shortening, faulting, folding and steep out-of-sequence-thrusting, but regional nappe stacking and large scale thrusting can be excluded.

sample nr.	location	geological unit	age of sedimentation (Ma)	central age (Ma)	error (Ma)
M24	Abrud-Zlatna	Upper Gosau	67	71.2	4
M27	Drocea	Upper Gosau	69	81	3.9
M15	Sălcuia	Upper Gosau	72	75.8	3.8
VS 107	Bihor	Variscan granite		62.6	3.5
VS109	autochthonous - crystalline units	Someș unit		77.3	4.3

Figure 3-66: Results of apatite fission-track dating. Note: the samples belonging to the Gosau sediments did not experience thermal overprint after sedimentation.

Apatite fission-track data of the crystalline rocks and thermal modeling

Two crystalline rock samples were collected for apatite fission-track processing. Both sample points are situated in the Bihor autochthonous unit (elevation: ~1500 m. asl). The first sample was taken from a Variscan granite (Muntele Mare granite). The second is a micaschist from the Someș unit. The cooling ages record values of 62 ± 3.5 and 77 ± 4.3 Ma (Fig. 3-66), which is corroborated by apatite fission-track data of Sanders (1998).

On sample 107, confined track lengths were measured in order to perform thermal modeling and to reconstruct the exhuming history. For explanation concerning the modeling method, see Appendix. The result of the modeling is presented in Figure 3-67. The following time/temperature pattern is visible:

- During the Upper Cretaceous slow cooling is identified.
- Modeling indicates a rapid cooling phase, which starts immediately after the Mesozoic/Tertiary boundary (65 Ma) and ceases approximately at 55 Ma (Paleocene/Eocene boundary).
- The following thermal evolution shows

a relaxation within the Bihor autochthonous unit from Eocene to Middle Miocene time.

- A second phase of increased cooling started in the Middle Miocene.

The presented model is in line with published data. Sanders (1998) performed apatite modeling on 6 samples of the Bihor autochthonous unit, which all show similar cooling patterns as the one described above, with low cooling in the Upper Cretaceous and rapid cooling in earliest Tertiary time; some samples, however, record a start of increased cooling rates in the Upper Cretaceous, between 70 and 80 Ma.

Own thermal modeling shows low exhumation rates during Upper Cretaceous, i.e. the sedimentation time of the Gosau sediments. Since the Upper Gosau Subgroup records the highest sedimentary input, an increased exhumation rate in the source area would be expected during the Maastrichtian. Based on the data of Sanders (1998), with increased cooling rates after 80 Ma, this contradiction can be solved: A low exhumation rate in the hinterland during the sedimentation of the Lower Gosau Subgroup was followed by a rapid exhumation, probably with regional

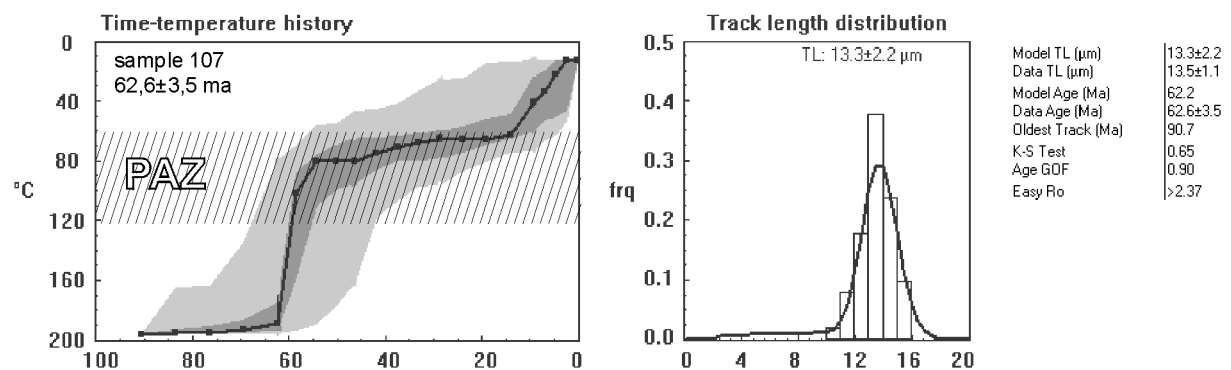


Fig. 3-67: Modeled thermal history from apatite fission track lengths of the Bihor autochthonous unit. The modeling was performed with AFTSolve® by using the "unsupervised search style". The left diagram displays the time/temperature path, the right one shows the frequency distribution of the measured confined track lengths. The light gray envelope (left diagram) comprises acceptable thermal paths, dark gray includes paths with good fit and black line represents the best fit (Ketcham et al., 2000). The PAZ (Partial Annealing Zone) illustrates the zone in which confined track experience shortening.

asynchrony. The rapid exhumation started between 70 and 80 Ma and was accompanied by rapid basin subsidence, which produced vast accommodation space for the eroded material and the deposition of the Upper Gosau Subgroup (cf. basin modeling based on vitrinite reflectance, chapter 3.3.). Change in heavy mineral spectra is in line with an uplift in the source area during deposition of the Upper Gosau Subgroup, reflecting increasing amount of minerals deriving from deep crustal levels (cf. chapter 3.2).

The rapid cooling of the crystalline rocks of the Bihor autochthonous unit during the uppermost Cretaceous to Early Paleogene indicates strong tectonic activity with increased exhumation rates. This correlates with the Early Tertiary compressive tectonics and the Paleocene sedimentary hiatus in the Apuseni Mts. and on the borderline to the Transylvanian basin. The following Upper Paleogene to Middle Miocene relaxation phase is accompanied by tectonic quiescence, which is also recorded by the shallow marine deposits of the Transylvanian and Pannonian basins. The Late Neogene exhumation is probably related to the block arrangement within the Carpathian bay (cf. chapter 1; Csontos, et al., 1992; Zweigel, 1997). The lateral drift of the Tisia-Dacia block along the northern border of the Moesian platform and the southern border of the ALCAPA block (Fig. 1-3) was probably accompanied by transpressive movements which caused regional uplift and exhumation within parts of the Tisia-Dacia block.

4. Interpretation and discussion

4.1. Evolution of the Gosau basin in the Apuseni Mts.

The evolution of the Gosau basins of the Apuseni Mts. can be reconstructed as follows:

Sedimentation started diachronously after the Late Turonian with a successive time shift from southwest to northeast. Conglomerates, sandstones, marls and limestones were deposited in a shallow marine basin. Heavy mineral spectra and paleocurrent data indicate sedimentary transport from both sides of the elongated basin. During this sedimentation period – Lower Gosau Subgroup – the basin experienced slow subsidence with low sedimentation rates.

Rapid subsidence accompanied by deep marine turbidite deposition occurred after Lower Campanian time. The onset of the second sedimentation period – Upper Gosau Subgroup – does not show the same diachronous pattern as recorded for the initial sedimentation of the Lower Gosau Subgroup. However, subsidence occurred asynchronously and scatters from Lower Campanian to Lower Maastrichtian. Continuous deep water sedimentation within the Upper Gosau Subgroup reflects ongoing basin subsidence. Basin modeling based on vitrinite reflectance data indicates a sedimentary fill of up to 3000 m of deep marine sediments (Fig. 3-50).

Heavy mineral and paleocurrent data prove the erosion of montaneous areas on both sides of the basin. This is also indicated by olistoliths and conglomerate pebbles within the Upper Gosau Subgroup. Subduction-related calc-alkaline magmatism started in the Apuseni Mts. after the Lower Campanian. Some heavy mineral associations record increasing amounts of minerals deriving from magmatic rocks (e.g. Sălciua-Ocoliș, Vidra, Vâldeasa).

Basin subsidence within the Upper Gosau Subgroup was accompanied by exhumation of the crystalline hinterland. The change within all heavy mineral

spectra reflects increasing regional exhumation of metamorphic units.

Fission-track data from detrital zircons record five age populations. Thus, five rock complexes, each with different thermal overprint, have been eroded. Apatite fission-track data show increasing exhumation of the autochthonous basement at the Cretaceous/Tertiary (K/T) boundary, which is explained by the compressive tectonics at this time (Fig. 3-67). Outcrop data suggest syn-sedimentary compressive tectonics, which reached its climax at the K/T boundary and terminated the sedimentation of the Gosau basin.

During the Upper Cretaceous, apart from the Gosau depositional area deep marine sediments have been deposited in a trench basin outside of the active orogenic wedge (Bozeș flysch, Fig. 3-54), reflecting continuous subduction syn-chronously to the Gosau sedimentation.

4.2. Geodynamic model

Based on own data, literature data and comparisons to basin evolutions in similar regional settings, a model for the formation and the geodynamic evolution of the Gosau basins of the Apuseni Mts. is proposed. The following paragraphs describe the geodynamic evolution of the Tisia and Dacia blocks from Early Cretaceous to Neogene time. Please note that the coordinates consider the Middle Miocene approx. 90° clockwise rotation.

The nappe emplacement of the Austrian Transylvanides and the Apusenides (in this order; cf. Fig. 2-1, 2-2) was a consequence of the compressive regime during the Early Cretaceous. Nappe stacking migrated from north (Austrian Transylvanides: presently in the east of the Apuseni Mts.) to the south. The Austrian Transylvanides (uppermost and oldest nappes) are proposed to be obduction nappes (Săndulescu, 1984). The lowermost and tectonically youngest is the Codru nappe unit (Balintoni, 1997). Nappe stacking occurred south-vergent

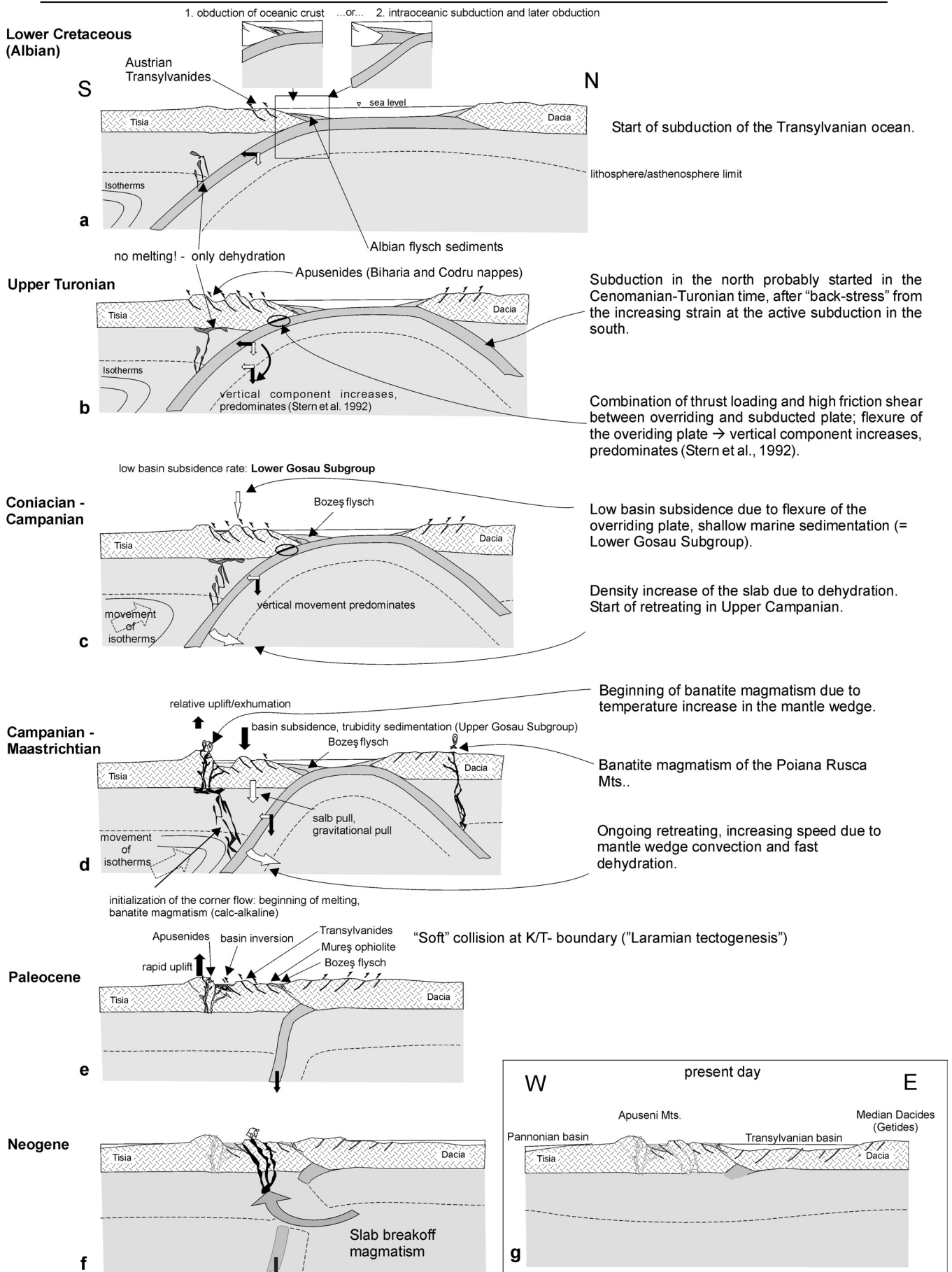


Fig. 4-1: Geodynamic model for the subduction of the Transylvanian ocean and the collision of the Tisia and Dacia microplates. Note: due to the Miocene rotation of the Tisia-Dacia block, the present day coordinates are E-W (g).

and thus, was opposite to the subduction polarity. The age of the nappe emplacement is not restricted to what is the so-called „Austrian“ or „pre-Gosauan“ orogenic phase, but to a long term compressional event during Lower to early Upper Cretaceous times. K/Ar ages of metamorphic rocks of the Biharia Unit record a plateau age of about 110 Ma (Dallmeyer et al., 1994, 1999). The Codru Unit (the lowermost nappe unit) does not record an Alpine metamorphic overprint (Dallmeyer et al., 1994, 1999). This signifies that tectonic forces were rather moderate, which can be explained by relative short nappe transport distances and steep thrust planes within the Apuseni nappe complexes.

The subduction of the Transylvanian /South Penninic ocean presumably started in Albian time. The first flysch sediments are recorded in Upper Aptian time. Upper Albian coarse grained sandstones and conglomerates within this flysch deposits reflect the onset of subduction.

The subduction onset was forced by the northward push of the Adriatic microplate. The young and hot oceanic crust was forced to an intra-oceanic subduction or to obduct parts of it onto the overriding plate (Fig. 4-1-a). An intra-oceanic subduction was suggested by Winkler (1996) and Wagneich (2000, 2001; Fig. 4-2) for the initial subduction of the South Penninic ocean beneath the Austroalpine basement in the Eastern Alps.

After the start of the subduction, the

compressional regime is likely to have decreased. Coarse-grained turbiditic flysch sediments were deposited in front of the active continental margin (Albian). During this short period the transgression extended into the inner parts of the Apuseni Mts., respectively south of the Austrian Transylvanides.

Because of the young and hot oceanic crust, the subduction speed decreased in the Upper Albian due to increasing frictional shear at the contact between the subducting and the overriding plate (Stern et al. 1992; Fig. 4-3). This scenario explains the uplift in the inner parts of the Apuseni Mts., where no Cenomanian sediments have been deposited. On the other hand: in front of the nappes (presently southeast and east of the Apuseni Mts., e.g. Bozeş flysch, there is an ongoing sedimentation throughout the Lower and Upper Cretaceous (equivalent to the Piemonte flysch in the Eastern Alps; Oberhauser, 1995).

Due to a combination of thrust loading and high frictional shear between the overriding and subducting plate (Stern, 1999; Fig. 4-1-b), a flexure of the overriding plate initiated subsidence within the upper plate in Upper Turonian time. This subsidence created the first accommodation space for the Lower Gosau Subgroup (Fig. 4-1-c). Stern et al. (1999) describe this process on the example of the Wanganui basin from New Zealand. The authors show that after a certain stress accumulation between the upper and lower plate a flexure of the upper plate will occur, together with a shift in the stress vectors of the subducted slab.

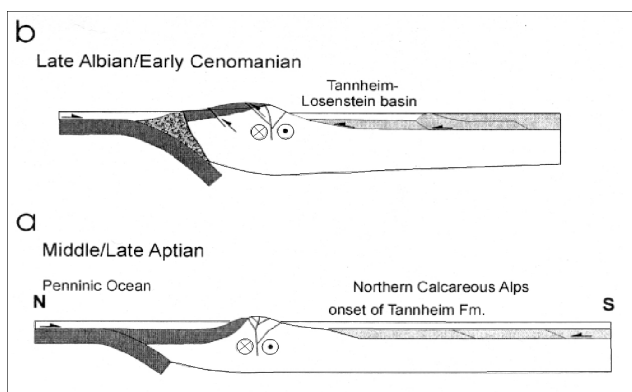


Fig. 4-2: Model of the Austroalpine intra-oceanic subduction (a) and later obduction (b) of Penninic oceanic crust proposed by Wagneich (2000). The oblique subduction is accompanied by transpression, thrusting in the frontal parts of the NCA and evolving of the Tannheim and Losentein basin.

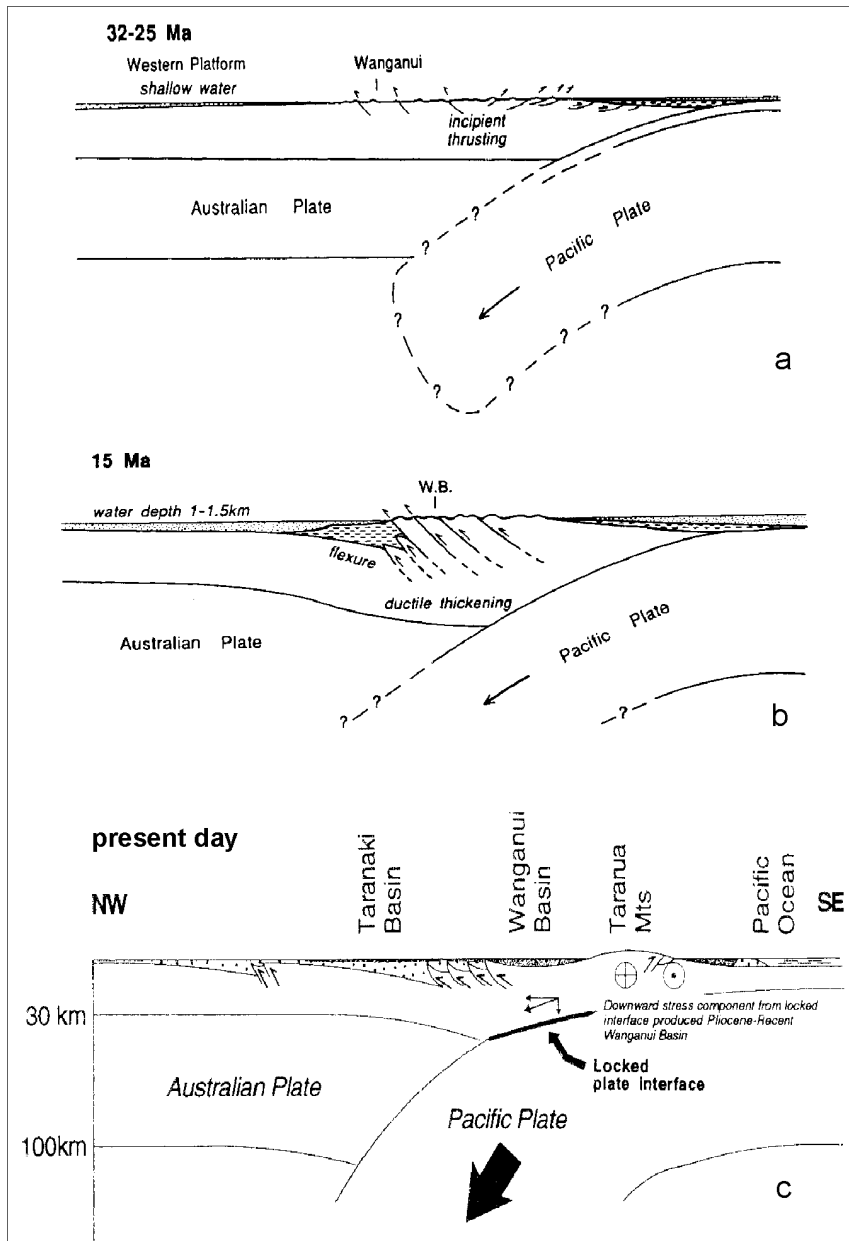


Fig. 4-3: Plate tectonic model for the forming of the Wanganui basin (New Zealand) proposed by Stern et al. (1992; Holt & Stern, 1994). The initial subduction is accompanied by thrusting (a). Crustal thickening and ongoing thrusting increases the "stress" along the overriding and subducting plate (b). This results in a locked plate interface and an increasing downward stress and slight basin subsidence due to the flexure of the overriding plate. The present day situation of the Wanganui basin is comparable with the initial sedimentation stage of the Gosau basin (Figures modified after Stern et al., 1992; Holt & Stern, 1994).

The vertical component increases, predominates, and forward movement of the subducted slab ceases. This situation was valid throughout the sedimentation of the Lower Gosau Subgroup and was characterized by moderate subsidence rates.

During this time the subducted slab dehydrated, but melting of upper mantle material was hampered by missing mantle wedge convection because of a low subduction angle. Thus, melting temperatures were not reached. Dehydration and eclogitization of the slab caused an increase of its density. The predominant vertical movement vector together with the

successive density increase of the subducted slab resulted in a prevailingly vertical movement of the slab. The necessary space for the installation of a mantle wedge convection was now available, thus hot material (cf. isotherms in Fig. 4-1) moved towards the wedge and started melting in the upper mantle. This resulted in the first intrusive and extrusive rocks of the calc-alkaline banatite magmatism (Fig. 4-1-d). The combination of these processes led to a positive feedback: downwarping and steepening of the slab caused enhanced cornerflow in the mantle wedge, which caused better dehydration, followed by faster sinking of

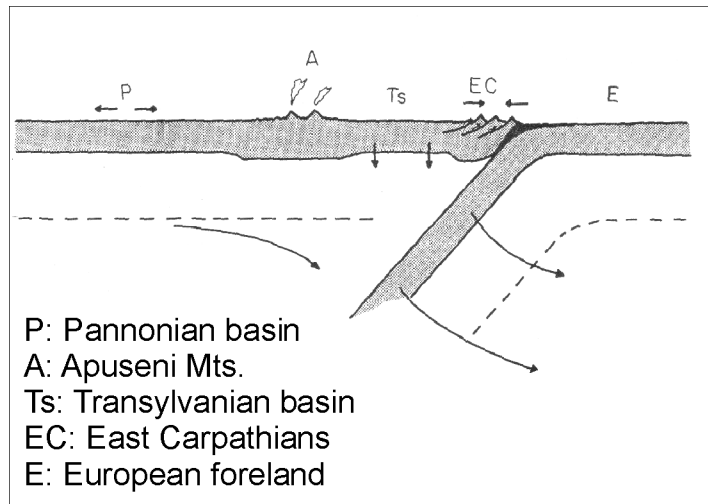


Fig. 4-4: Proposed model for slab rollback and retreating subduction for the Eastern Carpathians (Burchfiel & Royden, 1982). The subsidence in the Transylvanian basin (Ts) is a consequence of a "suction process" in order to fill the space formerly occupied by the downbending subducting plate. Note: the authors indicate that the Neogene magmatism of the Apuseni Mts. is related to subduction. This is in contradiction to the fact that Neogene magmatism is calc-alkaline and alkaline.

the slab, which intensified the heatflow in the mantle wedge etc.. As a result, the subduction type changed to a retreating type of subduction, where slab pull is the main controlling force of the subduction process (Burchfiel & Royden, 1982; Royden, 1993; Fig. 4-4). Retreating subduction is always accompanied by subsidence in the upper plate caused by "the downward pull and temporary suction from the downbending plate" (Burchfiel & Royden, 1982; Royden, 1993). This rapid and strong subsidence created the accommodation space for the deep water turbiditic sequences of the Upper Gosau Subgroup.

A crucial role in this model is attributed to the calc-alkaline basaltic magmatism, as its generation is still a subject of debate. With this model the magmatic activity starting about 20-30 Ma later than the initiation of the subduction can be reasonably explained (zircon age of subcrustal sills 70-75 Ma).

The northward subduction of oceanic crust probably started in Turonian/Cenomanian time after back-stress from increasing strain at the plate boundary between the Tisia block and the oceanic crust in the south (Fig. 4-1-b). As proposed by Burchfiel (1980), this scenario is able to explain the generation of the calc-alkaline magmatism within the Dacia block (Poiana Rusca Mts., South Carpathians; Fig. 4-1-d).

The collision of the two continental plates (Tisia and Dacia) occurred around the Cretaceous/Tertiary (K/T) boundary (Fig.

4-1-e). The last sedimentary record is from the Upper Maastrichtian. No sediments were deposited in the Apuseni Mts. until the Early Eocene, showing general erosion of this area during Paleocene times. As a characteristic for retreating subduction (Burchfiel & Royden, 1982; Royden, 1993), the following collision was weak, causing reverse faults but no large-scale thrusting (e.g. out of sequence thrusting). Apatite fission track analysis do not show Lower Tertiary overprint, although the samples have been collected from parts of the Upper Cretaceous basins where intensive faulting and folding is recorded. The tectonics around the K/T boundary is commonly described as "Laramian tectogenesis"; in this work the term "Early Tertiary tectogenesis" will be used (cf. chapter 2).

An additional implication of this model is that it is able to explain the Neogene magmatic activity in the Apuseni Mts.. As also proposed by Seghedi et al. (1998), the generation of the Neogene magmatism can be related to slab breakoff a subducted oceanic crust. Although the time gap between the collision and the magmatic activity of about 50 Ma is relatively long, the total detachment of the slab of the subducted Transylvanian ocean is able to explain the generating of breakoff-related magma.

The present situation is shown in profile (Fig. 4-1-g). The Transylvanian basin covers most of the Mesozoic basement of the Dacia block. The Median Dacides (Săndulescu, 1984; Getides after

Balintoni, 1997) exposed in the Eastern Carpathians are the easternmost nappes of the Dacia block. The Middle Miocene 90° clockwise rotation results in the orientation of the coordinates as shown in Figure 4-1-g.

Brief summary of the evolutionary stages:

- Upper Albian: start of the subduction, relaxation on the continental margin, transgressive onlap onto the active continental margin.
- Cenomanian: increasing of frictional shear between the subducting and overriding plate, uplift of the upper plate (no Cenomanian sedimentation on continental crust).
- Upper Turonian/Lower Coniacian: flexure of overriding plate, subsidence: Lower Gosau sedimentation.
- Campanian/Maastrichtian: change to retreating subduction, high subsidence rate: Upper Gosau sedimentation, calc-alkaline basaltic magmatism.
- K/T boundary: soft collision.
- Neogene: slab breakoff (Neogene magmatism).

4.3. Discussion

Several models have been proposed for the Mesozoic geodynamic evolution of the Gosau basins of the Eastern Alps and the Apuseni Mts.. A comparative discussion should help to support the model proposed in this study.

One distinct feature of the Gosau basins of both orogens is the rapid subsidence marked by the onset of the deep sedimentation phase, which did not cease until the final closure of the basin. The model of Wägreich (1994, 1995; Fig. 4-5) proposes the subduction of an oceanic high (e.g. ocean ridge), which caused subduction erosion. The oblique convergence of the two plates resulted in a diachronic subduction of this oceanic high. Thus, the change from shallow marine (Lower Gosau Subgroup) to deep marine sedimentation (Upper Gosau Subgroup) shifted from west to east. In the Apuseni Mts. no clear shift of facies can be identified. Although a shift for the initial (Lower Gosau) sedimentation is recorded,

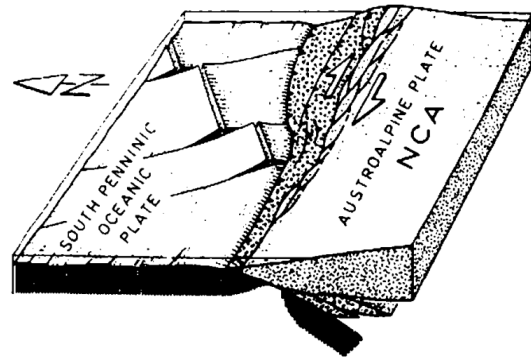


Fig. 4-5: Model of the oblique subduction of the South Penninic ocean with subcrustal erosion due to subduction of an intra-oceanic high (disected ridge). The oblique subduction resulted in a diachronous subsidence within the overriding austroalpine plate (Wägreich, 1995).

the change from shallow to deep marine sedimentation does not show any significant lateral shift. Thus I can not support the model of subduction of an oceanic high, whose existence can not be proven anyhow.

The collision of the two plates (Tisia and Dacia) and the final closure of the Transylvanian ocean is proposed by Săndulescu (1984; Fig. 4-6) and Neubauer (2002) to have occurred during the mid-Cretaceous. Following their model, the thick Upper Cretaceous sediments on the outer side of the orogenic wedge (east and southeast of the Apuseni Mts., eg. Bozeş flysch) are only explainable as parts of intramontaneous basins, which have deposited after the collision of the two continental plates. However, boreholes throughout the Transylvanian basin record thick Upper Cretaceous successions (Ciupagea et al., 1970; Ștefănescu 1985; Ciulavu & Bertotti, 1994). Upper Cretaceous deposits are also known from some outcrops in the Outer Transylvanides (Median Dacides after Săndulescu, 1984) in the Eastern Carpathians. This would result in a Upper Cretaceous sedimentation area of approx. 350 km in diameter (also keeping in mind the shortening at the K/T boundary), which is not realistic for the deep marine Gosau basin. In the concept of Neubauer (2002), the mid-Cretaceous continental collision was followed by slab breakoff in the Upper

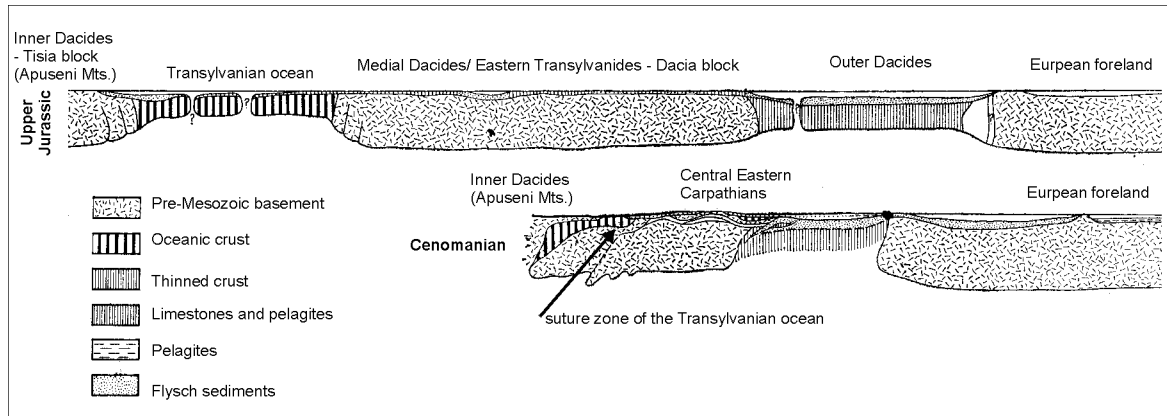


Fig. 4-6: Geotectonical evolution of the Carpathian-Transylvanian-Apuseni area after Săndulescu (1984). Note: closure of the Transylvanian ocean is proposed to have happened in Cenomanian time.

Cretaceous, which was responsible for the generation of the banatite magmatism.

Lupu et al. (1993; Fig. 4-7) propose that the ophiolitic rocks in the South Apuseni Mts. have been formed in a back arc basin during the Late Jurassic. The oceanic crust of the back-arc basin has been subducted in the Early Cretaceous leading to the collision of a magmatic arc with the Tisia block in mid-Cretaceous time and the nappe emplacement in the Apuseni Mts.. However, it can not be understood why the warm oceanic crust of the back-arc basin is subducted, and not the older and relatively cooler oceanic crust of the Transylvanian ocean. The ongoing subduction of the Transylvanian ocean in front of the proposed island arc is able to compensate the compressive regime which is assumed as the force initiating the subduction of the oceanic back-arc crust. The ophiolites of the South Apuseni Mts. are more likely a result of obduction during the subduction process. Additional arguments against the model of Lupu et al. (1993) are (1) that the Austrian Transylvanides include parts of continental crust comparable to those of the crystalline basement of the Bihor and Biharia units and (2) that back-arc ophiolites can not be found in-between the Austrian Transylvanides and the Apusenides (cf. Fig 2-1, 2-2). Therefore the Austrian Transylvanides are part of an active continental margin rather than an island arc.

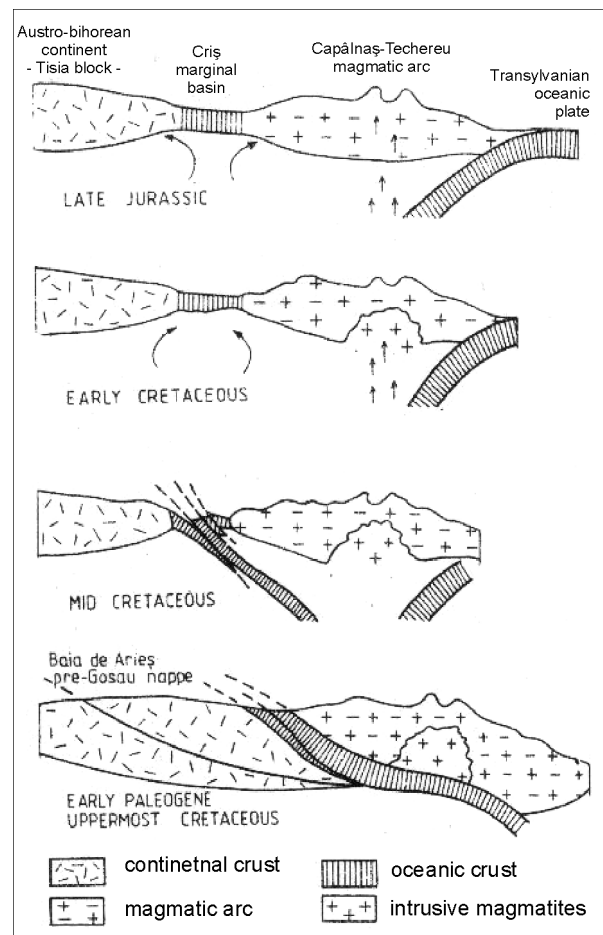
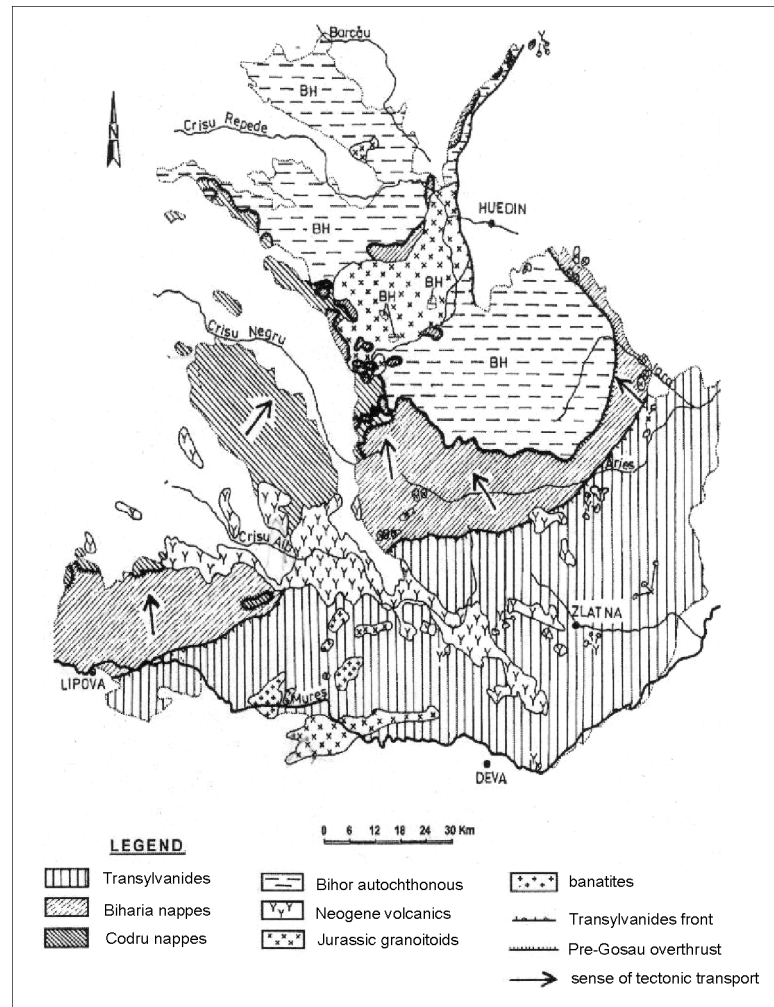


Fig. 4-7: Geodynamic model of the southern rim of the Tisia block considering a magmatic arc evolution, proposed by Lupu et al. (1993).

Fig. 4-8: Tectonic nappe transport directions of the Apuseni Mts., after Balintoni (2002).

Concerning the Austrian Transylvanides, Balintoni (2002; Figure 4-8) adopts the model of a back-arc basin proposed by Lupu et al. (1993). He furthermore points out that the Codru nappe unit was formed during a compressional regime in which nappe transport direction differs 90° (in some regions) from that of the Transylvanides and the Biharia Unit. He proposes that the Codru nappe is the nearest to the Meliata ocean and therefore should be transported from south to north. This assumption implies that nappes have been transported from south (Meliata ocean) and from north (respectively east in present coordinates) from the Transylvanian/South Penninic ocean. This would infer a difference in the transport direction of 180°, but it is still a point of discussion.



Emphasis of the main arguments

The low basin subsidence followed by the rapid subsidence is a consequence of the change from high-strain subduction to retreating subduction, latter which is also responsible for the generation of calc-alkaline magmatism. The Gosau sedimentation and simultaneous deposition of deep marine sediments into a trench basin ceased due to continental collision at the Cretaceous /Tertiary (K/T) boundary. Slab breakoff the subducted oceanic crust is responsible for the Neogene magmatism.

The proposed model explains:

- the low subsidence during the Lower Gosau Subgroup sedimentation
- the high subsidence during the Upper Gosau Subgroup sedimentation
- the ongoing deepwater sedimentation throughout almost the entire Cretaceous over a large area in front of the orogen (comparison to Piemont flysch in the Eastern Alps)
- the calc-alkaline banatite magmatism
- tectonics at the Cretaceous/Tertiary boundary
- the Neogene magmatism

5. Conclusions and paleogeographic implications

The sedimentation of the Upper Cretaceous Gosau succession of the Apuseni Mts. evolved in the same geotectonic frame as that of the Eastern Alps. The similarities, but also differences elaborated in this study, are evident.

The sedimentary facies successions are similar. The stratigraphic range covers nearly the same time interval. Deposition thickness is approximately equal. The provenance studies and fission-track analysis in both mountain ranges are leading to geotectonic interpretations, which prove the erosion and uppermost Cretaceous exhumation history in the basin hinterland. A diachronous time shift for the second subsidence phase (Lower Gosau to Upper Gosau facies change) has not been detected within the Apuseni Mts., although such a shift is well documented for the Eastern Alps.

The subduction of the Transylvanian ocean - which is the prolongation of the South Penninic ocean of the Eastern Alps - was responsible for the generation of the Gosau basins of the Apuseni Mts.. The process leading to rapid basin subsidence (the change from Lower Gosau Subgroup to Upper Gosau Subgroup) happened in both orogens, but did not migrate throughout the entire subduction line. It was more likely a regional pattern which might be due to subduction erosion in the Eastern Alps, but not in the Apuseni Mts..

A combination of high-strain, forced subduction followed by a retreating subduction is proposed for the basin subsidence processes in the Apuseni Mts.. Retreating subduction is able to explain rapid subsidence, calc-alkaline magmatism and "soft" continent-continent collision.

A further implication of the presented model is the possibility of regional geologic and paleogeographic reconstruction. Some concluding statements will be made,

concerning the paleogeographic evolution from Mid-Cretaceous to Neogene time:

- Together with the ALCAPA and the Tisia-block, the Eastern Alps formed one continental unit with an adjacent ocean in the north (South-Penninic/Transylvanian). The subduction of this ocean happened during the Upper Cretaceous (Fig. 5-1-a).
- The collision of the Austroalpine with a continental block (namely: Middle Penninic unit) is known from the Eastern Alps and comparable to the collision of the Tisia- and Dacia block in the Apuseni Mts.. In contrast to the Apuseni Mts., the Middle Penninic unit was overthrust by the Austroalpine Units (Frisch, 1979). The easternmost prolongation of the Middle Penninic unit was the Dacia block, which evolved as a larger continental slice.
- The convergent drift of the two microplates ended in a continent-continent collision, although a "soft one" due to slab rollback and retreating subduction. The continuous continental block has been dissected after Paleocene time (Fig. 5-1-b).
- The closure of the North Penninic ocean happened in the Eastern Alps during Eocene times (Fig. 5-1-c). The closure of the eastward prolongation of the North Penninic ocean with its resulting continental collision migrated towards the east along the ALCAPA block in the Western Carpathians (Fig. 5-1-d) and ended in the Eastern Carpathians in uppermost Miocene time.

In accordance to the proposed correlation of Săndulescu (1984, Fig. 5-2), the remnants of the Upper Cretaceous suture zone are exposed in the Tauern and Rechnitz windows of the Eastern Alps, within the Pieniny Klippen belt of the Western Carpathians, the Pienides (Săndulescu, 1984) of the East

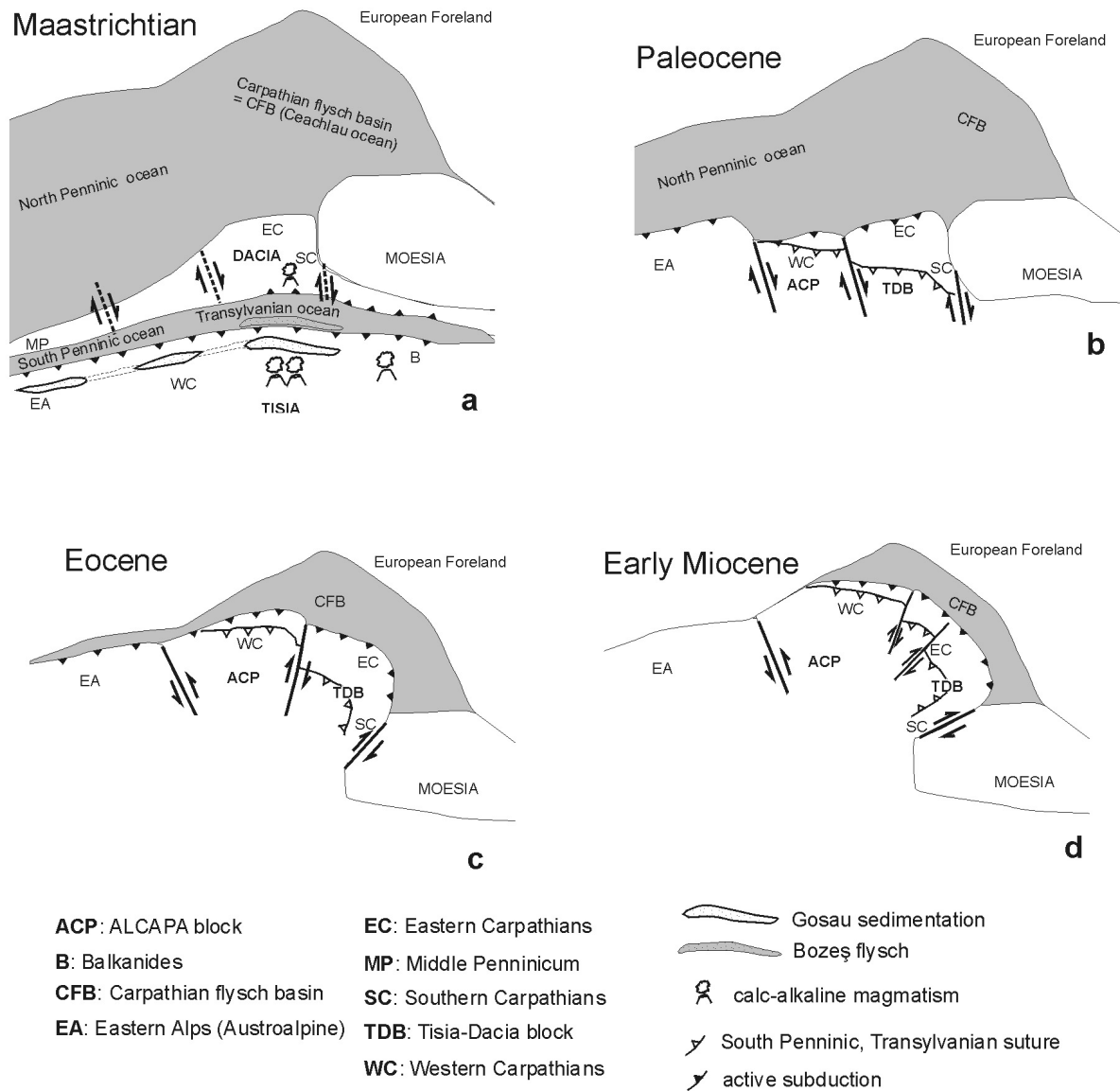


Fig 5-1: Position of continental blocks within the Eastern Alpine - Carpathian region from Late Cretaceous to Early Miocene. (a) The South Penninic ocean subducted beneath the Austroalpine Unit. At least in the Tisia-Dacia region subduction happened on both sides of the oceanic crust, since calc-alkaline magmatism is known on both plates. The Gosau sediments were deposited on the entire non-fragmented block, in elongated basins, which probably were connected to each other. The collision with the northern continental slice happened in the Upper Cretaceous in the Eastern Alps and at the K/T boundary in the Apuseni Mts.. (b) The Paleocene collision on the western margin of Moesia resulted in dissection of the continuous continental block during the Paleocene (Zweigel, 1997). (c) The closure of the North Penninic ocean happened in the Eocene in the Eastern Alps. Its eastward prolongation (Ceahlău ocean, after Zweigel, 1997) was subducted until the Upper Miocene (figures b, c, d: modified after Zweigel, 1997).

Carpathians (north Romania) and the Transylvanides. Additionally to these correlations, which describe the suture zone as Tethys suture in the broadest sense, it was possible to

show that the South Penninic ocean and its eastward prolongation (Transylvanian ocean) can be correlated as far as the South Carpathians.

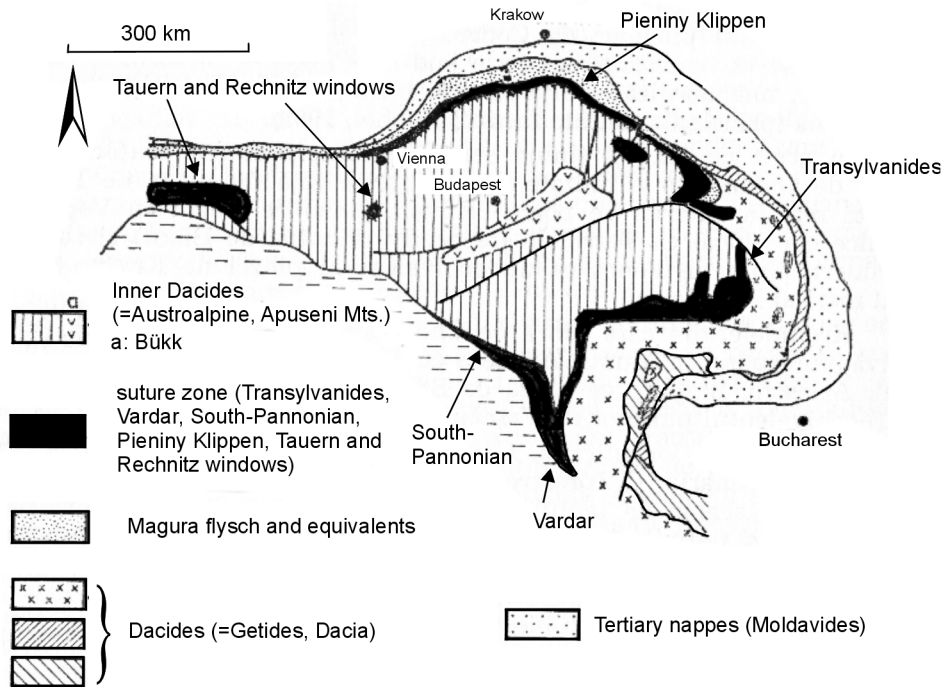


Fig. 5-2: Correlations of main geologic units of the Alpine-Carpathian chain after Săndulescu (1984).

References

- Avram, S. (1980): Petrographic study of the eastern part of the Vlădeasa eruptive massif. *Anuarul Institutului de Geologie si Geofizica*, vol.55, pp.207-325.
- Balintoni, I., Lupu, M., Iancu, V. and Lazar, C. (1987): Geological Map of Romania sc. 1:50.000, Poșaga sheet, Inst. Geol. Geofiz. București.
- Balintoni, I. (1997), *Geotectonica terenurilor metamorfice din România*. Univ."Babeș-Bolyai" Cluj-Napoca, 241 p.
- Balintoni, I. (2002): Short outlook on the structure of the Apuseni Mountains. In: Bucur, I.I., Filipescu, S., Săsăran, E. (eds.), *Algae and carbonate platforms in western part of Romania*. Field Trip Guidebook, Cluj University Press.
- Baciu, C. (2003): *Charophytele paleogene din nord-vestul Depresiunii Transilvaniei*. Casa Cărtii de Știință, 198 p., Cluj-Napoca.
- Berza, T.; Constantinescu, E., Vlad, S. N. (1998): Upper Cretaceous magmatic series and associated mineralisation in the Carpathian-Balkan Orogen. - *Resource Geology* (Tokyo 1998). 48; 4, Pages 291-306. 1998. In: SRG-SEG joint symposium on Granite types and mineralization., Ishihara, Shunso (convener); Izawa, Eiji (convener); Shimazaki, Hidehiko (editor).
- Bleahu, M., Soroiu, M., Catilina, R. (1984) On the Cretaceous tectonic-magmatic evolution of the Apuseni Mountains as revealed by K-Ar dating. *Rev Roum Phys* 29: 123-130.
- Borcoș, M., Berbeleac, I., Bordea, S., Mantea, G., Boștinescu, S. (1981): Geological Map of Romania sc. 1:50.000, Zlatna sheet, Inst. Geol. Geofiz. București.
- Bordea, J., Berbeleac, I., Borcoș, M., Mantea, G., Stancu, M. (1978): Geological Map of Romania sc. 1:50.000, Geoagiu sheet, Inst. Geol. Geofiz. București.
- Brinkmann, R. (1934): Zur Schichtfolge und Lagerung der Gosau in den Nördlichen Ostalpen. – *Beiträge zur Kenntnis der alpinen Oberkreide* 1, S. 1-8.
- Brinkmann, R. (1935): Die Ammoniten der Gosau und des Flysch in den nördlichen Ostalpen. *Mitt.Geol.Staatsinst. Hamburg*, 15: 1-14.
- Bucur I., Săsăran I., Săsăran E. & Schuller V. (2004): Micropaleontological Study Of The Limestone Olistoliths Within The Upper Cretaceous Wildflysh From Hășdate (Eastern Border Of The Gilău Mountains). *Studia Univ. Babeș-Bolyai, Geologia-Geographia*, , p. 33-38 (in press).
- Burchfiel, B.C. (1980). Eastern European Alpine system and the Carpathian orocline as an example of collision tectonics. *Tectonophysics*, 63, 31-61.
- Burchfiel B. C. and Royden L. (1982): Carpathian Foreland Fold and Thrust Belt and its relation to Pannonian and other Basins. *Bull. Am. Ass. Petrol. Geol.*, 66 (9): 1179–1195.
- Ciulavu, D., Bertotti, G. (1994): The Transylvanian Basin and its Upper Cretaceous substratum. *Romanian Journal of Tectonics and Regional Geology* 75/2: 59-64.
- Ciupagea, D. et al. (1970): *Geologia Depresiunii Transilvaniei*. Editura Academiei, Bucharest, pp 1-256.
- Cotta, von, B. (1864): *Über Eruptivgesteine und Erzlagerstätten im Banat und Serbien*. Edit. V. Braunmüller, Wien, 105.
- Csontos, et al. (1992): Tertiary tectonic evolution of the intra-Carpathian area; a model. *Tectonophysics* 208/1-3: 221-241.
- Csontos, L. (1995): Tertiary tectonic evolution of the Intra-Carpathian area. *Acta Vulcanologica* 7/2: 1-13.
- Dallmeyer, R. D., Neubauer, F., Pana, D., Fritz, H. (1994): Variscan vs. Alpine tectonothermal evolution within the Apuseni Mountains Romania.- *Romanian Journal of Tectonics and Regional Geology* 75 2.- ALCAPA II Fieldguide South Carpathians and Apuseni Mountains, 65-76.
- Dallmeyer R. D., Pana, D., Neubauer, F. & Erdmer, P. (1999): Tectonothermal Evolution of the Apuseni Mountains, Romania: Resolution of Variscan vs. Alpine Events with 40Ar/39Ar ages. - *J. Geol.*, 107 (3): 329-352.
- Dimitrescu, R., Bordea, S. (1974): Geological Map of Romania sc. 1:50.000, Cămpeni sheet, Inst. Geol. Geofiz. București.

- Dimitrescu, R., Bleahu, M. and Lupu, M. (1977): Geological Map of Romania sc. 1:50.000, Avram Iancu sheet, Inst. Geol. Geofiz. București.
- Dimitrescu, R. (1996): Geological Map of Romania sc. 1:50.000, Gilău sheet, Inst. Geol. Geofiz. Bucuresti (unpublished).
- Dunkl, I., Frisch, W., Kuhlemann, J. (1999): Fission track record of the thermal evolution of the Eastern Alps – review of the main zircon age clusters and the significance of the 160 Ma event. Abstracts of the 4th Workshop on Alpine Geological Studies, Tübingen 21-24 Sept. 1999.
- Dragoș, I. (1971): Flora și fauna cretacică din regiunea Vlădeasa (Munții Apuseni). Centrul de multiplicare al Universității București.
- Faupl, P., Wagreeich, M. (1992): Cretaceous flysch and pelagic sequences of the Eastern Alps: correlations, heavy minerals, paleogeographic implications. - *Cretac. Res.*, 13, 387-403.
- Frisch, W., Gawlick, H. J. (2003): The nappe structure of the central Northern Calcareous Alps and its disintegration during Miocene tectonic extrusion; a contribution to understanding the orogenic evolution of the Eastern Alps. *International Journal of Earth Sciences*, vol.92, no.5, pp.712-727.
- Har, N. (2001): Andezite bazaltice Apline din Munții Apuseni. Casa Cărții de Știință, Cluj-Napoca, 2001.
- Hârtoșanu, I., Hârtoșanu, P., Balintoni, I., Borcoș, M., Rusu, A. and Lupu, M. (1982): Geological Map of Romania sc. 1:50.000, Valea Ierii sheet, Inst. Geol. Geofiz. București.
- Holt, W.E., and T.A. Stern (1994): Subduction and foreland thrust loading: The late Tertiary development of Taranaki Basin, New Zealand, *Tectonics*, 13, 1068-1092.
- Ianovici, V., Borcos, M., Bleahu, M., Patrulius, D., Lupu, M., Dimitrescu, R., Savu, H. (1976): *Geologia Munților Apuseni. The geology of the Apuseni Mountains*. Ed. Acad. Repub. Soc. Rom., Bucharest, Romania.
- Kühn, O. (1947): Zur Stratigraphie und Tektonik der Gosauschichten. – *Sitzungsber. Österr. Akad. Wiss.* 146, S. 181-200.
- Leiss, O. (1990): Neue Aspekte zur Geodynamic und Deckenbildung als Ergebnis der Beckenanalyse von synorogenen Kreidevorkommen innerhalb der nördlichen Kalkalpen; *Geol. Rundsch.* 97/1; Stuttgart.
- Linzer, H.G. et al. (1998): Kinematic evolution of the Romanian Carpathians. *Tectonophysics* 297: 133-156.
- Lupu, M. (1970): Die obere Kreide der rumänischen Karpaten. - *Mitt. Geol. Ges. Wien*, 62, 17-34.
- Lupu, D. (1974): Contribuții la cunoașterea faunei de inocerami senonieni din depresiunea Rosia (Munții Apuseni de N). The Senonian Inoceramus fauna in the Rosia Depression, northern Apuseni Mountains. *Dări de Seama ale Sediștelor - Institutul de Geologie și Geofizică*. 3. Paleontologie, vol.60, (1972-1973), 3. Paleontologie, pp.71-84.
- Lupu, D., (1976): Contributions à l'étude des Rudistes Sénoniens des Monts Apuseni. *Mémoires de Institut de Géologie et de Géophysique*; Vol. XXIV, Bucarest.
- Lupu, D., Sornay, J. (1978): Noi date biostratigrafice asupra senonianului din regiunea Vidra (Munții Metaliferi). New biostratigraphic data on the Senonian of the Vidra region, Metalliferous Mountains. *Studii și Cercetări de Geologie, Geofizică, Geografie. Seria Geologie*, vol.23, no.1, pp.73-82.
- Lupu, D., Lupu, M. (1983): Biostratigraphische und fazielle merkmale der "Gosau formation" im Apuseni Gebirge. Biostratigraphy and facies indicators in the Gosau Series in the Apuseni Mountains. In: *The Twelfth congress of the Carpathian-Balkan Geologic Association*, Anuarul Institutului de Geologie și Geofizică, vol.59, pp.95-100.
- Lupu, D., (1985): Biostratigraphie und Faziesentwicklungen der Mittel- und Oberkreide des Apuseni-Gebirges. In: *Beitraege zur Stratigraphie und Palaeogeographie der mittleren Kreide Zentral*. Schriftenreihe der Erdwissenschaftlichen Kommissionen, vol.7, pp.15-25.

- Lupu, M., Avram, E., Antonescu, E., Dumitrică, P., Lupu, D., Nicolae, I., (1993): The Neojurassic and the Cretaceous of the Drocea Mts: The Stratigraphy and the Structure of an Ensialic Marginal Basin. - Rom. J. Tect. & Reg. Geol., 75, 53-66
- Lupu, M., Zacher, W. (1996): Faziesentwicklung und Tektogenese im Jungmesozoikum und Alttertiär der Rumänischen Karpaten und Vergleiche mit den Alpen. Zeitschrift der Deutschen Geologischen Gesellschaft, Band 147, Heft 1 . p. 81-99.
- Mantea, G. (1985): Geological studies in the upper basin of the Someșul Cald Valley and the Valea Seacă region (Bihor-Vlădeasa Mountains). Anuarul Institutului de Geologie și Geofizică; vol.66, 90 pp., 1985.
- Mantea, Gh., Ștefan, A., Rusu, A. and Dimitrescu, R. (1987): Geological Map of Romania sc. 1:50.000, Rachitele sheet, Inst. Geol. Geofiz. București.
- Mauritsch, H.J. & Marton, E. (1995): Escape models of the Alpine-Carpathian-Pannonian region in the light of palaeomagnetic observations. - Terra Nova, Vol.7, 44-50.
- Moser, F. (2001): Tertiäre Deformation in den Rumänischen Südkarpaten: Strukturelle Analyse eines Blattverschiebungskorridors am Westrand der Moesischen Plattform. Tübinger Geowissenschaftliche Arbeiten, Reihe A, 63, 169 pp.
- Neubauer, F. (2002): Contrasting Late Cretaceous with Neogene ore provinces in the Alpine-Balkan-Carpathian-Dinaride collision belt. In: Blundell, Derek J; Neubauer, F; von Quadt, Albrecht The timing and location of major ore deposits in an evolving orogen. Geological Society Special Publications, vol.204, pp.81-102.
- Neugebauer, J., Greiner, B., Appel, E. (2001): Kinematics of the Alpine-West Carpathian Orogen and palaeogeographic implications. Journal of the Geological Society of London, vol.158, Part 1, pp.97-110.
- Oberhauser, R. (1965): Zur Geologie der West-Ostalpen-Grenzzone in Vorarlberg und im Praetigau unter besonderer Berücksichtigung der tektonischen Lagebeziehungen. Deut. Geol. Ges., Z. vol.116, no.2, pp.440-446.
- Oberhauser, R. (1995): Zur Kenntnis der Tektoik und der Paläogeographie des Ostalpenraumes zur Kreide-, Paleozän- und Eozönzeit. Jb. Geol. B.-A. 138/2 , 369 - 432, Wien.
- Ortner, H. (1994): Die Muttekopfgosau (Lechtaler Alpen, Tirol/Oesterreich); Sedimentologie und Beckenentwicklung. The Muttekopf Gosau Basin, Lechtal Alps, Tyrol, Austria; sedimentology and basin development SO: Geologische Rundschau, vol.83, no.1, pp.197-211.
- Ortner, Hugo. (2001): Growing folds and sedimentation of the Gosau Group, Muttekopf, Northern Calcareous Alps, Austria Fourth workshop on Alpine geological studies International Journal of Earth Sciences, vol.90, no.3, pp.727-739.
- Ortner, H., Reiter, F. & Acs, P. (2002): Easy handling of tectonic data: the programs TectonicVB for Mac and TectonicsFP for Windows. Computers & Geosciences(28/10), 1193-1200
- Papainopol, I., Popescu, Ag. and Campeanu, St. (1977): Geological Map of Romania sc. 1:50.000, Plopiș sheet, Inst. Geol. Geofiz. București.
- Pătrașcu, St., Panaiotu, C., Șeclaman, M., Panaiotu, C. E. (1994): Timing of the rotational motion of Apuseni Mountains (Romania) : paleomagnetic data from Tertiary magmatic rocks. Tectonophysics, 233, 163-176.
- Patruluiș, D., Popa, E., Câmpeanu, St. and Orășanu, St. (1973): Geological Map of Romania sc. 1:50.000, Remeți sheet, Inst. Geol. Geofiz. București.
- Patruluiș, D. (1974): Duranddelgaia et Miseia, deux nouveaux genres de rudistes du Senonien de Padurea Craiului (Monts Apuseni), Dări de Seama ale Ședințelor - Institutul de Geologie și Geofizică. 3. Paleontologie, vol.60, (1972-1973), 3. Paleontologie, pp.170-180.
- Patruluiș, D., Bordea, S., Bordea, J., Manthea, G. (1983): Harta Geologică a Munților Pădurea Craiului – 1: 25 000; Institutul de Geologie Geofisica Romania, București.
- Perch-Nielsen, K. (1985): Mesozoic calcareous nannofossils. In Bolli, H.M., Saunders, J.B., and Perch-Nielsen, K. (Eds.), Plankton Stratigraphy: Cambridge (Cambridge Univ. Press), 329-426.

- Pitulea, G., Lupu, D. (1978): Contribuții la cunoașterea biostratigrafiei senonianului din Depresiunea Sălciua (Munții Apuseni). *Studii și Cercetari de Geologie, Geofizică, Geografie. Seria Geologie*, vol.23, no.1, pp.83-93.
- Reiter, F., Acs, P. (1996-2002): *TectonicsFP*.
- Royden LH (1993): Evolution of retreating subduction boundaries formed during continental collision. *Tectonics* 12/3: 629-638.
- Sachsenhofer, R.F., (1987): Fazies und Inkohlung mesozoischer Kohlen der Alpen Ostösterreichs. *Mitt. Österr. Geol. Ges.* 80, 1-45.
- Sanders, C. (1998): Tectonics and Erosion - Competitive Forces in a Compressive Orogen; A Fission Track Study of the Romanian Carpathians. Netherlands Research School of Sedimentary Geology (NSG)Publication no. 980505.
- Săndulescu, M. (1984): *Geotectonica României*. Et. Tehn., București, 336pp.
- Seghedi, I., Balintoni, I., Szakács, A. (1998): Interplay of tectonics and Neogene post-collisional magmatism in the Intracarpethian region; *Lithos*, vol.45, no.1-4, pp.483-497.
- Sissingh, W. (1977): Biostratigraphy of Cretaceous calcareous nannoplankton. *Geol. Mijnbouw*, 56:37-65.
- Stach E., Mackowsky M-Th., Teichmüller M., Taylor G.H., Chandra D., Teichmüller R. (1982): *Stach's Textbook of Coal Petrology*. 3rd edition. Gerbrüder Borntraeger, Berlin, Stuttgart.
- Stefan, A. (1980): Petrographic study of the eastern part of the Vlădeasa eruptive massif. *Anuarul Institutului de Geologie și Geofizică*, vol.55, pp.207-325.
- Ștefănescu, M. (1985): Geologic profiles, scale 1:200.000. Geological Institute, Bucharest.
- Stern, T.A., G.M. Quinlan, and W.E. Holt, (1992): Basin formation behind an active subduction zone: three-dimensional flexural modeling of Wanganui Basin, New Zealand, *Basin Research*, 4, 197-214.
- Stern, T.A., and W. E. Holt (1994): Platform Subsidence behind an active subduction zone, *Nature*, 368, 233-236.
- Szadetzki, J. (1930): Insula cristalină dintre comunele Petridul de Jos – Buru și Ocoliș. *D. d. S. Inst. Geol.*, vol. 13 (1924-1925): 125-129; București.
- Tari, G., Horváth, F. and Csontos, L. (1995). Palinspastic reconstruction of the Carpathian/Pannonian system. *AAPG Vienna*, p. A57.
- Tollmann, A. (1976): Analyse des klassischen nordalpinen Mesozoikums. – Stratigraphie, Fauna und Fazies der Nördlichen Kalkalpen. – Wien (Deuticke).
- Winkler, W. (1996): The tectono-metamorphic evolution of the Cretaceous northern Adriatic margin as recorded by sedimentary series (western part of the Eastern Alps). *Eclogae geol. Helv.* 89, p 527-551.
- Wagreich, M. & Faupl, P.(1994): Palaeogeography and geodynamic evolution of the Gosau Group of the Northern Calcareous Alps (Late Cretaceous, Eastern Alps, Austria). - *Palaeogeogr., Palaeoclimatol., Palaeoecol.*, 110, 235-254, Amsterdam.
- Wagreich, M. (1995): Subduction tectonic erosion and Late Cretaceous subsidence along the northern Austroalpine margin (Eastern Alps, Austria). *Tectonophysics*, 242, 63–78.
- Wagreich, M. (2000): A slope-apron succession filling a mid-Cretaceous piggyback basin: The Tannheim and Losenstein Formation of the eastern part of the Northern Calcareous Alps (Austria). *Mitt. Geol. Ges. Wien*, 93.
- Wagreich, M. (2001): A 400-km-long piggyback basin (upper Aptian-lower Cenomanian) in the Eastern Alps; *Terra Nova*, vol.13, no.6, pp.401-406.
- Wagreich, M. (2001): Paleocene - Eocene paleogeography of the Northern Calcareous Alps (Gosau Group, Austria). - In: Piller, W.E. & Rasser, M.W. (Eds.): *Paleogene of the Eastern Alps*. - *Österr. Akad. Wiss., Schriftenr. Erdwiss. Komm.*, 14, 57-75, Wien.
- Woletz, G. (1967): Schwermineralvergesellschaftungen aus ostalpinen Sedimentbecken der Kreidezeit. - *Geol. Rundschau*, 56, 308-320.
- Zweigel, P. (1997): The Tertiary tectonic evolution of the Eastern Carpathians (Romania): Orogenic arc formation in response to microplate movements. *Tübinger Geowissenschaftliche Arbeiten A/33*: pp 1-154.

Appendix (methodology and data tables)

A.1 Nannofossil determinations

Fig. A-1: Nannofossil and Nannozones after zonations of Sissingh (1977) and Perch-Nielsen (1985)

Sample	Origin	Preservation	Nannofossils	Nannozone	Age
186	Vlădeasa	moderate to good	Ceratolithoides aculeus, Watznaueria barnesae, W. ovata, Cribrosphaerella ehrenbergii, Ahmuellerella octoradiata, Prediscosphaera cretacea, Eiffellithus turriseiffelii, Calculites obscurus, C. ovalis, Orastrum campanensis, Lucianorhabdus cayeuxii, L. maleformis, Micula decussata, M. concava, Microrhabdulus decoratus, M. belgicus, Reinhardtites anthophorus, Lithostrinus grillii	CC20	upper Lower Campanian – lower Upper Campanian
206	Gilău	moderate	Watznaueria barnesae, W. ovata, Cyclagelosphaera margerelii, Cribrosphaerella ehrenbergii, Ahmuellerella octoradiata, Prediscosphaera cretacea, Eiffellithus turriseiffelii, E. eximius, Calculites obscurus, Lucianorhabdus cayeuxii, Quadrum gartneri, Micula decussata, M. concava, Microrhabdulus decoratus, M. belgicus, Nannoconus truitti s.l., Reinhardtites anthophorus, Eprolithus floralis	CC17	Lower Campanian
208	Gilău	moderate to good	Watznaueria barnesae, Cyclagelosphaera margerelii, Cribrosphaerella ehrenbergii, Ahmuellerella octoradiata, Prediscosphaera cretacea, Eiffellithus turriseiffelii, E. eximius, Calculites obscurus, Lucianorhabdus cayeuxii, L. maleformis, Quadrum gartneri, Micula decussata, M. concava, Microrhabdulus decoratus, Nannoconus truitti s.l., N. regularis, Tranolithus orionatus, Marthasterites furcatus, Broinsonia parca parca	CC18	Lower Campanian
211	Gilău	moderate	Watznaueria barnesae, Cyclagelosphaera margerelii, Cribrosphaerella ehrenbergii, Biscutum constans, Zeugrhabdotus embergeri, Prediscosphaera cretacea, P. grandis, Eiffellithus turriseiffelii, E. eximius, Cribrocorona gallica, Calculites obscurus, Lucianorhabdus cayeuxii, Quadrum gartneri, Micula decussata, M. concava, Microrhabdulus decoratus, Orastrum campanensis, Arkhangelskiella cymbiformis, Broinsonia enormis, Broinsonia parca parca	CC 18-19	upper Lower Campanian
210	Gilău	moderate	Watznaueria barnesae, Cyclagelosphaera margerelii, Cribrosphaerella ehrenbergii, Cribrocorona gallica, Prediscosphaera cretacea, P. spinosa, Eiffellithus turriseiffelii, E. eximius, Calculites obscurus, Lucianorhabdus cayeuxii, Lithastrinus grillii, Uniplanarius gothicus, Micula decussata, M. concava, Microrhabdulus decoratus, M. belgicus, Broinsonia parca parca, Arkhangelskiella cymbiformis, Ceratolithoides aculeus	CC20	lower Upper Campanian
266	Borod	good	Lithastrinus grillii, Marthasterites furcatus, Watznaueria barnesae, Cyclagelosphaera margerelii, Cribrosphaerella ehrenbergii, Prediscosphaera cretacea, P. spinosa, Eiffellithus turriseiffelii, E. eximius, Lucianorhabdus maleformis, Micula decussata, M. concava, Microrhabdulus decoratus, Chiastozygus literarius, Zeugrhabdotus embergeri, Z. erectus, Thoracosphaera sp., Corollithion signum, C. exiguum, Rotelapillus laffitei, Thoracosphaera sp.	CC15	Upper Coniacian
265	Borod	good	Lithastrinus grillii, L. septenarius, Watznaueria barnesae, Cribrosphaerella ehrenbergii, Ahmuellerella octoradiata, Prediscosphaera cretacea, Eiffellithus turriseiffelii, E. eximius, Calculites obscurus, C. ovalis, Lucianorhabdus cayeuxii, L. maleformis, L. quadrifidus, Quadrum gartneri, Micula decussata, M. concava, Microrhabdulus decoratus, M. belgicus, Nannoconus truitti s.l., Reinhardtites anthophorus, Eprolithus floralis, Nannoconus truitti truitti, N. multicaudus.	CC17	Upper Santonian
144	Ocoliș	moderate	Uniplanarius sissinghi, Ceratolithoides aculeus, Watznaueria barnesae, Cribrosphaerella ehrenbergii, Ahmuellerella octoradiata, Prediscosphaera cretacea, Eiffellithus turriseiffelii, Calculites obscurus, Lucianorhabdus cayeuxii, Micula decussata, M. concava, Microrhabdulus decoratus, M. belgicus, Nannoconus truitti, Reinhardtites anthophorus, Tranolithus orionatus, Placozygus fibuliformis.	CC21	Upper Campanian

Fig. A-1 (continued)

Sample	Origin	Preservation	Nannofossils	Nanno-zone	Age
138	Ocolis	moderate	Reinhardtites levis, R. anthophorus, Uniplanarius trifidus, U. sissinghi, Watznaueria barnesae, W. ovata, Cyclagelosphaera margerelii, Cribrosphaerella ehrenbergii, Ahmuellerella octoradiata, Prediscosphaera cretacea, P. stoveri, Eiffellithus turriseiffelii, E. eximius, Calculites obscurus, Lucianorhabdus cayeuxii, Micula decussata, M. concava, Microrhabdulus decoratus, Lithraphidites praequadratus, Arkhangelskiella cymbiformis.	CC 22C	Upper Campanian – Lower Maastrichtian
174	Sălcuia	moderate	Uniplanarius trifidus, U. sissinghi, Ceratolithoides aculeus, Watznaueria barnesae, W. ovata, Cribrosphaerella ehrenbergii, Prediscosphaera cretacea, Eiffellithus turriseiffelii, E. eximius, Calculites obscurus, Lucianorhabdus cayeuxii, L. maleformis, Quadrum gartneri, Micula decussata, M. concava, Microrhabdulus decoratus, M. belgicus, Reinhardtites anthophorus.	CC22C	Upper Campanian – Lower Maastrichtian
173	Sălcuia	moderate	Uniplanarius trifidus, U. sissinghi, Ceratolithoides aculeus, C. verbeeki, Watznaueria barnesae, Cribrosphaerella ehrenbergii, Prediscosphaera cretacea, P. spinosa, P. stoveri, Eiffellithus turriseiffelii, E. gorkae, E. eximius, Calculites obscurus, C. ovalis, Lucianorhabdus cayeuxii, Micula decussata, Microrhabdulus decoratus, M. belgicus, Reinhardtites anthophorus, Tranolithus orionatus	CC22C	Upper Campanian – Lower Maastrichtian
170	Sălcuia	moderate	Lithraphidites quadratus, Reinhardtites levis, Watznaueria barnesae, Cribrosphaerella ehrenbergii, Ahmuellerella octoradiata, Prediscosphaera cretacea, Eiffellithus turriseiffelii, Calculites obscurus, Orastrum campanensis, Lucianorhabdus cayeuxii, Micula decussata, M. concava, Microrhabdulus decoratus, Lithraphidites praequadratus, Arkhangelskiella cymbiformis, Tranolithus orionatus, Placozygus fibuliformis.	CC 25B	Upper Maastrichtian
147	Ocoliș	moderate	Lithraphidites quadratus, L. praequadratus, Arkhangelskiella cymbiformis, Watznaueria barnesae, W. ovata, Cyclagelosphaera margerelii, Cribrosphaerella ehrenbergii, Ahmuellerella octoradiata, Prediscosphaera cretacea, P. stoveri, Eiffellithus turriseiffelii, Lucianorhabdus cayeuxii, Micula decussata, M. concava, M. swastica, Microrhabdulus decoratus	CC25B	upper Lower – lower Upper Maastrichtian
151	Ocoliș	moderate	M. murus, M. decussata, M. concava, M swastica, Lithraphidites quadratus, L. camiolensis, Watznaueria barnesae, Cyclagelosphaera margerelii, Cribrosphaerella ehrenbergii, Placozygus fibuliformis, Prediscosphaera cretacea, P. spinosa, P. stoveri, Eiffellithus turriseiffelii, Lucianorhabdus cayeuxii, Microrhabdulus decoratus, M. belgicus, Semihololithus priscus, Ceratolithoides aculeus, Reinhardtites levis	CC25C	Upper Maastrichtian
176	Sălcuia	moderate	M. murus, M. swastica, M. decussata, M. concava, Watznaueria barnesae, W. ovata, Cyclagelosphaera margerelii, Cribrosphaerella ehrenbergii, Ahmuellerella octoradiata, Prediscosphaera cretacea, P. stoveri, Eiffellithus turriseiffelii, Calculites obscurus, Lucianorhabdus cayeuxii, Microrhabdulus decoratus, M. belgicus, Reinhardtites levis, Tranolithus orionatus, Placozygus fibuliformis	CC25C	Upper Maastrichtian
178	Arieș Vale / Mușca	moderate to good	Orastrum campanensis, Eiffellithus turriseiffelii, E. eximius, Broinsonia enormis, Broinsonia parca constricta, Watznaueria barnesae, Cribrosphaerella ehrenbergii, Ahmuellerella octoradiata, Prediscosphaera cretacea, Calculites obscurus, Lucianorhabdus cayeuxii, L. maleformis, Micula decussata, M. concava, Microrhabdulus decoratus, M. belgicus, Reinhardtites anthophorus.	CC18	Lower Campanian
226	Drocea	poor	Watznaueria barnesae, Cyclagelosphaera margerelii, Prediscosphaera cretacea, Eiffellithus turriseiffelii, E. eximius, Gartnerago segmentatum, Lithraphidites camiolensis, Quadrum gartneri, Microrhabdulus decoratus, Thoracosphaera sp.	CC12	Middle - Upper Turonian

Fig. A-1 (continued)

Sample	Origin	Preservation	Nannofossils	Nannozone	Age
227	Drocea	poor	Watznaueria barnesae, Cyclagelosphaera margerelii, Cribrosphaerella ehrenbergii, Biscutum constans, Zeugrhabdotus embergeri, Prediscosphaera cretacea, Eiffellithus turriseiffelii, E. eximius, Quadrum gartneri, Lithraphidites carniolensis, Lucianorhabdus maleformis, Marthasterites furcatus, Tranolithus gabalus	CC13	Upper Turonian - Lower Coniacian
231	Drocea	moderate	Watznaueria barnesae, Zeugrhabdotus embergeri, Z. erectus, Prediscosphaera cretacea, Eiffellithus turriseiffelii, E. eximius, Helicolithus trabeculatus, Nannoconus regularis, N. truittii truittii, Quadrum gartneri, Micula decussata, M. concava, Microrhabdulus decoratus, Lithraphidites carniolensis, Reinhardtites anthophorus, Lucianorhabdus cayeuxii (straight and curved specimens), L. maleformis, L. quadrifidus, Eprolithus floralis, .	CC16	Santonian
201	Drocea	moderate to good	Lucianorhabdus cayeuxii, L. quadrifidus, Watznaueria barnesae, W. ovata, Cyclagelosphaera margerelii, Cribrosphaerella ehrenbergii, Ahmuellerella octoradiata, Prediscosphaera cretacea, Eiffellithus turriseiffelii, E. eximius, Calculites obscurus, C. ovalis, Quadrum gartneri, Micula decussata, M. concava, Microrhabdulus decoratus, Nannoconus truittii truittii, N. multicaudus, Reinhardtites anthophorus, Eprolithus floralis, Lithastrinus septenarius, Reinhardtites anthophorus.	CC16	uppermost Coniacian – lowermost Santonian
236	Drocea	moderate to good	Watznaueria barnesae, Cyclagelosphaera margerelii, Eprolithus floralis, Prediscosphaera cretacea, Eiffellithus turriseiffelii, E. eximius, Lithraphidites carniolensis, Calculites obscurus, C. ovalis, Lucianorhabdus cayeuxii (straight and curved specimens), L. arcuatus, L. maleformis, L. quadrifidus, Quadrum gothicum, Micula decussata, M. concava, Microrhabdulus decoratus, M. undosus, Reinhardtites anthophorus, Lithstranus grillii	CC16	Santonian
239	Drocea	moderate to good	Watznaueria barnesae, Cretarhabdus conicus, Cyclagelosphaera margerelii, Cribrosphaerella ehrenbergii, Helicolithus trabeculatus, Prediscosphaera cretacea, Eiffellithus turriseiffelii, E. eximius, E. parallelus, Cribrocorona gallica, Tranolithus gabalus, Calculites obscurus, Lucianorhabdus cayeuxii, Quadrum gartneri, Micula decussata, M. concava, M. praemurus, Microrhabdulus decoratus, Lithraphidites praequadratus, Arkhangelskiella cymbiformis, Reinhardtites levis	CC24	Lower Maastrichtian
262	Drocea	moderate	Uniplanarius trifidus, U. sissinghi, Ceratolithoides aculeus, C. verbeeki, Watznaueria barnesae, W. ovata, Cyclagelosphaera margerelii, Cribrosphaerella ehrenbergii, Ahmuellerella octoradiata, Prediscosphaera cretacea, P. spinosa, Eiffellithus turriseiffelii, E. eximius, Calculites obscurus, Lucianorhabdus cayeuxii, L. maleformis, L. quadrifidus, Micula decussata, M. concava, Microrhabdulus decoratus, M. belgicus, Reinhardtites anthophorus	CC22C	Upper Campanian - Lower Maastrichtian
246	Roşia		Watznaueria barnesae, Russelia bukryi, Russelia laswelli, Prediscosphaera cretacea, Calculites ovalis, Microrhabdulus decoratus, Lucianorhabdus maleformis, , Calculites obscurus, Eiffellithus turriseiffelii, Retecapsa crenulata, Cylindralithus serratus, Cribrosphaerella daniae, Eiffellithus eximius, Rhagodiscus angustus, Lucianorhabdus cayeuxii, Quadrum bengalensis, Octolithus multiplus, Kamptnerius magnificus, Microrhabdulus undosus, Micula praemurus, Watznaueria quadri radiata, Calculites percensis, Lithastrinus grillii, Arkhangelskiella cymbiformis, Arkhangelskiella maastrichtiana, Ceratolithoides sp., Reinhardtites levis, Tranolithus orionatus, Chiastozygus litterarius, Lucianorhabdus maleformis, Microrhabdulus decoratus, Arkhangelskiella confusa.	CC24	Lower Maastrichtian

A.2 Heavy mineral analysis

The extraction of heavy mineral populations requires medium grained sandstones. The samples were taken from unweathered outcrops. For laboratory work ~500 g of each sample was crushed (<2 mm) and sieved. The fraction 100-200 μm was treated with acetic acid to dissolve carbonate components. The separation of the heavy mineral fraction has been made by using a fluid density of 2.8 g/cm^3 . Two compounds were embedded in immersion fluid with refractivity indices of $n=1.5$ and $n=1.7$. Counting and determination of the minerals was performed under transmitted light along a scanning line. Each mineral on the scanning line was determined and counted. For the quantitative calculations lithic grains and layer silicates were excluded. The diagram in Figure A-2-1 contains the percentages of non-opaque monominerals (without layer silicates) of each sample. For further data interpretation some minerals have been grouped, concerning their weathering resistivity, transport stability or lithologic predominance (e.g. exclusively metamorphic minerals; cf. chapter 3.2.). Although Cr-spinel is easily detectable with the transmitted light microscope some back-scattered electron scanning has been performed, in order to ensure the Cr-spinel occurrences (Fig. A-2-2, A-2-3).

Fig. A-2-1 (continued)

Sample Location	Garnet	Tourmaline	Staurolite	Epidote	Zoisite	Amphibole	Apatite	Zircon	Rutile	Cr-Spinel	Chloritoid	Anatas	Glaucofanane	Pyroxene	Sphalerite	Titanite	Cassiterite	Glauconite	Dolomite	Spinel	Xenotim	Orthit	mono-minerals (m.m.)	(m.m.) without layer silicates
Sălciuma-Ocoliș-Abrud																								
M16	89.2	2.5	0.0	1.3	2.5	0.6	0.6	0.6	1.3	0.0	1.3	0.0	0.0	0.0	0.0	0.0	0.0	0.0	0.0	0.0	0.0	0.0	203	158
M7	89.7	1.0	2.6	0.5	0.0	0.0	1.5	1.5	1.0	0.0	2.1	0.0	0.0	0.0	0.0	0.0	0.0	0.0	0.0	0.0	0.0	0.0	200	195
M8	40.3	14.9	26.9	4.5	0.0	0.0	3.0	3.0	3.0	0.0	4.5	0.0	0.0	0.0	0.0	0.0	0.0	0.0	0.0	0.0	0.0	0.0	202	67
M6	88.8	3.4	0.0	0.0	0.0	0.0	4.5	0.0	2.2	0.0	1.1	0.0	0.0	0.0	0.0	0.0	0.0	0.0	0.0	0.0	0.0	0.0	90	89
M15	60.1	19.6	0.6	0.0	0.0	0.0	15.2	0.0	3.8	0.0	0.0	0.0	0.0	0.0	0.0	0.0	0.0	0.0	0.0	0.0	0.0	0.0	190	158
M5	93.3	1.0	1.4	0.0	0.0	0.0	0.0	0.0	0.0	0.0	3.8	0.0	0.0	0.5	0.0	0.0	0.0	0.0	0.0	0.0	0.0	0.0	229	209
M4	78.4	3.1	7.2	0.0	0.0	0.0	0.0	0.0	10.3	0.0	1.0	0.0	0.0	0.0	0.0	0.0	0.0	0.0	0.0	0.0	0.0	0.0	152	97
M3	11.7	2.1	9.6	1.1	11.7	0.0	58.5	1.1	3.2	0.0	0.0	0.0	0.0	0.0	0.0	0.0	0.0	1.1	0.0	0.0	0.0	0.0	96	94
M1	63.8	0.5	26.2	0.0	0.0	0.0	9.5	0.0	0.0	0.0	0.0	0.0	0.0	0.0	0.0	0.0	0.0	0.0	0.0	0.0	0.0	0.0	227	210
M18	62.1	5.3	0.0	0.0	0.0	0.8	28.0	0.0	3.8	0.0	0.0	0.0	0.0	0.0	0.0	0.0	0.0	0.0	0.0	0.0	0.0	0.0	148	132
M24	23.9	5.4	0.0	0.0	0.0	1.1	31.5	6.5	31.5	0.0	0.0	0.0	0.0	0.0	0.0	0.0	0.0	0.0	0.0	0.0	0.0	0.0	121	92
M64	68.8	5.5	0.0	0.0	1.6	0.0	17.2	2.3	4.7	0.0	0.0	0.0	0.0	0.0	0.0	0.0	0.0	0.0	0.0	0.0	0.0	0.0	266	128
Vidra																								
1	67.2	25.4	0.0	0.0	0.0	0.0	1.5	6.0	0.0	0.0	0.0	0.0	0.0	0.0	0.0	0.0	0.0	0.0	0.0	0.0	0.0	0.0	270	67
4	1.9	46.5	0.0	0.0	0.0	0.6	50.3	0.0	0.6	0.0	0.0	0.0	0.0	0.0	0.0	0.0	0.0	0.0	0.0	0.0	0.0	0.0	173	159
7	1.2	75.9	0.0	0.0	0.0	0.0	20.5	1.2	1.2	0.0	0.0	0.0	0.0	0.0	0.0	0.0	0.0	0.0	0.0	0.0	0.0	0.0	111	83
8	0.5	64.1	0.0	0.0	0.0	0.0	2.3	2.7	30.5	0.0	0.0	0.0	0.0	0.0	0.0	0.0	0.0	0.0	0.0	0.0	0.0	0.0	241	220
15	2.8	35.9	0.0	0.0	2.1	0.0	52.8	0.7	5.6	0.0	0.0	0.0	0.0	0.0	0.0	0.0	0.0	0.0	0.0	0.0	0.0	0.0	166	142
23	13.1	26.3	4.0	0.0	2.0	0.0	34.3	5.1	13.1	0.0	0.0	0.0	0.0	0.0	0.0	0.0	0.0	0.0	2.0	0.0	0.0	0.0	119	99
30	22.3	39.1	0.0	0.0	2.8	0.0	21.8	1.7	11.7	0.0	0.0	0.6	0.0	0.0	0.0	0.0	0.0	0.0	0.0	0.0	0.0	0.0	357	179
33	8.1	35.1	0.0	0.0	0.0	0.0	45.9	2.7	6.8	0.0	0.0	0.0	0.0	0.0	0.0	1.4	0.0	0.0	0.0	0.0	0.0	0.0	204	74
M65	7.2	19.0	0.0	0.0	0.0	0.0	3.6	16.9	10.8	0.0	0.0	35.9	0.0	0.0	0.0	0.0	6.7	0.0	0.0	0.0	0.0	0.0	372	195
41	54.2	3.2	0.0	0.0	0.0	0.0	14.9	6.4	9.2	3.2	0.0	1.2	0.0	0.0	7.2	0.0	0.0	0.0	0.0	0.4	0.0	0.0	256	249
64	83.8	10.2	0.0	0.0	0.0	0.0	3.5	0.5	1.7	0.2	0.0	0.0	0.0	0.0	0.0	0.0	0.0	0.0	0.0	0.0	0.0	0.0	413	401
M66	70.6	18.2	0.0	0.0	0.0	0.0	9.1	1.4	0.7	0.0	0.0	0.0	0.0	0.0	0.0	0.0	0.0	0.0	0.0	0.0	0.0	0.0	411	143
M67	47.0	15.8	0.0	4.0	11.9	0.0	11.9	2.0	5.0	0.0	0.0	1.5	0.0	0.0	0.0	1.0	0.0	0.0	0.0	0.0	0.0	0.0	283	202
Vlădeasa																								
M26	0.0	38.7	0.0	0.0	0.0	0.0	25.8	12.9	19.4	3.2	0.0	0.0	0.0	0.0	0.0	0.0	0.0	0.0	0.0	0.0	0.0	0.0	68	31
186	44.4	14.4	0.0	0.0	0.0	0.0	16.7	24.4	0.0	0.0	0.0	0.0	0.0	0.0	0.0	0.0	0.0	0.0	0.0	0.0	0.0	0.0	185	90
162	69.9	9.2	0.0	0.0	0.0	0.0	21.0	0.0	0.0	0.0	0.0	0.0	0.0	0.0	0.0	0.0	0.0	0.0	0.0	0.0	0.0	0.00	324	229
163	16.3	4.6	0.0	0.0	0.0	0.0	3.9	7.2	0.0	0.0	0.0	0.7	0.0	0.0	0.0	0.0	0.0	0.0	0.0	0.0	0.0	67.32	77	153

Fig. A-2-2: Spectra of back-scattered electron scanning of Cr-spinel (sample 64).

Scan Nr 1: mineral 1												
64 Vidra	Element	Line	raw data (not corrected)	k-ratio	Intensity correct.	Weight%	Wweight % Sigma	Atom%	Component%	Formula	Ion number	Standard
	Mg	K_SERIES	0.19	0.00128	0.4436	4.62	0.31	5.53	7.66	MgO	0.78	MgO 1-Jun-99
	Al	K_SERIES	0.24	0.0018	0.536	5.01	0.26	5.41	9.47	Al ₂ O ₃	0.76	Al ₂ O ₃ 1-Jun-1999
	Cr	K_SERIES	3.31	0.03315	0.9498	38.32	0.48	21.46	56.01	Cr ₂ O ₃	3.03	Cr 1-Jun-1999
	Fe	K_SERIES	1.61	0.01607	0.8453	20.88	0.45	10.88	26.86	FeO	1.54	Fe 1-Jun-1999
	O					31.17	0.48	56.72			8	
Scan Nr. 2 mineral 2												
	Mg	K_SERIES	0.16	0.00109	0.4422	4.04	0.29	4.86	6.7	MgO	0.68	MgO 1-Jun-1999
	Al	K_SERIES	0.19	0.00143	0.5393	4.04	0.24	4.38	7.63	Al ₂ O ₃	0.61	Al ₂ O ₃ 1-Jun-1999
	Si	K_SERIES	0.03	0.00025	0.6401	0.54	0.18	0.56	1.15	SiO ₂	0.08	SiO ₂ 1-Jun-1999
	Cr	K_SERIES	3.49	0.03489	0.9469	41.31	0.5	23.22	60.38	Cr ₂ O ₃	3.25	Cr 1-Jun-1999
	Fe	K_SERIES	1.41	0.01407	0.8407	18.76	0.44	9.82	24.14	FeO	1.37	Fe 1-Jun-1999
	O					31.31	0.5	57.18			8	
Scan Nr. 3 mineral 3												
	Mg	K_SERIES	0.31	0.0021	0.4599	5.24	0.25	6.07	8.69	MgO	0.86	MgO 1-Jun-1999
	Al	K_SERIES	0.6	0.00438	0.5454	8.57	0.25	8.95	16.2	Al ₂ O ₃	1.27	Al ₂ O ₃ 1-Jun-1999
	Cr	K_SERIES	3.79	0.03793	0.947	31.47	0.38	17.05	46	Cr ₂ O ₃	2.41	Cr 1-Jun-1999
	Fe	K_SERIES	2.45	0.0245	0.851	22.63	0.39	11.42	29.12	FeO	1.62	Fe 1-Jun-1999
	O					32.08	0.41	56.5			8	

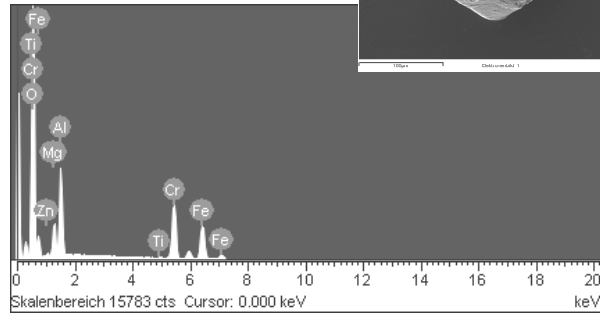
Spektrumverarbeitung :
Keine Peaks weggelassen

Verarbeitungsoption : Sauerstoff nach Stöchiometrie (Normalisiert)
Anzahl Iterationen = 3

Standard :
Mg MgO 1-Jun-1999 12:00 AM
Al Al2O3 1-Jun-1999 12:00 AM
Ti Ti 1-Jun-1999 12:00 AM
Cr Cr 1-Jun-1999 12:00 AM
Fe Fe 1-Jun-1999 12:00 AM
Zn Zn 1-Jun-1999 12:00 AM

Element	Gewichts%	Atom%	Komp.%	Formel
Mg K	4.68	5.36	7.76	MgO
Al K	11.35	11.72	21.45	Al2O3
Ti K	0.41	0.24	0.69	TiO2
Cr K	24.49	13.12	35.80	Cr2O3
Fe K	25.50	12.72	32.80	FeO
Zn L	1.21	0.51	1.50	ZnO
O	32.36	56.33		
Insgesamt	100.00			

sample M26



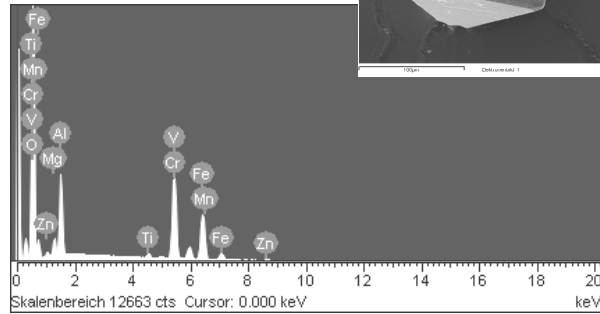
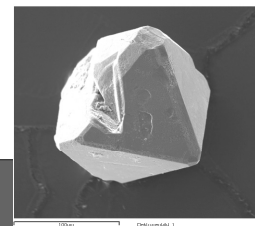
Spektrumverarbeitung :
Keine Peaks weggelassen

Verarbeitungsoption : Sauerstoff nach Stöchiometrie (Normalisiert)
Anzahl Iterationen = 3

Standard :
Mg MgO 1-Jun-1999 12:00 AM
Al Al2O3 1-Jun-1999 12:00 AM
Ti Ti 1-Jun-1999 12:00 AM
V V 1-Jun-1999 12:00 AM
Cr Cr 1-Jun-1999 12:00 AM
Mn Mn 1-Jun-1999 12:00 AM
Fe Fe 1-Jun-1999 12:00 AM
Zn Zn 1-Jun-1999 12:00 AM

Element	Gewichts%	Atom%	Komp.%	Formel
Mg K	1.96	2.37	3.25	MgO
Al K	8.29	9.00	15.66	Al2O3
Ti K	0.95	0.58	1.58	TiO2
V K	0.36	0.21	0.64	V2O5
Cr K	28.54	16.08	41.72	Cr2O3
Mn K	0.87	0.46	1.12	MnO
Fe K	26.26	13.78	33.78	FeO
Zn L	1.80	0.81	2.24	ZnO
O	30.97	56.72		
Insgesamt	100.00			

sample 41



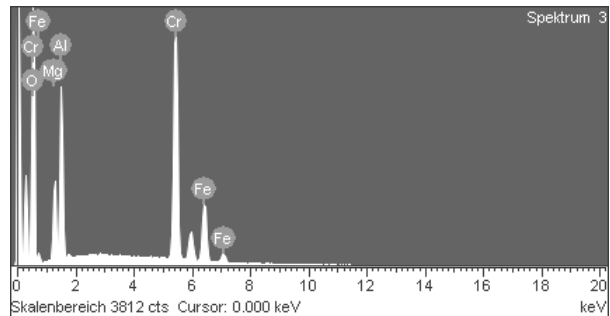
Spektrumverarbeitung :
Möglicherweise Peak weggelassen : 0.269keV

Verarbeitungsoption : Sauerstoff nach Stöchiometrie (Normalisiert)
Anzahl Iterationen = 3

Standard :
Mg MgO 1-Jun-1999 12:00 AM
Al Al2O3 1-Jun-1999 12:00 AM
Cr Cr 1-Jun-1999 12:00 AM
Fe Fe 1-Jun-1999 12:00 AM

Element	Gewichts%	Atom%	Komp.%	Formel
Mg K	4.20	4.86	6.96	MgO
Al K	8.25	8.61	15.58	Al2O3
Cr K	38.26	20.74	55.93	Cr2O3
Fe K	16.74	8.45	21.54	FeO
O	32.55	57.34		
Insgesamt	100.00			

sample M27 (1)



Spektrumverarbeitung :
Möglicherweise Peak weggelassen : 0.268keV

Verarbeitungsoption : Sauerstoff nach Stöchiometrie (Normalisiert)
Anzahl Iterationen = 2

Standard :
Mg MgO 1-Jun-1999 12:00 AM
Al Al2O3 1-Jun-1999 12:00 AM
Si SiO2 1-Jun-1999 12:00 AM
Cr Cr 1-Jun-1999 12:00 AM
Mn Mn 1-Jun-1999 12:00 AM
Fe Fe 1-Jun-1999 12:00 AM

Element	Gewichts%	Atom%	Komp.%	Formel
Mg K	3.94	4.77	6.54	MgO
Al K	3.39	3.69	6.40	Al2O3
Si K	0.62	0.65	1.33	SiO2
Cr K	41.71	23.59	60.96	Cr2O3
Mn K	0.80	0.43	1.03	MnO
Fe K	18.45	9.72	23.74	FeO
O	31.09	57.15		
Insgesamt	100.00			

sample M27 (2)

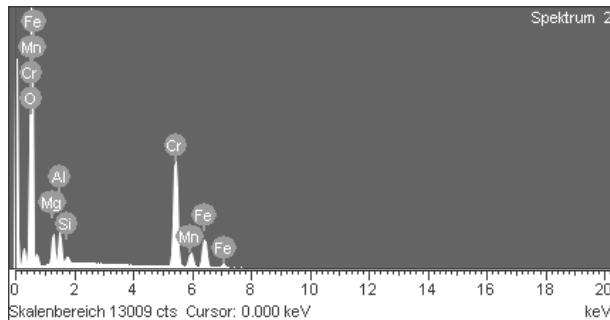


Fig. A-2-3: SEM (Scanning Electron Microscope) images and spectra of back-scattered electron scanning of Cr-spinel.

A.3 Paleocurrent data

Bedding planes with lineations of paleocurrents measured in the field were rotated into a horizontal position in order to obtain the paleocurrent direction. Note: some paleocurrent measurements did not record unimodal transport directions.

Fig. A-3: Paleocurrent data table.

Location	Stratigraphy	Lineation	Bedding	Paleocurrent direction	Unimodal transport direction
Hășdate-Gilău	Lower Gosau	331/44	317/30	325	no
	Upper Gosau	06/16	100/85	25	no
		09/44	278/85	324	no
		14/28	101/85	39	yes
		182/26	260/75	18	no
		142/16	62/70 (overturned)	350	yes
		332/8	246/70	147	no
		339/35	50/67	360	yes
		321/09	26/20	320	yes
		354/8	26/15	350	yes
		355/21	26/16	352	yes
344/5	26/17	340	yes		
Borod	Lower Gosau	192/16	88/15	192	yes
Drocea	Upper Gosau	171/52	151/58	162	yes
		185/05	135/31	180	yes
		171/52	135/32	170	yes
Vidra	Lower Gosau	222/35	292/6	45	no
		115/30	352/15	125	yes
		128/30	352/15	135	yes
		112/30	352/15	121	yes
		183/15	38136	185	yes
		65/5	268/10	58	no
		88/5	42339	85	yes
		150/3	116/10	150	no
		130/2	116/10	130	no
		226/15	285/15	226	no
		170/15	285/15	170	no
		180/15	285/15	180	no
		141/15	285/15	141	no
		294/15	285/15	294	no
		193/30	257/44	15	yes
	Upper Gosau	40/5	302/6	40	no
Salciua	Upper Gosau	0/0	268/66	358	yes
		100/78	120/83 (overturned)	304	yes
		335/32	284/82	338	yes
		228/37	120/83	240	yes
Areis-Tal	Lower Gosau	344/44	293/60	147	no
	Upper Gosau	66/03	151/44	66	yes
		175/10	82/54	181	no
		120/15	194/45	305	no
Rosia	Lower Gosau	306/70	293/69	295	no
	Upper Gosau	314/5	34/45	307	no

A.4 Vitrinite reflection

Sample preparation and measurement

Mainly dark colored siltstones and claystones were sampled for the preparation of coalification analysis. Besides, fine grained sandstones were collected. If organic matter was macroscopically identifiable. Since organic matter has a very low weathering resistivity, the samples were taken from unweathered outcrops. The samples were cut in 2-3 cm thick rectangles, embedded in epoxy resin and dried in a vacuum oven in order to displace pore gases. Several steps of wet grinding have been made by using abrasive emery paper up to grit size 1200. Polishing of the samples was performed by using diamond polishing fluid (3 μ m) and oxide polishing suspension (SiO₂, 00.1 μ m).

Principles of methods, examinations and determinations are precisely described by Stach et al. (1982). The vitrinite reflection of the dispersed particles was measured on a binocular incident-light microscope by using immersion oil. The intensity of the light reflected by a vitrinite particle is calculated by incorporating the reflectance of a standard substance:

R_{vi} = reflectance of vitrinite (%R)

R_s = reflectance of the standard substance (%R)

A_{vi} = deflection of when measuring vitrinite particles

A_s = deflection when measuring standard

$$R_{vi} = R_s \frac{A_{vi}}{A_s}$$

A mean value from all measured point within one sample has been calculated by using the standard deviation method. Measured mean values and standard deviations are shown in Fig (A-4-1).

Basin modeling

Numerical 1 D-modeling was performed by using the computer program BasinMod 1 D for Windows (Platte River Associates. Inc.). The constant input parameters are a reconstructed pseudo-well and measured vitrinite reflectance values. The kinetic LLNL Easy % Ro approach of the Lawrence Livermore National Laboratories (LLNL) was used for the calibration. Modeling was performed by varying the heatflow parameters and presumed erosion until the best fit curve to the measured vitrinite values was obtained. The input data for both models are presented in Figure A-4-2.

Fig. A-4-1: Values of the vitrinite reflectance measurements (%Rr = random vitrinite reflectance).

Sample	measured points	%Rr	standard deviation	Sample	measured points	%Rr	standard deviation
Remeți				Gilău			
V38	59	4.47	0.40	V34	74	0.95	0.16
V39	52	4.80	0.44	V33	12	1.07	0.06
V40	51	5.08	0.22	V31	52	1.05	0.13
V36	41	2.30	1.00	V30	49	0.96	0.12
V37	51	3.80	0.23	Sălcuia			
Vlădeasa				V101	55	1.42	0.09
164	50	1.97	0.13	V104	54	0.96	0.10
193	60	3.78	0.21	V102	38	1.48	0.09
Roșia				V107	52	0.92	0.11
V116	53	0.55	0.11	V103	52	0.85	0.14
V68	50	1.55	0.16	V 11	18	1.23	0.22
V117-1	57	0.47	0.04	V 12	50	0.88	0.09
V70	53	1.48	0.13	V 13	50	1.64	0.12
V69	52	1.18	0.16	V 16	50	1.06	0.12
V72	55	0.61	0.12	V 19	50	1.51	0.08
V76	53	0.59	0.12	V 10	50	1.17	0.06
Drocea				37-1	50	0.87	0.09
V64	51	1.22	0.14	Ocoliş			
V61	52	1.16	0.09	V4	55	1.27	0.12
202	50	0.94	0.11	140	50	1.17	0.16
199	53	1.08	0.13	V 8	35	1.54	0.12
V62	57	0.74	0.10	V 9	50	1.52	0.15
V54	57	0.63	0.07	Câmpeni-Abrud			
V67	56	1.02	0.10	V109	49	1.23	0.12
Vidra				V78	54	0.92	0.10
V114	54	1.24	0.10	V77	58	1.46	0.12
V113	55	1.62	0.09	V110	35	1.02	0.16
5	52	1.59	0.11	V111	53	0.94	0.11
11	50	1.48	0.13	V 23	50	0.95	0.12
16	140	1.33	0.11	V 25	50	1.20	0.06
25	60	2.86	0.17	Borod			
32	50	1.83	0.12	V45	56	0.72	0.14
40	50	1.56	0.10	V46	39	0.78	0.08
59	50	1.85	0.14	V48	45	0.82	0.11
Hașdate				Geoagiu valley			
V91	53	1.24	0.10	L13	52	0.38	0.04
V93	46	1.14	0.11	CV9	57	0.44	0.06
V98	53	0.95	0.12	CV7	52	0.37	0.05
V95-1	94	0.95	0.20	CV2	43	0.57	0.1
V97	511	1.10	0.10	CV3	66	0.55	0.13
V94	60	1.05	0.17	CV1	63	0.7	0.13
111	50	0.83	0.09				
121	50	1.26	0.14				
128	50	0.78	0.10				

Fig. A-4-2: Input parameters and calculation options of the basin modeling (modeling report).

BasinMod 1-D Data Report						
Licensed to: Eberhard-Karls-Universitat						
Release Name: May 2002 Release						
Build Date: 2002-05-06						
File Name: beckenmod cimpeni.mod						

Stratigraphy Table						
Formation or Event Name	Type	Begin Age (my)	Top Depth (m)	Present Thick (m)		
erros	E	65				
ma	F	70	0	1268		
st-ma	F	83.5	1268	380		
st2_cp	F	84	1648	82		
st1	F	85	1730	340		
Formation or Event Name	Type	Eroded Thick (m)	Lithology			
erros	E	-1100				
ma	F		flysch			
st-ma	F		mergel			
st2_cp	F		Limestone			
st1	F		basiskong			
Formation or Event Name	Type	Total Conduct (W/m*C)				
erros	E	1.5				
ma	F					
st-ma	F					
st2_cp	F					
st1	F					
Lithology Name	% Sandstone	% Siltstone	% Shale	% Limestone	% Dolomite	
Limestone	0	0	0	100	0	
Dolomite	0	0	0	0	100	
flysch	70	20	10	0	0	
mergel	0	0	70	30	0	
basiskong	95	5	0	0	0	

All Mixed Parameters Table						
Lithology Name	Initial Porosity	Reciprocal Compaction Factor	Exponential Compaction Factor	Matrix Density		
	1D.2D.3D (fraction)	1D (1/km)	1D (1/km)	1D.2D.3D (g/cm^3)		
Limestone	0.6	1.5	0.22	2.72		
flysch	0.485	1.905	0.322	2.636		
mergel	0.6	2.13	0.423	2.636		
basiskong	0.455	1.773	0.277	2.64		
Lithology Name	Koz-Car Grain Size	Quartz Grain Size	Quartz Fraction	Clay Coat Fraction		
	1D.2D.3D (mm)	1D.2D (mm)	1D.2D (fraction)	1D.2D (fraction)		
Limestone	0.5	0.5	0	0		
flysch	0.122493	0.047317	0.366	0.73		
mergel	0.003397	0.012253	0.014	0.665		
basiskong	0.420415	0.09095	0.478	0.663		
Lithology Name	Matrix Thermal Conductivity	Matrix Therm Cond	Matrix Heat Capacity	Matrix Therm Cond		
	1D.2D.3D (W/m*C)	1D (factor)	1D.2D.3D (kJ/m^3*C)	2D.3D (ratio)		
Limestone	2.9	350	2600	1.55		
flysch	3.375	205	2700	1.55		
mergel	1.828	-21	2250	1.55		
basiskong	4.23	265	2792.5	1.55		
Lithology Name	FF Fraction of A	FF A Initial Porosity	FF B Initial Porosity	FF A Poro Exponential		
	1D (fraction)	1D (factor)	1D (factor)	1D (factor)		
Limestone	1	0.6	0	-0.8		
flysch	0.3	0.567	0.45	-0.8		
mergel	1	0.6	0	-0.8		
basiskong	0.05	0.55	0.45	-0.8		

Fig. A-4-2 (continued)

Lithology Name	FF B Poro Reciprocal 1D (1/Pa)	FF B Redux 1D	Porosity Reduction Factor 1D.2D (factor)	Initial Vertical Permeability 1D.2D.3D (md)	Permeability Reduction Factor 1D.2D (factor)
Limestone	0	0	0.00019	5000	6
flysch	1.35e-008	0	1.951e-4	4305.12	6.7
mergel	0	0	2.616e-4	64.5195	6
basiskong	1.35e-008	0	1.774e-4	22556.2	6.95

Lithology Name	Irreducible Water Saturation 2D (fraction)	Fracture Gradient Factor 2D (factor)	Permeability Anisotropy 1D.2D.3D (ratio)	Statoil Permeability Factor 1D (md)
Limestone	0.2	0.5	0.5	0.001
flysch	0.26	0.28	0.324901	1.58489
mergel	0.34	0.71	0.263276	7.94328e-006
basiskong	0.21	0.205	0.386375	56.2341

Lithology Name	Statoil Permeability Exponent 1D.3D (unitless)	Statoil Compaction Exponent 1D.3D (1/Pa)	Statoil Matrix Therm Cond Temp Corr 1D (1/C)
Limestone	17	1.8e-008	-0.0017
flysch	16.3	2.84e-008	-0.001464
mergel	12.1	2.99e-008	-0.001028
basiskong	17	2.715e-008	-0.001665

Lithology Name	Statoil Matrix Therm Cond Press Corr 1D (1/Pa)	Statoil Matrix Therm Cond Anis Mean Depth 1D (m)	Statoil Matrix Therm Cond Max Anis 1D (ratio)
Limestone	3e-011	2000	1
flysch	3.7e-011	2000	1.12951
mergel	7.9e-011	2000	1.6245
basiskong	3e-011	2000	1.0132

Time Values Table

Time (my)	Heat Flow (mW/m ²)	Surface Temp (C)
0.4445	71.11	
7.4695	71.43	
18.769	69.54	
22.357	57.21	
48.903	58.64	
50.696	70.18	
53.388	85.58	
57.691	98.66	
63.072	106	
68.812	108.51	
79.932	106.54	
88.004	101.7	
92.308	88.63	
95.358	77.34	
99.842	52	

Measured %Ro Table

Depth	%Ro
300	0.94
380	0.95
718	1.02
770	0.92
1300	1.23
1710	1.46

Model Units
Depth = (m)
Distance = (m)
Thermal Conductivity = (W/m*C)
Heat Capacity = (kJ/m ³ *C)
Heat Flow = (mW/m ²)
Temperature = (C)
Heat Generation = (muW/m ³)
Gradient = (C/100 m)
Activation Energy = (kcal/mole)
Frequency Factor = (1/sec)
HC Density = (g/cm ³)
Pressure = (MPa)
Grain Size = (mm)
Seismic Velocity = (m/sec)
Event Time = (msec)

Thermal Options

Geothermal Calculation = Transient Heat Flow

Current Surface Temp = 10.00

Current Heat Flow = 41.60

Conductivity Calculation = Deming/Chapman

Fig. A-4-2 (continued)

Geothermal Gradient Table
 Time Depth 1 Gradient 1 Depth 2 Gradient 2

 0 0 2.1 2000 3.5

 Delta Heat Table

 Event Name Time Start

 st-ma4 65

 End Generated Time Heat

 60 80
 Calculation Options Permeability Calculation = Power Function
 Expulsion Calculation = Saturation Method
 Default Max Time Interval = 2.00
 Automatic Time Interval = Yes
 Use Depth Interval = No
 Compaction Options Compaction = Exponential
 Advanced Options TTI Reference Temp = 105.00
 TTI Doubling Temp = 10.00
 Rock-Eval Correction = 35.00
 Critical Fracturing Fraction = 0.850
 Fracture Closure Rate = 0.050
 Initial S1 = 3.00
 Abbreviated Well Name = geoagiu

```

+-----+
| BasinMod 1-D Data Report |
| Licensed to: Eberhard-Karls-Universitat |
| Release Name: May 2002 Release |
| Build Date: 2002-05-06 |
| Model Name: |
| File Name: beckenmod geoagiu.mod |
+-----+
    
```

Stratigraphy Table

Formation or Event Name	Type	Begin Age (my)	Top Depth (m)	Present Thick (m)
neog	F	15.7	0	200
erros	E	65		
st-ma4	F	67	200	620
st-ma3	F	73	820	620
st-ma2	F	77	1440	620
st-ma	F	80	2060	620
co-st	F	85	2680	50
co	F	88	2730	60

Formation or Event Name	Type	Eroded Thick (m)	Lithology
neog	F		Sandstone
erros	E	-4000	
st-ma4	F		flysch
st-ma3	F		flysch
st-ma2	F		flysch
st-ma	F		flysch
co-st	F		mergel
co	F		basiskong

Formation or Event Name	Type	Total Conduct (W/m°C)
neog	F	1.5
erros	E	1.5
st-ma4	F	1.5
st-ma3	F	1.5
st-ma2	F	1.5
st-ma	F	1.5
co-st	F	1.5
co	F	1.5

Lithology Mixes Table

Lithology Name	Lithology Color	Lithology Pattern
flysch	Light Green	Coarse Sand
mergel	True Green	Shale
basiskong	Brown	Conglomerate

Lithology Name	% Sandstone	% Siltstone	% Shale	% Limestone	% Dolomite
flysch	70	20	10	0	0
mergel	0	0	70	30	0
basiskong	95	5	0	0	0

Fig. A-4-2 (continued)

Lithology		%	%	%	%	%
Name	Evaporite	Kerogen	Igneous	User	Lith1	User Lith2
flysch	0	0	0	0	0	0
mergel	0	0	0	0	0	0
basiskong	0	0	0	0	0	0
Lithology		% Total				
Name	User	Lith3	%			
flysch	0	0	100			
mergel	0	0	100			
basiskong	0	0	100			
All Mixed Parameters Table						
Lithology	Initial Porosity	Reciprocal Compaction Factor	Exponential Compaction Factor	Matrix Density		
Name	1D.2D.3D (fraction)	1D (1/km)	1D (1/km)	1D	1D.2D.3D	1D.2D.3D (g/cm^3)
flysch	0.485	1.905	0.322	2.636		
mergel	0.6	2.13	0.423	2.636		
basiskong	0.455	1.773	0.277	2.64		
Lithology	Koz-Car Grain Size	Quartz Grain Size	Quartz Fraction	Clay Coat on Quartz		
Name	1D.2D.3D (mm)	1D.2D (mm)	1D.2D (fraction)	1D.2D	1D.2D	1D.2D (fraction)
flysch	0.122493	0.047317	0.366	0.73		
mergel	0.003397	0.012253	0.014	0.665		
basiskong	0.420415	0.09095	0.478	0.663		
Lithology	Matrix Thermal Conductivity	Matrix Therm Cond Temp Corr	Matrix Heat Capacity	Matrix Therm Cond Anisotropy		
Name	1D.2D.3D (W/m^C)	1D (factor)	1D.2D.3D (kJ/m^3*C)	1D	1D.2D.3D	2D.3D (ratio)
flysch	3.375	205	2700	1.55		
mergel	1.828	-21	2250	1.55		
basiskong	4.23	265	2792.5	1.55		
Lithology	Fraction of A	FF A Initial Porosity	FF B Initial Porosity	FF A Poro Redux Exponential		
Name	(fraction)	1D (factor)	1D (factor)	1D	1D	1D (factor)
flysch	0.3	0.567	0.45	-0.8		
mergel	1	0.6	0	-0.8		
basiskong	0.05	0.55	0.45	-0.8		
Lithology	FF B Poro Redux Reciprocal	Porosity Reduction Factor	Initial Vertical Permeability	Initial Permeability Reduction Factor		
Name	1D (1/Pa)	1D.2D (factor)	1D.2D.3D (md)	1D.2D.3D	1D.2D	1D.2D (factor)
flysch	1.35e-008	1.951e-4	4305.12	6.7		
mergel	0	2.616e-4	64.5195	6		
basiskong	1.35e-008	1.774e-4	22556.2	6.95		
Lithology	Irreducible Water Saturation	Fracture Gradient Factor	Permeability Anisotropy	Statoil Permeability Factor		
Name	2D (fraction)	2D (factor)	1D.2D.3D (ratio)	1D.2D.3D	1D	1D (md)
flysch	0.26	0.28	0.324901	1.58489		
mergel	0.34	0.71	0.263276	7.94328e-006		
basiskong	0.21	0.205	0.386375	56.2341		
Lithology	Statoil Permeability Exponent	Statoil Compaction Exponent	Statoil Therm Cond Temp Corr	Matrix Therm Cond		
Name	1D.3D (unitless)	1D.3D (1/Pa)	1D (1/C)	1D		
flysch	16.3	2.84e-008	-0.001464			
mergel	12.1	2.99e-008	-0.001028			
basiskong	17	2.715e-008	-0.001665			
Lithology	Statoil Therm Cond Press Corr	Statoil Matrix Therm Cond Anis	Statoil Matrix Mean Depth	Statoil Matrix Therm Cond Max Anis		
Name	1D (1/Pa)	1D	1D (m)	1D	1D	1D (ratio)
flysch	3.7e-011	2000	1.12951			
mergel	7.9e-011	2000	1.6245			
basiskong	3e-011	2000	1.0132			

Fig. A-4-2 (continued)

Time Values Table

Time (my)	Heat Flow (mW/m ²)	Surface Temp (C)
4.5325	99.1	
8.813	96.62	
19.336	31.89	
39.491	23.4	
66.542	21.27	
74.448	21.31	
79.489	26.86	
87.111	27.77	
90.663	29.65	
91.749	29.59	

Depth	%Ro
500	0.38
650	0.44
1310	0.37
2370	0.550
2475	0.570
2645	0.700

Comment Log
 Model Units

- Depth = (m)
- Distance = (m)
- Thermal Conductivity = (W/m*C)
- Heat Capacity = (kJ/m³*C)
- Heat Flow = (mW/m²)
- Temperature = (C)
- Heat Generation = (muW/m³)
- Gradient = (C/100 m)
- Activation Energy = (kcal/mole)
- Frequency Factor = (1/sec)
- HC Density = (g/cm³)
- Pressure = (MPa)
- Grain Size = (mm)
- Seismic Velocity = (m/sec)
- Event Time = (msec)

Thermal Options

- Geothermal Calculation = Transient Heat Flow
- Current Surface Temp = 10.00
- Current Heat Flow = 41.90
- Conductivity Calculation = Deming/Chapman

Geothermal Gradient Table

Time	Depth 1	Gradient 1	Depth 2	Gradient 2
0	0	2.1	2000	3.5

Delta Heat Table

Event Name	Start Time
st-ma4	65

End Generated

Time	Heat
60	80

Calculation Options

- Permeability Calculation = Power Function
- Expulsion Calculation = Saturation Method
- Default Max Time Interval = 2.00
- Automatic Time Interval = Yes
- Use Depth Interval = No

Compaction Options

- Compaction = Exponential

Advanced Options

- TTI Reference Temp = 105.00
- TTI Doubling Temp = 10.00
- Rock-Eval Correction = 35.00
- Critical Fracturing Fraction = 0.850
- Fracture Closure Rate = 0.050
- Initial S1 = 3.00

Abbreviated Well Name = geoagiu

A.5 Kinematic analysis

For calculations of paleostress directions fault planes, fault axes and axial fault planes were measured. The sense of slip of fault planes was determined from sense of growth of fibrous minerals (mainly calcite and quartz), stylolites, Riedel fractures or offset markers. For each measurement a quality parameter was assigned. It expresses a confidence value of the fault sense value visible in the outcrop. A quality parameter of 1 means a excellently preserved sense of to slip, 4 signifies an inferred sense of slip. This quality parameters will be included in the calculation of principal stress axes, which has been performed by using the computer program TectonicsFP 1.6 (Ortner et al., 2002). The angle between the contraction axis (P) and the fault plane was empirically set to 30° (Fig. A-5-1).

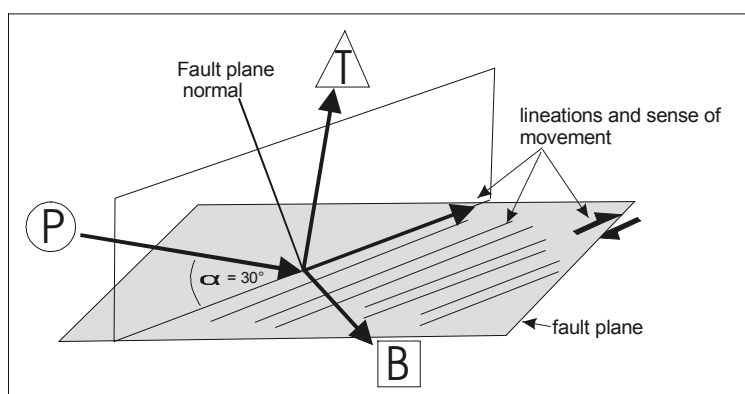


Fig. A-5-1: Principle and geometric relations for the P-T-B axis calculations. The P, B and T axis form 90° angles with each other. The P - T plane is defined by the fault plane normal and the lineation on the fault plane (e.g., mineral fibres). The B axis is perpendicular to the constructed plane.

The heterogeneous data sets have been separated in order to detect individual tectonic events. Thus, accumulation fields of main axes have been separated and interpreted as recording distinct tectonic events. Data sets with oblique kinematic axis (non-horizontal, non-vertical) have been rotated (by the amount of measured layer dip) in order to obtain subhorizontal or subvertical kinematic axes. If rotation resulted in the required axes orientation, the faults were considered to be pre-tilting/folding, thus belonging to stratigraphically older events than those which show subhorizontal or subvertical kinematic axes without rotation. Furthermore, age differences of fault movements have been separated by superposed mineral fibers or fault intersections.

Fig. A-5-2: Fault planes measurements and calculated main stress axes. Sense of slip: 1=reverse, 2=normal, 3= dextral, 4=sinistral.

Dip Direction	Dip	Azimuth	Plunge	Sense of slip	Quality	P- Azimuth	P-Plunge	T- Azimuth	T-Plunge	B- Azimuth	B- Plunge
origin: Sălciua; data set: salciua.t30											
250	20	279	18	1	1	94	12	312	75	186	9
130	26	112	25	2	1	105	54	300	35	205	7
322	55	359	49	2	2	45	69	154	7	246	19
155	62	117	56	2	2	54	72	145	0	235	18
323	84	49	31	2	2	84	30	349	10	243	58
157	76	73	24	2	2	40	28	310	0	219	62
118	78	41	48	2	2	356	48	99	11	198	40
257	40	270	39	2	1	281	69	82	20	174	6
124	27	111	26	2	1	105	56	297	33	203	5
308	20	317	20	2	1	319	50	133	40	226	3
110	80	41	64	2	1	335	60	98	17	196	24
origin: Ocoliş; data set: oclis rotiert1.t30											
122	85	205	56	2	1	254	49	139	20	35	34
196	75	282	14	3	1	313	20	45	6	151	69
310	35	303	35	1	1	305	5	159	84	35	3
310	75	257	66	1	2	288	41	143	43	35	18
320	74	232	6	3	1	81	2	171	17	343	73
322	55	263	36	1	2	284	13	177	52	23	35
218	71	304	13	4	1	275	2	6	23	180	67
283	30	294	30	1	2	111	0	17	85	201	5
122	85	35	30	1	2	68	23	329	19	204	59
58	56	78	54	1	1	69	25	225	63	334	10
52	48	53	48	1	1	53	18	231	72	322	0
68	55	68	55	1	1	68	25	248	65	338	0
97	77	61	74	1	2	85	46	283	43	185	9
56	25	143	1	1	1	309	26	180	53	52	24
322	55	348	52	1	1	337	23	126	63	241	13
origin: Hășdate; data set: hasdate-3+1+5.t30											
248	65	325	25	1	1	299	9	35	35	196	53
258	65	340	16	4	1	314	2	45	30	221	60
257	67	332	31	1	1	305	15	46	37	197	49
165	72	86	30	1	1	115	16	15	31	229	54
168	74	84	19	3	1	113	9	19	24	221	64
151	68	71	24	1	1	99	9	3	32	203	57
212	60	299	6	4	1	93	9	357	29	199	59
146	68	68	28	1	2	96	13	357	34	203	53
224	76	137	12	4	1	106	17	15	6	265	72
94	41	118	38	1	1	110	9	237	75	18	12
140	76	56	23	1	1	86	13	350	24	201	62
122	75	44	37	1	1	75	23	329	32	194	49
153	78	67	20	3	1	97	11	3	20	214	67
240	41	316	12	0	0	117	12	14	49	217	39
160	63	94	38	1	1	119	18	10	45	225	40

Fig. A-5-2 (continued)

Dip Direction	Dip	Azimuth	Plunge	Sense of slip	Quality	P- Azimuth	P-Plunge	T- Azimuth	T-Plunge	B- Azimuth	B- Plunge
origin: Hășdate; data set: hasdate-3+1+5.t30											
90	40	133	31	1	1	121	4	220	67	29	22
173	60	104	32	1	1	129	12	26	44	231	43
173	59	104	31	1	2	128	10	27	44	228	44
132	50	218	4	3	1	243	23	348	31	123	50
150	56	67	10	3	3	271	7	7	35	171	54
240	85	326	39	1	1	291	30	35	23	156	51
234	80	319	25	1	2	289	16	25	21	164	63
315	45	270	35	1	1	285	8	177	64	18	24
250	82	333	39	1	1	299	29	45	26	170	50
217	82	297	50	1	1	260	36	15	30	134	39
202	80	285	34	1	1	253	23	355	25	126	54
122	62	206	11	3	1	235	24	333	18	96	59
168	45	82	4	3	1	283	17	29	40	175	45
233	72	312	29	1	1	283	16	23	31	170	55
310	45	269	37	1	1	282	10	170	66	16	22
origin: Hășdate; data set: hasdate-4+2+6.t30											
97	54	63	49	2	1	19	71	266	8	174	17
106	58	99	58	2	1	49	86	284	2	194	3
71	49	80	49	2	1	98	78	254	11	345	5
68	36	58	36	0	0	61	6	281	83	151	5
268	72	221	64	2	1	139	69	259	11	352	18
199	81	130	66	2	1	61	61	188	19	285	22
338	70	293	63	2	1	214	70	329	9	61	18
66	61	76	61	2	1	171	86	68	1	338	4
302	81	17	59	2	1	73	55	317	17	217	29
50	65	51	65	2	2	226	85	50	5	320	0
198	65	271	32	2	1	307	42	42	6	139	48
80	86	136	83	2	1	248	63	83	26	350	6
39	88	312	53	2	1	267	45	20	22	127	37
82	89	354	67	2	1	297	53	69	26	172	23
300	80	353	74	1	1	317	48	112	39	212	13
82	72	8	40	2	1	327	45	60	3	153	45
191	84	109	54	1	1	149	40	31	30	277	36
219	52	159	33	2	1	127	51	17	15	276	35
163	76	91	51	1	2	125	34	5	37	243	35
257	73	188	49	2	1	139	53	239	7	334	36
84	89	173	52	1	1	130	42	244	24	355	38
origin: Vlădeasa; data set: vladeasa komplet rotiert-1.t30											
22	59	71	47	2	1	117	63	217	5	309	26
35	66	59	64	2	1	162	79	40	6	309	9
49	89	320	70	2	2	260	55	37	27	138	20
11	69	355	68	2	1	222	80	8	9	99	6
16	70	326	61	2	1	255	68	5	8	98	21
8	69	330	64	2	1	241	74	0	8	92	14
203	90	292	65	1	1	238	52	9	27	112	25
8	84	63	79	2	1	169	65	13	23	279	9

Fig. A-5-2 (continued)

Dip Direction	Dip	Azimuth	Plunge	Sense of slip	Quality	P-Azimuth	P-Plunge	T-Azimuth	T-Plunge	B-Azimuth	B-Plunge
origin: Vlădeasa; data set: vladeasa komplet rotiert-1.t30											
8	90	279	78	2	1	208	58	2	29	98	12
19	72	339	67	2	1	243	72	12	11	104	14
75	77	13	64	2	1	303	63	64	15	159	22
26	75	86	61	2	1	152	62	38	12	302	25
37	63	28	62	2	1	270	85	35	3	125	4
46	69	357	60	2	1	286	69	35	7	127	20
38	75	68	73	2	1	192	73	42	15	310	8
228	85	196	84	1	2	223	55	50	35	318	3
193	30	215	28	2	1	226	57	24	31	120	10
294	15	234	8	2	1	226	37	72	50	326	13
154	16	230	4	2	1	239	33	27	53	139	15
217	85	215	85	0	0	217	55	37	35	307	0
256	80	207	75	1	1	241	49	83	39	344	11
272	50	268	50	2	1	259	80	91	10	0	2
62	60	88	57	2	3	155	78	249	1	339	12
115	41	100	40	2	1	86	69	289	19	196	7
146	52	151	52	2	1	165	82	328	8	58	2
origin: Vlădeasa; data set: vladeasa komplet rotiert-rest.t30											
246	75	326	32	1	1	296	19	37	29	177	54
271	83	183	15	4	1	152	17	242	1	336	73
78	70	8	43	2	1	325	49	58	2	150	41
286	73	198	5	4	2	168	13	75	12	305	72
origin: Roșia; data set: lazurii alle nach rotation.t30											
206	85	267	80	1	2	219	54	21	35	117	9
14	54	325	42	2	1	286	61	177	10	82	27
25	88	25	88	1	2	25	58	205	32	115	0
19	44	25	44	2	1	32	74	201	16	292	3
24	19	12	19	2	1	9	49	197	41	103	4
30	65	26	65	2	1	227	85	29	5	119	2
183	50	195	49	2	1	217	78	7	10	98	6
92	86	10	64	2	1	312	54	78	23	180	26
356	66	14	65	2	1	129	81	360	6	269	7
108	80	146	77	2	1	267	69	112	19	19	8
315	46	265	34	2	1	235	56	115	19	15	28
128	88	205	81	2	1	292	61	133	28	37	8
280	61	286	61	2	1	28	87	282	1	191	3
234	72	184	63	2	1	107	68	224	10	317	19
313	86	277	86	1	1	308	56	135	34	42	3
306	87	239	83	1	1	295	56	131	33	36	7
101	88	183	78	2	1	261	60	108	27	11	12
85	84	158	69	1	1	112	49	253	34	357	20
68	39	357	14	2	1	335	37	215	33	97	36
257	80	175	39	2	1	136	39	234	10	334	49
181	67	232	55	2	1	292	65	194	4	101	25

Fig. A-5-2: (continued)

Dip Direction	Dip	Azimuth	Plunge	Sense of slip	Quality	P- Azimuth	P-Plunge	T- Azimuth	T-Plunge	B- Azimuth	B- Plunge
origin: Drocea; data set: drocea-alle rotiert.t30											
293	87	19	50	2	1	62	43	313	19	205	40
293	87	210	65	1	1	259	49	127	30	20	24
268	86	182	45	1	3	219	35	111	24	354	45
294	85	221	73	1	1	271	52	124	34	23	16
176	53	167	53	2	3	142	82	354	7	263	4
56	71	329	9	4	2	300	17	206	12	84	69
267	85	285	85	1	1	269	55	86	35	177	2
135	79	219	30	2	1	254	32	161	5	63	58
299	70	235	50	1	2	264	30	142	43	15	33
303	66	30	7	3	1	59	18	154	17	285	65
359	55	70	25	1	1	47	5	142	45	313	45
278	65	253	63	1	1	266	34	107	54	3	10
281	64	240	57	1	1	260	31	118	53	2	18
283	83	194	5	4	1	164	8	74	4	319	81
358	75	268	2	4	1	239	9	147	13	4	74
283	33	265	32	2	1	255	61	95	28	0	8

A.6 Fission-track analysis.

Sample preparation

Medium grained sandstones were sampled for fission track analysis. The processing methods are similar to those of heavy minerals (Cf. A.2), except that the sieved fraction <250 μm was treated with the Wilfley shaking table and, after heavy fraction separation, the sample underwent a magnetic separation. The separated zircons and apatites were embedded in Teflon respectively epoxy resin. The mounts were polished with diamond suspension down to 1 μm . Zircon mounts were etched with KOH-LiOH eutectic melt (at 205° C, 27 to 166 hours), apatites with 1 % HNO₃ (3 minutes, room temperature), to allow later microscopic detection. A detector (low uranium muscovite) was placed on the mount during irradiation to record the induced tracks from fission near the surface of the crystal mount. For visibility of the tracks, the muscovite was etched with 40 % HF (35 minutes) after irradiation. A minimum of two crystal mounts was made from sedimentary rocks and etched for different time lengths. Since the ages and provenances of crystals from sedimentary rocks are inferred to be unevenly distributed, this procedure insures that all tracks will be etched (low-uranium zircons/high-uranium zircons, old zircons/young zircons).

Principles

The fission-track dating method is based on the natural decay of ²³⁸U, which is a accessory element in zircon and apatite crystals. The spontaneous decay produces two radiogenic nuclides with approximately equal energy, which themselves cause damaging of the crystal lattice. The damage tracks have a length of approximately 17 μm for apatite and 15 μm for zircon. For age calculations the confined tracks were counted individually for each mineral. The fission track age is a relation of counted tracks and uranium content, which is determined by irradiation.

The basic equation for the dating method is:

$$N_D = N_P(e^{\lambda t} - 1)$$

N_D = number of daughter atoms

N_P = number of parent atoms

λ = decay constant

The determined density of spontaneous tracks is expressed by the equation:

$$\rho_s = \frac{\lambda_f^{238}}{\lambda_d} N(e^{\lambda_d t} - 1)$$

the density of induced tracks by:

$$\rho_i = {}^{238}\text{NI}\sigma\phi$$

By replacing NP with pi and ND with ps the age determination equation is represented by the following term (Naeser, 1967; Price & Walker, 1963):

$$t = \frac{1}{\lambda_\alpha} \ln \left(\frac{\rho_s \lambda_\alpha}{\rho_i \lambda_f} I \sigma \phi + 1 \right)$$

λ_d = total decay constant = $\lambda_\alpha + \lambda_f$ of ${}^{238}\text{U}$;

λ_α = decay constant of ${}^{238}\text{U}$ α emission ($1.55125 \times 10^{-10} \text{a}^{-1}$; Jaffrey et al., 1973);

λ_f = decay constant for the spontaneous fission of ${}^{238}\text{U}$;

$I = {}^{235}\text{U}/{}^{238}\text{U}$ isotope ratio (7.2527×10^{-3} ; Cowan and Adler, 1976);

σ = cross-section for neutron fission reaction of ${}^{235}\text{U}$ ($580.2 \times 10^{-24} \text{cm}^2$, Hanna et al., 1969);

Φ = thermal neutron fluence;

ρ_s = density of spontaneous tracks;

ρ_i = density of induced tracks.

ζ -calibration method

The ζ -calibration method has been introduced in order to calibrate the fission-track dating procedure. The method eliminates variables and uncertainties like λ_f , σ , Φ and individual determination statistics. An age standard (with independently measured age) and uranium glass with uniform distributed uranium is to be analysed. Two age standards and the two uranium glasses were added to the crystal mount (with muscovite detector sheet) during irradiation. For each mineral species (apatite or zircon) an individual, nontransferable ζ -value has to be calculated. The ζ -value is determined by the ratio of spontaneous and induced tracks of the age standard and the track density of the uranium glass

$$\zeta = \frac{(e^{\lambda_\alpha t_{std}} - 1)}{\lambda_\alpha \left(\frac{\rho_s}{\rho_d} \right)_{std} G \rho_d}$$

G = geometry factor (0.5 for external detector method);
 pd = dosimeter track density (counted from uranium glass standards);
 t_{std} = age of the standard;
 $(\rho_s/\rho_i)_{std}$ = track density ratio in the standard.

The ζ -value is introduced in the age determination equation and results in the final equation:

$$ts = \frac{1}{\lambda_\alpha} \ln \left[\lambda_\alpha \left(\frac{\rho_s}{\rho_i} \right) \rho_d G \zeta + 1 \right]$$

ts = age of the sample;
 $(\rho_s/\rho_i)_s$ = track density ratio in the sample.

Irradiation

The irradiation procedure has been realized at the HIFAR nuclear reactor of the Oregon State University (USA), by using a neutron flux of 1.8×10^{15} n/cm² for zircon, and 4.8×10^{15} n/cm² for apatite.

Used age standards for zircon irradiation

Tardree rhyolithe (Northern Ireland, U.K), age: 58.7 ± 1.1 Ma (Hurford and Green, 1983)

Used age standard for zircon irradiation

Fish Canyon volcanic tuff (Colorado, USA), age: 27.8 ± 0.2 Ma (Hurford and Hammerschmidt, 1985)

Dosimeter uranium glasses:

for zircon irradiation: CN2, 38 ppm natural uranium (Hurford and Green, 1983)

for apatite irradiation: CN5, 12 ppm natural uranium (Hurford and Green, 1983)

Counting of fission-tracks

Spontaneous and induced tracks were determined by using the External Detector Method (EDM; Naeser and McKee, 1970). This method allows single grain age determination, which is required for zircon age population separation. A minimum of 25 grains has been counted for crystalline rocks and 50 grains for sedimentary rocks.

Track counting was made by using a Zeiss optical microscope and a magnification of 1000. The tracks of the crystals were counted by using immersion oil, whereas induced tracks of the muscovite detector sheet were counted without oil. Only crystals with homogeneous track distribution, without fractures or fluid inclusions have been counted. Crystals with curved tracks have been excluded, since their orientation was not parallel to the optical c-axis. The microscopic analysis was made by using the calibration tablet controlled by the computer program FTStage, version 3.11 (Dumitru, 1993). The program TRACKKEY has been utilized for age determination (Dunkl, 2002).

Figure A-4-1 displays the measured ages of the standards with calculated ζ -values. The weighted mean value, which was used for age determination was calculated with the FIT program.

Age	N	ρ_s	N_s	ρ_i	N_i	ρ_d	$P\chi^2$	ρ_s/ρ_i	N_d	$\zeta \pm 1\sigma$	
Std.		$\times 10^5$ (cm ²)		$\times 10^5$ (cm ²)		$\times 10^5$ (cm ²)	(%)				
ZT	25	66.55	1616	67.29	1634	8.23	0.04	0.99	5182	144.8	6.1
ZF	25	51.17	2314	82.29	3721	7.30	8.03	0.626	5802	122.3	4.23
ZF	25	55.27	1918	104.87	3639	7.29	7.72	0.521	5802	147.27	5.29
ZF	27	38.88	1659	75.40	3217	8.34	0.17	0.514	6612	130.45	4.86
weighted mean \pm standard error									133.54 \pm 2.5		

Fig. A-6-1: Calculation of ζ -values

Age populations

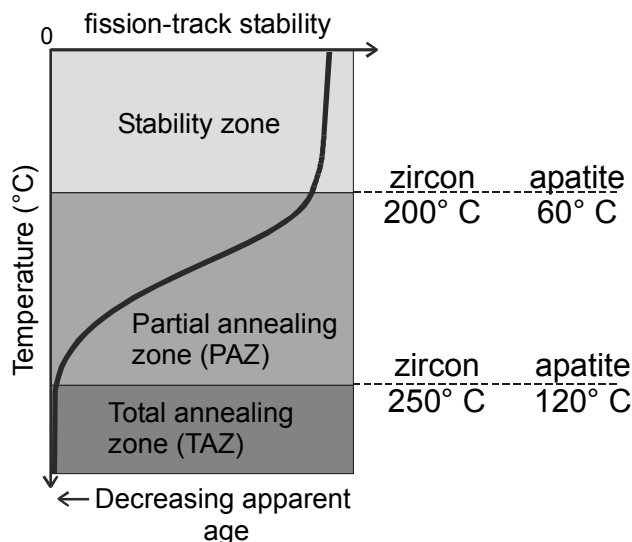
Sedimentary rocks contain minerals and mineral fragments from different source rocks with different geologic history. If fission-track ages of zircons from sedimentary rocks are determined and these sediments did not suffer high temperatures (above total annealing, cf. following paragraphs), the determined ages of the individual zircons display the fission-track ages of the source rocks. With the age population method the fission-track ages of the eroded rocks were determined by using statistical methods of separation. If $P\chi^2$ is lower than 5 %, more than one age population was presumed and the measured data set underwent a statistical separation process. Almost all whole rock determined fission-track ages of sedimentary samples fail the $P\chi^2$ test. For the separation process the program PopShare v1.K (Dunkl & Szekely, 2003) was used. The root mean square statistical method was used to separate the age populations.

Fission-track annealing

Increasing temperature causes track healing, a total or partly closure of the spontaneous tracks and thus recovering of the initial zircon or apatite lattice. The temperature zone in which the fission track starts to heal is called Partial Annealing Zone (PAZ, Wagner, 1979; Naeser, 1979). Below the PAZ (within the zone of total annealing: TAZ, Fig. A-6-2), higher temperatures causes immediately healing of spontaneous tracks and thus, no tracks are retained. The governing factors for track annealing are temperature, time, and chemical composition of the crystals, whereas temperature is the most important factor.

The difference of chemical composition and lattice defects in zircon and apatite make them more or less temperature sensitive. Thus, the PAZ for apatite lies within approximately 60° C and 120° C (Wagner, 1968; Naeser and Faul, 1969) and for zircon within approximately 200° C and 250° C (Fleischer et al., 1964, 1965).

Fig. A-6-2: Stability zones of fission-tracks for zircon and apatite. Bold line indicates decrease in apparent fission-track age with increasing temperature and depth during a steady-state period (modified after Naeser, 1979).



Apatite track length measurements and T-t path modelling

Shortening of the apatite track occurs within the partial annealing zone (PAZ), between 60-120° C. Time and temperature are the main controlling variables for this process. Reduction of track length will increase with increasing temperature and time within the PAZ. Therefore, the reconstruction of thermal histories of rocks is possible by using track length distributions. Track lengths were determined by measuring horizontal confined track lengths (Bhandari et al., 1971).

Modelling of the low-temperature thermal history, based on the apparent FT ages and the confined track length data, was carried out using the AFTSolve 1.1.3 modelling program (Ketcham et al., 2000). The FT age data together with track lengths distributions were used to model individual thermal histories of the samples, by using the AFTSolve 1.1.3 modelling program (Ketcham et al., 2000). The annealing model of Ketcham et al. (1999) was used for the modelling, the initial track length was set at 16.0 μm , and the searching algorithm ran in 50 000 iterations.

Fig. A-6-2. Table with zircon fission-track results. Except for sample 130., the sedimentary samples derive from the Gosau succession

Code	Locality	Lithology	Sedi- mentation age ma	Sample location	Altitude (masl)	Cryst.	Spontaneous		Induced		Dosimeter		P(x ²)	FT age (Ma ± 1σ)
							P _s	N _s	P _i	N _i	P _d	N _d		
159	Băișoara	banatite	-	06 88 552/51 62 312	532±23	25	159.68	2433	122.93	1873	8.11	5182	54.2	70.0 ± 2.7
163	Viădeasa	banatite	-	06 40 551/51 78 160	1037±24	23	172.94	1972	131.72	1502	8.07	5182	96.1	70.4 ± 2.9
M11	Ocoliș	banatite	-	06 89 588/51 49 858	453±10	25	124.80	1926	102.38	1580	7.96	5182	81.6	64.4 ± 2.7
130	Linteni	sandstone	54	06 88 228/51 65 196	642±22	50	96.69	3764	45.21	1760	7.40	5802	0.0	107.8 ± 5.9
M64	Mușca	sandstone	66	06 64 852/51 33 184	992±52	44	157.28	4499	33.35	954	9.00	6612	0.5	274.2 ± 14.0
M24	Abrud-Zlatna	sandstone	67	06 63 028/51 18 486	822±33	49	123.60	3402	41.60	1145	7.80	5182	0.0	148.3 ± 10.8
M27	Drocea	sandstone	69	05 80 222/51 04 691	242±41	48	114.40	4847	50.37	2134	7.42	5182	5.2	112.6 ± 4.4
M52	Drocea	sandstone	70	05 84 457/51 07 772	245±43	49	113.05	4734	42.79	1792	8.67	6612	0.0	149.3 ± 8.0
M15	Sălciuma	sandstone	72	06 85 422/51 43 377	530±22	47	126.31	4321	57.94	1982	7.69	5182	0.0	110.9 ± 7.1
VS 127	Hășdate	sandstone	78	06 84 998/51 71 043	612±84	50	98.15	3126	42.95	1368	7.07	5182	0.1	107.7 ± 5.3
M26	Viădeasa	sandstone	78	06 37 897/51 70 939	1160±19	50	107.63	4867	36.07	1631	7.34	5802	0.0	144.2 ± 7.8
Mai 82	Hășdate	sandstone	79	06 84 704/51 86 812	670±53	50	89.35	4787	46.12	2471	7.34	5182	0.1	94.3 ± 3.8
247	Roșia	sandstone	80	06 09 791/51 82 466	346±25	24	169.71	1368	83.49	673	8.79	6612	0.0	111.4 ± 11.7
Mai 8-	Vidra	sandstone	82	06 44 571/51 36 746	682±14	49	95.27	4280	48.51	2179	7.57	5182	0.5	99.1 ± 4.1
Mai 89	Hășdate	sandstone	83	06 83 701/51 69 276	825±19	50	99.78	4610	45.61	2107	7.35	5802	0.0	104.6 ± 5.1
M61	Gilau	sandstone	83	06 81 035/51 79 332	468±150	50	103.29	4498	46.39	2020	8.88	6612	0.0	128.9 ± 7.3
VS 44	Vidra	sandstone	83	06 45 170/51 37 659	712±45	49	105.24	3238	52.78	1624	7.88	5182	0.0	102.5 ± 5.0
M49-	Drocea	sandstone	84	05 79 401/51 07 443	210±15	50	133.34	4417	47.73	1581	9.06	6612	0.0	166.9 ± 10.4
Mai92b-	Hășdate	sandstone	85	06 83 693/51 69 171	774±33	49	80.47	3971	37.02	1827	7.49	5182	0.0	106.9 ± 5.0
M16	Sălciuma	sandstone	87	06 85 141/51 44 992	563±56	49	118.26	3406	56.66	1632	7.76	5182	0.0	108.5 ± 5.3
165	Viădeasa	sandstone	87	06 42 754/51 78 850	915±150	50	73.71	3543	38.74	1862	7.22	5182	8.7	91.4 ± 3.7
204	Drocea	sandstone	89	05 89 835/51 13 934	357±20	48	119.40	3791	46.36	1472	7.15	5182	0.0	121.4 ± 7.0
107	Valea Șoimului	Variscan granite (Granit de Mt. Mare)	-	06 67 018/51 56 119	1516±40	25	48.44	1457	27.19	818	8.03	5182	64.4	94.8 ± 4.7
109	Băișoara Mt.	micaschist (Someș Unit)	-	06 65 555/51 66 166	151±100	26	148.97	1889	92.35	1171	8.00	5182	68.7	85.5 ± 3.8
105	lara valley	micaschist	-	06 75 121/51 64 378	846±25	25	180.36	1702	93.46	882	7.38	5802	69.1	94.4 ± 4.5
106	lara valley	micaschist	-	06 71 787/51 62 470	1005±82	15	110.12	1050	64.71	617	7.6093	5182	3.9	85.9 ± 4.8

Cryst: number of dated crystals.

Track densities (ρ) are as measured (x105 tr/cm2); N: number of tracks counted.

Zircon ages were calculated using dosimeter glass: CN 2 with ζ = 345.95 ± 10.78

P(x²): probability obtaining Chi-square value (x²) for n degree of freedom (where n = no. of crystals - 1).

FT age: central age ± 1 standard error

Fig. A-6-3: Zircon fission-track results of data sets with deselected euhedral crystals.

Code	Locality	Lithology	Sedi- mentation age ma	Cryst.			Induced	Dosimeter			$P(X^2)$	FT age
				Spontaneous	ρ_s	N_s		ρ_i	N_i	ρ_d		
130	Linteni	sandstone	54	21	108.91	2077	36.97	705	7.40	5802	0.0	134.3 \pm 14.0
M27	Drocea	sandstone	69	12	94.18	1222	38.30	497	7.42	5182	20.4	120.9 \pm 7.9
VS127	Hășdate	sandstone	78	33	98.89	2258	43.05	983	7.07	5182	0.1	108.2 \pm 6.4
Mai 82	Hășdate	sandstone	79	25	74.03	2154	39.18	1140	7.34	5182	2.5	92.1 \pm 4.8

Fig. A-6-4: Age populations of detrital zircon fission track ages.

Code	Locality	Crystal	M1 -Pu	SD1 -Pu	%C1 -Pu	M2 -Pu	SD2 -Pu	%C2 -Pu	M3 -Pu	SD3 -Pu	%C3 -Pu	Method	Model
130	Linteni	50	85.7	17.2	81.5	127.5	7.4	16.5	398.7	34.6	32.3	RMS	Gaussian
M64	Musca	44	216.9	34.5	51.2	290.2	23.5	45.7	255.4	9.8	18.1	RMS	Gaussian
M24	Abrud-Zlatna	49	92.2	37.6	36.2	180.5	29.6	77.4	153.3	3.6	7.1	RMS	Gaussian
M 27	Drocea	48	95.6	4.6	15.5	117.4	26.6	59.5				RMS	Gaussian
M52	Drocea	49	139.4	27.9	40.5	171.6	68.7	76.4				RMS	Gaussian
M15	Sălciuma	47	79.4	9.9	23.6	134.7	52.2	35.7				RMS	Gaussian
VS 127	Hășdate	50	101.6	25.6	64.3	137.4	36.2	9.4	172.6	63.0	68.4	RMS	Gaussian
M26	Viădeasa	50	110.5	16.0	22.2	143.0	1.9	74.7				RMS	Gaussian
Mai 82	Hășdate	50	77.0	6.1	25.3	103.2	24.1	24.7				RMS	Gaussian
247	Roșia	24	98.0	41.5	75.3	201.0	37.5	33.3				RMS	Gaussian
Mai 8-	Vidra	49	93.0	17.9	66.7	133.0	19.8	7.7				RMS	Gaussian
Mai 89	Hășdate	50	102.1	24.0	92.3	178.0	13.0	34.7	170.0	69.8	47.0	RMS	Gaussian
M61	Gilau	50	85.9	5.7	18.3	122.4	9.7	14.2				RMS	Gaussian
44-B	Vidra	49	97.9	22.7	85.8	1528.0	11.5	22.3	216.0	65.8	67.7	RMS	Gaussian
M49-	Drocea	50	89.2	1.9	10.0	128.3	7.7	46.9				RMS	Gaussian
Mai 92	Hășdate	49	85.0	10.7	53.1	129.0	14.4	18.7				RMS	Gaussian
M16	Sălciuma	49	104.0	25.6	81.3	166.9	47.9	29.2	205.8	21.1	19.2	RMS	Gaussian
204	Drocea	48	95.7	28.2	51.6	145.6	15.8					RMS	Gaussian

Fig. A-6-5: Fission track age populations of detrital zircons from datasets with deselected euhedral zircons.

Code	Locality	Crystal	M1 -Pu	SD1 -Pu	%C1 -Pu	M2 -Pu	SD2 -Pu	%C2 -Pu	M3 -Pu	SD3 -Pu	%C3 -Pu	Method	Model
130	Linteni	21	115.5	5.5	25.0	154.0	85.4	75.0				RMS	Gaussian
M27	Drocea	12	109.5	21.1	70.9	150.8	2.4	29.1				RMS	Gaussian
VS 127	Hășdate	33	108.2	28.4	83.0	140.8	49.5	17.0				RMS	Gaussian
Mai 82	Hășdate	25	85.7	17.2	81.5	127.8	7.4	18.5				RMS	Gaussian

SD1 - Pu: standard deviation of population 1

%C1 - Pu: percentage of population group 1

Fig. A-6-6: Apatite fission track data table.

Code	Locality	Lithology	Sedi- mentat. age ma	Cryst.	Spontaneous	Induced	Dosimeter	$P(X^2)$	FT age
					ρ_s	ρ_i	N_d	N_d	(Ma $\pm 1\sigma$)
107	Valea Șoimului	Variscan granite (Granit de Mt. Mare)	-	20	6.39	11.83	1139	4291	62.6 \pm 3.5
109	Baișoara Mt.	micaschist (Someș Unit)	-	20	7.58	12.07	1263	4291	77.3 \pm 4.3
M15	Sălcium	sandstone	72	20	9.49	14.90	1354	4291	75.8 \pm 3.8
M24	Abrud/Zaitna	sandstone	67	20	6.68	11.37	1049	4291	71.2 \pm 4
M27	Drocea	sandstone	69	20	10.00	14.56	1394	4291	81 \pm 3.9

References

- Bhandari, N., Bhat, S. G., Lal, D., Rajagopalan, G., Tamhane, A. S. J., and Venkatavaradan, V. (1971): Fission fragment track in apatite: recordable track lengths. *Earth Planet. Sci. Lett.*, 13, 191-199.
- Cowan, G.A., and Adler, H. H. (1976): The variability of the natural abundance of ^{235}U . *Geochim. Cosmochim. Acta*, 40, 1487-1490.
- Dumitru, T. A. (1993): A new computer-automated microscope stage system for fission-track analysis. *Nucl. Tracks Radiat. Meas*, 21, 575-580.
- Dunkl, I. (2002): TRACKKEY: a windows program for calculation and graphical presentation of fission track data. *Computers and Geosciences*, 28(2).
- I. Dunkl and B. Székely (2003): Component Analysis With Visualization of Fitting - Popshare, A Freeware program For Evaluation Of Mixed geochronological Data. *Geophysical Research Abstracts*, Vol. 5, 02657.
- Fleischer, R. L., Price, P. B., and Walker, R. M. (1964): Fission-track ages of zircons. *Journal of Geophysical Research*, v.69, no. 22, 4885-4888.
- Fleischer, R. L., Price, P. B., and Walker, R. M. (1965): Effects of temperature, pressure and ionization of the formation and stability of fission tracks in minerals and glasses. *Journal of Geophysical Research*, 70, 1497-1502.
- Hurford, A. J., and Green, P. F. (1983): The zeta age calibration of fission-track dating. *Chem. Geol., Isot. Geosci.*, 41, 285-312.
- Hurford, A. J., and Hammerschmidt, K. (1985): ^{40}Ar - ^{39}Ar and K-Ar dating of the Bishop and Fish Canyon tuffs: calibration ages for fission track dating standard. *Chem. Geol. (Isotope Geol. Section)* 58, 23-32.
- Jaffrey, A. H., Flynn, K. F., Glendenin, L. E., Bentley, W. C., and Essling, A. M. (1973): Precision Measurements of the half-lives and specific activities of ^{235}U and ^{238}U . *Phys. Rev.*, v. 4, 1889-1906.
- Ketcham, R. A., Donelick, R.A. and Carlson, W.D., (1999): Variability of apatite fission-track annealing kinetics: III. Extrapolation to geological time scales. *Am. Mineral.*, 84, 1235-1255.
- Ketcham, R. A., Donelick, R. A. and Donelick, M.B., (2000): AFTSolve: a program for multi-kinetic modelling of apatite fission-track data. *Mineral. Soc. Am. Geol. Mater. Res.* 2, 1-32.
- Naeser, C. W. (1967): The use of apatite and sphene for fission track age determination. *Bull. Geol. Soc. Am.* 78, 1523-1526.
- Naeser, C. W., and Faul, H. (1969): Fission track annealing in apatite and sphene. *Jour. Geophys. Res.*, 74, 705-710.
- Naeser, C. W. (1979): Fission-track dating and geologic annealing of fission tracks. In Jäger, E., and Hunziker, J. C. (eds.), 1979: *Lectures in isotope Geology*, Springer-Verlag, Heidelberg, 154-169.
- Ortner, H., Reiter, F., Acs, P. (2002): Easy handling of tectonic data: the programs TectonicVB for Mac and TectonicsFP for Windows. *Comput. Geosci V.* 28/10 p. 1193—1200.
- Price, P. B., and Walker, R. M. (1963): A simple method for measuring low uranium concentrations in natural crystals. *Appl. Phys. Lett.* 2, 23-25.
- Wagner, G. A. (1968): Fission track dating of apatites, *Earth Planet. Sci. Lett.* 4, 411-415.
- Stach E., Mackowsky M-Th., Teichmüller M., Taylor G.H., Chandra D., Teichmüller R. (1982): *Stach's Textbook of Coal Petrology*. 3rd edition. Gebrüder Borntraeger, Berlin, Stuttgart.
- Wagner, G. A. (1979): Correction and interpretation of fission-track ages. In: Jäger, E., and Hunziker, J. C. (eds): *Lectures in isotope geology*, Springer, 170-177.

Acknowledgements

I want to express my thanks to Prof. Wolfgang Frisch, who supported the idea of this research project and accompanied my work with suggestions, discussions, revealing of contradictions and useful critical comments.

Dr. Horst Hann, for his professional and mental support, for reviewing the first drafts of my work, for introducing me to important geologists of Romania and of course for his friendship.

Dr. Istvan Dunkl for showing me the world of “fissioned tracks” and “heavy minerals”, his help concerning data processing, his field guide, various suggestions concerning my work, for counting my apatite samples and for suffering some hard times with me.

Martin Danišík for his help in innumerable situations, during laboratory work, discussions and especially for measuring and modeling apatite fission-track length.

Dr. Joachim Kuhlemann for helpful critics and for reviewing my thesis.

Many thanks to Dr. Thomas Rainer, Prof. Reinhard Sachsenhofer and “Siggi” Schieder from the University of Leoben for showing me the tricks and art of vitrinite sample preparation and reflectance measurements. Special thanks to Thomas, who friendly offered me his second bed during the work in Leoben and suffered some headaches during this time.

The collaboration of the University Tübingen and the University Babeş-Bolyai, Cluj-Napoca (Romania) is a result of several common research projects of the past. This work has been strongly supported by the colleagues from the University Babeş-Bolyai. At this point I want to thank all the colleagues and friends from the University Babeş-Bolyai who will not be named below:

Prof. Ion Balintoni for several interesting and important geological (but not only!) discussions, Prof. Ion Bucur, Dr. Sorin Filipescu (for his “microfauna”-effort) and Dr. Călin Baciuc.

Dr. Nicu Har, for hospitality during my fieldwork breaks in Cluj, several evening with a lot of interesting discussion and other nice spontaneous or organized events.

Liana and Emanoil Săsăran for their hospitality and the several common field works, with many geological discussions, which resulted in several ideas incorporated in this work.

Cristian Bâzdăra, Cristian Lazăr and Cosmin Tat for choosing their diploma thesis on heavy mineral analysis and studies on the Upper Cretaceous turbidites of the Geoagiu flysch.

Ramona Bâlc for processing and determining some nannoplankton samples.

I appreciated the help and discussions with several Romanian geologists: Dr. Denisa and Dr. Marcel Lupu, which doubtless performed most of the work on the Gosau sediments of the Apuseni Mts., for their helps in form of discussions, informations (outcrop locations) and several reference material. Dr. Nicolae Ionel, Dr. Tudor Berza and Dr. Sever Bordea for hosting and several other helps in Bucharest. Furthermore, I want to specially thank Dr. Mihaela Melinte for processing and determination of most of the nannoplankton samples.

Many thanks to all the colleagues and friends in the Frisch-workgroup at the University of Tübingen.

Special thanks to Dr. Radu Gârbacea, who introduced me in Romanian geology and helped me defining the project, but also for discussions during the work.

Many thanks to the cosmoproleten (www.cosmoproleten.de) for pleasant and useful distraction.

The last very important acknowledgements are dedicated to my partner and my children who suffered me several times during overworked periods.

This work was financed by the DFG (Deutsche Forschungsgemeinschaft, Project Nr.: Fr 610/18-1). Additional financial support was given by the DAAD (Deutscher Akademischer Austausch Dienst) and IAS (International Association of Sedimentologists). Acknowledgments are expressed to Plate River Association, Inc., for supporting me with their modeling software.